GROWTH KINETICS OF FACETED SOLID-LIQUID INTERFACES

By

STATHIS D. PETEVES

A DISSERTATION PRESENTED TO THE GRADUATE SCHOOL
OF THE UNIVERSITY OF FLORIDA IN
PARTIAL FULFILLMENT OF THE REQUIREMENTS
FOR THE DEGREE OF DOCTOR OF PHILOSOPHY

UNIVERSITY OF FLORIDA

1986

To the antecedents of phase changes: Leucippus, Democritus, Epicurus and, the other Greek Atomists, who first realized that a material persists through a succession of transformations (e.g. freezing-melting-evaporation-condensation).

ACKNOWLEDGEMENTS

The assumption of the last stage of my graduate education at the University of Florida has been due to people, aside from books and good working habits. It is important that I acknowledge all those individuals who have made my stay here both enjoyable and very rewarding in many ways.

Professor Reza Abbaschian sets an example of hard work and devotion to research, which is followed by the entire metals processing group. Although occasionally, in his dealings with other people, the academic fairness is overcome by his strong and genuine concern for the research goals, I certainly believe that I could not have asked more of a thesis advisor. I learned many things through his stimulation of my thinking and developed my own ideas through his strong encouragement to do so. His constant support and guidance and his unlimited accessibility have been much appreciated. I am grateful to him for making this research possible and for passing his enthusiasm for substantive and interesting results to me. At the same time, he encouraged me to pursue any side interests in the field of crystal growth, which turned out to be a very exciting and "lovable" field. Finally, I thank him for his understanding and his tolerance of my character and habits during "irregular" moments of my life.

Professors Robert Reed-Hill and Robert DeHoff have contributed to my education at UF in the courses I have taken from them and discussions of my class work and research. Their reviews of this manuscript and

their insight to several parts of it was greatly appreciated. Professor Ranganathan Narayanan has been very helpful with his expertise in fluid flow; his suggestions and review of this work is very much acknowledged. I thank Professor Tim Anderson for many helpful comments and for critically reviewing this manuscript. My thanks are also extended to Professor Robert Gould for his acceptance when asked to review this work, for his advice, and for his continuous support.

Julio Alvarez deserves special thanks. We came to the University at the same time, started this project, and helped each other in closing many of the "holes" in the crystal growth of gallium story. He introduced me to the world of minicomputers and turned my dislike for them into a fruitful working tool. He did the work on the thermoelectric effects across the solid-liquid interface. His collaboration with me in the laboratory is often missed.

I am also grateful to several colleagues and friends for their moral support. I thank Robert Schmees and Steve Abeln for making me feel like an old friend during my first two semesters here. Both hardcore metallurgists helped me extend my interest in phase transformations; I shared many happy moments with them and nights of Mexican dinners and "mini skirt contests" at the Purple Porpoise. With Robert, I also shared an apartment; I thank him for putting up with me during my qualifying exams period, teaching me the equilibrium of life and making the sigma phase an unforgettable topic. Joselito Sarreal, from whom I inherited the ability to shoot pictures and make slides, taught me to

My very special thanks to Stephanie Gould for being the most important reason that the last two years in my life have been so happy. I am so grateful to her for her continuous support and understanding and particularly for forcing me to remain "human" these final months.

I also especially thank my parents and my sister for 29 and 25 years, respectively, of love, support, encouragement, and confidence in me.

TABLE OF CONTENTS

APPENDICES

LIST OF TABLES

LIST OF FIGURES

GROWTH KINETICS OF FACETED SOLID-LIQUID INTERFACES

By

STATHIS D. PETEVES

December 1986

A novel method based on thermoelectric principles was developed to
monitor in-situ the interfacial conditions during unconstrained crystal
growth of Ga crystals from the melt and to measure the solid-liquid
(S/L) interface temperature directly and accurately. The technique was
also shown to be capable of detecting the emergence of dislocation(s) at
the crystallization front, as well as the interfacial instability and
breakdown.

The dislocation-free and dislocation-assisted growth kinetics of
(111) and (001) interfaces of high purity Ga, and In-doped Ga, as a
function of the interface supercooling (ΔT) were studied. The growth
rates cover the range of 10^{-3} to 2×10^4 μm/s at interface supercoolings
from 0.2 to 4.6°C, corresponding to bulk supercoolings of about 0.2 to
53°C. The dislocation-free growth rates were found to be a   function

of $\exp(-1/\Delta T)$ and proportional to the interfacial area at small super-coolings. The dislocation-assisted growth rates are proportional to $\Delta T^2 \tanh(1/\Delta T)$, or approximately to ΔT^n at low supercoolings, with n around 1.7 and 1.9 for the two interfaces, respectively. The classical two-dimensional nucleation and spiral growth theories inadequately describe the results quantitatively. This is because of assumptions treating the interfacial atomic migration by bulk diffusion and the step edge energy as independent of supercooling. A lateral growth model removing these assumptions is given which describes the growth kinetics over the whole experimental range. Furthermore, the results show that the faceted interfaces become "kinetically rough" as the supercooling exceeds a critical limit, beyond which the step edge free energy becomes negligible. The faceted-nonfaceted transition temperature depends on the orientation and perfection of the interface. Above the roughening supercooling, dislocations do not affect the growth rate, and the rate becomes linearly dependent on the supercooling.

The In-doped Ga experiments show the effects of impurities and microsegregation on the growth kinetics, whose magnitude is also dependent on whether the growth direction is parallel or antiparallel to the gravity vector. The latter is attributed to the effects of different connective modes, thermal versus solutal, on the solute rich layer ahead of the interface.

CHAPTER I
INTRODUCTION

Melt growth is the field of crystal growth science and technology of "controlling" the complex process which is concerned with the formation of crystals via solidification. Melt growth has been the subject of absorbing interest for many years, but much of the recent scientific and technical development in the field has been stimulated by the increasing commercial importance of the process in the semiconductors industry. The interest has been mainly in the area of the growth of crystals with a high degree of physical and chemical perfection. Although the technological need for crystal growth offered a host of challenging problems with great practical importance, it sidetracked an area of research related to the fundamentals of crystal growth. The end result is likely obvious from the common statement that "crystal growth processes remain largely more of an art rather than a science." The lack of indepth understanding of crystal growth processes is also due, in part, to the lack of sensors to monitor the actual processes that take place at the S/L interface. Indeed, it is the "conditions" which prevail on and near the crystal/liquid interface during growth that govern the formation of dislocations and chemical inhomogeneities of the product crystal. Therefore, a fundamental understanding of the melt growth process requires a broad knowledge of the solid-liquid (S/L) interface and its energetics and dynamics; such an understanding would, in turn, result in many practical benefits.

Crystal growth involves two sets of processes; one on the atomic scale and the other on the macroscopic scale. The first one deals with the attachment of atoms to the interface and the second with the transport of heat and mass to or from the growth front. Information regarding the interfacial atomistic process, both from a theoretical and technical point of view, can be obtained from the interfacial growth kinetics. Growth kinetics, in turn, express the mathematical relationship between the growth rate (V) and the thermodynamic driving force, as related to the supercooling (ΔT) or supersaturation (ΔC), the analytical form of which portrays a particular growth mechanism related to the nature of the interface.

The main emphasis of this dissertation is to study the atomistic processes occurring in the S/L interfacial region where the atoms or molecules from the liquid assume the ordered structure of the crystal, and to evaluate the effects of different factors, such as the structure and nature of the interface, the driving force, and the crystal orientation, physical defects, and impurities on the growth behavior and kinetics. Another aim of the work is to obtain accurate and reliable growth kinetics that would a) allow further insight to the growth mechanisms and their dependence on the above mentioned factors and b) provide accurate data against which the existing growth models can be tested. In this respect, the growth behavior at increased departures from equilibrium and any possible transitions in the kinetics is of prime interest.

A reliable kinetics determination, however, cannot be made without the precise determination of the interface temperature and rate. This

investigation plans to overcome the inherent difficulty of measuring the actual S/L interface by using a recently developed technique during a conjunct study about thermoelectric effects across the S/L interfaces.[1] As shown later, this technique will also provide the means of a sensitive and continuous way of in-situ monitoring of the local interfacial conditions. The growth rates will also be measured directly and correlated with the interfacial supercoolings for a wide range of supercoolings and growth conditions, well suited to describe the earlier mentioned effects on the growth processes.

High purity gallium, and gallium doped with known amounts of In were used in this study because, a) it is facet forming material and has a low melting temperature, b) it is theoretically important because it belongs to a special class of substances which are believed to offer the most fruitful area of S/L interfacial kinetics research, and c) of practical importance in the crystal growth community. Furthermore, detailed and reliable growth rate measurements at low rates are already available for Ga;[2] the latter study is among the very few conclusive kinetics studies for melt growth which provides a basis of comparison and a challenge to the present study for continuation of the much needed remaining work at high growth rates.

The remainder of this introduction will briefly describe the following chapters of this thesis. Chapter II is a critical overview of the theoretical and experimental aspects of crystal growth from the melt. This subject demands an unusually broad background since it is a truly interdisciplinary one in the sense that contributions come from many scientific fields. The various sections in the chapter were

arranged so that they follow a hierarchal scheme based on a conceptual view of approaching this subject. The chapter starts with a broad discussion of the S/L interfacial nature and its morphology and the models associated with it, together with their assumptions, predictions, and limitations. The concept of equilibrium and dynamic roughening of interfaces are presented next, which is followed by theories of growth mechanisms for both pure and doped materials. Finally, transport phenomena during crystal growth and the experimental approaches for determination of S/L interfacial growth kinetics are presented.

In Chapter III the experimental set-up and procedure are presented. The experimental technique for measuring the growth rate and interface supercooling is also discussed in detail.

In Chapter IV the experimental results are presented in three sections; the first two sections are for two interfaces of the pure material, while the third one covers the growth kinetics and behavior of the doped material. Also, in this chapter the growth data are analyzed and, whenever deemed necessary, a brief association with the theoretical models is made.

In Chapter V the experimental results are compared with existing theoretical growth models, emphasizing the quantitative approach rather than the qualitative observations. The discrepancies between the two are pointed out and reasons for this are suggested based on the concepts discussed earlier. The classical growth kinetics model for faceted interfaces is also modified, relying mainly upon a realistic description of the S/L interface. Finally, the effects of segregation and fluid flow on the growth kinetics of the doped material are interpreted.

Final comments and conclusions are found in Chapter VI. The Appendices contain detailed calculations and background information on the Ga crystal structure, Ga-In system, morphological stability, heat transfer, computer programming, and supercooling/supersaturation relations.

CHAPTER II
THEORETICAL AND EXPERIMENTAL BACKGROUND

The Solid/Liquid (S/L) Interface

Nature of the Interface

The nature and/or structure of interfaces between the crystalline and fluid phases have been the subject of many studies. When the fluid phase is a vapor, the solid-vapor (S/V) interface can easily be described by associating it with the crystal surface in vacuum,[3,4] which can be studied directly on the microscopic scale by several experimental techniques.[5] However, this is not the case for the S/L interface, which separates two adjacent condensed phases, making any direct experimental study of its properties very difficult, if not impossible. In contrast with the S/V interface, here the two phases present (S and L) have many properties which are rather similar and the separation between them may not be abrupt. Furthermore, liquid molecules are always present next to the solid and their interactions cannot be neglected, as can be done for vapors. The S/L interface represents a far more peculiar and complex case than the S/V and L/V interfaces; therefore, ideas developed for the latter interfaces do not properly portray the actual structure of the solid/liquid interface. In the following section, the conceptual description of the various types of S/L interfaces will be given, and each type of interface will be briefly related to a particular growth mechanism.

Two criteria have been used to classify S/L interfaces. The first one, which is mainly an energetic rather than a structural criterion,

6

considers the interface as a region with "intermediate" properties of the adjacent phases, rather than as a surface contour which separates the solid and the liquid side on the atomic level. According to this criterion, the interface is either <u>diffuse</u> or <u>sharp</u>.[6-10] A diffuse interface, to quote,[6] "is one in which the change from one phase to the other is gradual, occurring over several atom planes" (p. 555). In other words, moving from solid to liquid across the interface, one should expect a region of gradual transition from solid-like to liquid-like properties. On the other hand, a sharp interface[8-10] is the one for which the transition is abrupt and takes place within one inter-planar distance. A specific feature related to the interfacial diffuse-ness, concerning the growth mode of the interface, is that in order for the interface to advance uniformly normal to itself (continuously), a critical driving force has to be applied.[6] This force is large for a sharp interface, whereas it is practically zero for an "ideally diffuse" interface.

The second criterion[8-12] assumes a distinct separation between solid and liquid so that the location of the interface on an atomic scale can be clearly defined. In a manner analogous to that for the S/V interface, the properties of the interface are related to the nature of the crystalline substrate and/or macroscopic (thermodynamic) properties via "broken-bonds" models. Based on this criterion, the interface is either <u>smooth</u> (singular,[*13] faceted) or <u>rough</u> (non-singular,[*] non-faceted). A smooth interface is one that is flat on a molecular scale, represented by a cusp (pointed minimum) in the surface free energy as a

---

* Sometimes these interfaces are called F- and K-faces, respectively.[13]

function of orientation plot (Wulff's plot[14] or γ-plot[15]). In contrast,
a rough interface has several adatoms (or vacancies) on the surface
layers and corresponds to a more gradual minimum in the Wulff's plot.
Any deviation from the equilibrium shape of the interface will result in
a large increase in surface energy only for the smooth type. Thus, on
smooth interfaces, many atoms (e.g. a nucleus) have to be added simul-
taneously so that the total free energy is decreased, while on rough
interfaces single atoms can be added.

Another criterion with rather lesser significance than the previous
ones is whether or not the interface is perfect or imperfect with re-
spect to dislocations or twins.[11] In principle this criterion is con-
cerned with the presence or absence of permanent steps on the interface.
Stepped interfaces, as will become evident later, grow differently than
perfect ones.

Interfacial Features

There are several interfacial features (structural, geometric, or
strictly conceptual) to which reference will be made frequently through-
out this text. Essentially, these features result primarily from either
thermal excitations on the crystal surface or from particular interfa-
cial growth processes, as will be discussed later. These features which
have been experimentally observed, mainly during vapor deposition and on
S/L interfaces after decanting the liquid,[16] are shown schematically in
Fig. 1a for an atomically flat interface. (Note that the liquid is
omitted in this figure for a better qualitative understanding of the
structure.) These are a) atomically flat regions parallel to the top-
most complete crystalline layer called terraces or steps; b) the edges

Terraces, Steps

Edge (ledge)

a)

Kinks

Liquid

b)

Diffuse
interface

Solid
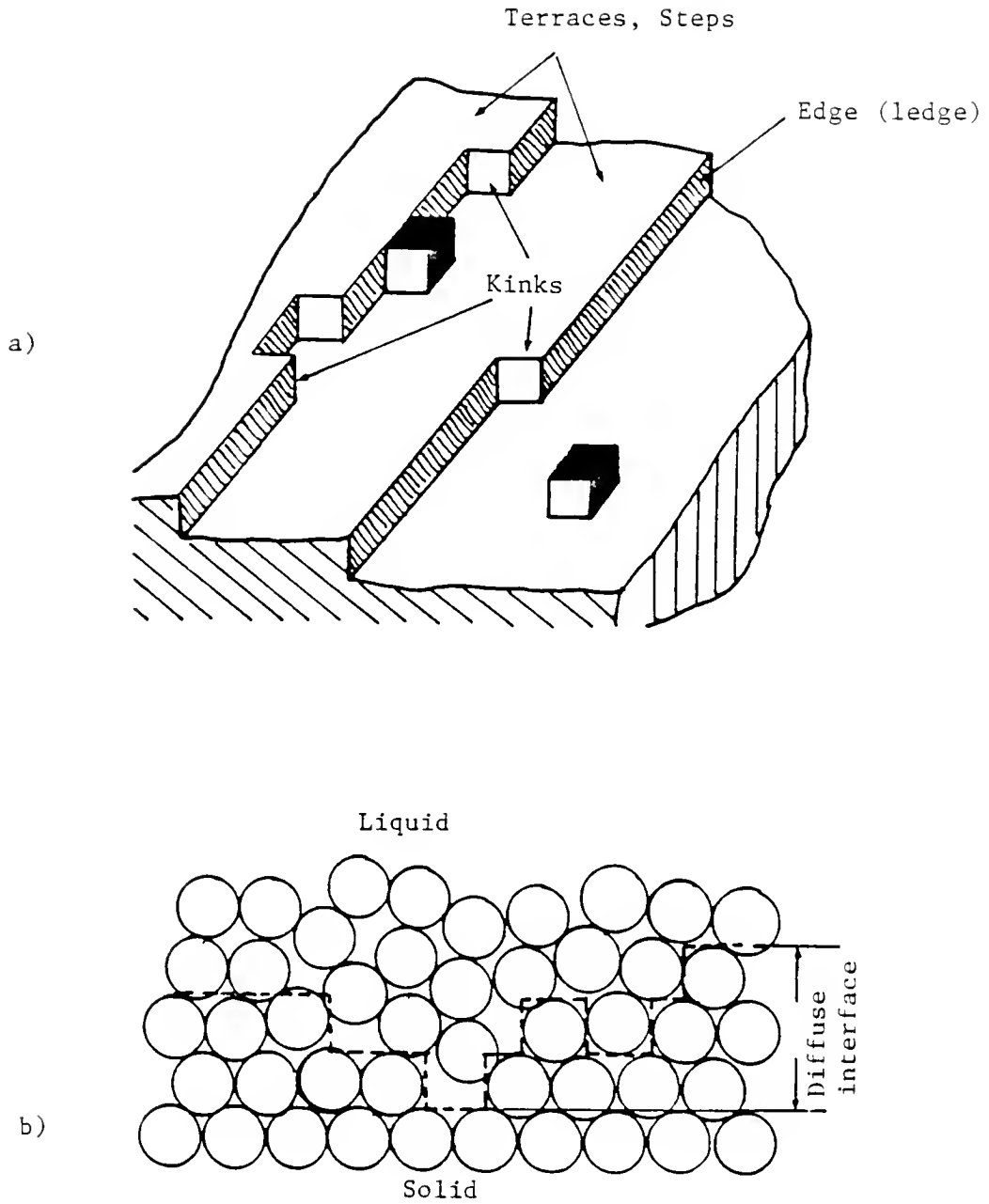
Figure 1   Interfacial Features.   a) Crystal surface of a sharp
interface; b) Schematic cross-sectional view of a
diffuse interface.   After Ref.(17)

(or ledges) of these terraces that are characterized by a step height h; c) the kinks, or jogs, which can be either positive or negative; and d) the surface adatoms or vacancies. From energetic considerations, as understood in terms of the number of nearest neighbors, adatoms "prefer" to attach themselves first at kink sites, second at edges, and lastly on the terraces, where it is bonded to only one side. With this line of reasoning, then, atoms coming from the bulk liquid are incorporated only at kinks, and as most crystal growth theories imply,[18] growth is strongly controlled by the kink-sites.

Although the above mentioned features are understood in the case of an interface between a solid and a vapor where one explicitly can draw a surface contour after deciding which phase a given atom is in, for S/L interfaces there is considerable ambiguity about the location of the interface on an atomic scale. However, the interfacial features (a-c) can still be observed in a diffuse interface, as shown schematically in Fig. 1b. Thus, regardless of the nature of the interface, one can refer, for example, to kinks and edges when discussing the atomistics of the growth processes.

Thermodynamics of S/L Interfaces

Solidification is a first order change, and, as such, there is discontinuity in the internal energy, enthalpy, and entropy associated with the change of state.[19] Furthermore, the transformation is spatially discontinuous, as it begins with nucleation and proceeds with a growth process that takes place in a small portion of the volume occupied by the system, namely, at the interface between the existing nucleus (crystal seed or substrate) and the liquid. The equilibrium thermodynamic

formulation to interfaces, first introduced by Gibbs[20] forms the basis of our understanding of interfaces. The intention here is not to review this long subject, but rather to introduce the concepts previously highlighted in a simple manner. If the temperature of the interface is exactly equal to the equilibrium temperature, T_m, the interface is at local equilibrium and neither solidification nor melting should take place. Deviations from the local equilibrium will cause the interface to migrate, provided that any increase in the free energy due to the creation of new interfacial area is overcome so that the total free energy of the system is decreased. On the other hand, the existence of the enthalpy change, $\Delta H = H_L - H_S$, means that removal of a finite amount of heat away from the interface is required for growth to take place.

At equilibrium ($T = T_m$) the Gibbs free energies of the solid and liquid phases are equal, i.e. $G_L = G_S$. However, at temperatures less than T_m, only the solid phase is thermodynamically stable since $G_S < G_L$. The driving force for crystal growth is therefore the free energy difference, ΔG_v, between the solid and the supercooled (or supersaturated) liquid. For small supercoolings, ΔG_v can be written as

$$\Delta G_v = \frac{L \Delta T}{V_m T_m} \qquad (1)$$

where L is the heat of fusion per mole and V_m is the solid molar volume. The S/L interfacial energy is likely the most important parameter describing the energetics of the interface, as it controls, among others, the nucleation, growth, and wetting of the solid by the liquid. According to the original work of Gibbs, who considered the interface as a physical dividing surface the S/L interfacial free energy is related to

the "work done to create unit area of interface." Analytically $\sigma_{s\ell}$ can be given by

$$\sigma_{s\ell} = U_{s\ell} - TS_{s\ell} + PV_i \approx U_{s\ell} - TS_{s\ell} \tag{2}$$

where $U_{s\ell}$ is the surface energy per unit area, $S_{s\ell}$ is the surface entropy per unit area, and the surface volume work, PV_i, is assumed to be negligible. A further understanding of the surface energy, as an excess quantity for the total energy of the two phase system (without the interface), can be achieved by considering Fig. 2. Here the balance in free energy across the interface is accomodated by the extra energy of the interface, $\sigma_{s\ell}$.

The step edge (ledge) free energy is concerned with the effect of a step on the crystal surface of an otherwise flat face. As discussed later, this quantity is a very important parameter related to the existence of a lateral growth mechanism versus a continuous one and the roughening transition. In order to understand the concept of edge free energy, consider the step (see Fig. 1) as a two-dimensional layer that perfectly wets the substrate. In this particular case, the extra interfacial area created (relative to that without the step) is the periphery; the energetic barrier for its formation accounts for the step edge energy. Based on this concept, the step edge free energy is comparable to the interfacial energy and, in some sense, the values of these two parameters are complementary. For example, it has been stated[21] that for a given substance and crystal structure, the lower the surface free energy of an interface, the higher the edge free energy of steps on it and vice-versa. However, such a suggestion is contradictory to the traditionally accepted analytical relation given as[6]
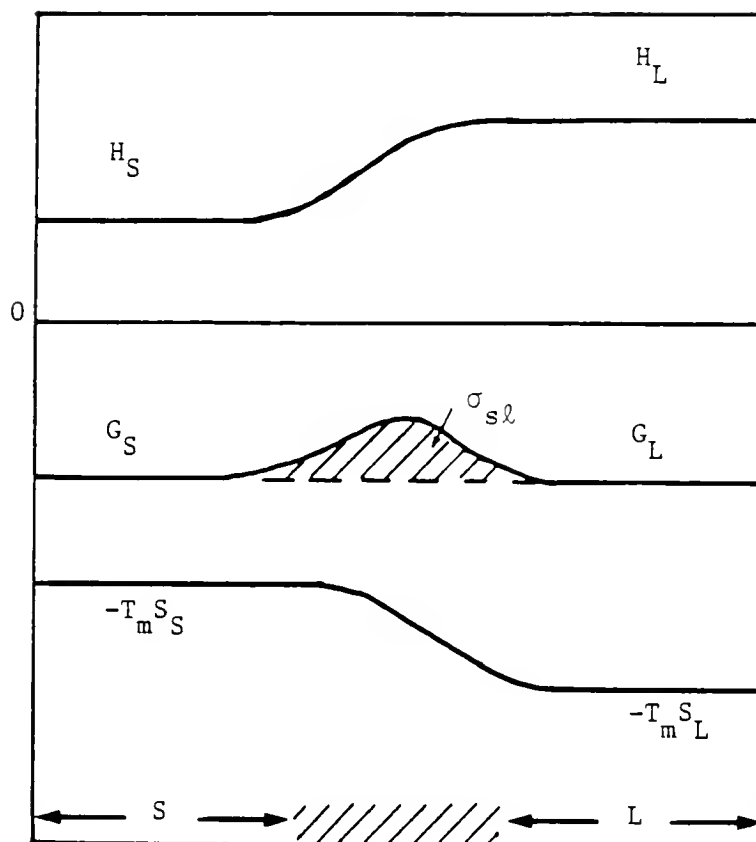
Figure 2 Variation of the free energy G at T_m across the solid-liquid interface, showing the origin of $\sigma_{s\ell}$. After Ref.(22).

$$\sigma_e = \sigma_{s\ell} \cdot h \qquad\qquad (3)$$

where σ_e is the edge energy per unit length of the step and h is the step height. However, this relation, as discussed later, has not been supported by experimental results.

Models of the S/L Interface

As may already be surmised, the most important "property" of the interface in relation to growth kinetics is whether the interface is rough or smooth, sharp or diffuse, etc. This, in turn, will largely determine the behavior of the interface in the presence of the driving force. Before discussing the S/L interface models, one should distinguish between two interfacial growth mechanisms, i.e. the lateral (step-wise) and the continuous (normal) growth mechanisms. According to the former mechanism, the interface advances layer by layer by the spreading of steps of one (or an integral number of) interplanar distance; thus, an interfacial site advances normal to itself by the step height only when it has been covered by the step. On the other hand, for the continuous growth mechanism, the interface is envisioned to advance normal to itself continuously at all atomic sites.

Whether there is a clear cut criterion which relates the nature of the interface with either of the growth mechanisms and how the driving force affects the growth behavior are discussed in the following sections.

Diffuse interface model

According to the diffuse interface growth theory,[6] lateral growth will take over "when any area in the interface can reach a metastable equilibrium configuration in the presence of the driving force, it will

remain there until the passage of the steps" (p. 555). Afterwards, obviously, the interface has the same free energy as before, since it has advanced by an integral number of interplanar spacings. On the other hand, if the interface cannot reach the metastable state in the presence of the driving force, it will move spontaneously. This model, which involves an analogy to the wall boundary between neighboring domains in ferromagnets,[23] assumes that the free energy of the interface is a periodic function of its mean position relative to the crystal planes, as shown in Fig. 3a. The maxima correspond to positions between lattice planes. The free energy, F (per unit area), of the interface is given as

$$F = a \sum_{-\infty}^{\infty} \{f(u_n) + Ka^{-2}(u_n - u_{n+1})^2\} \qquad (4)$$

where a is the interplanar distance and the subscripts n, n + 1, represent lattice planes and K is a constant; u is related to some degree of order, and $f(u_n)$ is the excess free energy of an intermediate phase characterized by u, formed from the two bulk phases (S and L). The second term represents the so-called gradient energy,[24] which favors a gradual change (i.e. the diffuseness) of the parameter u_n. Leaving aside the analytical details of the model, the solution obtained for the values of u's which minimize F are given as

$$u(z) = \tanh\left(\frac{2z}{na}\right) \qquad (5)$$

where z is a distance normal to the interface and the quantity
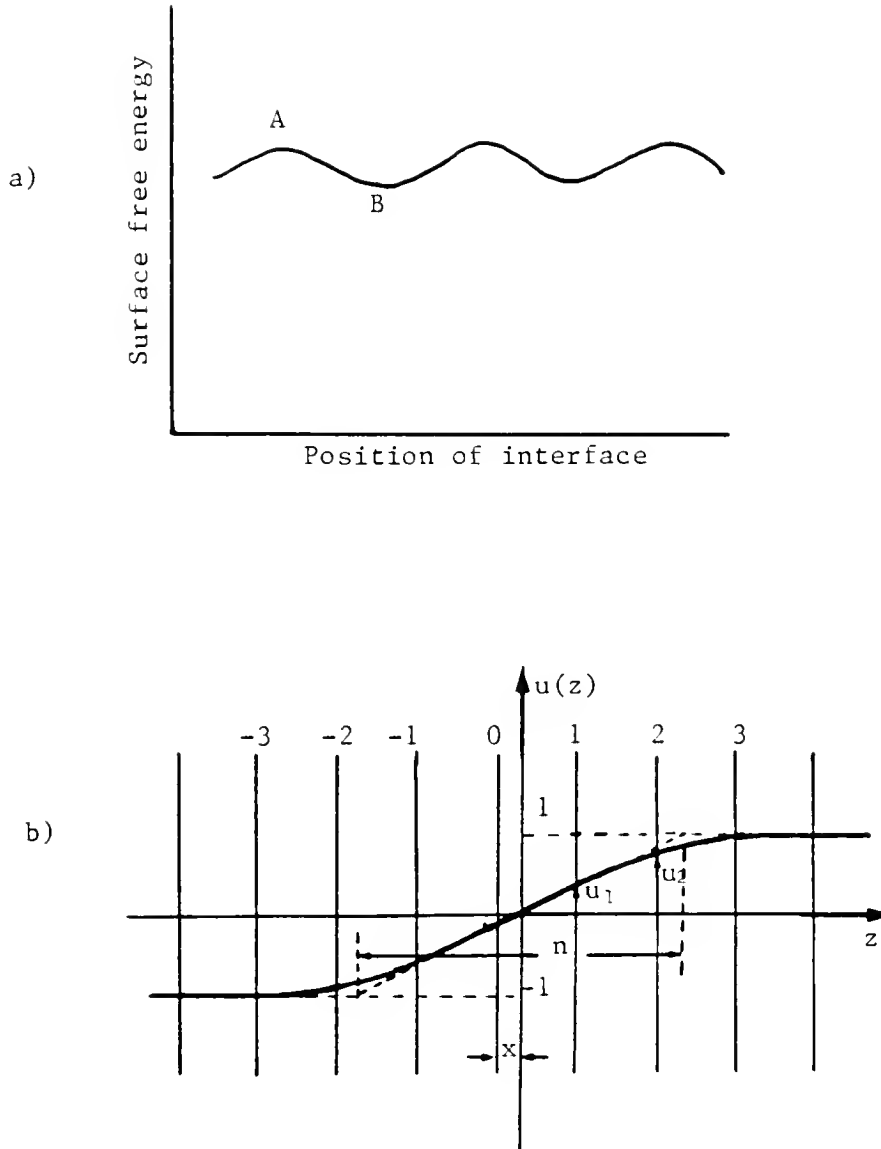
Figure 3   Diffuse interface model.   After Ref. (6).   a) The
surface free energy of an interface as a function
of its position.   A and B correspond to maxima and
minima configuration; b) The order parameter u as
a function of the relative coordinate x of the
center of the interfacial profile, i.e. the 0th
lattice place is at -x.

$$n = (2/a) \cdot (K/f_o)^{1/2} \tag{6}$$

signifies the thickness of the interface in terms of lattice planes. As expected, the larger diffuseness of the interface, the larger is the coefficient K characterizing the gradient energy and the smaller the quantity f_o which relates to the function $f(u_n)$. The interesting feature of this model is that the surface energy is not constant, but varies periodically as a function of the relative coordinate x of the center of the interface where the lattice planes are at $z = na - x$ (see Fig. 3b). Assuming the interface profile to be constant regardless of the value of x we have

$$\sigma(x) = \sigma_o + g(x)\sigma_o \tag{7}$$

where σ_o is the minimum value for σ, and $\sigma_o g(x)$ represents the "lattice resistance to motion" and $g(x)$ is the well known diffuseness parameter that for large values of n is given as

$$g(x) = 2^{-4}\pi^4 n^3 (1 - \cos \frac{2\pi x}{a}) \exp (- \frac{\pi^2 n}{2}) \tag{8}$$

Note that $g(x)$ decreases with the increasing diffuseness n. Its limits are 0 and 1, which represent the cases of an ideally diffuse and sharp interface, respectively.

In the presence of a driving force, ΔG_v, if the interface moves by δx, the change in free energy is given as

$$\delta F = (\Delta G_v + \sigma_o \frac{dg(x)}{dx}) \delta x \tag{9}$$

For the movement to occur, δF must be negative. The critical driving force is given by

$$-\Delta G_v^c = \sigma \left. \frac{dg(x)}{dx} \right|_{max} = \frac{\pi \sigma_o g_{max}}{a} \tag{10}$$

where

$$g_{max} = \frac{\pi^2 n^3}{8} \exp \left(- \frac{\pi^2 n}{2} \right) \tag{11}$$

Thus, if the driving force is greater than the right hand side of eq. (10), which represents the difference between the maxima and minima in Fig. 3a, the interface can advance continuously. The magnitude of the critical driving force depends on g(x), which is of the order of unity and zero for the extreme cases of sharp and ideally diffuse interfaces, respectively. In between these extremes, i.e. an interface with an intermediate degree of diffuseness, lateral growth should take place at small supercoolings (low driving force) and be continuous at large ΔT's.

Detailed critiques from opponents and proponents of this theory have been reported elsewhere.[25-27] A summary is given next by pointing out some of the strong points and the limitations of this theory: 1) The concept of the diffuse interface and the gradient energy term were first introduced for the L/V interface,[24] which exhibits a second order transition at the critical temperature, T_c, where the thickness of the interface becomes infinite.[28] Since a critical point along the S/L line in a P-T diagram has not been discovered yet, the quantities $f(u_n)$ and the gradient energy are hard to qualify for the solid-liquid interface. The diffuseness of the interface is determined by a balance between the energy associated with a gradient, e.g. in density, and the energy required to form material of intermediate properties. The concept of the diffuseness was extended to S/L interfaces[6] after observing[29] that the grain boundary energy (in the cases of Cu, Au, and Ag) is larger than two times the $\sigma_{s\ell}$ value. 2) The theory does not provide any analytical

form or rule for prediction of the diffuseness of the interface for a given material and crystal direction. However, the model predicts[6] that the resistance to motion is greatest for close-packed planes and, thus, their diffuseness will comparatively be quite small. 3) The theory, which has been reformulated for a fluid near its critical point[30] (and received experimental support[24,31]), provides a good description of spinodal decomposition[32,33] and glass formation.[34]

The present author believes that this theory's concept is very reasonable about the nature of the S/L interface. Indeed, recent studies, to be discussed next, indirectly support this theory. However, there are several difficulties in "following" the analysis with regard to the motion of the interface, which stem primarily from the fact that it a) does not explicitly consider the effect of the driving force on the diffuseness of the interface, and b) conceives the motion of the interface as an advancing averaged profile rather than as a cooperative process on an atomic scale, which is important for smooth interfaces.

In a later development[7] about the nature of the S/L interface, many aspects of the original diffuse interface theory were reintroduced via the concept of the many-level model.* Here the thickness of the interface, i.e. its diffuseness, is considered a free parameter that can adjust itself in order to minimize the free energy of the interface (F); the latter is evaluated by introducing the Bragg-Williams[35] approxima-

---

* As contrasted to other models where the transition from solid to liquid is assumed to take place within a fixed and usually small number of layers, e.g. two-level or two-dimensional models.

tion,[*] and depends on two parameters of the model, namely β and γ, given as

$$\beta = \frac{\Delta G_v}{KT} \text{ and } \gamma = \frac{4W}{KT}$$

here $W = E_{s\ell} - (E_{ss} + E_{\ell\ell})/2$ is the mixing energy, $E_{s\ell}$ is the bond energy between unlike molecules and E_{ss}, $E_{\ell\ell}$ are the bond energies between solid-like and liquid-like molecules, respectively; K is the Boltzman's constant.

Numerical calculations show that the interface under equilibrium is almost sharp for $\gamma > 3$ and increases its diffuseness with decreasing γ. It can also be shown that the roughness of the interface defined as[10,36]

$$S = \frac{U - U_o}{U_o} \tag{12}$$

where U_o is the surface energy of a flat surface and U that of the actual interface. The latter increases with decreasing γ, with a sharp rise at $\gamma \sim 2.5$. This is expected since U is related to the average number of the broken bonds (excess interfacial energy).[37]

When the interface is undercooled, $\Delta G_v < 0$, the theory shows a pronounced feature. The region of positive values of the parameters β and γ can be divided into two subregions, as shown in Fig. 4. In region A there are two solutions, each corresponding to a minimum and a maximum of F, respectively, while in region B there are no such solutions. In

---

[*] The Bragg-Williams or Molecular or Mean Field approximation[35] of statistical mechanics assumes that some average value E can be taken as the internal energy for all possible interfacial configurations and that this value is the most probable value. Then, the free energy of the interface becomes a solvable quantity. Qualitatively speaking, this approximation assumes a random distribution of atoms in each layer; therefore, clustering of atoms is not treated.
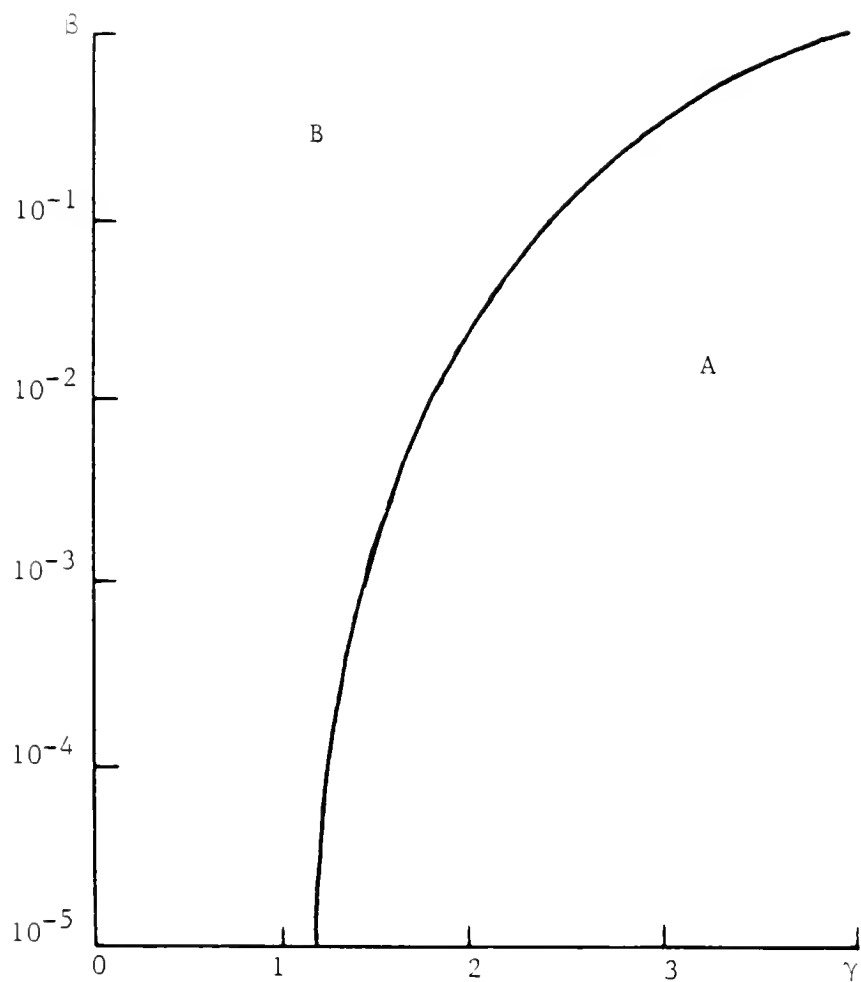
Figure 4 Graph showing the regions of continuous (B) and lateral
(A) growth mechanisms as a function of the parameters
β and γ, according to Temkin's model.[7]

this region, F varies monotonically so that the interface can move continuously. On the other hand, in region A the interface must advance by the lateral growth mechanism. Moreover, depending on the γ value, a material might undergo a transition in the growth kinetics at a measurable supercooling. For example, if $\gamma = 2$, the transition from region A to region B should take place at an undercooling of about .05 T_m (assuming that $L/KT_m \sim 1$, which is the case for the majority of metals). However, to make any predictions, W has to be evaluated; this is a difficult problem since an estimate of the $E_{s\ell}$ values requires a knowledge of the "interfacial region" a-priori. It is customarily assumed that $E_{s\ell} = E_{\ell\ell}$, which leads to a relation between W and the heat of fusion, L. But this approximation, the incorrectness of which is discussed elsewhere, leads, for example, to negative values of $\sigma_{s\ell}$ for pure metals.[38] Nevertheless, if this assumption is accepted for the moment, it will be shown that Temkin's model stands somehow between those of Cahn's and Jackson's (discussed next).

The "α" factor model: roughness of the interface

Before discussing the "α" factor theory,[8,9] the statistical mechanics point of view of the structure of the interface is briefly described. The interfacial structure is calculated by the use of a partition function for the co-operative phenomena in a two-dimensional lattice. Indeed, the change of energy accompanying attachment or detachment of a molecule to or from a lattice site on the crystal surface cannot be independent of whether the neighboring sites are occupied or not. A large number of models[39] have been developed under the assumptions i)

the statistical element is capable of two states only and ii) only interactions between nearest neighbors are important.

The "α" factor theory, introduced by Jackson,[8] is a simplified approach based on the above mentioned principles for the S/L interface. This model considers an atomically smooth interface on which a certain number of atoms are randomly added, and the associated change in free energy (ΔG) with this process is estimated. The problem is then to minimize ΔG. The major simplifications of the model are a) a two-level model interface: as such it classifies the molecules into "solid-like" and "liquid-like" ones, b) it considers only the nearest neighbors, and c) it is based on Bragg-Williams statistics.

The main concluding point of the model is that the roughness of the solid-liquid interface can be discriminated according to the value of the familiar "α" factor, defined as

$$\alpha = \frac{L}{KT_m} \xi \tag{13}$$

where ξ represents the ratio of the number of bonds parallel to the interface to that in the bulk; its value is always less than one and it is largest for the most close-packed planes, e.g. for the f.c.c. structure ξ (111) = .5, ξ (100) = 1/3, and ξ (110) = 1/6. It should be noted that the α factor is actually the same with γ in Temkin's theory. For values of $\alpha < 2$, the interface should be rough, while the case of $\alpha > 2$ may be taken to represent a smooth interface. Alternately, for materials with $L/KT_m < 2$, even the most closely packed interface planes should be rough, while for $L/KT_m > 4$ they should be smooth. According to this, most metallic interfaces should be rough in contrast with those of most organic materials which have large L/KT_m factors. In between

these two extremes (2 and 4) there are several materials of considerable importance in the crystal growth community, such as Ga, Bi, Ge, Si, Sb, and others such as H_2O. For borderline materials ($\alpha \approx 2$), the effect of the supercooling comes into consideration. For these cases, this model qualitatively suggests[26,40] that an interface which is smooth at equilibrium temperature may roughen at some undercooling.

Jackson's theory, because of its simplicity and its somewhat broad success, has been widely reviewed in many publications.[25,26,27,34] The concluding remarks about it are the following:

a) In principle, this model is based on the interfacial "roughness" point of view.[10,36] As such, it attempts to ascribe the interfacial atoms to the solid or the liquid phase, which, as mentioned elsewhere, is likely to be an unrealistic picture of the S/L interface. Thus, the model excludes a probable "interface phase" that forms between the bulk phases so that its quantitative predictions are solely based on bulk properties (e.g. L).

b) The model is essentially an equilibrium one since the effect of the undercooling on the nature of the interface was hardly treated. Hence, it is concluded that a smooth interface will grow laterally, regardless of the degree of the supercooling. A possible transition in the nature of the interface with increasing ΔT is speculated only for materials with $\alpha \sim 2$. Indeed, it is for these materials that the model actually fails, as will be discussed later.

c) The anisotropic behavior of the interfacial properties is lumped in the geometrical factor ξ, which could be expected to make sense only

for flat planes or simple structures, but not for some complex structures.[41]

d) In spite of the limitations of this model, the success of its predictions is generally good, particularly for the extreme cases of very smooth and very rough interfaces.[26,27,34]

Other models

The goal of most other theoretical models of the S/L interface is the determination of the structural characteristics of the interface that can then be used for the calculation of thermodynamic properties which are of experimental interest; the majority of these models follow the same approaches that have been applied for modeling bulk liquids.[4] Therefore, these are concerned with spherical (monoatomic) molecules that interact with the (most frequently used) Lennard-Jones, 12-6, potential.[42] The L-J potential, which excludes higher than pair contribution to the internal energy, is a good representation of rare gasses and its simple form makes it ideal for computer calculations. The model approach can be classified into three groups:[4]

a) hard-sphere,

b) computer simulations (CS); molecular dynamics (MD), or Monte Carlo (MC), and

c) perturbation theories.

In the Bernal model (hard-sphere),[43] the liquid as a dense random packing of hard spheres is set in contact with a crystal face, usually with hexagonal symmetry (i.e. FCC (111), HCP (0001)). Computer algorithms of the Bernal model have been developed[4] based on tetrahedral packing where each new sphere is placed in the "pocket" of previously

deposited spheres on the crystalline substrate. Under this concept, the model[44],[45] shows how the disorder gradually progresses with distance from the interface into the liquid. The beginning of disorder, on the first deposited layer, is accounted by the existence of "channels"[44] (p. 6) between atom clusters, whose width does not allow for an atom to be placed in direct contact with the substrate. As the next layer is deposited, new sites are eventually created that do not continue to follow the crystal lattice periodicity, which, when occupied, lead to disorder. However, the very existence of the formed "channels" is explained by the peculiarity of the hcp or fcc close-packed crystal face that has two interpenetrating sublattices of equal occupation probabilities.[4] The density profiles calculated at the interface also show a minimum associated with the existence of poor wetting; on the other hand, perfect wetting conditions were found when the atoms were placed in such a way that no octahedral holes were formed.[46] Thermodynamic calculations from these models allow for an estimate of the interfacial surface energy ($\sigma_{s\ell}$), which are in qualitative agreement with experimental findings. In conclusion, these models give a picture of the structure of the interface which seems reasonable and can calculate $\sigma_{s\ell}$. However, they neglect the thermal motion of atoms and assume an undisturbed crystal lattice up to the S/L interface, eliminating, therefore, any kind of interfacial roughness.

Computer simulation of MC and MD techniques are linked to microscopic properties and describe the motion of the molecules. In contrast with the MD technique, which is a deterministic process, the MC technique is probabilistic. Another difference is that time scale is only

involved in the MD method, which therefore appears to be better suited to study kinetic parameters (e.g. diffusion coefficients). From the simulations the state parameters such as T, P, kinetic energy, as well as structural (interfacial) parameters, can be obtained. Furthermore, free energy (entropy) differences can be calculated provided that a reference state for the system is predetermined. The limitations of the CS techniques are[4] a) a limited size sample (~1000 molecules), as compared to any real system, because of computer time considerations; the small size (and shape) of the system might eliminate phenomena which might have occurred otherwise. b) The high precision and long time required for the equilibriation of the system (for example, the S/L interface is at equilibrium only at T_m, so that precise conditions have to be set-up). c) The interfacial free energy cannot be calculated by these techniques.

MD simulations of a L-J substance have concluded[47] for the fcc (100) interface that it is rather diffuse since the density profile normal to the interface oscillates in the liquid side (i.e. structured liquid) over five atomic diameters. Similar conclusions were drawn from another MD[48] study where it was shown that, in addition to the density profile, the potential energy profile oscillates and that physical properties such as diffusivity gradually change across the interface from those of the solid to those of the liquid. Note that none of these studies found a density deficit (observed in the hard sphere models) at the interface. However, in an MC simulation[49] of the (111) fcc interface with a starting configuration as in the Bernal model, a small deficit density was observed in addition to the "channeled-like" structure

of the first 2-3 interfacial layers. A more precise comparison of the (100) and (111) interfaces concluded[50] that the two interfaces behave similarly. Interestingly enough, this study also indicates that the L → S transition, from a structural point of view, as examined from molecular trajectory maps parallel to the interface, is rather sharp and occurs within two atomic planes, despite the fact that density oscillations were observed over 4-5 planes. However, these trajectory maps, in terms of characterizing the atoms as liquid- or solid-like, are very subjective and critically depend on the time scale of the experiment;[51] an atom that appears solid on a short time could diffuse as liquid on a longer time scale.

The perturbation method of the S/L interface[52] has not yet been widely used to determine the interfacial free energy or the structure of the liquid next to the solid, but only to determine the density profiles at the interface. The latter results are shown to be in good agreement with those found from the MD simulations, but do not provide any additional information. In a study of the (100) and (111) bcc interfaces,[51,53] calculations suggest that the interfacial liquid is "structured," i.e. with a density close to that of the bulk liquid and a solid-like ordering. The interfacial thickness was estimated quite large (10-15 layers) and the observed density profile oscillations were less sharp than those observed[47-50] for the fcc interfaces. This was rationalized by the lower order and plane density (area/atom) for the bcc interfaces. Despite the differences in the density profiles among the (100) and (111) interfaces, the interfacial potential energies and S/L surface energies were found to be nearly equal (within 5%).[51]

The interfacial phenomena were also studied by a surface MD method,[54],[55] meant to investigate the epitaxial growth from a melt. It was observed that the liquid adjacent to the interface up to 4-5 layers had a "stratified structure" in the direction normal to the interface which "lacked intralayer crystalline order"; intralayer ordering started after the establishment of the three-dimensionally layered interface regions. In contrast with the previously mentioned MD studies, non-equilibrium conditions were also examined by starting with a supercooled melt. For the latter case, the above mentioned phenomena were more pronounced and occurred much faster than the equilibrium situation. These results are supported by calculations[56] of the equilibrium S/L interface (fcc (001) and (100)) in a lattice-gas model using the cluster variation method. In addition, it was shown that for the nonclose-packed face (110), the S → L transition was smoother and the "intermediate" layer observed for the (001) face was not found for the (110) face. However, despite these structural differences, the calculated interfacial energies for these two orientations differed only by a few percent.[57]

Most of the methods presented here give some information on the structure and properties of the S/L interface, particularly of the liquid adjacent to the crystal. In spite of the fact that these models provide a rather phenomenological description of the interface, their information seems to be useful, considering all the other available techniques for studying S/L interfaces. In this respect, they rather suggest that the interfacial region is likely to be diffuse, particularly if one does not think of the solid next to the liquid as a rigid wall.[48] Such a picture of the interface is also suggested from recent

experimental works that will be reviewed next. These simulations re-sults then raise questions about the validity of current theories on crystal growth[58,59] and nucleation[60] which, based on theories discussed earlier, such as the "α" factor theory, assume a clear cut separation between solid and liquid; this hypothesis, however, is significantly different from the cases given earlier.

Experimental evidence regarding the nature of the S/L interface

Apparently, the large number of models, theories, and simulations involved in predicting the nature of the S/L interface rather illus-trates the lack of an easy means of verifying their conclusions. In-deed, if there was a direct way of observing the interfacial region and studying its properties and structures, then the number of models would most likely reduce drastically. However, in contrast to free surfaces, such as the L/V interface, for which techniques (e.g. low-energy dif-fraction, Auger spectroscopy, and probes like x-rays[61]) allow direct analysis to be made, no such techniques are available at this time for metallic S/L interfaces. Furthermore, structural information about the interface is even more difficult to obtain, despite the progress in techniques used for other interfaces.[62] Therefore, it is not surprising that most existing models claim success by interpreting experimental re-sults such that they coincide with their predictions. Some selected examples, however, will be given for such purposes that one could relate experimental observations with the models; emphasis is given on rather recent published works that provide new information about the interfa-cial region. A detailed discussion about the S/L interfacial energies will also be given. Indirect evidence about the nature of the

interface, as obtained from growth kinetics studies, will not be covered here; such detailed information can be found, for example, in several review papers[25,26,63] and books.[64,65]

Interfacial energy measurements for the S/L interface are much more difficult than for the L/V and S/V interfaces.[62]   For this reason, the experiments often   rely upon indirect measurement of this property; indeed, direct measurements of $\sigma_{s\ell}$ are available only for a very few cases such as Bi,[66] water,[67] succinonitrile,[68] Cd,*[69] NaCl and KCl,*[70] and several metallic alloys.[62]   However, even in these systems, excepting Cd, NaCl, and KCl, information regarding the anisotropy of $\sigma_{s\ell}$ is lacking.[71-76] Nevertheless, most evaluations of the S/L interfacial energies come from indirect methods.   In this case, the determinations of $\sigma_{s\ell}$ deal basically with the conditions of nucleation or the melting of a solid particle within the liquid.   For the former, that is the most widely used technique, $\sigma_{s\ell}$ is obtained from measured supercooling limits, together with a crystal-melt homogeneous nucleation theory in which $\sigma_{s\ell}$ appears as a parameter[60,77] in the expression

$$J = K_v \exp \left(- \frac{M \, \sigma_{s\ell}^3}{\Delta T^2} \right) \qquad (14)$$

Here J is the nucleation frequency, K_v is a factor rather insensitive to small temperature changes, and M is a material constant.   On the

---

* Strictly speaking, only these measurements are direct; the rest, still considered direct in the sense that the S/L interface was at least observed, deal with measurements of grain boundary grooves or intersection angles (or dihedral angles) between the liquid, crystal, and grain boundary.[71-74] The level of confidence of these measurements[75] and whether or not the shape of the boundaries were of equilibrium or growth form[76] remain questionable.

other hand, the latter method, i.e. depression of melting point of small particles (spherical with radius r) by ΔT, is based on the well known Gibbs-Thomson equation[78]

$$\Delta T = \frac{2\sigma_{s\ell}\, T_m}{Lr} \qquad (15)$$

Homogeneous nucleation experiments were performed by subdividing liquid droplets and keeping them apart by thin oxide films, or by suspending the particles in a suitable fluid in a dilatometer and measuring the nucleation rates (J) and associated supercoolings (ΔT).[77,79] The determined values were correlated with the latent heat of fusion with the well known known relation[77,80]*

$$\sigma_{s\ell} \propto .45\ L\ (\text{units of } \frac{\text{cal}}{\text{g-atom}}).$$

However, more recent experiments have shown that much larger supercoolings than those observed earlier are possible,[81] and the ratio $\Delta T/T_m$ considerably exceeds the value of $.2\ T_m$,[77,79] which is often taken as the limiting undercooling at which homogeneous nucleation occurs in pure metals. As a consequence, many of the experimentally determined values are in error by as much as a factor of 2. The main criticism of the $\sigma_{s\ell}$ values determined from nucleation experiments includes the following: a) the influence of experimental conditions (e.g. droplet size, droplet coating, cooling rates, and initial melt superheat) on the amount of maximum recorded undercooling,[81b] b) whether a crystal nucleus (of atomic dimensions, a few hundred atoms)/melt interface can be adequately described with $\sigma_{s\ell}$ of an infinite interface, which is a macroscopic

---

* A slope of .45 has also been proposed[80] for the empirical relation of the ratio $\sigma_{s\ell}/\sigma_{gb}$ (σ_{gb} is the grain boundary surface tension).

quantity,[76] c) whether the observed nucleation is truly homogenous or rather if it is taking place on the surface of the droplets,[82] d) the assumption that the nucleus has a spherical shape or that $\sigma_{s\ell}$ is isotropic,[83]* and e) the fact that the values obtained represent some average interfacial energy over all orientations. In spite of these limitations, the $\sigma_{s\ell}$ values deduced from nucleation experiments still constitute the major source of S/L interfacial energies; if used with skepticism, they provide a reference for comparison with other inter-facial parameters. Moreover, it should be mentioned that these values have been confirmed in some cases using other techniques or theoretical approaches which have not been reviewed here. However, the theoretical approaches[84-87] have also been criticized because they assume complete wetting, atomically smooth interfaces, and that the liquid next the interface retains its bulk character.

Experimental attempts to find a critical point between the solid and the liquid by going to extreme temperatures and pressures (high or low) have always resulted in non-zero entropy or volume changes at the limit of the experiment, suggesting that a critical point does not exist. Similar conclusions are drawn from MD studies,[88] despite the wide range of T and P accessible to computer simulations. Theoretical studies,[89] which disregard lattice defects, also predict that no crit-ical point exists for the S/L transition because the crystalline sym-metry cannot change continuously. In contrast to these results, a critical point was found in the vicinity of the liquidus line of a K-Cs

---

* Note that the temperature coefficient of $\sigma_{s\ell}$ has also been neglected in most studies.

alloy;[90] also, a CS of a model for crystal growth from the vapor found that the phase transition proceeds from the fluid phase to a disordered solid and afterwards to the ordered solid.[91]

Strong molecular ordering of a thin liquid layer next to a growing S/L interface has been suggested[92] as an explanation of some phenomena observed during dynamic light scattering experiments at growing S/L interfaces of salol and a nematic liquid crystal.[93] In an attempt to rationalize this behavior, it was proposed that only interfaces with high "α" factors can exert an orienting force on the molecules in the interfacial liquid; however, such an idea is not supportive of the observation regarding the water/ice (0001) interface ($\alpha \approx 1.9$).[94-96] The ice experiments[94,95] have shown that a "structure" builds up in the liquid adjacent to the interface (1.4-6 μm thick), when a critical growth velocity ($\sim$1.5 μm/s) is exceeded, that has different properties from that of the water (for example, its density was estimated to be only .985 g/cc, as compared to 1 g/cc of the water) and ice, but closer to that of water. Interpreting these results from such models as that of the sharp and rough interface, of nucleation (critical size nuclei) ahead of the interface and of critical-point behavior, as in second-order transition* were ruled out. Similar experiments performed on salol revealed[97] that the S/L interface resembles that of the ice/water system, only upon growth along the [010] direction and not along the [100] direction. The "structured" (or density fluctuating) liquid layer

_____

* It should be noted they[95] determined the critical exponent of the relation between line width and intensity of the scattered light in close agreement with that predicted[29,30] for the diffuse liquid-vapor interface at the critical point.

was estimated to be in the order of 1 μm. An explanation of why such a layer was not formed for the (100) interface was not given. Still, these results agree in most points with the ones mentioned earlier[92] and are indirectly supported by the MD simulations[54],[56] discussed earlier. However, despite the excellence of these light scattering experiments for the information they provide, there is still some concern regarding the validity of the conclusions which strongly depend on the optics framework.[98]

Aside from the computer simulations and the dynamic light-scattering experiments, experimental evidence of a diffuse interface is usually claimed by observing a "break" in the growth kinetics $V(\Delta T)$ curve; this is associated with the transition from lateral to continuous growth kinetics. As such, these will be discussed in the section regarding kinetic roughening and growth kinetics at high supercoolings.

Confirmation of the "α" factor model has been provided via observations of the growth front (faceted vs. non-faceted morphology) for several materials.[26] Although experimental observations are in accord with the model for large and small "α" materials, there are several materials which facet irrespective of their "α" values. These are Ga,[2],[63],[99] Ge[100],[101] Bi,[63] Si,[102] and H_2O,[103] which have L/KT_m values between 2 and 4 and P_4[104] and Cd[69] whose L/KT_m values are about 1. Other common features of these materials are a) complex crystal structures, oriented molecular structure; b) semi-metallic properties; c) some of their interfaces have been found to be non-wetted by their melts; and d) their S/L interfacial energies do not follow the empirical rule of $\sigma_{s\ell} \sim .45$ L. Hence, these materials belong to a special group and it would be

difficult to imagine that simple statistical models could be adequate to describe their interfaces. However, these materials are of great theoretical importance in the field of crystal growth, as well as of technical importance referring to the electronic materials industry.

Next, the effect of temperature and supercooling on the nature of the interface is discussed.

Interfacial Roughening

For many years, one of the most perplexing problems in the theory of crystal growth has been the question of whether the interface undergoes some kind of smooth to rough transition connected with thermodynamic singularities at a temperature below the melting point of the crystal. This transition is usually called the "roughening transition" and its existence should significantly influence both the kinetics during growth and the properties of the interface. The transition could also take place under non-equilibrium or growing conditions, called the "kinetic roughening transition," which differs from the above mentioned equilibrium roughening transition. These subjects, together with the topic of the equilibrium shape of crystals, are discussed next.

Equilibrium (Thermal) Roughening

The concept of the roughening transition, in terms of an order-disorder transition of a smooth surface as the temperature increases was first considered back in 1949-1951.[10,36] The problem then was to calculate how rough a (S/V) interface of an initially flat crystal face (close-packed, low-index plane) might become as T increases. This was possible after realizing that the Ising model for a ferromagnet could be

adapted to the treatment of phase transformations (order-disorder, second-order phase transformation) by recognizing that the equilibrium structure of the interface is mathematically equivalent to the structure of a domain boundary in the Ising model for magnetism.

Statistical mechanics,[39] as mentioned previously, have long been associated with co-operative phenomena such as phase transition; moreover, in recent years, the important problem of singularities related with them has been a central topic of statistical mechanics. Its application to a system can be reduced to the problem of calculating the partition function of the system. One of the most popular tractable models for applications to phase changes is the Ising or two-dimensional lattice gas model.* The Ising model is a square two-dimensional array of magnetic atomic dipoles. The dipoles can only point up or down (i.e. an occupied and a vacant site, respectively); the nearest neighbor interaction energy is zero when parallel and $\varphi/2$ when antiparallel. Thus, this model restricts atoms to lattice sites and assumes only nearest neighbor interactions with the potential energy being the sum of all such pair interactions. This simple model has been rigorously solved[106] to obtain the partition function and the transition temperature T_c (Curie temperature) for the ferromagnetic phase transition (paramagnetic → ferromagnetic). Hoping that this discussion provides a link between the roughening transition and statistical mechanics, the earlier discussion about roughening continues.

---

* Strictly speaking, the two models are different, but because of their exact correspondence,[105] they are considered similar.

Burton et al.[10] considered a simple cubic crystal (100) surface with $\varphi/2$ nearest neighbor interaction energy per atom. Proving that this two level problem corresponds exactly to the Ising model, a phase transition is expected at T_c. This transition then is related to the roughening of the interface ("surface melting") and the temperature at which it takes place is related to the interaction energy as

$$\exp\left(-\frac{\varphi}{2KT_R}\right) = \sqrt{2} - 1, \text{ or } \frac{KT_R}{\varphi} = .57$$

where T_R is the roughening temperature. For a triangular lattice, e.g. (111) f.c.c. face KT_R/φ is approximately .91. The authors also considered the transition for higher (than two) level models of the interface using Bethe's approximation.* It was shown that, with increasing the number of levels, the calculated T_R decreases substantially, but remains practically the same for a larger number of levels. Although this study did not rigorously prove the existence of the roughening transition,[107] it gave a qualitative understanding of the phenomenon and introduced its influence on the growth kinetics and interfacial structure. The latter, because of its importance, motivated in turn a large number of theoretical works[108] during the last two decades. This upsurge in interest about interfacial roughening brought new insight in the nature of the transition and proved[59,109,110] its existence from a theoretical point of view. In principle, these studies use mathematical transformations to relate approximate models of the interface to other systems, such as

---

* Exact treatments of phase transitions can be discussed only for special systems and two dimensions, as discussed previously. For more than two dimensions, approximate theories have to be considered. Among them are the mean field, Bethe, and low-high temperature expansions methods.

two-dimensional Coulomb gas, ferroelectrics, and the superfluid state, which are known to have a confirmed transition. As mentioned previously, it is out of the scope of this review to elucidate these studies, detailed discussion about which can be found in several reviews.[107,111,112]

At the present time, the debate about the roughening transition seems to be its universality class or whether or not the critical behavior at the transition depends on the chosen microscopic model. Based on experiments, the physical quantities associated with the phase transition vary in manner $|T-T_c|^{\mu}$ when the critical temperature T_c is approached. The quantities such as μ in the above relation that characterize the phase transition are called <u>critical exponents</u>. They are inherent to the physical quantities considered and are supposed to take universal values (<u>universality class</u>) irrespective of the materials under consideration. For example, in ferromagnetism, one finds as $T \rightarrow T_c$ (Curie temperature):

$$\text{susceptibility, } x \propto (T - T_c)^{-\gamma}$$
$$\text{specific heat, } C(T) \propto (T - T_c)^{-a} \qquad (T > T_c)$$

Another important quantity in the critical region is the <u>correlation length</u>, which is the average size of the ordered region at temperatures close to T_c. In magnetism, the ordered region (i.e. parallel spin region) becomes large at T_c, while in particle systems the size of the clusters of the particles become large at T_c. The correlation length also obeys the relation[105]

$$\xi \propto \begin{cases} |T - T_c|^{-\nu} & (T > T_c) \\ |T_c - T|^{-\nu} & (T < T_c) \end{cases} \qquad (16)$$

or, according to a different model, ξ diverges in the vicinity of T_R as[113]

$$\xi \propto \exp \left(C/\left(\frac{T_R - T}{T_R}\right)^{1/2}\right) \qquad (T < T_R)$$

$$\xi \propto \infty \qquad (T > T_R) \qquad (17)$$

where C is a constant (about $1.5^{[113]}$ or $2.1^{[114]}$). The above mentioned illustrates that the universality class can be different depending on the model in use. To be more specific, the difference in behavior can be realized by comparing the relations (16) vs. (17); the former, which belongs to the two-dimensional Ising model, indicates that ξ diverges by a power law, while the latter of the Kosterlitz-Thouless[113] theory shows that ξ diverges exponentially.

One, however, may wonder what the importance of the correlation length is and how it relates, so to speak, to "simpler" concepts of the interface. In this view, ξ relates to the interfacial width;[59] hence, for temperatures less than the roughening transition, the interfacial width is finite in contrast with the other extreme, i.e. for T's > T_R; ξ also corresponds to the thickness of a step so that the step free energy can then be calculated from ξ. Indeed, it has been shown that σ_e is related to the inverse of ξ.[110,115] Thus, these results predict that the step edge free energy approaching T_R diverges as

$$\sigma_e \propto \exp \left(-C/\left(\frac{T_R - T}{T_R}\right)^{1/2}\right) \qquad (18)$$

and is zero at temperatures higher than T_R.[116] Hence, the energetic barrier to form a step on the interface does not exist for T's higher than T_R.

In summary, the key points of the roughening transition of an interface between a crystal and its fluid phase (liquid or vapor) are the following: a) At $T = T_R$ a transition from a smooth to a rough interface takes place for low Miller index orientations. At $T < T_R$ the interface is smooth and, therefore, is microscopically flat. The edge free energy of a step on this interface is of a finite value. Growth of such an interface is energetically possible only by the stepwise mode. On the other hand, for $T > T_R$, the interface is rough, so it extends arbitrarily from any reference plane. The step edge energy is zero, so that a large number of steps (i.e. arbitrarily large clusters) is already present on a rough interface. It can thus grow by the continuous mechanism. Pictorial evidence about the roughening transition effects can be considered from the results of an MC simulation[117] of the SOS model* (S/V interface), shown in Fig. 5. Also, a transition with increasing T from lateral kinetics to continuous kinetics above T_R was found for the interfaces both on a SC[118] and on an fcc crystal[117] for the SOS model. b) It is claimed that most theoretical points of the transition have been clarified. Based on recent studies, the temperature of the roughening transition is predicted to be higher than that of the BCF model. Furthermore, its universality class is shown to be that of the Kosterlitz-Thouless transition. Accordingly, the step edge free

---

* If, for the ordinary lattice gas model in a SC crystal, it is required that every occupied site be directly above another occupied site, one ends up with the solid-on-solid (SOS) model. This model can also be described as an array of interacting solid columns of varying heights, $h_r = 0, \pm 1, \ldots, \pm\infty$; the integer h_r represents the number of atoms in each column perpendicular to the interface, which is the height of the column. Neighboring sites interact via a potential $V = K|h_r - h_r'|$. If the interaction between nearest neighbor columns is quadratic, one obtains the "discrete Gaussian" model.
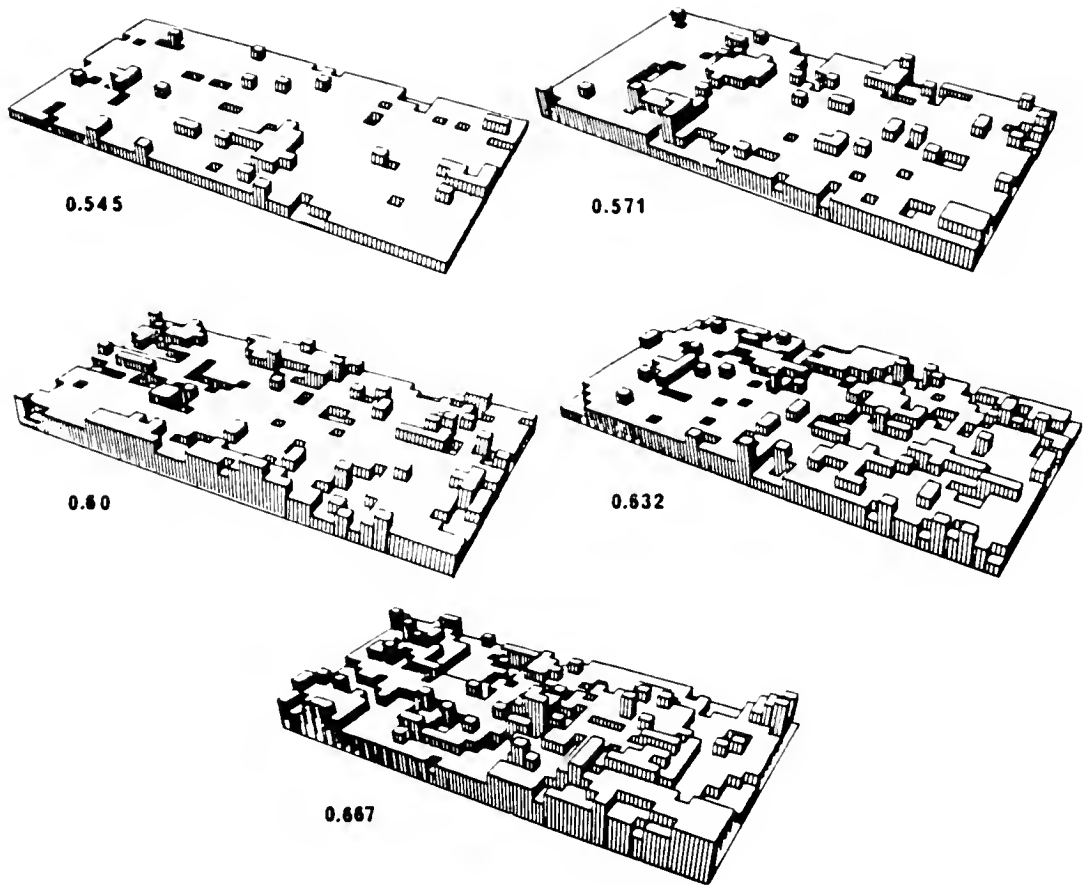
Figure 5   Computer drawings of crystal surfaces (S/V interface,
Kossel crystal, SOS model) by the MC method at the
indicated values of KT/ϕ.   After Ref. (112).

energy goes to zero as $T \rightarrow T_R$, vanishing in an exponential manner. These points have been supported and/or confirmed by several MC simulations results,[119] in particular, for the SOS model.

As may already be surmised, the roughening transition is also expected to take place for a S/L interface. Indeed, its concept has been applied, for example, in the "α" factor model;[8,9] the "α" factor is inversely related to the roughening transition temperature T_R, assuming that the nearest neighbor interactions (φ) are related to the heat of fusion. Such an assumption is true for the S/V interface where only solid-solid interactions are considered ($E_{ss} = φ$, $E_{sv} = E_{vv} \approx 0$). Then, for the Kossel crystal,[120]* $L_v \approx 3φ$ where L_v is the heat of evaporation. Unfortunately, however, for the S/L interface all kinds of bonds (E_{ss}, $E_{s\ell}$, $E_{\ell\ell}$) are significant enough to be neglected so that one could not assume a model that accounts only vertical or lateral (with respect to the interface plane) bonds. Assumptions such as $E_{\ell\ell} = E_{s\ell}$ cannot be justified, either. Several ways have been proposed[121] to calculate $E_{s\ell}$. Their accuracy, however, is limited since both $E_{s\ell}$ and $E_{\ell\ell}$, to a lesser extent, depend on the actual properties of the interfacial region which, in reality, also varies locally. Nevertheless, such information is likely to be available only from molecular dynamics simulations at the present.[4]

Quantitative experimental studies of the roughening transition are rare, and only a few crystals are known to exhibit roughening. Because of the reversible character of the transition, it is necessary to study

---

* As Kossel crystal[120] is considered a stacking of molecules in a primitive cubic lattice, for which only nearest neighbor interactions are taken into account.

a crystal face under growth and equilibrium conditions above and below T_R. That means the "α" factor, which is said to be inversely proportional to T_R, has to change continuously (with respect to the equilibrium temperature) or that L/KT_m has to be varied. For a S/V interface, depending on the vapor pressure, the equilibrium temperature can be above or below T_R, so that "α" can vary. The only exception in this case is the ^{4}He S/L (superfluid) interface, at T < 1.76 K. For this system, by changing the pressure, the "α" factor can be varied over a wide range, in a small experimental range (i.e. .2 K < T < 1.7 K), where equilibrium shapes, as well as growth dynamics, can be quantitatively analyzed.[96] For a metallic solid in contact with its pure melt though, this seems to be impossible because only very high pressure will influence the melting temperature. Thus, at T_m a given crystal face is either above or below its T_R;[122] crystals facet at growth conditions provided that $T_i < T_R$, where T_i is the interface temperature. Thus, the roughening transition of a S/L interface of a metallic system cannot be expected, or experimentally verified.

In spite of the fact that most of the restrictions for the S/L interface do not exist for the S/V one, most models predict T_R's (for metals) higher than T_m, thus defying experimentation on such interfaces.

The majority of the reported experiments are for non-metallic materials such as ice,[123] naphthalene,[124] C_2Cl_6 and NH_4Cl,[125] diphenyl,[126] adamantine,[127] and silver sulphide;[128] in these cases the transition was only detected through a qualitative change in the morphology of the crystal face (i.e. observing the "rounding" of a facet). The likely conclusions from these experiments are that the transition is gradual

and that the most close-packed planes roughen the last (i.e. at higher T). Also, it can be concluded that the phenomena are not of universal character (e.g. for diphenyl and ice the most dense plane did not roughen even for $T \approx T_m$, while for adamantine the most close-packed plane roughened below the bulk melting point) and that the theoretically predicted T_R's for S/V interfaces are too high (e.g. for C_2Cl_6 the theoretical value of KT_R/L_v is 1/16 compared with the theoretical value of 1/8). It was also found that impurities reduce T_R.[127]

The roughening transition for the hcp ^{4}He crystals has been experimentally found for at least three crystal orientations ((0001), (1100), (1101)[129,130]). Moreover, a recent study[130] of the (0001) and (1100) interfaces, is believed to be the first quantitative evidence that couples the transition with both the growth kinetics and the equilibrium shape of the interface. Below T_R the growth kinetics were of the lateral type; that allowed for a determination of the relationship $\sigma_e(T)$. At T_R it was shown that σ_e vanished as

$$\exp\left(-C/\left(\frac{T_R - T}{T_R}\right)^{1/2}\right)$$

in accord with the earlier mentioned theories. At $T > T_R$ the interfaces advanced by the continuous mechanism.

As far as S/L interfaces of pure metallic substances are concerned, the roughening transition is likely non-existent experimentally. A faceted to non-faceted transition, however, has been observed for a metallic solid-solution (other liquid metals or alloys) interface in the Zn-In and Zn-Bi-In systems.[131,132] The transition, which was studied isothermally, took place in the composition range where important

changes in $\sigma_{s\ell}$ occurred. Evidence about roughening also exists for several solvent-solute combinations during solution growth.[133]

Additional information about the roughening transition concept comes from experimental studies on the equilibrium shape of microscopic crystals. This topic is briefly reviewed in the next section.

Equilibrium Crystal Shape (ESC)

The dynamic behavior of the roughening transition can also be understood from the picture given from the theory of the evolution of the equilibrium crystal shape (ECS). In principle, the ECS is a geometrical expression of interfacial thermodynamics. The dependence of the interfacial free energy (per unit area) on the interfacial orientation $\hat{n}$ determines $r(T,\hat{n})$, where r is the distance from the center of the crystal in the direction of $\hat{n}$ of a crystal in two-phase coexistence.[14,15] At T = 0, the crystal is completely faceted.[134]* As T increases, facets get smaller and each facet disappears at its roughening temperature $T_R(\hat{n})$. Finally, at high T, the ECS becomes completely rounded, unless, of course, the crystal first melts. As discussed earlier, facets on the ECS are represented with cusps in the Wulff plot, which, in turn, are related to nonzero free energy per unit length necessary to create a step on the facet;[135] the step free energy also vanishes at $T_R(\hat{n})$, where the corresponding facets disappear. Below T_R, facets and curved areas on the crystal meet at edges with or without slope discontinuity (i.e. smooth or sharp); the former corresponds to first-order phase transition and the latter to second-order transitions. The edges are the

---

* It is generally believed that macroscopic crystals at T = 0 are faceted; however, this claim that comes only from quantum crystals still remains controversial.[134]

singularities of the free energy $r(T,\hat{n})$[136] that determines the ECS phase diagram.[137] The shape of the smooth edge varies

$$y = A(x - x_c)^\theta + \text{higher-order terms}$$

where x_c is the edge position; x, y are the edge's curvature coordinates. The critical exponent θ is predicted to be as $\theta = 2$[136] or $\theta = 3/2$.[137,138] The 3/2 exponent is characteristic of a universality class[139,140] and it is therefore independent of temperature and facet orientation as long as $T < T_R$. Indeed, the 3/2 value has been reported from experimental studies on small equilibrium crystals (Xe on Cu substrate[141] and Pb on graphite[134]). For the equilibrium crystal of Pb grown on a graphite substrate, direct measurements of the exponent θ via SEM yielded a value of $\theta \simeq 1.60$, in the range of temperatures from 200-300°C, in close agreement with the Pokrovsky-Talapov transition[139] and smaller than the prediction of the mean-field theory.[137] Sharp edges have also been seen in some experiments, as in the case of Au,[142,143] but they have received less theoretical attention.

At the roughening transition, the crystal curvature is predicted to jump from a finite universal value for $T = T_R^+$ to zero for $T = T_R^-$,[130,138,144] as contrasted to the prediction of continuously vanishing curvature.[136] Similarly, the facet size should decrease with T and vanish as $T \to T_R^-$, like $\exp(-C/\sqrt{(T_R - T)})$,[113] as opposed to the behavior as $(T_R - T)^{1/2}$.[136] The jump in the crystal curvature has been exactly related[59] to the superfluid jump of the Kosterlitz-Thouless transition in the two-dimensional Coulomb gas.[113,130,134,141] In addition, the facet size of Ag_2S crystals[128] was found (qualitatively) to decrease, approaching T_R, in an exponential manner.

Although the recent theoretical predictions seem to be consistent with the experimental results, the difficulty of achieving an ECS on a practical time scale imposes severe limitations on the materials and temperatures that can be investigated. The only ideal system to study these phenomena is the ^{4}He (see an earlier discussion), for which several transitions have already been discovered in the hcp phase. Whether the superfluid ^{4}He liquid resembles a common metallic liquid and how the quantum processes affect the interface still remain unanswered.

Kinetic Roughening

In the last decade or so, MC simulations of SOS kinetic model[*] of (001) S/V interface of a Kossel crystal have revealed[117,145,146] a very interesting new concept, the "kinetic roughening" of the interface; in distinction with the equilibrium roughening caused by thermal fluctuations, the kinetic roughening is due to the effect of the driving force on the interface during growth. The simulations show that when a crystal face is growing at a temperature below T_R ($T < T_R$) under a driving force ΔG less than a critical value ΔG_c, it is smooth on an atomic scale and it advances according to a lateral growth mechanism. However, if the crystal face is growing at $T < T_R$, but at a driving force such that $\Delta G > \Delta G_c$, it will be rough on an atomic scale and a continuous growth

---

[*] This is an extension of the SOS model for (S/V) growth kinetics studies. Atoms are assumed to arrive at the interface with an externally imposed rate K^+. The evaporation rate K^-, on the other hand, is a function of the number of nearest neighbors, i.e. $f_{n,m}$, which is the fraction of surface atoms in the n/th layer with m lateral neighbors. The net growth rate is then the difference between condensation and evaporation rates in all layers. Unless some specific assumptions are made concerning K^-, and/or about $f_{n,m}$, the system cannot be solved. Indeed, all the existing kinetic SOS models essentially differ only in the above mentioned assumptions. (See, for example, references 117 and 119.)

mechanism will be operative. The transition in the interface morphology and growth kinetics as a function of the driving force is known as kinetic roughening. Computer drawings of the above mentioned simulations, shown in Figs. 6a and 6b, show the kinetic roughening phenomenon. It can be seen that at a low driving force the growth kinetics are non-linear, as contrasted with the high driving force region where the kinetics are linear. These correspond respectively to lateral and continuous growth kinetics, as discussed in detail later. It is believed that the high driving force results in a relatively high condensation rate with respect to the evaporation rate. In addition, the probability of an atom arriving on an adjacent site of an adatom and thus stabilizing it, is overwhelming that of the adatom evaporation. These result in smaller and more numerous clusters, as contrasted to the low driving force case where the clusters are large and few in number.

As far as the author knows, an experimental verification of kinetic roughening for a S/L interface in a quantitative way is non-existent. There are a few studies which identify the transition with morphological changes occurring at the interface with increasing supercooling.[133] Such conclusions are of limited qualitative character and under certain circumstances could also be erroneous, because 1) there may be a clear-cut distinction between equilibrium and growth forms of the interface,[12] 2) even when the growth is stopped, the relaxation time for equilibrium may be quite long[130] for macroscopic dimensions, and 3) a "round" part of a macroscopically faceted interface does not necessarily have to be rough on an atomic scale. Such microscopic detailed information can be gained only from the standpoint of interfacial kinetics, which also

a)

$\beta\Delta\mu = 2$ $\beta\Delta\mu = 10$
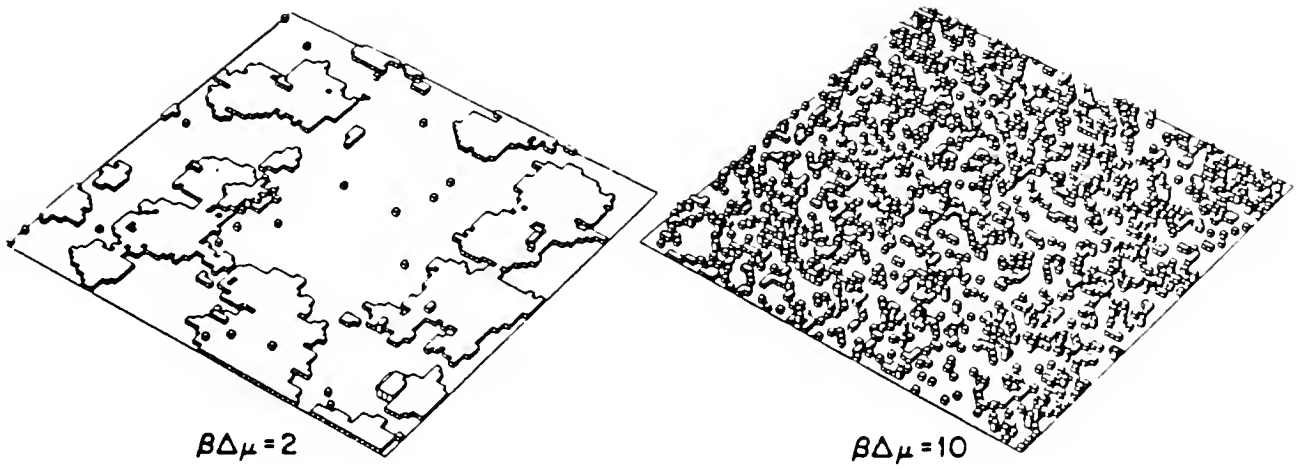
b)
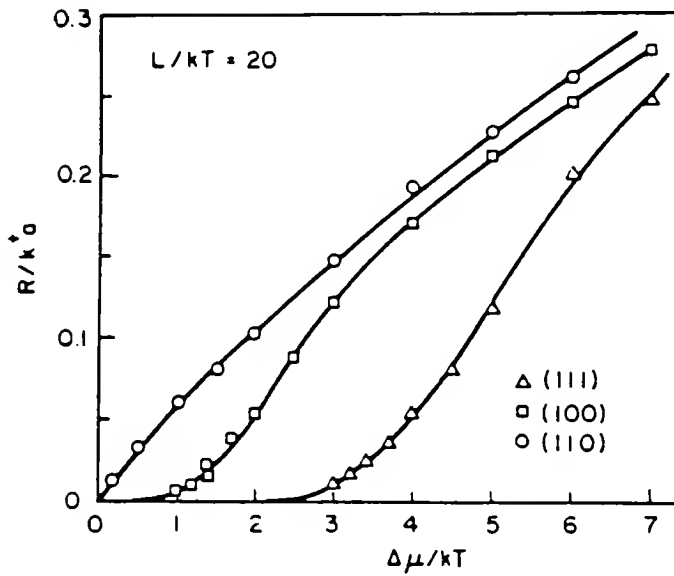
Figure 6   Kinetic Roughening. After Ref. (117). a) MC interface drawings after deposition of .4 of a monolayer on a (001) face with $KT/\phi = .25$ in both cases, but different driving forces ($\Delta\mu$). b) Normalized growth rates of three different FCC faces as a function of $\Delta\mu$, showing the transition in the kinetics at large supersaturations.

allow for a reliable determination of critical parameters linked to the transition. There are a few growth kinetics studies which provide a clue regarding the transition from lateral to continuous growth; these will be reviewed next rather extensively due to the importance of the kinetic roughening in this study.

A faceted (spiky) to non-faceted (smooth spherulitic) transition was observed for three high melting entropy (L/KT_m ~ 6-7) organic substances, salol, thymol, and O-terphenyl.[147] The transition that took place at bulk supercoolings ranging from 30-50°C for these materials was shown to be of reversible character; it also occurred at temperatures below the temperature of maximum growth rate.* An attempt to rationalize the behavior of all three materials in accord with the predictions of the MC simulation results[117] was not successful. The difference in the transition temperatures (20, 13, and -10°C for the O-terphenyl, salol, and thymol, respectively) were attributed to the dissimilar crystal structures and bonding.

Morphological changes corresponding to changes from faceted to nonfaceted growth form together with growth kinetics have been reported[148] for the transformation I-III in cyclohexanol with increasing supercooling. The morphological transition was associated with the change in growth kinetics, as indicated by a non-linear to linear transition of the logarithm of the growth rates, normalized by the reverse reaction term [1 - exp(- $\Delta G_v/KT$)], as a function of 1/T (i.e. $\log(V/1-\exp(- \Delta G_v/KT))$ vs. 1/T plot); the linear kinetics (continuous growth)

---

* This feature will be further explained in the continuous growth section.

took place at supercoolings larger than that for the morphological change and also larger than the supercooling for the maximum growth rate. The change in the kinetics was found to be in close agreement with Cahn's theory.[25] It should be noted that the low supercoolings data, which presumably represented the lateral growth regime, were not quantitatively analyzed; also, the "α" factor of cyclohexanol lies in the range of 1.9-3.7, depending on the ξ value. It was also suggested[149] that normalization of the growth rates by the melt viscosity at high ΔT's might mask the kinetics transition.

The morphological transition for melt growth has also been observed[133] for the (111) interface of biphenyl at a ΔT about .03°C; the "α" factor of this interface was calculated to be about 2.9. For growth from the solution, the transition has been observed at minute supercooling for facets of tetraoxane crystals with an "α" factor in the order of 2.[150]

Based on kinetic measurements, it was initially suggested that P_4 undergoes a transition from faceted to non-faceted growth at supercoolings between 1-9°C.[151] However, this was not confirmed by a later study by the same authors, who reported that P_4 grew with faceted dendritic form at high supercoolings.[41]

In conclusion, a complete picture of the kinetic roughening phenomenon has not been experimentally obtained for any metallic S/L interface. It seems that for growth from the melt because of the limited experimental range of supercoolings at which a change in the growth morphology and kinetics can be accurately recorded, only materials with

an "α" factor close to the theoretical borderline of 2 are suitable for testing. Even in such cases the transition cannot be substantiated and quantified in the absence of detailed and reliable growth kinetics analysis.

Interfacial Growth Kinetics

Lateral Growth Kinetics (LG)

It is generally accepted that lateral growth prevails when the interface is smooth or relatively sharp; this in turn implies the following necessary conditions for lateral growth: 1) the interfacial temperature T_i is less than T_R and 2) the driving force for growth is less than a critical value necessary for the dynamic roughening transition, and/or the diffuseness of the interface.

The problem of growth on an atomically flat interface was first considered by Gibbs,[20] who suggested that there could be difficulty in the formation of a new layer (i.e. to advance by an interplanar or an interatomic distance) on such an interface. When a smooth interface is subjected to a finite driving force (i.e. a supercooling ΔT), the liquid atoms, being in a metastable condition, would prefer to attach themselves on the crystal face and become part of the solid. However, by doing so as single atoms, the free energy of the system is still not decreased because of the excess surface energy term associated with the unsatisfied lateral bonds. Thus, an individual atom, being weakly bound on the surface and having more liquid than solid neighbors, is likely to "melt" back. However, if it meant to stay solid, it would create a more favorable situation for the next arriving atom, which would rather take

the site adjacent to the first atom rather than an isolated site. From this simplified atomistic picture, it is obvious that atoms not only prefer to "group" upon arrival, but also choose such sites on the sur- face as to lower the total free energy. These sites are the ones next to the edges of the already existing clusters of atoms. The edges of these interfacial steps (ledges) are indeed the only energetically favorable growth sites, so that steps are necessary for growth to pro- ceed (stepwise growth). The interface then advances normal to itself by a step height by the lateral spreading of these steps until a complete coverage of the surface area is achieved. Although another step might simultaneously spread on top of an incomplete layer, it is understood that the mean position of the interface advances one layer at a time (layer by layer growth).

Steps on an otherwise smooth interface can be created either by a two-dimensional nucleation process or by dislocations whose Burgers vec- tors intersect the interfaces; the growth mechanisms associated with each are, respectively, the two-dimensional nucleation-assisted and screw dislocation-assisted, which are discussed next. Prior to this, however, we will review the atomistic processes occurring at the edge of steps and their energetics, since these processes are rather independent from the source of the steps.

Interfacial steps and step lateral spreading rate (υ_e)

In both lateral growth mechanisms the actual growth occurs at ledges of steps, which, like the crystal surface, can be rough or smooth; a rough step, for example, can be conceived as a heavily kinked step. For S/V interfaces it has been shown[107,112] that the roughness of

the steps is higher than that of their bonding surfaces and it decreases with increasing height; moreover, MC simulations find that steps roughen before the surface roughening temperature T_R. On the other hand, for a diffuse interface, the step is assumed[6] to lose its identity when the radius of the two-dimensional critical nucleus, r_c, becomes larger than the width of the step defined as

$$w = h/(g)^{1/2} \tag{19}$$

Note that the width of the step is thought to be the extent of its profile parallel to the crystal plane; hence, the higher the value of w, the rougher the step is and vice versa. Interestingly enough, even for relatively sharp interfaces, i.e. when g ~ .2-.3, the step is predicted to be quite rough. Based on this brief discussion, the edge of the steps is always assumed to be rough.

Atoms or molecules arrive at the edge of the steps via a diffusive jump across the cluster/liquid interface. Diffusion towards the kink sites can occur either directly from the liquid or vapor (bulk diffusion) or via a "surface diffusion" process from an adjacent cluster, or simultaneously through both. For the case of S/L interfaces, however, it is assumed that growth of the steps is via bulk diffusion only.[152] Furthermore, anisotropic effects (i.e. the edge orientation) are excluded.

The growth rate of a straight step is derived as[152]*

$$\upsilon_e = \frac{3DL\Delta T}{hRTT_m} = K_E \, D \, \frac{\Delta T}{T} \tag{20}$$

---

* For detailed derivation, see further discussion in the continuous growth section.

where D is the liquid self-diffusion coefficient and R is the gas constant. Cahn et al.[25] have corrected eq. (20) by introducing the phenomenological parameter β and the g factor as

$$\upsilon_e = \beta(2 + g^{-1/2}) \frac{DL\Delta T}{hRTT_m} \tag{21}$$

Here β corrects for orientation and structural factors; it principally relates the liquid self-diffusion coefficient to interfacial transport, which will be considered next. β is expected to be larger than 1 for symmetrical molecules (i.e. molecularly simple liquids for which "the molecules are either single atoms or delineate a figure with a regular polyhedral shape"[153]) and less or equal to 1 for asymmetric molecules. In spite of these corrections, the concluding remark from eqs. (20) and (21) is that υ_e increases proportionally with the supercooling at the interface.

When the step is treated as curved, then the edge velocity is derived as[17]

$$\upsilon = \upsilon_e (1 - r_c/r) \tag{22}$$

where r is the radius of curvature. In accord with eq. (22), the edge of a step with the curvature of the critical nucleus is likely to remain immobile since $\upsilon = 0$.

If one accounts for surface diffusion, υ_e is given according to the more refined treatment of BCF[10] as

$$\upsilon_e = 2\sigma x_s \nu \exp(-W/KT) \tag{23}$$

where σ is the supersaturation, x_s is the mean diffusion length, ν is the atomic frequency ($\nu \sim 10^{13}$ sec^{-1}), and W is the evaporation energy. For parallel steps separated by a distance y_o, the edge velocity is derived as

$$\upsilon_e \simeq 2\sigma x_s \upsilon \exp(- W/KT) \tanh(y_0/2x_s) \tag{24}$$

which reduces to (23) when y_0 becomes relatively large.

Interfacial atom migration

The previously given analytical expression (eq. (20)) for the edge velocity can be written more accurately as

$$\upsilon_e \approx c \, \Delta G_v \cdot \exp(- \Delta G_i/KT) \tag{25}$$

where c is a constant and ΔG_i is the activation energy required to transfer an atom across the cluster/L interface. This term is customarily assumed[154] to be equal to the activation energy for liquid self-diffusion, so that υ_e in turn is proportional to the melt diffusivity or viscosity (see eq. (20)).

Before examining this assumption, let it be supposed that the transfer of an atom from the liquid to the edge of the step takes place in the following two processes: 1) the molecule "breaks away" from its liquid-like neighbors and reorients itself to an energetically favorable position and 2) the molecule attaches itself to the solid. Assuming that the second process is controlled by the number of available growth sites and the amount of the driving force at the interface, it is expected that ΔG_i to be related to the first process. As such, the interfacial atomic migration depends on a) the nature of the interfacial region, or, alternatively, whether the liquid surrounding the cluster or steps retains its bulk properties; b) how "bonded" or "structured" the liquid of the interfacial region is; c) the location within the interfacial region where the atom migration is taking place; and d) the molecular structure of the liquid itself. Thus, the combination and the magnitude of these effects would determine the "interfacial

diffusivity," D_i. Alternatively, suggesting that $D_i = D$, one explicitly assumes that the transition from the liquid to the solid is a sharp one and that the interfacial liquid has similar properties to those of the bulk. Although this assumption might be true in certain cases,[25,153] its validity has been questioned[25,153,155] for the case of diffuse interface, clustered, and molecularly complex liquids. These views have been supported by recent experimental works[92,95,156] and previously discussed MD simulations of the S/L interface,[50,53,54-56] which indicate that a liquid layer, with distinct properties compared to those of the bulk liquid and solid, exists next to the interface. Within this layer then the atomic migration is described by a diffusion coefficient D_i that has been found to be up to six orders of magnitude smaller[92,95] than the thermal diffusivity of the bulk liquid; if this is the case, the transport kinetics at the cluster/L interface should be much slower than eq. (20) indicates. Moreover, if the interfacial atom migration is 3-6 orders of magnitude slower than in the bulk liquid, one should also have to question whether atoms reach the edge of the step as well by surface diffusion. As mentioned earlier, these factors are neglected in the determination of υ_e. Finally, it should be noted that ΔG_i also enters the calculations of the two-dimensional nucleation rate via the arrival rate of atoms (R_i) at the cluster, which is discussed next.

Two-dimensional nucleation-assisted growth (2DNG)

As indicated earlier, steps at the smooth interface can be created by a two-dimensional nucleation (2DN) process, analogous to the three-dimensional nucleation process. The main difference between the two is that for 2DN there is always a substrate, i.e. the crystal surface,

where the nucleus forms. The growth mechanism by 2DN, conceived a long time ago;[157] can be described in terms of the random nucleation of two-dimensional clusters of atoms that expand laterally or merge with one another to form complete layers. In certain limiting cases, the growth rate for the 2DNG mechanism is predominantly determined by the two-dimensional nucleation rate, J, whereas in other cases the rate is determined by the cluster lateral spreading velocity (step velocity), υ_e as well as the nucleation rate. These two groups of 2DNG theories are discussed next, succeeding a presentation of the two-dimensional nucleation theory.

Two-dimensional nucleation. The prevailing two-dimensional nucleation theory is based on fundamental ideas formulated several decades ago.[158-161] These classical treatment, which dealt with nucleation from the vapor phase, and the basic assumptions were later followed in the development of a 2DN theory in condensed systems.

The classical theory assumes that clusters, including critical nuclei, have an equilibrium distribution in the supercooled liquid or that the growth of super-critical nuclei is slow compared with the rate of formation of critical size clusters. It also assumes, as the three-dimensional nucleation theory, single atom addition and removal from the cluster, as well as the kinetic concept of the critical size nucleus.[162]* The expression for the nucleation rate is given as

$$J = Z \; \omega_i^* \; n_i^*$$

_____

* The validity of these assumptions has been the subject of great controversy and continues to be so. For detailed discussion, see, for example, ref. 162.

where ω_i^* is the rate at which individual atoms are added to the critical cluster (equal to the product of arrival rate, R_i, and the surface area of the cluster, S), n_i^* is the equilibrium concentration of critical nuclei with i^* number of atoms, and Z is the Zeldovich non-equilibrium factor which corrects for the depletion of the critical nuclei when nucleation and growth proceed. Z has a typical value of about 10^{-2},[163] and is given as

$$Z = (\frac{\Delta G_i^*}{4\pi KT})^{1/2} \frac{1}{i^*}$$

where ΔG_i^* is the free energy of formation of the critical cluster. For the growth of clusters in the liquid, it is assumed that the clusters fluctuate in size by single atom increments so that the edge of the cluster is rough. The arrival rate R_i is then defined as described previously for the growth of a step. Finally, the concentration of the critical nuclei is given as

$$n_i^* = n \exp (- \frac{\Delta G_i^*}{KT})$$

where n is the atom concentration. For a disk-like nucleus of height h, the work needed to form it is given as

$$\Delta G^* = - \frac{\pi \sigma_e^2}{h \Delta G_v} \tag{26}$$

where σ_e is the step edge free energy per unit length of the step. For small supercoolings at which the work of forming a critical two-dimensional nucleus far exceeds the thermal energy (KT), the nucleation rate per unit area can be approximately written, as derived by Hillig,[164] in the form of

$$J \approx \frac{N}{V_m} \left(\frac{L\Delta T}{RTT_m}\right)^{1/2} \frac{3\beta D}{2a_o} \exp\left(-\frac{\Delta G^*}{KT}\right) \qquad (27)$$

where N is Avogadro's number and a_o is the atomic radius. This expression, that confirmed an earlier derivation,[165] is the most widely accepted for growth from the melt. The main feature of eq. (27) is that J remains practically equal to zero for up to a critical value of supercooling. However, for supercoolings larger than that, J increases very fast with ΔT, as expected from its exponential form. Relation (27) can be rewritten in an abbreviated form as

$$J = K_o D\left(\frac{\Delta T}{T}\right)^{1/2} \exp\left(-\frac{\Delta G^*}{KT}\right) \approx K_n \exp\left(-\frac{\Delta G^*}{KT}\right) \qquad (28)$$

where K_o is a material constant and K_n is assumed to be constant within the usually involved small range of supercooling. Although theoretical estimates of K_n are generally uncertain because of several assumptions, its value is commonly indicated in the range of $10^{21\pm2}$.[163] The very large values of K_n, and the fact that it is essentially insensitive to small changes of temperature, have made it quite difficult to check any refinements of the theory. Indeed, such approaches to the nucleation problem that account for irregular shape clusters[166] and anisotropy effects[167] lead to same qualitative conclusions as expressed by eq. (28). Also, a recent comparison of an atomistic nucleation theory from the vapor[145] with the classical theory leads to the same conclusion. In contrast, the nucleation rate is very sensitive to the exponential term, therefore to the step edge free energy and the supercooling at the cluster/liquid (C/L) interface. The nature of the interface affects J in two ways. First, in the exponential term, ΔG^*, through its dependence upon σ_e and in the pre-exponential term through the energetic barrier

for atomic transport across the C/L interface. The assumptions of the classical theory are simple in both cases, since σ_e is taken as constant, regardless of the degree of the supercooling, and the transport of atoms from the liquid to the cluster is described via the liquid self-diffusion coefficient. These assumptions are not correct when the interface is diffuse[6] and at large supercoolings.[32] These aspects will be discussed in more detail in a later chapter.

Mononuclear growth (MNG). As was mentioned earlier, two-dimensional nucleation and growth (2DNG) theories are divided into two regions according to the relative time between nucleation and layer completion (cluster spreading). The first of these is when a single critical nucleus spreads over the entire interface before the next nucleation event takes place (see Fig. 7a). Alternatively, this is correct when the nucleation rate compared with the cluster spreading rate is such that

$$1/JA > \ell/\upsilon_e \quad \text{or for a circular nucleus } A \leq (\upsilon_e/J)^{2/3} \quad (29)$$

where A, ℓ are the area and the largest diameter of the interface, respectively. If inequality (29) is satisfied, each nucleus then results in a growth normal to the interface by an amount equal to the step (nucleus) height, h. Thus, the net crystal growth rate for this classical mononuclear (and monolayer) mechanism (MNG) is given as[164,168]

$$V = hAJ \quad (30)$$

In this region, the growth rate is predicted to be proportional to the interfacial area (i.e. crystal facet size). The practical limitations of this model, as well as the experimental evidence of its existence, will be given later.
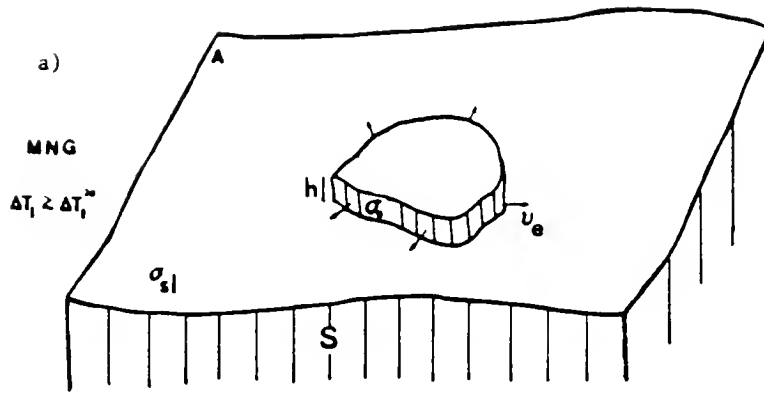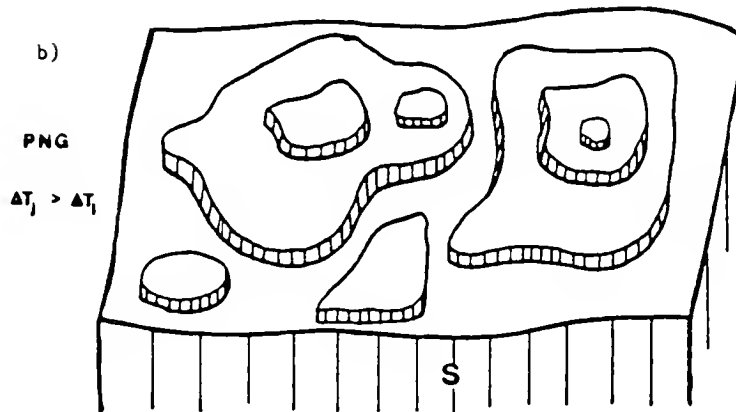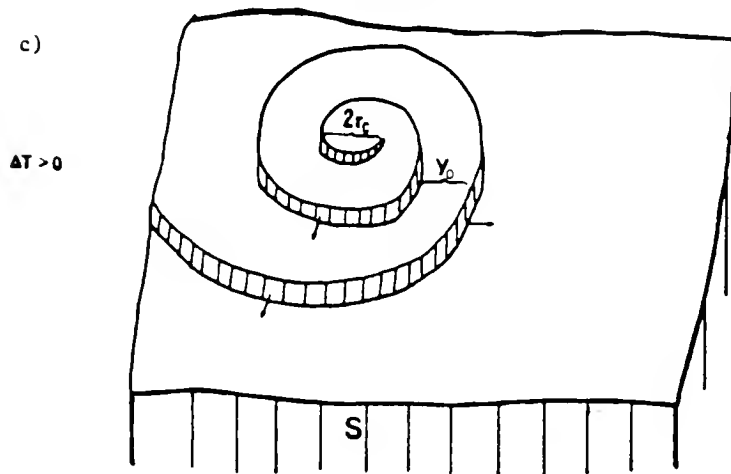
Figure 7 Schematic drawings showing the interfacial processes for the lateral growth mechanisms a) Mononuclear. b) Poly-nuclear. c) Spiral growth. (Note the negative curvature of the clusters and/or islands is just a drawing artifact.)

Polynuclear growth (PNG). At supercoolings larger than those of the MNG region, condition (29) is not fulfilled and the growth kinetics are described by the so called polynuclear (PNG) model.[*] According to this model, a large number of two-dimensional clusters nucleate at random positions at the interface before the layer is completed, or on the top of already growing two-dimensional islands, resulting in a hill- and valley-like interface, as shown in Fig. 7b. Assuming that the clusters are circular and that υ_e is independent of the two-dimensional cluster size, anisotropy effects, and proximity of neighboring clusters, the one layer version of this model was analytically solved.[169] This was possible by considering that for a circular nucleus the time, τ, needed for it to cover the interface is equal to the mean time between the genesis of two nuclei (i.e. the second one on top of the first), or otherwise given by

$$\pi \int_0^\tau J(\upsilon_e t)^2 \, dt = 1 \tag{31}$$

Integration of this expression and use of the relation $V = h/\tau$ yields the steady state growth rate (for the polynuclear-monolayer model) given as

$$V = h \, (\pi J \upsilon_e^2/3)^{1/3} \tag{32}$$

This solution has been shown by several approximate solutions[164,168,170] and simulations[168,171,172] to represent well the more complete picture of multilevel growth by which several layers grow concurrently through

---

[*] It should be mentioned that the use of the term "polynuclear growth" in this study should not be confused with the usually referred unrealistic model,[18] which considers completion of a layer just by deposition of critical two-dimensional nuclei.

nucleation and spreading on top of lower incomplete layers. The more general and accurate growth rate equation in this region is given by

$$V = ch \ (J\upsilon_e^2)^{1/3}$$ (33)

where the constant c falls between 1-1.4. It is interesting that eq. (32), being an approximation to the asymptotic multilevel growth rate, has been shown to be very close to the exact value of steady state conditions that are achieved after deposition of 3-4 layers.[173] It was also suggested from these studies that for irregularly shaped nuclei the transient period is shorter than for the circular ones. Nevertheless, the growth rate is well described by eq. (33).

The effect of the nucleus shape upon the growth rate has been considered in a few MC simulation experiments for the V/Kossel crystal interface.[174] Square-like[172] and irregular nuclei result in higher growth rates. This increase in the growth rate can be understood in terms of a larger cluster periphery, which, in turn, should (statistically) have a larger number of kink sites than the highly regular cluster shapes assumed in the theory. This situation would cause a higher atom deposition to evaporation flux ratio. Furthermore, surface diffusion during vapor growth was found to cause a large increase in the growth rate.[174]

As indicated earlier, eqs. (32) and (33) were derived under the assumption that the nucleus radius increases linearly with time. Although this assumption does not really affect the physics of the model, it plays an important role in the kinetics because it determines the 1/3 exponent in the rate equations. For example, assuming that the cluster radius grows as $r(t) \propto t^{1/2}$ (i.e. the cluster area increases linearly

with time) as in a diffusion field, the growth rate equation is derived as[175,176]

$$V \approx c'h \ (J\upsilon_e^2)^{1/2} \tag{34}$$

where c' is a constant close to unity. Indeed, growth data (S/V) of a MC simulation study were represented by this model.[176] Alternatively, if the growth of the cluster is assumed to be such that its radius increases with time as $r(t) \propto t + t^{1/2}$ (i.e. a combined case of the above mentioned submodels), it can be shown that the growth rate takes the form of

$$V \approx c''h \ (J\upsilon_e^2)^{2/5} \tag{35}$$

where c" is a constant. Therefore, according to these expressions, the power in the growth rate equation varies from 1/3 to 1/2.[177]

A faceted interface that is dislocation free grows by any of the two previously discussed 2DN growth mechanisms. At low supercoolings the kinetics are of the MNG mode, while at higher supercoolings the interface advances in accord with PNG kinetics. The predicted growth rate equations (eqs. (30) and (32)) can be rewritten with the aid of eqs. (27), (26), and (20) as

$$(MNG) \qquad V = K_1 \ A \ (\frac{\Delta T}{T})^{1/2} \ \exp \ (- \frac{M\sigma_e^2}{T\Delta T}) \tag{36}$$

$$(PNG) \qquad V = K_2 \ (\frac{\Delta T}{T})^{5/6} \ \exp \ (- \frac{M\sigma_e^2}{3T\Delta T}) \tag{37}$$

Here, K_1, K_2, and M are material and physical constants whose analytical expressions will be given in detail in the Discussion chapter. The growth rates as indicated by eqs. (36) and (37) are strongly dependent upon the exponential terms, and therefore upon the step edge free energy

and the interfacial supercooling. Although the pre-exponential terms of the rate equations, strictly speaking, are functions of ΔT and T, practically they are constant within the usually limited range of supercoolings for 2DNG. The distinct features associated with 2DNG kinetics are the following: a) A finite supercooling is necessary for a measurable growth rate ($\sim 10^{-3}$ μm/s); this is related to the threshold supercooling for 2DN, mentioned earlier, and it is governed by σ_e in the exponential term. The smaller σ_e is, the smaller the supercooling at which the interfacial growth is detectable. b) Only the MNG kinetics are dependent on the S/L interfacial area. c) Since the pre-exponential terms are relatively temperature independent, both MNG and PNG kinetics should fall into straight lines in a $\log(V)$ vs. $1/\Delta T$ plot. d) From the slope of the $\log(V)$ vs. $1/\Delta T$ curve (i.e. $- M\sigma_e^2/T$), the step edge free energy can be calculated,[63,177-181] provided that the experimental data have been measured accurately. σ_e can then be used to estimate the diffuseness parameter "g" via the proposed relation[6]

$$\sigma_e = \sigma_{s\ell} \ h \ (g)^{1/2} \tag{38}$$

e) Furthermore, in the semilogarithmic plot of the growth data, the ratio of the slopes for the MNG and PNG regimes should be 3, according to the classical theory; however, as discussed earlier, this ratio can actually range from 2 to 3 depending on the details of the cluster spreading process.

Detailed 2DNG kinetics studies are very rare, in particular for the MNG region, which has been found experimentally only for Ga[2] and Ag.[182] The major difficulties encountered with such studies are 1) the necessity of a perfect interface; 2) the commonly involved minute growth

rates;   3) the   required close   control of the interfacial supercooling and, therefore, its accurate determination; and 4) the   problems associated with analyzing the growth data analysis when the experimental range of ΔT's is small or it falls close to the   intersection of the two MNG and PNG kinetic regimes for a given sample size. Nevertheless, there are a couple of experimental studies which rather accurately have verified the 2DN assisted growth for faceted metallic interfaces.[2,63,99,182]

Screw dislocation-assisted growth (SDG)

Most often crystal interfaces contain lattice defects such as screw dislocations and these can have a tremendous effect on the growth kinetics.   The importance of dislocations in crystal growth was first proposed by Frank,[183] who indicated that they could enhance the growth rate of singular faces by many orders of magnitude relative to the 2DNG rates. For the past thirty years since then, researchers have observed spirals caused by growth dislocations on a large variety of metallic and non-metallic crystals grown from the vapor and solutions,[16] and on a smaller number grown from the melt.[184]

When a dislocation intersects the interface, it gives rise to a step initiating at the intersection, provided that the dislocation has a Burgers vector $(\vec{b})$ with a component normal to the interface.[185] Since the step is anchored, it will rotate around the dislocation and wind up actually in a spiral (see Fig. 7c). The edges of this spiral now provide a continuous source of growth sites. After a transient period, the spiral is assumed to reach a steady state, becoming isotropic, or, in terms of continuous mechanics, an archimedian spiral.   This further means that the spiral becomes completely rounded since anisotropy of the

kinetics and of the step edge energy are not taken into account. How-
ever, it has been suggested[119] that on S/V interfaces sharply polygoni-
zed spirals may occur at low temperatures or for high "α" factor mater-
ials. Nonrounded spirals have been observed during growth of several
materials,[186,187] as well as on Ga monocrystals during the present
study.

Most theoretical aspects of the spiral growth mechanism were first
investigated by BCF in their classical paper,[10] which presented a revo-
lutionary breakthrough in the field of crystal growth. Interestingly
enough, although their theory assumes the existence of dislocations in
the crystal, it does not depend critically on their concentration. The
actual growth rate depends on the average distance (y_0) between the arms
of the spiral steps far from the dislocation core. This was evaluated
to be equal to $4\pi r_c$; later, a more rigorous treatment estimated it as
$19 r_c$.[188] The curvature of the step at the dislocation core, where it is
pinned, is assumed to be equal to the critical two-dimensional nucleus
radius r_c. On the other hand, for polygonized spirals, the width of the
spiral steps is estimated[186] to be in the range of $5 r_c$ to $9 r_c$.

According to the continuum approximation, the spiral winds up with
a constant angular velocity ω. Thus, for each turn, the step advances
y_0 in a time $y_0 / \upsilon_e = 2\pi/\omega$. Then the normal growth rate V is given as[10]

$$V = b\omega/2\pi = by_0/\upsilon_e \tag{39}$$

where b is the step height (Burgers vector normal component). According
to the BCF notation, from eq. (24) where $y_0 = 4\pi r_c \approx 4\pi\gamma_e/KT\sigma$ (here γ_e
is the step edge energy per molecule), one gets the BCF law

$$V \approx f \cdot \nu \exp(-W/KT)(\sigma^2/\sigma_1)\tanh(\sigma_1/\sigma) \tag{40}$$

where

$$\sigma_1 = \frac{2\pi\gamma_e b}{KTx_s} \text{ and } f \text{ is a constant.}$$

BCF also considered the case when more than one dislocation merges at the interface. For instance, for a group of S dislocations, each at a distance smaller than $2\pi r_c$ from each other, arranged in a line of length L, eq. (40) holds with a new $y_o = y_o/S$ when $L < 4\pi r_c$ and $y_o \approx 2L/S$ when $L > 4\pi r_c$. Nevertheless, the growth rate V can never surpass the rate for one dislocation, regardless of the number and kind of dislocations involved.

For growth from the melt, the rate equation for the screw dislocation growth (SDG) mechanism has been derived as[152,189]

$$V = \frac{DL \, \Delta T^2}{4\pi T_m^2 RT\sigma_{s\ell} V_m} \qquad (41)$$

Canh et al.[25] have modified eq. (41) for diffuse interfaces with a multiplicity factor β/g. The physical reason for this parabolic law is that both the density of spiral steps and their velocity increases proportionally with ΔT. Models for the kinetics of nonrounded spirals also predict a parabolic relationship between V and ΔT.[190] However, another model that accounts for the interaction between the thermal field of the dislocation helices has shown that a power less than two can be found in the kinetic law $V(\Delta T)$.[191]

The influence of the stress field in the vicinity of the dislocation has shown to be significant on the shape of growth and dissolution (melting) of spirals in several cases.[192] It can be shown[188] that the effect of the stress field extends to a distance r_s from the core of the dislocation given as

$$r_s = (\frac{\mu b^2 r_c}{8\pi^2 \sigma_{s\ell}})^{1/2}$$

where μ is the shear modulus. Nevertheless, corrections due to the stress field are usually neglected since most of the time $r_s < y_o$.

In conclusion, dislocations have a major effect on the kinetics of growth by enhancing the growth rates of an otherwise faceted perfect interface, as it has been shown experimentally for several materials.[2,25,26,34,63] Predictions from the classical SDG theory describe the phenomena well enough, as long as spiral growth is the dominant process.[145] As far as growth from the melt is concerned, most experimental results are not in agreement with the commonly referred parabolic growth law, eq. (41); indeed, the majority of the S/L SDG kinetics found in the literature are expressed as $V \propto \Delta T^m$ with $m < 2$.

In contrast with the perfect (and faceted) interface, a dislocated interface is mobile at all supercoolings. Moreover, the SDG rates are expected to be several orders of magnitudes higher than the respective 2DNG rates, regardless of the growth orientation. Like the 2DNG kinetics, the dislocation-assisted rates can fall on two kinetic regimes according to the BCF theory. This can be understood by considering the limits of SDG rate equation, eq. (40), with respect to the supersaturation σ. It is realized that when $\sigma \ll \sigma_1$, i.e. low supersaturation, then one has the parabolic law

$$V \propto \sigma^2$$

and for $\sigma \gg \sigma_1$ the linear law

$$V \propto \sigma$$

For the parabolic law case, y_o is much greater than x_s and the reverse is true for the linear law. In between these two extreme cases, i.e. at intermediate supersaturations, the growth rates are expected to fall in a kinetics mode faster than linear but slower than parabolic; such a mode could be, for example, a power law, $V \propto \Delta T^n$, with n such that $1 < n < 2$.

For growth from the melt, the BCF rate equation can be rewritten as[*]

$$V = N \Delta T^2 \tanh (P/\Delta T) \tag{42}$$

where N and P are constants. Equation (42) reduces to a parabolic or to a linear growth when the ratio $P/\Delta T$ is far less or greater, respectively, than one.

Lateral growth kinetics at high supercoolings

According to the classical LG theory, the step edge free energy is assumed to be constant with respect to supercooling, regardless of possible kinetics roughening effects on the interfacial structure at high ΔT's. Based on a constant σ_e value, the only change in the 2DNG growth kinetics with ΔT is expected when the exponent $\Delta G^*/3KT$ (see eq. (37)) is close to unity. In this range, the rate is nearly linear ($\sim \Delta T^n$, n = 5/6). An extrapolation to zero growth rates from this range intersects the ΔT axis to the right of the threshold supercooling for 2DN growth. For SDG kinetics, based on the parabolic law (eq. (40)), no changes in the kinetics are expected at high ΔT's. However, the BCF law (eq.

---

[*] For detailed relations between supersaturation and supercooling see Appendix VI.

(39)), as discussed later, for large supercoolings reduces to an equation in the form

$$V = A' \Delta T - B' \tag{43}$$

where A' and B' are constants. Note: if eq. (43) is extrapolated to V = 0, it does not go through the origin, but intersects the ΔT axis at a positive value.

It should be mentioned that none of the above discussed transitions has ever been found experimentally for growth from a metallic melt. The parabolic to linear transition in the BCF law has been verified through several studies of solution growth.[181,193]

Continuous Growth (CG)

The model of continuous growth, being among the earliest ideas of growth kinetics, is largely due to Wilson[194] and Frenkel[195] (W-F). It assumes that the interface is "ideally rough" so that all interfacial sites are equivalent and probable growth sites. The net growth rate then is supposed to be the difference between the solidifying and melting rates of the atoms at the interface. Assuming also that the atom motion is a thermally activated process with activation energies as shown in Fig. 8, and from the reaction rate theory, the growth rate is given as[154,196]

$$V = V_o \exp\left(-\frac{Q_i}{KT}\right)\left[1 - \exp\left(-\frac{L\Delta T}{KT_m T}\right)\right] \tag{44}$$

where V_o is the equilibrium atom arrival rate and Q_i is the activation energy for the interfacial transport. As mentioned earlier, for practical reasons, Q_i is equated to the activation energy for self-diffusion in the liquid, Q_L, and $V_o \approx a\nu_i$ where a is the jump distance (interlayer spacing/interatomic distance) and ν_i is the atomic vibration frequency.
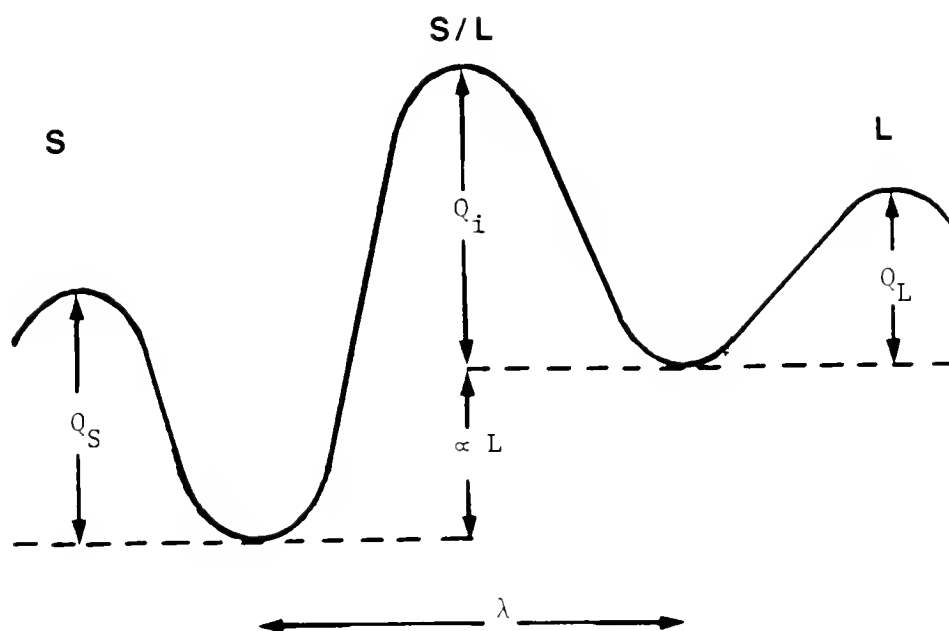
Figure 8 Free energy of an atom near the S/L interface. Q_L and Q_s are the activation energies for movement in the liquid and the solid, respectively. Q_i is the energy required to transfer an atom from the liquid to the solid across the S/L interface.

Hence, $a\nu_i \exp(-Q_i/KT) = D/a$ where D is the self-diffusion coefficient in the liquid. A similar expression can be derived based on the melt viscosity, η, by the use of the Stokes-Einstein relationship $aD\eta = KT$. Therefore, eq. (44) can be rewritten as

$$V = F(T)\left[1 - \exp\left(-\frac{L\Delta T}{KT_m T}\right)\right] \tag{45}$$

where $F(T)$ in its more refined form is given as[197]

$$F(T) \approx \frac{Da}{\lambda^2}\, f \propto \frac{1}{\eta}$$

in which f is a factor (≤ 1) that accounts for the fact that not all available sites at the interface are growth sites and λ is the mean diffusional jump distance. Note that if $\lambda = a$, then $F(T) = Df/a$. Furthermore, for small supercoolings, where $L\Delta T/KT_m T \ll 1$, eq. (45) can be rewritten as (in molar quantities)[25]

$$V = \frac{DL}{aRTT_m}\Delta T = K_c \Delta T \tag{46}$$

which is the common linear growth law for continuous kinetics. For most metals the kinetic coefficient K_c is of the order of several cm/sec·°C, resulting in very high growth rates at small supercoolings. Because of this, CG kinetics studies for metallic metals usually cover a small range of interfacial supercoolings close to T_m; in view of this, most of the time linear and continuous kinetics are used interchangeably in the literature. However, this is true only for small supercoolings, since for large supercoolings the temperature dependence of the melt diffusivity has to be taken into account. Accordingly, the growth rate as a function of ΔT is expected to increase at small ΔT's and then decrease at high ΔT's. On the other hand, a plot of the logarithm of

$$V/[1 - \exp\left(-\frac{L\Delta T}{kT_m T}\right)]$$

as a function of $1/T$ should result in a straight line, from the slope of which the activation energy for interfacial migration can be obtained. Indeed, such behavior has been verified experimentally[25,26,63,198] in a variety of glass-forming materials and other high viscosity melts.

An alternative to eqs. (45) and (46) was proposed by suggesting that the arrival rate at the interface for simple melts might not be thermally activated;[199,200] the kinetic coefficient K_c then was assumed to depend on the speed of sound in the melt. This treatment was in good agreement with the growth data for Ni,[201] but not with the data of glass-forming materials. Another approach suggested that the growth rate is given as[202]

$$V = \frac{a}{\lambda}\left(\frac{3KT}{m}\right)^{1/2} f\left[1 - \exp\left(-\frac{L\Delta T}{KTT_m}\right)\right]$$

where the atom arrival rate is replaced by $(3KT/m)^{1/2}$, which is the thermal velocity of an atom. This equation was in good agreement with recent MD results on the crystallization of a Lennard-Jones liquid.[202,203]

Other approaches for continuous growth are mostly based on the kinetic SOS model for a Kossel crystal in contact with the vapor.[117,145] As mentioned elsewhere, the basic difference among these models is the assumption concerning clustering (i.e. number of nearest neighbors), which strongly effects the evaporation rate and, therefore, the net growth rate.[204] In addition, these MC simulations only provide information about the relative rates in terms of the arrival rate of atoms. For vapor growth, the latter is easily calculated from gas kinetics.

For melt growth, however, the arrival rate strongly depends on the structure of the liquid at the interface, which is not known in detail. Therefore, these models cannot treat the S/L continuous growth kinetics properly. Some general features revealed from these models are discussed next to complete this review.

All MC calculations for rough interfaces indicate linear growth kinetics. The calculated growth rates are smaller than those of the W-F law, eq. (44). This is understood since the latter assumes $f = 1$. Interestingly enough, the simulations show that some growth anisotropy exists even for rough interfaces. For example, for growth of Si from the melt, MC simulations predicted[205] that there is a slight difference in growth rates for the rough (100) and (110) interfaces. The observed anisotropy is rather weak as compared to that for smooth interfaces, but it is still predicted to be inversely proportional to the fraction of nearest neighbors of an atom at the interface (ξ factor). Nevertheless, true experimental evidence regarding orientation dependent continuous growth is lacking. If there is such a dependence, the corresponding form of the linear law would then be

$$V = K_c(\hat{n}) \; \Delta T \qquad\qquad (47)$$

This is illustrated by examining the prefactor of ΔT in eq. (46). Note that the only orientation dependent parameter is (a), so that the growth rate has to be normalized by the interplanar spacing first to further check for any anisotropy effect. If there is any anisotropy, it could only relate to the diffusion coefficient D, otherwise D_i to be correct, and, therefore, to the liquid structure within the interfacial region. At present, the author does not know of any studies that show such

anisotropy. In contrast, it is predicted[117] that there is no growth rate difference between dislocation-free and dislocated rough interfaces. This is because a spiral step created by dislocation(s) will hardly alter the already existing numerous kink sites on the rough interface.

A summary of the interfacial growth kinetics together with the theoretical growth rate equations is given in Fig. 9. Next, the growth mode for kinetically rough interfaces is discussed.

Growth Kinetics of Kinetically Roughened Interfaces

As discussed earlier, an interface that advances by any of the lateral growth mechanisms is expected to become rough at increased supercoolings. Evidently, the growth kinetics should also change from the faceted to non-faceted type at supercoolings larger than that marking the interfacial transition.

In accord with the author's view regarding the kinetic roughening transition, the following qualitative features for the associated kinetics could be pointed out: a) Since the interface is rough at driving forces larger than a critical one, its growth kinetics are expected to resemble those of the intrinsically rough interfaces. Thus, the growth rate is expected to be unimpeded, nearly isotropic, and proportional to the driving force. Moreover, the presence of dislocations at the interface should not affect the kinetics. b) It is clear that the faceted interface gradually roughens with increasing ΔT over a relatively wide range of supercoolings. The transition in the kinetics should also be a gradual one. c) In the transitional region the growth rates should be faster than those predicted from the lateral, but slower than the

INTERFACIAL KINETICS

THEORETICAL GROWTH RATE EQUATIONS

Rough Interface

Continuous

$$V = f_e D_L a /_\lambda [1 - \exp(-L\Delta T / K T T_e)],$$

or

$$V = D_L \beta \Delta T \, L /_{K T T_e} \quad \propto \Delta T$$

Smooth Interface

Dislocation Assisted , (SDG)

$$V = k_3 \, \Delta T^2 /_{\Delta T_t} \tanh[\Delta T /_{\Delta T}]$$

or

$$V_\alpha \quad \nearrow \Delta T^2 \atop \searrow \Delta T \quad \longrightarrow \Delta T^n \quad n < 2$$

2-D Nucleation, (2DNG)

$$J = \frac{N}{V_m} \left(\frac{L}{R T_e}\right)^{1/2} \frac{3\beta}{2a_o} D_L \, \Delta T^{1/2} \exp(-s\sigma_e^2 T_e /_{L K h T \Delta T})$$

$$V_e = k_e D_L \, \Delta T$$

$$A < (v_e / J)^{2/3}$$

$$A > (v_e / J)^{2/3}$$

Mononuclear, (MNG)

$$V = h J A , \text{ or}$$

$$V = k_1 A \, \Delta T^{1/2} \exp(-M\sigma_e^2 / T \Delta T)$$

Polynuclear, (PNG)

$$V = c h (J v_e^2)^{1/3}$$

$$V = k_2 \, \Delta T^{5/6} \exp(-M\sigma_e^2 / 3 T \Delta T)$$
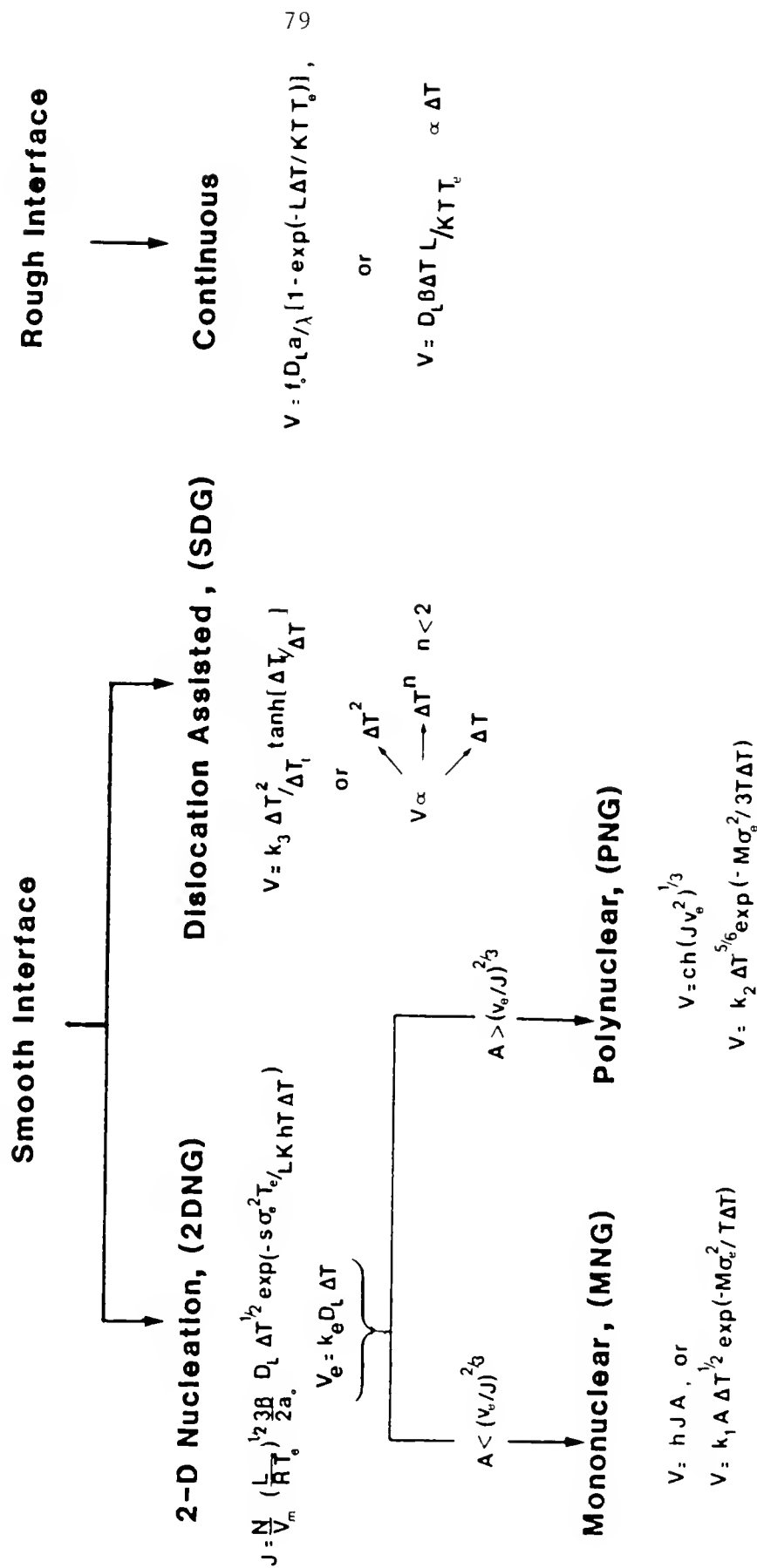
Figure 9   Interfacial growth kinetics and theoretical growth rate equations.

continuous growth. Although referred to continuous growth, it would be possible, to differentiate between two linear growth mechanisms, A) the continuous growth which takes place at all supercoolings for a rough interface and B) the normal growth which is the upper limit of the lateral growth, due to the kinetic roughening of the initially faceted interface. The former, at low ΔT's,[*] is represented by a line ($V = K_c \Delta T$) in a $V(\Delta T)$ plot that passes through the origin.

For growth from the melt, the only indication of a kinetic transition of both 2DNG and SDG kinetics has become available from a previous detailed kinetic study for the Ga (001) interface.[2] It was shown that, with increasing ΔT, the 2DN and SD growth rates approach each other and finally fall under the same kinetics. Analogous qualitative results have been published for salol,[63] where it was found that, at high ΔT's, the growth velocities scatter between a maximum and a minimum; the first with parabolic dependence on ΔT and the second with exponential dependence. However, the large scatter did not allow for any quantitative conclusion.

The transition from lateral to continuous growth kinetics with increasing ΔT is also predicted from the diffuse interface theory, as shown in Fig. 10. As discussed previously, this theory assumes that classical LG should prevail as long as

$$w < r_c \quad \text{or} \quad \frac{h}{\sqrt{g}} < - \frac{\sigma_e}{h \Delta G_v} \tag{48}$$

which with the aid of eqs. (38) and (1) determines the range of ΔT's for LG kinetics as

---

[*] Note that for metallic melts any effects because of decreased atomic mobility are not to be expected up to relatively high supercoolings.
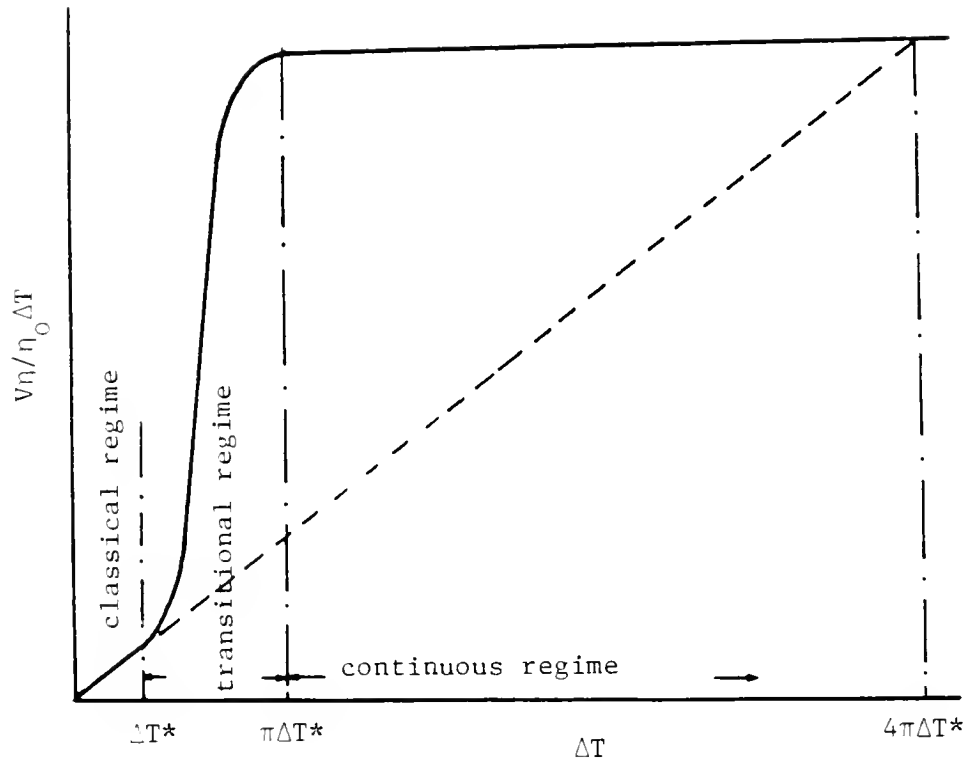
Figure 10   Transition from lateral to continuous growth according
to the diffuse interface theory;[25] η_o is the melt
viscosity at T_m.

$$0 \le \Delta T^* = \frac{\sigma_{s\ell} \, g \, V_m \, T_m}{Lh} \tag{49}$$

On the other hand, the critical driving force for continuous growth is derived from eq. (9) as

$$\Delta G_v + \sigma_o \frac{dg}{dx} = 0 \quad \rightarrow \quad -\Delta G_v^c = \frac{\pi \, \sigma_{s\ell} \, g}{h}$$

or that continuous growth should operate for supercoolings such that

$$\Delta T > \pi \, \Delta T^* \tag{50}$$

At intermediate supercoolings, i.e. $\Delta T^* < \Delta T < \pi \, \Delta T^*$, there is a transitional regime where growth deviates off those extrapolated from the low ΔT's regime towards the direction of faster growth rates.

To account for such a deviation, it was suggested that within the transitional region the step edge free energy should decrease with ΔT and finally become zero when the growth becomes continuous. For the SDG kinetics, starting from inequality (48), it was also concluded that the departure from the classical SDG law ($\propto \Delta T^2$) should occur at the same supercooling ΔT^* as for 2DNG kinetics. Note that here the width of the step is compared to r_c and not to y_o, the distance between the steps. The latter would result in an increased ΔT^* by a factor 2π.

In spite of the fact that the theory attempts to quantify the transition in the kinetics, it leaves unexplained the following key points: a) in accordance with their proposed analytical equation for σ_e, i.e. $\sigma_e = h \, \sigma_{s\ell} \sqrt{g}$, it is hard to rationalize how it is possible for σ_e to decrease with ΔT as long as g,* $\sigma_{s\ell}$ and h are constant. However, if

---

* It is obvious from their analysis and discussion of experimental growth kinetics[25] that g is a constant number.

the diffusiveness of the interface increases with ΔT (i.e. g decreases), then σ_e should decrease. b) The growth kinetics in the transitional regime are not described quantitatively. c) The quantitative parameter, ΔT^*, of the theory is not predicted, instead it has to be obtained ex- perimentally. Nevertheless, this model is the only existing phenomeno- logical approach attempting to describe the lateral to continuous growth transition at high ΔT's.

Growth Kinetics of Doped Materials

The presence of impurities in the melt is expected to affect growth kinetics in several ways. However, the role and the mechanism of the influence of the impurity on the interfacial growth processes have not yet been studied in detail. Needless to say, this question is of im- portance and considerable interest because small quantities of impur- ities are almost always present in the melt, intentionally in the case of doped semiconducting substances or unintentionally in other cases. As discussed later, the possibility of negligible amounts of impurities in the melt and its influence on kinetics has created questions regard- ing the reliability of reported crystal growth kinetics for supposedly pure materials. Moreover, the effects of these impurities and their understanding would help to better understand the crystal growth mechan- ism of pure materials. Thus, as a whole, the complicated problem of solute influence on growth kinetics requires further attention and in- vestigation.

This problem will be reviewed rather qualitatively since for growth from melt the existing theories are mostly empirical or just deal with the diffusion-diffusionless growth mode at high growth rates. Especial

attention will be given to the possible effects of the solute on the two-dimensional nucleation assisted growth, since they will be utilized in discussing the results of the current experiments on the influence of the In dopant on the 2DNG kinetics of Ga.

The overall crystal growth rate will depend on the interaction of the solute with the "pure" interfacial processes. The effect of impurities on the 2DNG kinetics mainly comes from its influence[*] on the step edge free energy (σ_e) and on the lateral spreading rate of the steps (υ_e). The first effect will alter the two-dimensional nucleation rate, while the latter will interfere with the coverage rate of the interfacial monolayer; hence, both MNG and PNG kinetics are expected to be affected by the impurity. Moreover, the additional transport process occurring at the interface, as compared with those encountered in the moving "pure" interface must be considered because of interfacial segregation, as discussed elsewhere. The transport process is concerned with the diffusion of solute away from the interface on both the liquid and solid sides. On the other hand, the presence of the solute rich (or depleted, depending on the value of the partition coefficient) layer on the growth front alters the diffusional barrier for the host atoms in crossing the nucleus/L interface. The thickness of the interfacial solute rich layer, among other factors (i.e. steady or transient growth conditions) depends on the growth rate and the segregation coefficient k, as discussed later.

---

[*] Note that the impurity influence on the equilibrium thermodynamics of the system (e.g. melting point temperature, heat of fusion, etc.) are not considered here. Since this study is concerned with very dilute solutions, these effects are quite small.

As mentioned previously, however, the effect of the solute on the 2DNG kinetics is two-fold; either on σ_e or on υ_e. If the impurity bonds strongly to the crystal surface (relative to the solvent atoms), the nucleation process could be facilitated, for example, by nucleation of clusters around the impurity. In return, this process would permit measurable growth to take place in a region of supercoolings where the faceted (dislocation-free) interface is essentially immobile without the impurity atoms.[206]* Similarly, the adsorption of the solute atoms at the periphery of the two-dimensional cluster can reduce the value of σ_e, thus increasing the nucleation rate and, therefore, the growth rate. Although there is not any experimental proof regarding a particular trend concerning the effect of solute on σ_e, it is believed[70,207] that, if its concentration exceeds a certain limit, the edge free energy will be reduced. Based on this, the loss of the faceted character of the interface at high concentrations of solute is then understood. On the other hand, the presence of the solute at the smooth interface (as an adsorbed atom) can affect the spreading rate, υ_e, of the two-dimensional nucleus. The overall effect on the macroscopic growth rate then depends on the magnitude of υ_e.[208,209] If υ_e is small (for example, at low supercoolings), the solute atom will have enough time to be exchanged by a host atom, and the growth rate will not then be affected. However, if υ_e is large, the adsorbed impurities on the terrace will create an energy barrier for the step motion, thus lowering the rate.

---

* If the impurities enhance the nucleation process on all types of interfaces, the growth rate would then be less sensitive to orientation (smoothing agents).[206]

The above mentioned conclusions are rather qualitative, at least theoretically, in the sense that they do not provide a background to make any predictions for a given system. The complex and usually conflicting effects of the impurity on nucleation and growth mechanisms and the poorly understood adsorption phenomena (between the solute, the solvent, and the interfacial sites) make the problem quite difficult to treat analytically. Furthermore, this important and yet complicated problem has not been investigated in detail; the recent theoretical treatments on this subject mainly treat the diffusion controlled to diffusionless solidification[210,211] transition at rapid rates rather than the "impure" interfacial kinetics. Although there are several investigations concerned with the impurity effects in crystal growth from solution,[212-214] the number of experiments dealing with growth from the melt is very limited.

The effects of small additions of Al,[209] In,[215] Ag and Cu,[63] and other impurities (Sn, Zn)[216] on the growth kinetics of Ga has been studied. However, only the Ga-Al study[209] is complete in the sense that the effect of solute build-up on the growth rate was reported. In all cases but those of Ag and 20 ppm Al addition, it was reported that the effect of solute was to decrease the growth rate progressively as the percent concentration increased. It was also observed[63,209] that the faceted interface would occasionally break down as a result of excessive interfacial build-up. Growth in the presence of Al[209] and In[215] occurred by the 2DNG mechanism with the major effect of the addition believed to be on υ_e rather than on the step edge free energy. At higher concentrations and supercoolings[209,215] (i.e. 1000 ppm Al, .1 wt% In,

and $\Delta T \approx 2$-$2.5°C$), it was thought that the interface lost its faceted character.

Additions of Ag, Cu[63] caused a sharp increase in the growth velocity of the pure Ga and a replacement of the two-dimensional nucleation by the dislocation growth mechanism. The source of the dislocations was attributed to impurity segregation and separation of second phases ($CuGa_2$, for example).

Whether the adsorption of the impurity on different crystal facets changes, resulting in habit modifications, is not clearly understood as yet. During growth of Si[217] and GaAs,[218] such effects have been observed. Although the role of impurities is quite important during growth of facet forming materials, there have been very few studies devoted to this field of research and the essential features of growth in the presence of impurities are not very well understood. Theoretical interpretations are not yet possible, but based on experimental results some interpretations allow for guidelines regarding the possible solute effects on the growth kinetics. However, aside from the technical point of view, the role of impurities is worth further investigation for the better comprehension of the crystal growth mechanisms, and, most importantly, of the S/L interface.

Transport Phenomena During Crystal Growth

Growth of a solid from the liquid phase involves two sets of processes; one on the atomic scale and the other on the macroscopic scale. The first is associated with the interfacial atomistic processes. The second involves the transport of matter (solute, impurities) and latent

heat away from the interface through the crystal and/or the undercooled
liquid.

It is well recognized that macroscopic mass and heat transport play
a very important role in crystal growth processes. Up to now, the
microscopic processes were examined, i.e. how molecules cross the S/L
interface and attach themselves to the crystal and how this process is
governed by the driving force and the nature of the interface. However,
for the molecules to reach the growth sites, they are transported in the
liquid by diffusive and/or convective fluxes over macroscopic distances.
The interface velocity at the same time depends on how fast the heat of
fusion is transported away from the growth front, on the concentration
of species present, and the nature of the interface. Hence, the rate
with which the interface advances is a coupled interfacial kinetics and
macroscopic transport process. This section is concerned only with the
macroscopic transport processes. The subjects that will be discussed
are interfacial heat transfer, segregation, and morphological stability
in relation to the growth of both the pure and doped materials.

Heat Transfer at the S/L Interface

The rate at which the heat of fusion can be removed away from the
growth front depends on the specifics of the experimental set-up and the
thermal properties of the solid and liquid. Whether or not this rate is
greater than the interfacial kinetics determines whether the growth is
limited by the interfacial kinetics (kinetics controlled) or by heat
transfer (heat flow controlled).   However, in many occasions during
growth from a supercooled melt, regardless of the thermal arrangements,
the growth is a heat flow-interface kinetics coupled process. Including

the growth kinetics in the transport (Stefan[219]) problem, the coupled boundary conditions at the interface can be described as[220]

$$\Delta T = \Delta T_b - h_c V, \quad \Delta T_b \geq \Delta T \geq 0$$

$$V = f(\hat{n}, T_i), \quad f(\hat{n}, T_m) = 0$$

where h_c is a heat transfer parameter to be described later and the function f depends upon the specific growth mechanism by which the interface advances. For faceted materials, the interface supercooling is appreciable so that the assumption of local equilibrium ($T_i = T_m$) does not apply. The interfacial supercooling ΔT may be a small fraction of other temperature differences within the system and, most importantly, of the bulk supercooling, ΔT_b, as shown in Fig. 11a. The interfacial conditions are even more complicated when growth involves additional matter transport, e.g. during growth from a supersaturated solution, schematically shown in Fig. 11b. Since the interfacial temperature (T_i) is higher than the bulk temperature (T_b), the growing interface has a higher equilibrium concentration (c_i^e) than that of the bulk (c_e). At the same time, the solute diffuses from the supersaturated solution (c_∞) to the growing interface, resulting in an interfacial composition of c_i. Although the magnitude of c_i depends, among other factors, on the growth rate and convection, it is the difference $\Delta c = c_i - c_i^e$ which governs the interfacial processes and, therefore, has to be evaluated in order to determine the growth kinetics.[221]

Since a direct measurement of the interfacial supercooling (S/L) is a difficult problem, most experimental investigations disregard the essential role of interfacial supercooling and describe growth kinetics in terms of the "Bulk Kinetics," i.e. the relationship $V(\Delta T_b)$.[222] As an
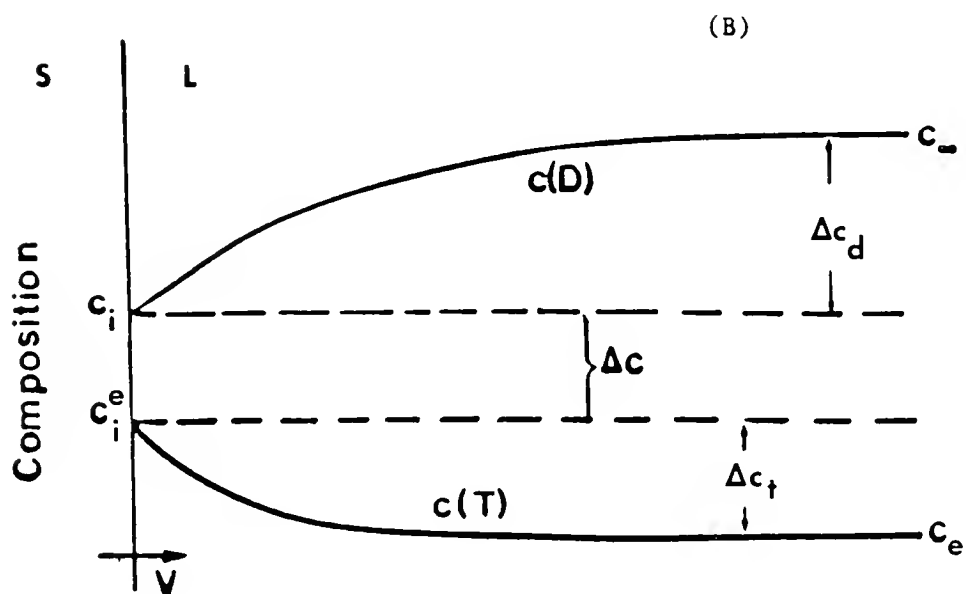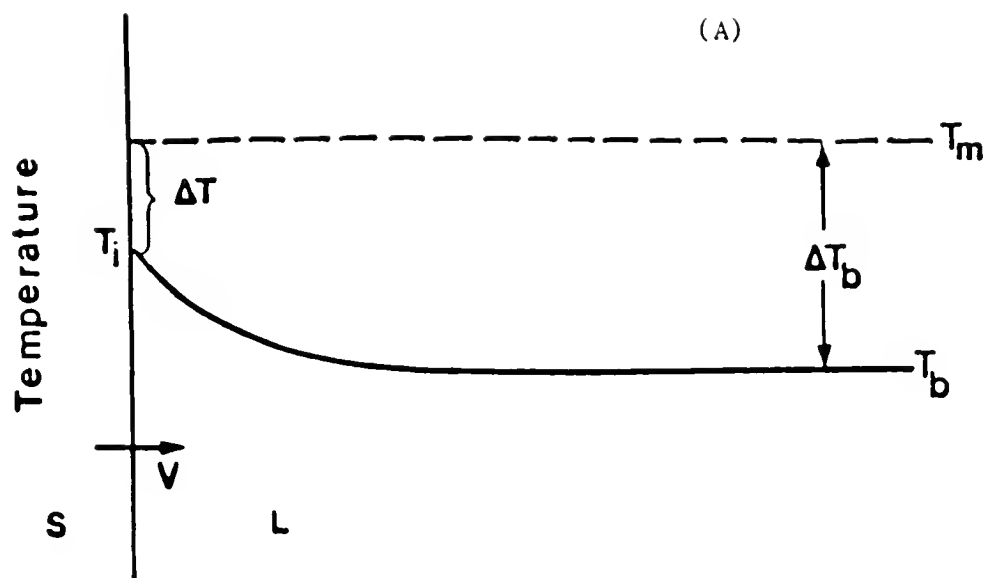
Figure 11 Heat and mass transport effects at the S/L interface.
a) Temperature profile with distance from the S/L inter-
face during growth from the melt and from solution. b)
Concentration profile with distance from the interface
during solution growth.

example, the bulk kinetics of Ni^{201} are shown in Fig. 12 for bulk super-coolings up to ~240°C. The ΔT_b dependence of V in the range of 0-175°C supercoolings can be approximately described by a $K_b(\Delta T_b)^2$ law with K_b = .14 cm/s(°C)^2. In comparison, a growth law of .28 $(\Delta T_b)^{1.8}$ has been determined from another investigation[223] for ΔT_b's in the range 20-200°C. However, calculations based on heat transport limited growth rates[200] and an upper limiting kinetic coefficient based on the speed of sound in the melt indicate that the interfacial supercooling is only a small fraction of ΔT_b, e.g. it is 26°C when the bulk supercooling is 175°C. Hence, the bulk kinetics relation in no way provides accurate information, even in a qualitative sense, as far as crystal growth kinetics is concerned, and may also be misleading[2,25,26,153] when a comparison is attempted with the existing theoretical treatments for crystal growth. This can be understood, considering that for growth into undercooled melts a parabolic relationship in the form of

$$V = K_b \, \Delta T_b^2 \tag{51}$$

is commonly obtained.[63] The above mentioned relationship could represent different growth mechanisms. For example, in the case of dendritic growth, a simple solution of the governing heat flow equations (neglecting interfacial kinetics) predicts[17] a growth rate that has an approximate parabolic dependence on the bulk supercooling. Another example is the growth rate by the dislocation mechanism, as discussed previously, which can also be a parabolic function of the supercooling.

Another difficulty in using bulk kinetics is that the value of the coefficient K_b depends on heat transfer conditions, sample and inter-face geometry, and the specifics of the experimental set-up. This
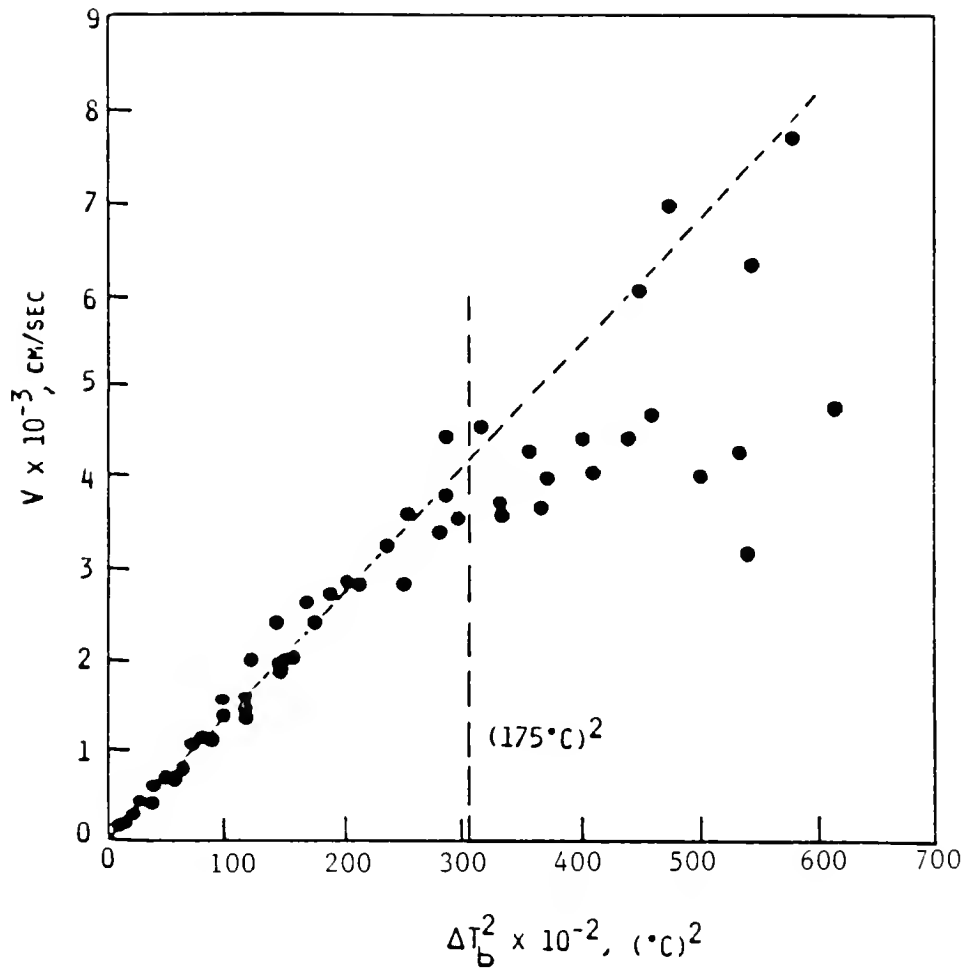
Figure 12 Bulk growth kinetics of Ni in undercooled melt.
After Ref. (201).

complicates interpretation of results and may explain the contradictory conclusions reached by various investigators on the growth mode and kinetics. The disagreement between kinetic coefficients found from various investigations for the same material is very common indeed. (See, for example, the reported kinetics laws for melt growth of Sn.[63,222a,224-231])

Morphological Stability of the Interface

The purpose of this section is to present an overview of theoretical and some experimental work on the morphological stability of the S/L interface during melt growth. The emphasis will be on the assumptions, conclusions, and predictions (in analytical forms) rather than the mathematical details of the topic, which are available in several reviews.[232-236] A detailed discussion of the stability analysis will be given only for the case of supercooled pure melt. An understanding of the morphological stability of the S/L interface during solidification in terms of all the pertinent, i.e. thermodynamic, kinetic, thermal, and hydrodynamic parameters, is essential for predicting the interface morphology on a microscopic scale.

Instability of a planar interface occurs whenever the shape of a smooth growing interface develops protrusions, depressions, or undulations, primarily because of the "point effect" of heat and/or solute diffusion. From the practical point of view, stability theories are to decide whether a growing flat interface will remain flat or will become irregular, cellular, or dendritic and therefore structurally and compositionally inhomogeneous under given growth conditions.

Until now, two fundamentally different theoretical approaches have been used to describe the interface stability. The first is the constitutional supercooling (CS) theory[237,238] which is based on an equilibrium thermodynamics argument describing the solute-rich (or depleted) liquid adjacent to the S/L interface. The stability criterion of this static analysis, which assumes a constant growth velocity (V) and no convection and solute diffusion in the solid is expressed as

$$\frac{G_L}{V} > \frac{C_\ell^* \; (1 - k) \; (-m)}{D} \qquad \text{(stable)} \qquad (52)$$

Here G_L is the thermal gradient in the liquid, D is the solute diffusion in the melt, and k is the equilibrium distribution coefficient, assumed to be independent of growth rate and kinetics. Here, the case of $k < 1$ only is considered and, thus, the liquidus slope m is negative in sign. C_ℓ^* is the liquid composition at the interface, which, for the equilibrium steady state conditions assumed by the CS theory, is given as

$$C_\ell^* = \frac{C_s^*}{k} = \frac{C_o}{k}$$

Here, C_s^* is the solid composition and C_o is the initial composition at the interface of the melt. Hence, eq. (52) can be rewritten as

$$\frac{G_L}{V} > \frac{C_o \; (1 - k) \; (-m)}{Dk}$$

or as

$$G_L > m \; G_c \qquad (53)$$

where G_c is the composition gradient at the interface and is given as

$$G_c = - \; \frac{V \; (1 - k)}{Dk} C_o$$

In the case of the solidification of pure material, $G_c = 0$, so eq. (53) can be written as

$$G_L > 0$$

Thus, for solidification into a supercooled liquid ($G_L < 0$), the constitutional supercooling criterion always predicts instability. Also, since the instability is predicted to be proportional to the growth rate, the interface is expected to be unstable during rapid solidification of alloys.

The second theoretical approach on the morphological stability (MS) of the interface is based on the dynamics of the entire process.[239-242] In this approach, small perturbation, which can be a temperature, concentration, or shape fluctuation at the S/L interface, is imposed on the system. When the mathematical equations are linearized with respect to perturbation, in order to make the problem solvable, the time dependence of the amplitude of the perturbation is calculated under given growth conditions. If the perturbation grows, the interface is unstable, while if it decays, the interface is stable. The morphological instability problem is then solved by taking into account CS, surface tension ($\sigma_{s\ell}$) and transport of heat from the interface through both the liquid and the solid. Assuming constant velocity during unidirectional solidification of a dilute binary alloy in the z-direction, the perturbation of the interface is given as

$$z = \delta \exp(\sigma t + i(\omega_x x + \omega_y y))$$

where δ is the perturbation amplitude and $\omega_{x,y}$ are its spatial frequencies. The interface is unstable if the real part of σ is positive for any perturbation (the imaginary part of σ has been shown rigorously to vanish[243] at the stability/instability demarcation ($\sigma = 0$)). The value of σ for local equilibrium conditions and isotropic S/L interface is given as[240,244,245]

$$\sigma = \frac{V\{- K_L G_L (\alpha_L - \frac{V}{\kappa_L}) - K_s G_s (\alpha_s + \frac{V}{\kappa_s}) - 2\, \bar{K} T_m \Gamma \omega^2 \bar{\alpha} + 2\bar{K} m G_c \bar{\alpha}(\alpha - \frac{V}{D})\, (\alpha - p\frac{V}{D})^{-1}\}}{L_v V + 2\bar{K} m G_c \bar{\alpha}(\alpha - p\frac{V}{D})^{-1}}$$

$$(eq. \ (54))$$

with

$$\alpha = (\frac{V}{2D}) + [(\frac{V}{2D})^2 + \omega^2 + \frac{\sigma}{D}]^{1/2}$$

$$\alpha_L = (\frac{V}{2\kappa_L}) + [(\frac{V}{2\kappa_L})^2 + \omega^2 + \frac{\sigma}{\kappa_L}]^{1/2}$$

$$\alpha_s = -(\frac{V}{2\kappa_s}) + [(\frac{V}{2\kappa_s})^2 + \omega^2 + \frac{\sigma}{\kappa_s}]^{1/2}$$

$$\bar{\alpha} = \frac{(K_s \alpha_s + K_L \alpha_L)}{(2\bar{K})}$$

$$\bar{K} = \frac{K_s + K_L}{2}$$

$$p = 1 - k$$

$$\Gamma = \frac{\sigma_{s\ell}}{L_v}$$

where G_s is the solid thermal gradient, $K_{L,s}$ and $\kappa_{L,s}$ are the liquid and solid thermal conductivities and diffusivities, respectively, L_v is the latent heat of fusion per unit volume, and T_m is the melting point in the absence of a solute.

In eq. (54) both terms in the denominator are always positive (k < 1). Therefore, the planar[246-252]* interface is unstable or stable depending on whether or not the numerator ever becomes positive. The numerator consists of four terms proportional to G_s, G_L, Γ, and G_c. For the usual case of positive temperature gradients (solidification of super-heated liquids), the thermal terms (first two terms) are negative, thus promoting stability. The surface tension term (third term) is always negative, therefore also favoring stability. The compositional gradient term (fourth term) is positive. Hence, instability happens when the de-stabilizing effect of the solute term is large enough to overcome the stabilizing influences of thermal gradients and surface tension.

In most practical cases, a sufficient and necessary condition for stability (after neglecting the surface tension term that becomes important at high growth rates as discussed later) is[240]

$$\frac{K_L G_L + K_s G_s}{K_s + K_L} > m\, G_c \tag{55}$$

which is the modified constitutional supercooling (MCS) criterion as compared with the original CS criterion given in eq. (53). The MS stability criterion is usually also expressed as

$$\frac{2K_L}{K_s + K_L} \frac{k}{(1-k)} \left(\frac{L_v}{2K_L} + \frac{G_L}{V}\right) \frac{D}{(-m)\, C_o} > S(A,k) \tag{56}$$

where S is the stability function[244] that ranges from 0 to 1 and A is a dimensionless parameter given as

$$\frac{k^2}{1-k} \frac{\Gamma V}{D} \frac{T_m}{(-m)\, C_o}$$

---

* There is a large number of theoretical work regarding the stability of a non-planar interface; the two geometries that have been studied the most are the spherical[246-249] and the cylindrical.[250-252]

Both CS and MS theories are very similar for the case of A < 0 (neglecting capillarity effect or low growth rates) and S ≃ 1 since both stability expressions (56) and (53) become identical by setting $K_L = K_s$ in eq. (56). The theories differ appreciably however, for S < 1 and in particular for large A (high growth rates); when S → 0, the interface is stable for all G_L/V below a critical concentration, as predicted by the absolute stability criterion that will be discussed next.

Absolute stability theory during rapid solidification

The situation where the CS and MS theories differ is the case of rapid solidification, where the MS theory[240] and its extended forms[253,254] predict an increased form of stability known as absolute stability. At high growth rates because of the limited time for solute diffusion away from the interface, instability can only occur for per-turbations at the S/L interface with very short wavelengths.[240] This, however, requires such a large increase in the area of the interface that the perturbations are stabilized by surface tension forces. The critical velocity is given by the expression

$$V = \frac{mD(1 - k)C_o}{k^2 T_m \Gamma} \quad (57)$$

Whenever V exceeds the value given by eq. (57), a planar S/L interface is stable. There are, however, several restrictions[255] on using eq. (57). First, eq. (57) is only valid if the interface is at local equilib-rium and k is the equilibrium partition coefficient. When k depends on the growth rate and/or the growth kinetics, which is the case during rapid solidification and solidification of facet forming materials (see the discussion in the next section), eq. (57) has to be modified

accordingly.[245]   The second restriction regarding the analytical form of absolute stability is that the net heat flow must be into the solid.

$$(i.e. \ \frac{K_L G_L + K_s G_s}{2\overline{K}} > 0).$$

The third one is that to use this criterion the conditions must be such that the regime of interest is far from the MSC regime.

Effect of interfacial kinetics

The effect of interfacial kinetics on morphological stability has been treated by several researchers[256-260] by incorporating non-equilibrium (kinetic) effects at the appropriate interfacial boundary conditions of the heat-flow and diffusion equations.   These treatments include growth rate and kinetics dependent interfacial supercooling and partition ratios.[261-263]*   (This subject will be treated in more detail in Appendix III.)   Briefly, the analysis indicates that, for small supercoolings (i.e. $V = f(\Delta T)$ and k is given by the phase diagram), the numerator of eq. (54) remains unchanged, but the denominator is increased by an extra kinetic term[253]

$$\mu_T = \frac{\partial f}{\partial(\Delta T)}$$

For slow kinetics (small μ_T), this term leads to a reduction of the velocity at which the perturbation grows; in other words, a larger value of concentration, as compared to the case of local equilibrium, is needed for instability at fixed V.   For fast kinetics ($\mu_T > 5$ cm/s°C), on the other hand, not only the stability/instability demarcation, but also the magnitude of σ (eq. (54)) are unaffected by the growth kinetics.

---

* Convection effects on k leading to longitudinal and lateral instabilities have also been incorporated in the stability analysis during unidirectional solidification.[261-263]

Furthermore, anisotropic interfacial kinetics leads to the translation of the perturbations parallel to the interface as they grow, with their peaks at an angle to the growth direction.[259] This conclusion may explain to the existence of preferred directions for cellular and dendritic growth.

Stability of undercooled pure melt

During solidification of a pure liquid, morphological instability of the planar growth front can occur when the melt is supercooled. Instability then arises from thermal supercooling rather than the constitutional supercooling; this is because the outflow of the latent heat into the supercooled liquid is aided by the protrusions and impeded by the intrusions at the interface ("point effect").

During solidification of an undercooled melt, the CS criterion always predicts instability, in contrast with experimental observations. According to the morphological stability theory, however, the interface can be stable despite the melt supercooling ($G_L < 0$) if G_S is sufficiently large (see eq. (55)). Providing that the thermal steady state approximation holds ($K_L G_L + K_S G_S > 0$) and the kinetics effects are negligible, the original MS criterion can be used to predict morphological instability conditions of the interface by setting G_C equal to zero. The remaining terms then in the stability criterion are the destabilizing thermal field and the stabilizing capillarity term.

Under conditions for which $K_L G_L + K_S G_S < 0$, detailed analysis shows that the thermal field is stabilizing for large wavelength perturbations ($\omega \to 0$) and is destabilizing for small wavelengths ($\omega \to \infty$). Since the capillarity term is always stabilizing and is rather important for large ω, it is concluded that the interface will most likely be stable at low

growth rates ($\omega \propto V$); at high growth rates interfacial stability will depend on the competitive effects of the thermal and the capillarity fields.

Incorporation of the effect of interfacial kinetics on the stability leads to conclusions analogous to those mentioned earlier that the stability-instability demarcation is virtually unaffected by the kinetics. Slow kinetics are expected to enhance stability, while rapid kinetics will have little effect on it. The mathematical analysis that leads to the above mentioned conclusions will be given in Appendix III.

Experiments on stability

The commonly used procedure to verify the CS and MS predictions is to plot G_L/V vs. C_O and determine the demarcation line between the cellular or dendritic substructure region and that with no substructure. The slope of the experimental line can then be compared to those of the CS and MS theories according to eqs. (53) and (55). However, the theoretical slopes are related to the diffusion coefficient D, which is often poorly known, and to the partition ratio k. Because of the above, and also the fact that the predictions of both theories are almost identical at low growth rates (or small G_L/V), it is difficult to discriminate the CS and MS theories as far as agreement with the experimental results is concerned. Nevertheless, there are several experiments which are supportive of dynamic theories. These include direct observation of the interface shape during evolution of instability[264],[265] and determination of the onset of the instability while varying the growth conditions.[266-269] The influence of thermal diffusion[270] (Soret effect) at large thermal gradients, convection,[271] thermosolutal convection under microgravity conditions,[272] and recent experimental results during rapid

solidification[273,274] are also other studies supporting the MS theory. It is generally agreed that, at low G_L/V values, experimental findings agree with the CS theory (or MCS criterion), while at high G_L/V values, the stability of the interface is in accord with the MS theory;[275,276] however, the experimental verification of the effect of non-equilibrium interfacial conditions upon the interfacial stability is still pending from the experimental point of view, mainly due to the lack of knowledge regarding the relationships $V(\Delta T)$ and $k(V, \Delta T)$.

Segregation

Partition coefficients

During solidification in the near-local equilibrium limit, the composition of the solid and liquid at the interface may be represented by the equilibrium phase diagram. The segregation coefficient k_o is then defined as

$$k_o = \frac{C_s}{C_\ell} \tag{58}$$

where k_o is generally a function of temperature, but can be treated as constant when the solidus and liquidus lines of the phase diagram are nearly straight. When the interface is not planar but has a curvature, R, the equilibrium coefficient k_o is expected to scale as

$$k_o(R) = k_o(1 + \Gamma R)$$

where Γ is the capillarity constant.

In the case of finite growth rates, however, the interfacial composition on either side of the S/L interface can no longer be represented by the equilibrium phase diagram since the solid forms at a temperature lower than that of the equilibrium because of the interfacial kinetics discussed earlier. Furthermore, solute trapping also may take place,

causing the solid composition to differ from the equilibrium one. The actual distribution coefficient k is related to the equilibrium one, the velocity and the interface supercooling of the advancing interface as

$$k = k_o f(V, \Delta T, \hat{n}) \qquad (59)$$

where the function f depends on the model under consideration and has to be determined for each model. It is obvious that for local equilibrium conditions (i.e. $V \to 0$, $\Delta T \to 0$) $f(0, 0, \hat{n}) = 1$. On the other extreme, at high growth rates or large deviations from equilibrium, no segregation should occur according to the solute trapping theories,[254],[277-279]* and, therefore, $f \to 1/k_o$ (i.e. $k \to 1$) as $V \to \infty$. For faceted materials, non-equilibrium segregation can be obtained even at low growth rates, since large undercoolings are required for finite growth rates when the growth mechanism is of the stepwise type. This manifestation of segregation anisotropy during growth from the melt has been experimentally observed[219a] in several doped semiconducting materials. This form of anisotropy is also referred to as the facet effect that expresses the verified common trend for higher solute concentration on facets than in off-facet areas of a macroscopic interface. Several mechanisms have been suggested to account for the interfacial segregation on faceted interfaces.[34],[280-283] Most of these theories involve an adsorbed layer and are based upon the difference of the lateral and continuous growth kinetics in order to explain the facet effect. The analytical result of such a model,[281],[283] is given as

$$k = k_o + (1 - k_o) \exp(-\frac{V_D}{V}) \qquad (60)$$

---

* The review of the solute trapping theories and related experiments is beyond the scope of the present review.

where V_D is the diffusive speed (i.e. $V_D = D/h$). The above equation predicts that $k \to k_o$ when $V \ll D/h$ (~5 m/s for Ga (111) interface) and $k \to 1$ when $V \gg D/h$. Although this model has been shown to agree with experiments of high growth rates ($V \geq 1$ m/s),[284] it cannot explain the observed increase[283] in k at much lower rates (~1 μm/s) than the diffusive speed, assuming that $D_i \simeq D$. It is clear that k depends more strongly on the interfacial supercooling (or growth rate) rather than the interface orientation. For example, if a macroscopic interface grows at an average constant rate (e.g. Czochralski technique), its faceted and non-faceted regions will have equal growth rates. Accordingly, the facets will require a much higher supercooling than the off-facet area if it grows by the 2DNG mechanism; the larger driving force, in turn, results in a higher k value. Alternatively, for a given growth rate, the growth direction "determines" the magnitude of the required driving force; therefore, orientation affects k indirectly through growth kinetics. Other factors that are expected to affect k are[282] i) the relative mobility of the solute and solvent atoms and ii) the bonding strength of the solute atom to the crystal.

Solute redistribution during growth

This section is related to the bulk mass transfer during unidirectional growth when the melt is convection free or that the solute transport in the liquid is purely diffusive. The composition of solid and liquid as a function of distance solidified is shown in Fig. 13. The initial region of the solid before reaching C_o composition (steady state) is termed transient with a characteristic distance in the order of D/kV. The last part of the solidified ingot is the final transient with a

105
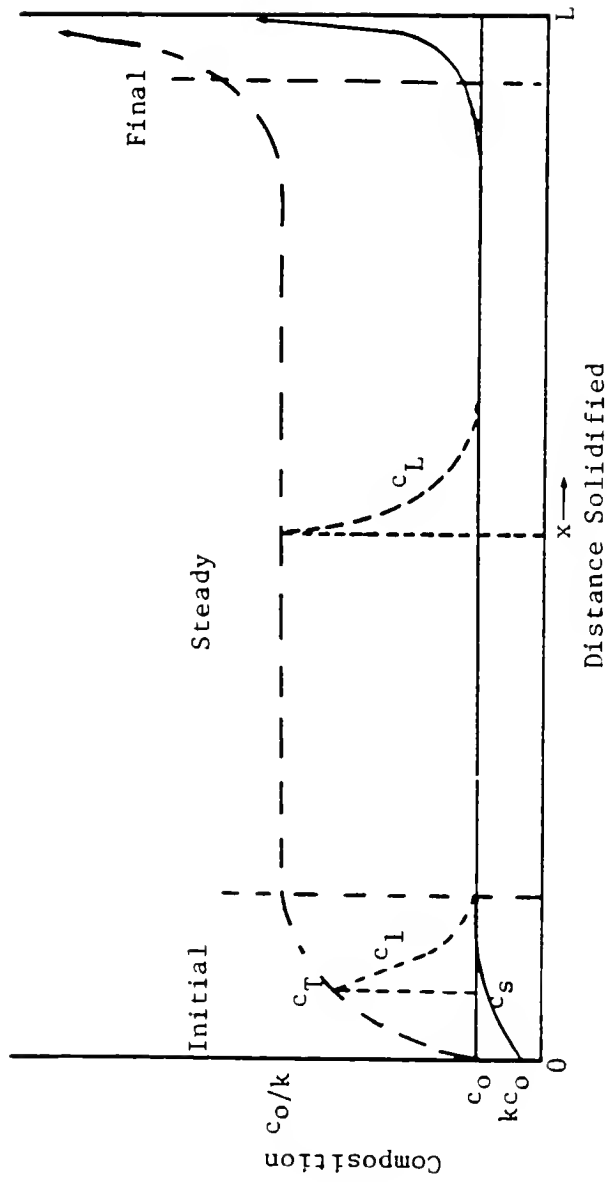
Figure 13 Solute redistribution as a function of distance solidified during unidirectional solidification with no convection.

characteristic distance about D/V. The solute concentrations in the liquid ahead of the interface for small values of k are given as[285,286]

$$C_L = C_0 \{ 1 + (\frac{1 - k}{k}) \exp(- \frac{Vx'}{D}) \} \qquad (61)$$

$$C_\ell = C_0 \{ \frac{1 - k}{k} [1 - \exp(- \frac{kVx}{D})] \exp(- \frac{Vx'}{D}) + 1 \} \qquad (62)$$

for the steady and the initial transient regions, respectively. Here x' is the distance from the interface into the liquid and x is the distance from the onset of growth. In both regions the solute profile decays within a distance D/V from the interface. However, since there is usually convection in the melt, as discussed later, the solute transport is purely diffusive only within a distance δ from the interface; beyond this distance the liquid is mixed by convection flows. Under such conditions, the distribution coefficient k_0 is replaced by an effective distribution coefficient, k_{eff}, defined as[287]

$$k_{eff} = \frac{k_0}{k_0 + (1 - k_0) \exp(- \frac{V\delta}{D})} \qquad (63)$$

Note that the equilibrium coefficient k_0, is usually used in calculating k_{eff}.

Convection

Macroscopic mass and heat transport play a central role in crystal growth processes. Fluid flow is beneficial to crystal growth, by reducing the diffusional barriers for interfacial heat and matter transport, provided that the flow is uniform (steady state). However, because of the complex geometries and boundary conditions, as well as the adverse vertical and nonvertical thermal fields encountered in crystal growth,

the detailed effects and nature of convection in these processes are not fully understood yet, and their understanding is likely to be limited at this point. In this section, a qualitative review of some convective phenomena during unidirectional solidification of a dilute alloy is given, in order to provide some background for the discussion related to the growth kinetics of the In-doped Ga. For complete information regarding this subject, the reader is referred to review papers[288-290] and books.[219a,291,292]

During crystal growth of multicomponent systems, temperature and compositional gradients needed to drive heat and mass flows. However, these gradients induce variations in the properties of the liquid from which the crystal grows. The most important property that changes is the density. In a gravitational field, a density gradient will always result in fluid motion[293] when the gradient is not aligned parallel to the gravity force. This type of flow is called natural or free convection; it is driven by body (buoyancy) forces (e.g. gravitational, electric, magnetic fields) and/or surface tension as contrasted with forced convection that arises from surface[*] (contact) forces.

Density gradients in a fluid can be due to existing thermal gradients, since density increases as temperature decreases (thermal expansion). The resulting convection is termed thermal convection. However, during growth of a multicomponent system, a density variation can be caused by compositional differences due to, for example, the interfacial

---

[*] Surface tension should not be confused with surface forces that require direct contact between matter elements. An example of surface force is the frictional force exerted from the rotating crystal on the melt during pulling.

segregation process. This form of convection is called <u>solutal</u> convection. When convection is caused simultaneously by thermal and concentration gradients, it is usually termed as <u>thermosolutal</u>. Other convective phenomena that occur during crystal growth are due to a) surface tension gradients along free surfaces (Marangoni convection), b) thermal diffusion of species in a solution in the presence of temperature gradients (Soret effect),[*] and c) externally applied body-forces other than gravity.

A fluid in a vertical configuration is statically stable if the density decreases with height, and is unstable for the reverse case. A statically stable density gradient does not cause convection. On the other hand, an unstable profile will cause convection when the density gradient is larger than a critical value necessary to initiate flow (i.e. to overcome the viscous forces). Following the thermal, solutal, and thermosolutal convection during unidirectional growth of a dilute alloy, that grows parallel or antiparallel to the gravity vector and whose solute density is higher than that of the solvent will be examined. This case is related to the present experiments on In doped-Ga, as will become apparent later. For different cases under the same principle, reference is made elsewhere.[294,295]

For unidirectional solidification of an undercooled alloy melt that grows upwards, as shown in Fig. 14a, the liquid is heated from below (i.e. hot at the interface and cold away from it) and the temperature

---

[*] Note that the compositional differences caused by the Soret effect will not be maintained when convection begins.
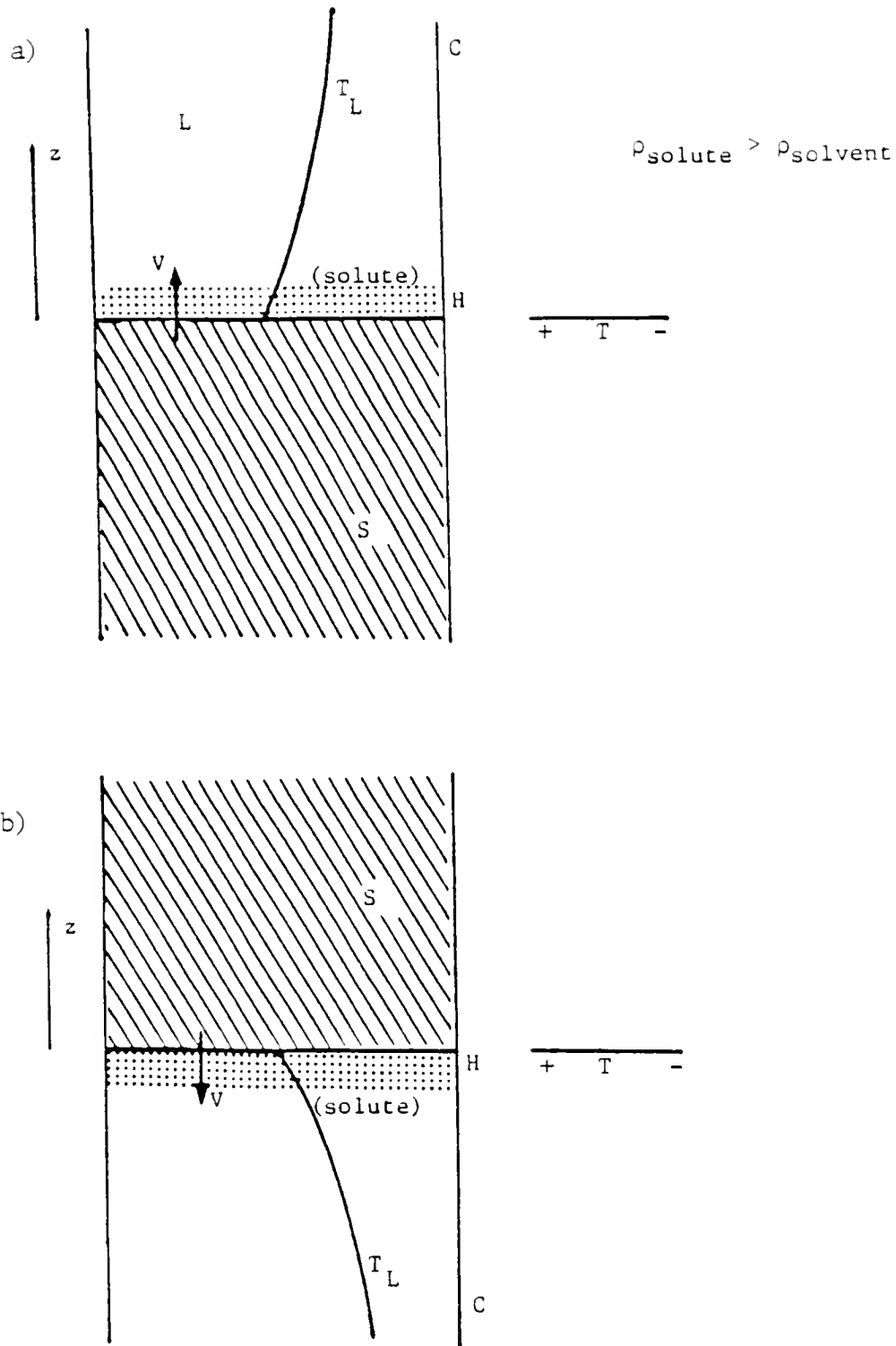
Figure 14 Crystal growth configurations. a) Upward growth with
negative G_L. b) Downward growth with positive G_L. In
both cases the density of the solute is higher than the
density of the solvent.

gradient, G_L, is negative. Assuming that the alloy is also of such composition that $k < 1$, there is more concentration of solute at the interface upon growth; hence, the solute gradient, G_c, is also negative. Considering the negative temperature gradient separately, it is realized that it would result in a positive density gradient (i.e. ρ_ℓ increases with distance from the interface) that makes the liquid statically unstable. The negative solute gradient alone would cause a negative density gradient (since the solute is assumed to be more dense than the solvent), stabilizing the liquid. The net liquid density profile then depends on the relative magnitude of the thermal and solutal gradients. Since the solute concentration decreases as $\exp(-D/V)$ away from the interface, the compositional gradient is important only within the decay distance (D/V). The temperature gradient on the other hand, decays with κ_L/V, which is much larger than the previous decay distance. Accordingly, convection may occur, depending on how large the temperature gradient is.

The second case to examine is the reverse of the first one, where the interface moves downward, as shown in Fig. 14b. Here, the positive thermal gradient (hot on top of cold) results in a negative density gradient, while the positive solute gradient leads to a positive density gradient. Thus, solutal convection may arise in this case, depending on the relative magnitudes of $\Delta\rho/\Delta c$ and $\Delta\rho/\Delta T$, only within a distance in the order D/V (or, more precisely, $2D/V$, which is the distance at which C_ℓ reaches $.93\ C_o$) away from the S/L interface.

Next, consider a disturbance of the bottom fluid[288,295] that makes a fluid element rise for both configurations. Since the thermal

diffusivity is much greater than the chemical diffusivity, the fluid will gain or lose heat much faster than solute. Thus, in the first case (upwards growth), the element will still be more dense than its new surrounding and will tend to return to its original position, i.e. at the interface. This is the case of an oscillatory instability. However, for the case of downward growth, the element that rises from the bottom is less dense than its surroundings because of the segregation profile, and, therefore, it will continue rising. Hence, convection may occur even though the overall density profile is stable.

Studies of thermosolutal convection in crystal growth experiments rely upon measuring segregation profiles and comparing them with those predicted theoretically. For example, macrosegregation profiles observed during unidirectional growth of Pb-Sn (Pb rich),[296] Al-Ti and Al-Cr,[297] Al-Cu and Al-Mg,[298] and Mn-Bi[299] have been correlated with thermosolutal convection. In these studies, all but the last study (Mn-Bi), growth took place upwards and for conditions of destabilizing solute gradients and stabilizing thermal gradients. For the Pb-Sn system, the boundary layer thickness (δ) was found to be independent of growth rate (.8-5.7 μm/s) and sample size (.3-.6 cm diameter) and equal to ~65 μm (< D/V for the rates studied). For the Al-Ti and Al-Cr experiments, it was concluded that convection is only important at low growth rates. This was based on the fact that, although for the Al-Cr experiments the gradient $d\rho/dx$ was larger than that for the Al-Ti system, convection affected solute segregation of the former at the growth rates around 15 μm/s, while for the latter convection was significant at much lower solidification rates (<1.8 μm/sec).

For the Al-Cu experiments,[298] the δ values (200-400 μm) appeared to be insensitive to the growth rates, but sensitive to the gradient and initial composition (for fixed C_O, $\delta\uparrow$ as $G_L\downarrow$ and for given G_L, $\delta\downarrow$ as $C_O\uparrow$). The Mn-Bi (Bi rich) system was studied solidifying both upwards and downward; the former resulting in solutal and the latter in thermal convection. As expected, a higher degree of convection was observed for the solutally unstable configuration. The determined δ (~250 μm) values were found to increase with concentration (note that here k > 1) and slightly with the growth rate. However, the important effect of the liquid gradient was overlooked in this study.

Experimental S/L Growth Kinetics

Shortcomings of Experimental Studies

Despite the numerous experimental studies reported over the past years, little conclusive information is available regarding crystal growth kinetics from the melt. To a large extent this is a consequence of the fact that experiments for melt growth kinetics, particularly for metals, are difficult. The difficulties associated with S/L interfacial kinetics are: high melting temperatures, opacity, impurities, sample perfection, i.e. the structural and chemical homogeneity of the sample, and, most importantly, the determination of the actual temperature at the interface. The latter because of its importance will be discussed separately next. There are also several shortcomings in interpreting growth kinetics results. This is because in most studies a) the S/L interfacial kinetics are "confused" with the bulk kinetics, b) the kinetics measurements are not carried out over a wide enough supercooling

range, c) the perfection (dislocation-free vs. dislocation-assisted) or morphology of the interface are not reported, and d) certain critical data such as L, $\sigma_{s\ell}$, $\eta(T)$, crystal structure along the growth direction, etc. were unavailable.

The methods of determination of the growth rate during crystal growth are: 1) optical measurements via a microscope by directly observing and timing the motion of the interface; 2) resistometric,[228] which utilizes the resistance change across the sample during growth; 3) photocells, where the passage of time of the growth front for a certain length is determined with the aid of two or more photocells;[63] 4) high-speed photography of the advancing interface and subsequent frame by frame analysis; and 5) conductance, which is related to the thickness of a molten layer so that the growth velocity can be calculated from the current transient.[300] During constrained growth experiments, the steady state growth rate is usually assumed to be equal to the rate with which the thermal zone moves along the sample. In the present study, methods (1) and (2) were utilized, as it will be further discussed later.

Interfacial Supercooling Measurements

Several methods of direct or indirect determination of the S/L interface temperature have been attempted in the past. The most commonly used direct method consists of embedding a thermocouple probe in the crystal or the melt.[100] However, the presence of the thermocouple not only disturbs the thermal and solutal fields at the interface, but it also affects the actual growth process; in several cases it has been reported[63] that thermocouples were used to intentionally introduce dislocations. Moreover, in controlled solidification experiments, this

technique is limited by the sharpness of the break in the temperature-time curve as the interface passes the thermocouple.

The thermal wave technique[301] was developed to evaluate the growth rate and interface supercooling from measurements of the attenuation of a periodic thermal wave, induced in the liquid, as it travelled through the S/L interface. The periodic variation at the interface allows only for determination of the supercooling, i.e. absolute temperature measurements cannot be made. Aside from the experimental difficulties, this technique has been subjected to criticism[302-304] as it induces convection flows in the melt and it does not account for thermal losses along the container walls. Moreover, it is restricted to small growth rates (< 50 μm/s)[301] and the reported kinetics using this technique[224,225] have been conflicting. Later, a similar method was proposed[305] that determines the growth parameters from an analysis of the response of the interface to a periodic heat input, introduced by using Peltier heating or cooling. Experimental results based on this technique have not been reported in spite of the fact that the Peltier effect has been widely used, particularly with semiconducting materials, during crystal growth related experiments.[306]*

The single and double thermoelectric probe technique was proposed[307] for measuring the interfacial temperature and velocity during growth in a pure material. This method, which also disturbs the actual growth process, is applicable under constrained growth conditions (i.e. G_L must be known). The accuracy of the technique depends on the Seebeck

---

* These experiments are not concerned with growth kinetics and, therefore, are not reviewed here.

coefficients of the solid and the liquid, the probe material, and the thermal field within the sample, as well as on the experimental details. This method has been further used[308] to determine the growth rate during constrained growth of Sn, Bi, and Sn-Pb.

Another method of determining the interface temperature relies upon mathematical analysis of heat flow conditions at the moving S/L boundary during unconstrained growth into a supercooled melt.[2,178,181] For these cases, the bulk and interfacial supercoolings are related via a temperature correction as

$$\Delta T = \Delta T_b - h_c V, \ \Delta T_b \geq \Delta T \geq 0$$

where h_c is the parameter representing the interfacial heat transfer coefficient which depends on the experimental design and the physical and thermal properties, such as latent heat, thermal conductivities, and densities of the materials involved. There are a few developed heat transfer models[2,178,181] that allow for calculation of h_c and, therefore, of ΔT if ΔT_b and V are measured (see detailed discussion in Appendix III). Besides the complex mathematics of these models and the dependence of their accuracy on thermal property data, their major drawback lies in the lack of verifying their validity as long as the interface temperature is not measured directly. Furthermore, at fast growth rates and for rapid interfacial kinetics, the problem of calculating the interface temperature is very complex.[309] Therefore, it seems rather difficult, if not impossible, to obtain accurate kinetic data as long as the interface supercooling has to be determined indirectly.

Because of the above mentioned limitations of the previous techniques, a novel technique for directly and accurately determining the

actual interface temperature has been used in this study as described in the next chapter.

CHAPTER III
EXPERIMENTAL APPARATUS AND PROCEDURES

Experimental Set-Up

The apparatus used to study the growth kinetics of Ga as well as In-doped Ga is shown in Fig. 15. It consisted of two constant temperature circulators, two observation baths, temperature measuring devices, and a computer interfaced to a nanovoltmeter, a multimeter, and a current source. The constant temperature bath circulators, (manufactured by Lauda, model K-4/R) were used in order to circulate and control the temperature of the liquid flowing inside the observation baths; the circulators could cool thirteen liters of fluid down to -30°C with a temperature control accuracy of ±0.02°C, and they feature a flow regulating valve to control the rate of liquid circulation. The circulating liquids used were water and aqueous ethylene glycol solutions (10-50 wt% $HOCH_2CH_2OH$) for the subzero temperatures. The cooling rate of the constant temperature circulators depended on several factors, such as environmental conditions, circulating fluid, and temperature range. Typical cooling rates for temperatures around 27, 5, and -10°C were .85, .7, and .2°C/ min, respectively. The temperature of each observation bath, constant within ±.025°C, was monitored using Chromel-Alumel thermocouples (I and II) in conjunction with an Omega model TRC-III ice point cell (0.1°C). The output of the thermocouples was recorded (one at a time through a switching device) by a Gould-110 dual channel model strip chart recorder with a high gain multi-span DC Preamplifier providing a

117

118
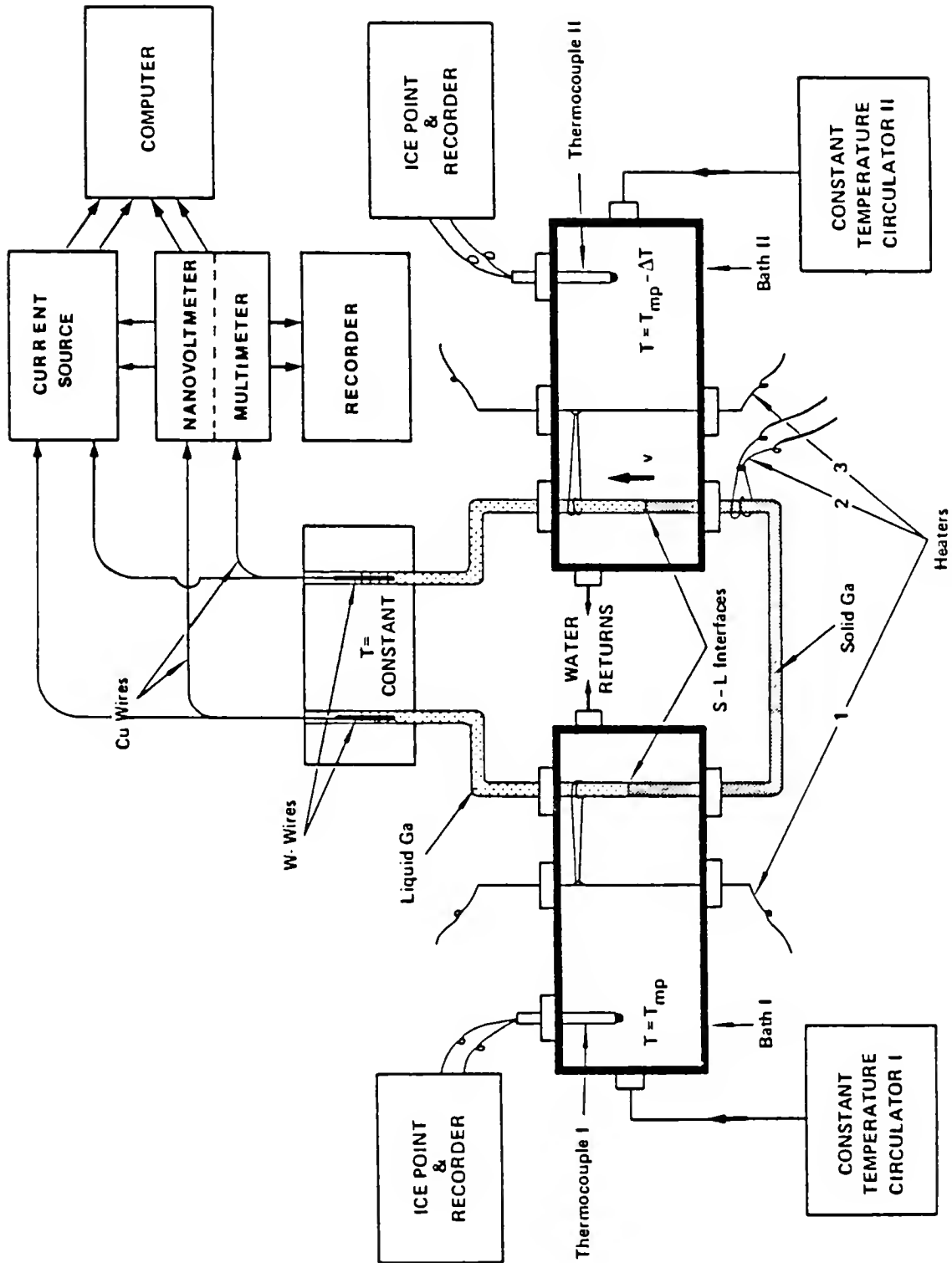
Figure 15 Experimental set-up.

maximum resolution of 4 μV/cm. The usually selected 20 μV full range resulted in a temperature reading accuracy of ±.0125°C. In addition, depending on the experimental procedures, as it will be discussed later, the thermocouple outputs were also read by the nanovoltmeter or the multimeter.

After the sample had been positioned inside the observation baths, it was electrically connected to a Keithley-181 model nanovoltmeter which measured the thermoelectric emf output of the sample with a precision of ±5nV; the sample was also electrically connected to a Hewlett-Packard model 3456A Voltmeter and to a Keithley model 220 programmable current source. The latter instruments and the nanovoltmeter were interfaced to an Apple IIe microcomputer using an IEEE-488 (GPIB) interface bus card.

The heaters 1, 2, and 3, shown in Fig. 15, were used to station the two S/L interfaces, respectively, in a desired position during the preliminary steps of an experimental run; they were turned off during the growth kinetics measurements. The heaters were made out of Kanthal wire (φ = .051 cm, .0708 Ω/cm resistance), which was wound into a two or three turn coil, were connected to a 12V battery through a variable resistor. The leads of the heater 3 were inserted into two-hole ceramic tube such that the coil could be moved up and down the observation bath.

The cell of the observation bath consisted of a copper frame (32 x 5 x 1 cm) with two circulating fluid inlets and outlets on its sides; the front and the back of the cell was enclosed by transparent plexiglass plates (.6 cm thick). A stereoscopic zoom microscope Nikon model SMZ-10 was used to observe the S/L interface with a magnification range

of 6.6-40X. The graduated eyepiece of the microscope was calibrated against a .01 mm standard micrometer slide by Bausch and Lomb. The thickness of the graduation lines was about 3 μm. Under ordinary experimental conditions a change in the position of the interface of about 10 μm could be resolved. The microscope was mounted on a hydraulic jack which allowed for continuous vertical movements while in focus.

Sample Preparation

The growth kinetics measurements were made on Ga single crystals contained in borosilicate glass capillary tubes with inside diameter and wall thickness ranging from .595 to .24 mm and .39 to .07 mm, respectively. The capillaries were freshly drawn, for each sample, from Corning or Kimble glass tubes of .8 cm o.d. (.6 cm i.d.) which were first thoroughly washed with aqua regia and then rinsed with distilled water; finally, the tubes were dried under vacuum and/or a high pressure flow of inert gas (Ar). Subsequently, the glass tube was subjected to gas flame heating for drawing. The two ends of a capillary tube, about 25 cm long, were connected to polyethylene tubes, with i.d.'s ranging from .7-1.1 mm, which had been cleaned by the previously mentioned procedure. Finally, the whole capillary assembly (65-75 cm long) was passed through the observation baths so that the glass portion of the tubing extended from about 5 cm above the top bath (II) to about 1-2 cm below the lower bath (I). The capillary, in place, was then filled with 99.9999%[*] or 99.99999% purity Ga (spectrographic analyses are given

---

[*] It should be noted that very few preliminary runs of this study were done on six 9's purity Ga; more than 95% of the reported experimental results are for the seven 9's purity Ga.

respectively in Tables 1 and 2). The as received Ga ingots (25g), sealed in polyethylene bags, was stored under vacuum until a portion of it was melted with a heating lamp and sucked into a polypropylene sterile syringe with a prewashed polyethylene tube, instead of a needle, attached to the needle hub. The molten metal contained in the syringe was subsequently injected smoothly in the capillary under ambient conditions. The tube was filled in excess in order to discard the first part of the liquid Ga which had come in contact with the atmospheric air.

Immediately following the capillary filling, solidification was initiated at one end of the sample by touching the liquid Ga with a fresh seed crystal. The Ga seeds were grown in advance by slowly cooling molten Ga, protected from oxidation by a dilute HCl (5-10%) solution. The monocrystal, floating on the surface of the liquid Ga, was separated from the bulk liquid by a tweezer whose ends were covered with polyethylene. The characteristic shape of the monocrystals are shown in Fig. 16, where the faces of interest (001) and {111} can be seen.

The seeding of the capillary tubes was done in such a way that the desired crystal face, (111) or (001), was essentially normal to the tube axis. Following the seeding, crystal growth proceeded through the top observation bath (II) and it was stopped when the S/L interface had reached about the middle of the lower bath (I). The first solidified end of the sample was then melted down so another S/L interface would form inside the top bath.

The above mentioned procedure resulted in the formation of a continuous sample consisting of two S/L interfaces, one inside each of the

Table 1.

Mass Spectrographic Analysis of Ga (99.9999%).[*]

Element	Concentration (ppm) <
Pb	.05
Sn	.1
Al	.05
Cu	.05
Ag	.03
Cr	.03
Fe	.05
Hg	.5
Mn	.01
Mg	.01
Si	.2
Na	.1
V	.1
Ti	.1
Ni	.1
Cd	.1
Zn	.1
Zr	.1
In	.1

[*] Analysis as provided by the Aluminum Company of America, Pittsburg, PA.

Table 2.
Mass Spectrographic Analysis of Ga (99.99999%).[*]

Element	Concentration (ppm) <
Al	.03
Ba	.03
Be	.03
Bi	.03
B	.03
Cd	.03
Ca	.03
Cr	.03
Co	.03
Cu	.03
Ge	.03
Au	.03
In	.005
Fe	.03
Pb	.03
Mg	.03
Mn	.03
Hg	.02
Mo	.03
Ni	.03
Nb	.03
K	.03
Si	.03
S	.03
Cl	.03
C	.03
Ag	.03
Ta	.03
Th	.03
Sn	.04
Ti	.03
W	.03
V	.03
Zn	.03
Zr	.03

[*] Analysis as provided by the United Mineral and Chemical Corporation, New York, NY.
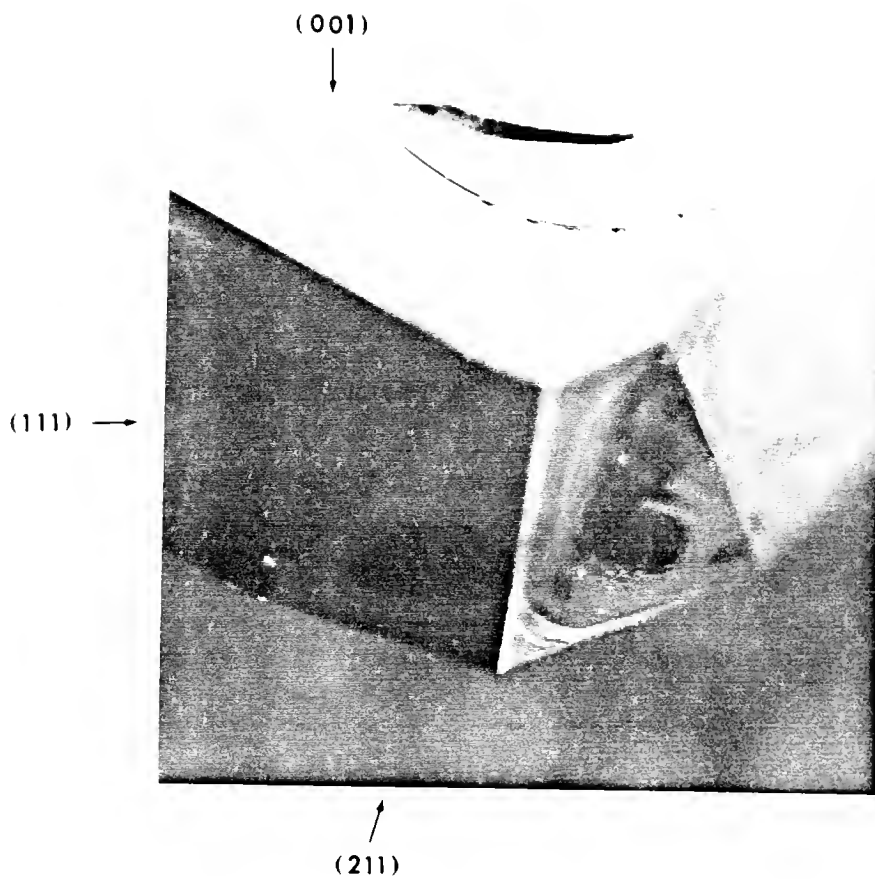
Figure 16 Gallium monocrystal, X 20.

observation baths, linked by a single crystal of Ga of a specific crystal orientation. The sample thus formed a circuit similar to those shown in Fig. 17.

The last step of the sample preparation was its electrical connection to the nanovoltmeter, multimeter, and the current source. This was achieved by inserting tungsten[*] electrodes (ϕ = .127 mm), in the liquid ends of the sample which were in turn connected via coaxial shielded copper cables to the leads of the nanovoltmeter (model 1506 low thermal cable), of the current source (model 6011 Triaxial Lead), and of the multimeter (Triaxial Shielded Cable). Extreme precautions were taken in making all the electrical connections, as well as in connecting the devices together, in order to minimize various noises and high contact resistances along the circuit which would be particularly troublesome for the Seebeck measurements. To achieve this, the copper leads were fusion welded to the W-electrodes and soldered to the instrument leads via copper splice tubes by low-thermal cadmium-tin solder. All the junctions were kept close together inside a Dewar's flask at a constant temperature. All instruments were connected to a common ground and the length of the leads was kept minimum.

Interfacial Supercooling Measurements

Thermoelectric (Seebeck) Technique

A novel technique founded on thermoelectric principles was used to directly measure the S/L interface temperature during growth from the melt. This technique, described in detail elsewher,[311-313] utilizes the

---

[*] The solubility of W in liquid Ga is negligible; for example, at 815°C is only ~.001 wt%.[310]
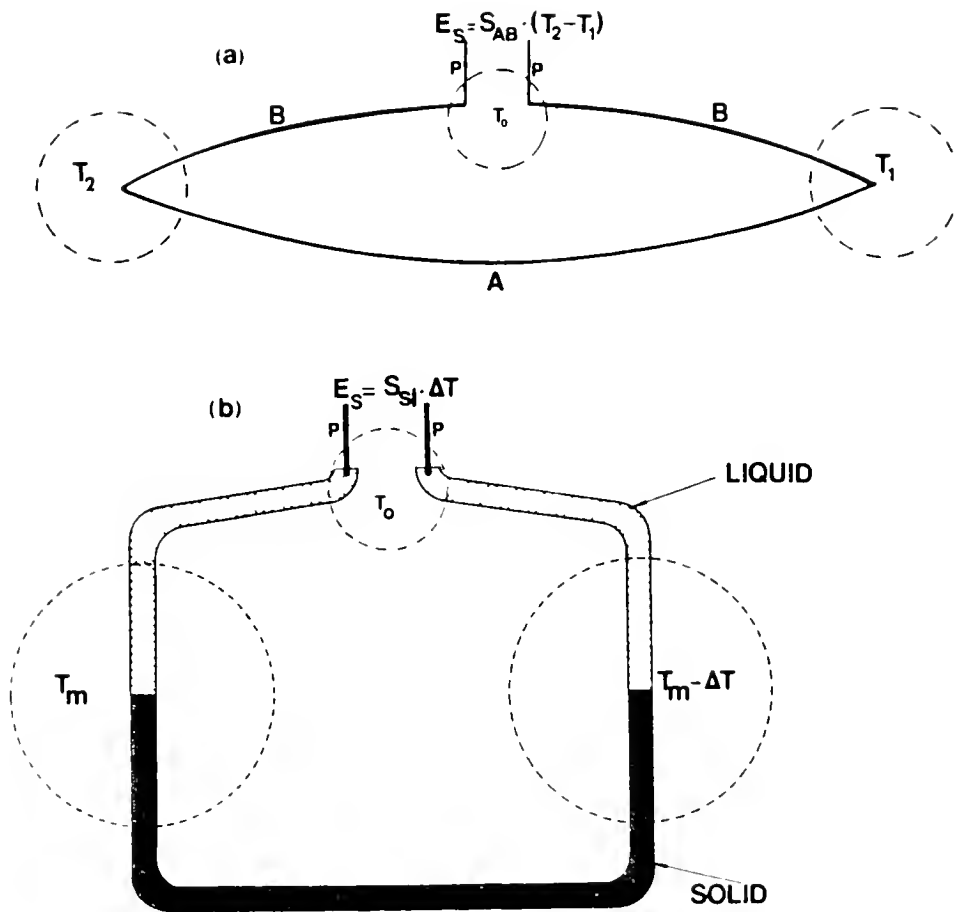
Figure 17   Thermoelectric circuits.   a) Seebeck open circuit.
b) Seebeck open circuit with two S/L interfaces.

dependence of the Seebeck emf generated across the S/L interface upon the interface temperature and crystal orientation, as well as the dopant concentration.

Thermoelectricity, in principle, is concerned with the generation of electromotive forces by thermal means in a circuit of conductors.[314] Since its discovery, the thermoelectric phenomenon has extensively been used to measure temperatures. The first discovered thermoelectric phenomenon is the Seebeck effect, upon which the method of determining ΔT in this study is entirely based. For the Seebeck effect, one generally envisages an open circuit, shown in Fig. 17a, constructed out of conductors A and B with their junctions 1 and 2 held at temperatures T_1 and T_2. The thermoelectric emf, E_s, developed by this couple is given by .

$$E_s = \int_{T_1}^{T_2} (S_A - S_B) \, dT \tag{64}$$

where S_A and S_B are the absolute thermopowers (the rate of change of the thermoelectric voltage with respect to temperature) or Seebeck coefficients of metals A and B. The thermoelectric power of the couple is defined as[314,315]

$$S_{AB}(T) = S_A(T) - S_B(T) = \lim_{\Delta T \to 0} (\Delta E_s / \Delta T) \tag{65}$$

This relation permits the determination of the Seebeck coefficient of the junction if the absolute thermoelectric powers of the components are known.

The Seebeck effect can be used to measure the S/L interfacial temperature by an arrangement that is shown in Fig. 17b. The thermoelectric loop in Fig. 17b is identical to that of Fig. 17a, except that conductors A and B are replaced with a solid and liquid metal; similarly, the

junctions AB and BA are replaced by two S/L interfaces, one of which being at equilibrium (T_m) is the "hot junction," while the other super-cooled by an amount ΔT is the "cold junction." According to eqs. (64) and (65) and taking into account the law of Magnus[316] and the law of intermediate metals,[317] the emf generated across the S/L interfaces is given by

$$E_s = S_{s\ell}\bigg|_{T_m} T_m + S_{\ell s}\bigg|_{T_i} T_i \approx S_{s\ell}(T_m - T_i) \qquad (66)$$

$$= S_{s\ell}\Delta T$$

where $S_{s\ell}$ is the Seebeck coefficient of the S/L interface. When the two interfaces are at equal temperatures, then $E_s = 0$. It should also be noted that the Seebeck coefficient of most materials is a function of temperature, but for small temperature intervals it can be approximated by a linear function, with a temperature coefficient in the order of 10^{-2} to 10^{-5} $\mu V/(°C)^2$. Hence, according to eq. (66), the interface supercooling can be determined from the recorded emf, provided that the Seebeck coefficient S_{s1} is known. This can be measured directly[312] or indirectly,[308,311,318] if the absolute Seebeck coefficients of the solid and liquid are known, with the aid of the relation

$$S_{s\ell}(T) = S_s(T) - S_L(T) \qquad (67)$$

where S_s and S_L are the absolute solid and liquid Seebeck coefficients. For the case of Ga, $S_{s\ell}$ was obtained in both ways, as discussed else-where;[1] the direct method of determining $S_{s\ell}$ will be further discussed later. In general, the coefficient $S_{s\ell}$ of a homogeneous solid is a second order tensor.[319] This means that for anisotropic crystals (non-cubic symmetry), the coefficient also varies with crystal orientation.

For example, in the case of Ga (orthorhombic structure, see more in Appendix I), the tensor is actually a diagonal matrix; the elements along the diagonal represent the Seebeck coefficient for the three principal axes of the Ga crystal. Furthermore, eqs. (64) -(67) are, strictly speaking, valid only if the circuit conductors are structurally and chemically homogeneous.[320] Strong textures and intense segregation in the conductors result in spurious emf's caused by secondary effects such as Bennedick and Volta effects.[321] Nevertheless, with a suitable experimental arrangement and instrumentation, the Seebeck voltage can be utilized to determine the interfacial temperature, as discussed next.

Determination of the Interface Supercooling

Prior to making the kinetics measurements, the following parameters for each sample were determined: a) the melting point, T_m. This temperature was used to double check and recalibrate, if necessary, the thermocouples. The thermocouple output would give the bulk supercooling of the liquid. b) The values of the "offset emf", E_{off}. According to the previous discussion about the thermoelectric technique, when the two S/L interfaces are at the same temperature, the recording emf (see eq. (66)) should be zero. However, in practice this is rarely the case because of the several other junctions involved in the circuitry and the possible minute temperature differences between them. For example, a constant temperature difference of .01°C between the W-Cu junctions would result in an offset emf of the order .02 μV. Other causes resulting in a non-zero E_{off} are inhomogeneities in the Cu-leads and the junction between Cu leads and the instrument's cables, and offset potentials of the recording instruments. For each sample, the value of E_{off}

remained constant;   values of it for several samples are listed in Table 3.   c) The Seebeck coefficient of the S/L interface, $S_{s\ell}$.   The values of the S/L interface thermoelectric   powers, $S_{s\ell}$, were determined directly for each sample and were verified by the results of the previous study.[311]   Direct determination of $S_{s\ell}$ was possible because of the faceted character of the involved Ga interfaces.   When these interfaces are free of dislocations, they remain practically stationary up to cer- tain values of ΔT (see earlier discussion on LG kinetics).   Therefore, within this range of supercoolings, the S/L interface temperature is not affected by the heat of fusion and it is equal to the bulk temperature T_b.   Based on this, the value of $S_{s\ell}$ was determined as follows.   Ini- tially, the two interfaces were brought just below T_m. Subsequently, interface II was cooled to about 1.4°C for the (111) type and about .6°C for the (001) interface below T_m and then heated up to its original temperature.   During the cooling and heating cycle of the S/L interface, the thermoelectric voltage generated was recorded as a function of temp- erature, as shown in Fig. 18 (also see print out of the computer program (#1) involved in Appendix V).   The slope of the fitted line is the $S_{s\ell}$ value at the mean temperature.   The determined $S_{s\ell}$ values for several samples for the (111) and (001) interfaces are listed in Table 3.   Dur- ing growth conditions, since the Seebeck emf changes proportionally to the interface supercooling, if the conditions (growth) at the interface remain then otherwise similar, it also "follows" proportionally the changes in ΔT_b. This is indeed shown in Fig. 19.

The Seebeck technique, as mentioned earlier, not only allows for direct and accurate measurement of the interface supercooling, but also

Table 3. Seebeck Coefficients ($S_{s\ell}$) of the S/L Ga Interfaces
and Offset Thermal emf's for Several of the Used Samples.

Sample	Interface	$S_{s\ell}$, μV/°C	E_{off}, μV
A-1	(111)	1.822	.086
B-1	(111)	1.84	.286
B-2	(111)	1.901	.63
B-3	(111)	1.906	.17
C1-1	(111)	1.89	.35
C-2	(111)	1.8805	-.035
D-1	(111)	1.78	-.2
D-2	(111)	1.792	.712
E-1	(111)	1.874	-.208
F-3	(111)	1.909	.413
G-1	(111)	1.886	.52
H-2	(001)	2.107	.932
K-1	(001)	2.218	.15
D-3	(001)	2.187	.299
L-1	(001)	2.22	-.071
M-2	(001)	2.171	.43
N-1	(001)	2.3	.121
K-2	(001)	2.43	.592
C-3	(001)	2.45	-.43
L-2	(001)	2.47	.632
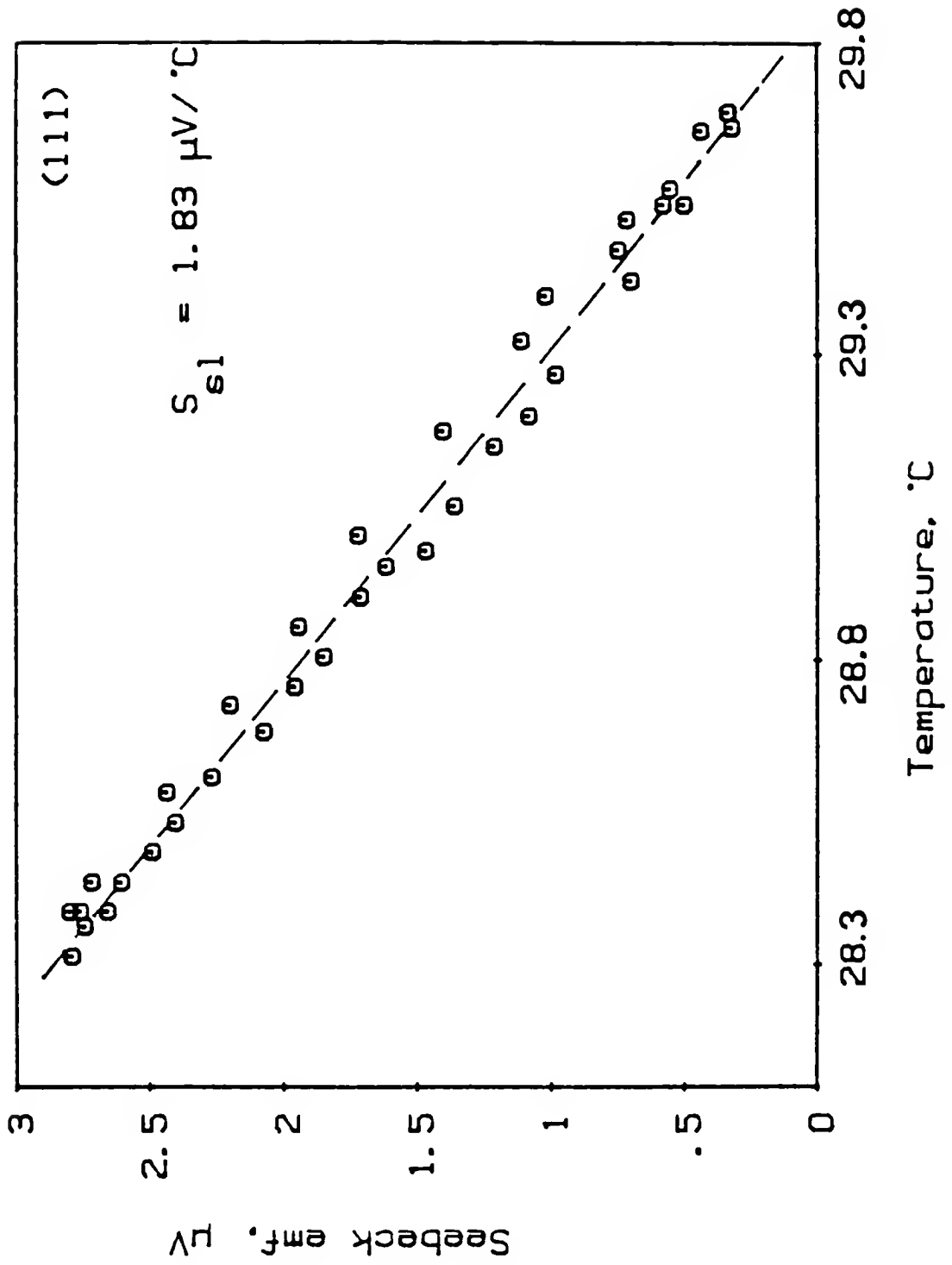
Figure 18   The seebeck emf as a function of temperature for the (111) S/L interface.
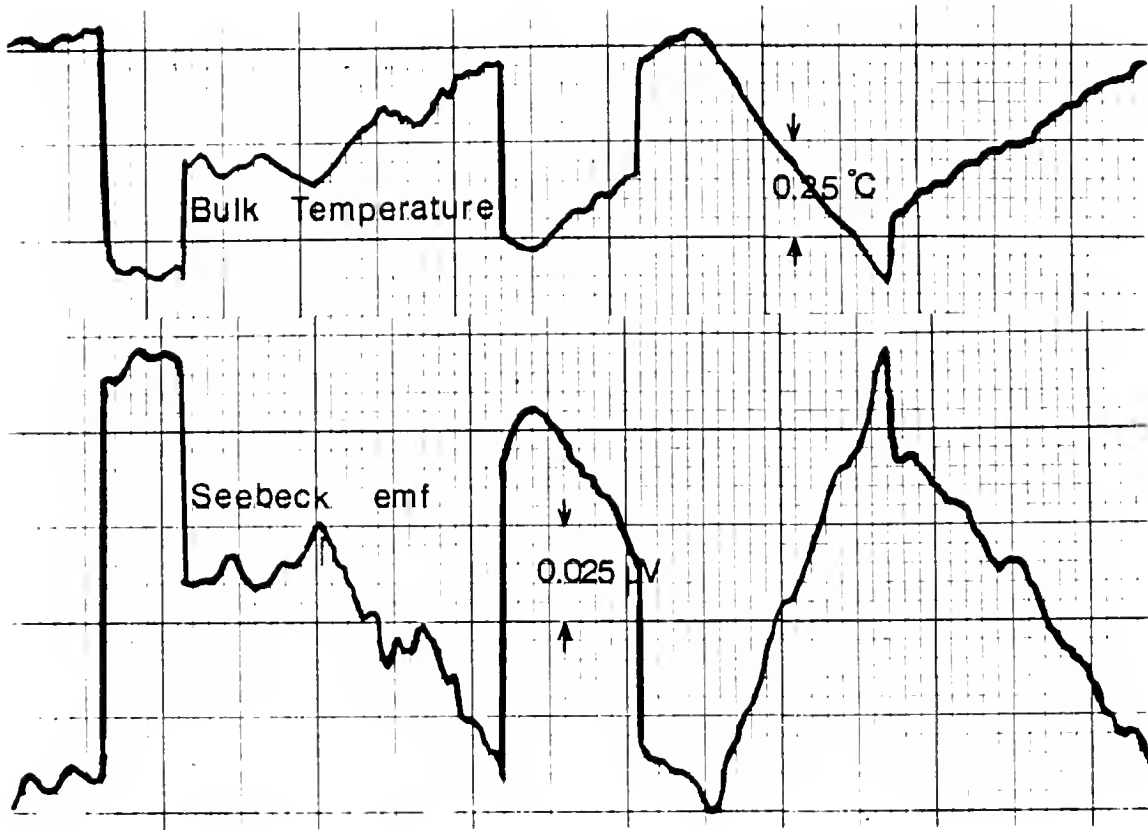
Figure 19   Seebeck emf of an (001) S/L Ga interface compared with the bulk temperature

detects the emergence of dislocations at the interface. This unique capability of the technique is illustrated in Fig. 20 where the Seebeck emf generated across the S/L interface of a (111) sample together with the bulk supercooling (emf of thermocouple II) are shown. The Seebeck emf changes proportionally to the interface temperature, which is in turn related to the bulk supercooling, heat transfer conditions, and the growth kinetics[313] (also see the previous discussion on transport phenomena at the interface). The abrupt peaks in the steady Seebeck emf indicate the emergence of screw dislocation(s) at the interface; when a dislocation intersects the faceted interface, the growth rate, is drastically altered, which changes the interface supercooling and, therefore, the Seebeck emf.

Growth Rates Measurements

To measure the growth rate, the interface was initially positioned outside the observation bath II by keeping the heater 2 on, while the water temperature was set at the desired level of bulk supercooling. After the temperature had reached the steady state, heater II was turned off, allowing the interface to enter the bath and to grow into the supercooled liquid inside the observation bath. The growth rate was then measured via the optical microscope and/or by the resistance change of the sample, as described below. For growth rates in the range of 10^{-3} to 1.5×10^3 µm/s, the interface velocity was measured directly by observing the motion of the trace of the interface on the capillary glass wall via the graduated optical microscope (20-40x) and timing it by a stop watch. Rate measurements were made only when the growth was
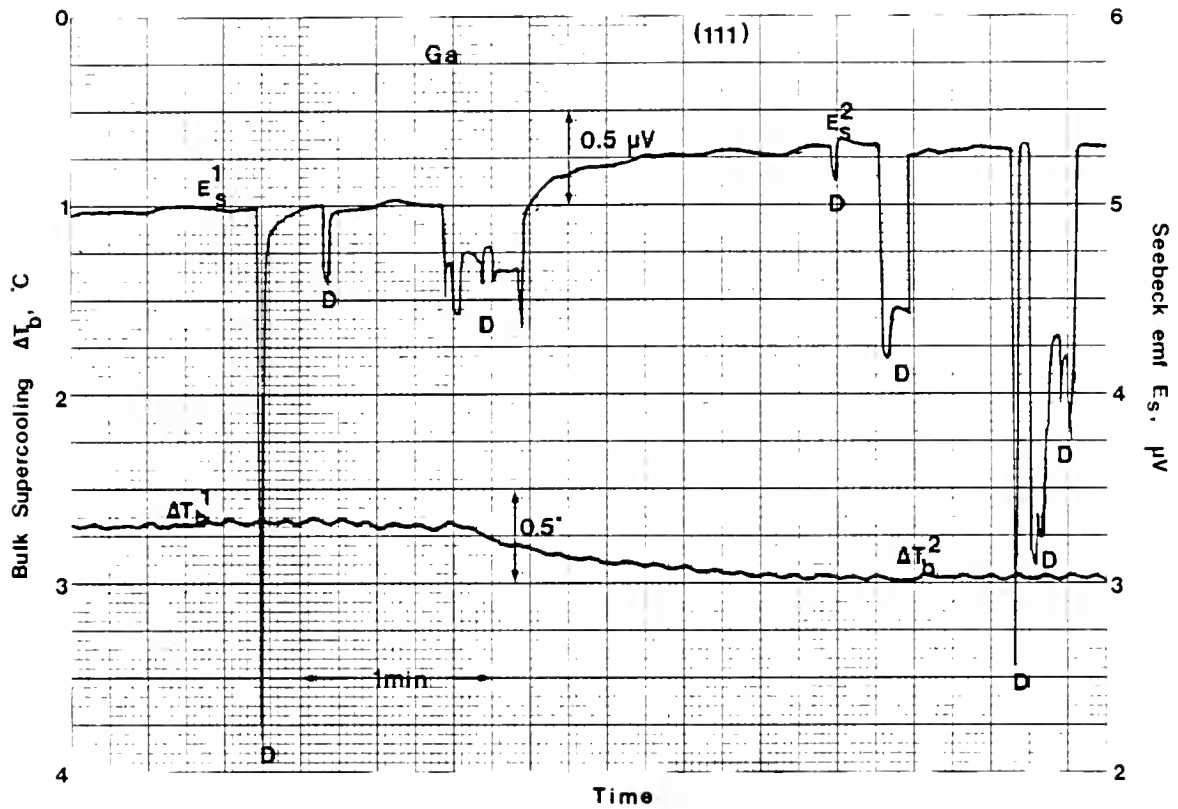
Figure 20   Seebeck emf as recorded during unconstrained growth of a
            Ga S/L (111) interface compared with the bulk supercooling;
            the abrupt peaks (D) show the emergence of dislocations at
            the interface, as well as the interactive effects of
            interfacial kinetics and heat transfer.

steady and the interface consisted of a single facet of the orientation under consideration. Whenever the trace of the interface was not normal to the tube axis, the measured rates were corrected by the cosine of the angle between the interface's normal and the capillary axis. For each bulk supercooling, at least six rate measurements were made; the standard deviation from the mean accounted up to about ±3%. A typical set of rate measurements for a sample along the (111) interface is given in Table 4.

For growth rates in the range of 500 - 1.5 x 10^{-3} μm/s, the interface velocity was determined from the resistivity change of the sample as a function of time, in addition to the above mentioned optical technique. For rates higher than 1.5 x 10^3 μm/s, the growth rates were determined only by the resistance change technique, since the accuracy of the optical measurements was limited at high growth rates. It should be noted that, although no optical growth rates measurements were taken at faster rates than 1.5 x 10^3 μm/s, the interface behavior and shape were directly observed (7-20X) and correlated with the rate measurements. For the resistivity technique, a square wave current at a specified periodicity (ranging from 100-500 milliseconds) alternating between less than a picoamp (<1 x 10^{-9} A) and a few milliamps (3 - 5 x 10^{-3} A) was passed through the sample. This technique, which was fully controlled from the microcomputer (see computer programs #2-#4 in Appendix V), made it possible to alternatively measure the interface supercooling and the growth rate. During the picoamps cycle, the Seebeck emf was recorded, which, in turn, yielded the ΔT values, while during the milliamps cycle the potential drop across the sample was measured; the latter

Table 4. Typical Growth Rate Measurements for the (111) Interface.

Lot: B, Sample: 1, T_m = 29.74°C, $S_{s\ell}$ (29°C) = 1.84 μv/°C, E_{off} = .28 μv, $\Delta R/\Delta \ell$ (27°C) = 1.17μΩ/μm, ΔT_b = 8.22°C, I = 5 x 10^{-3} A, Δt = 1.4 sec.

Distance Solidified μm	Time, Optical, sec	ΔU μV	V, optical μm/s	V, resistance μm/s	Results
1750	2.13		821.6		
1750	2.18		802.7		
1750		7.09		837	
1750	2.15		815		
1750		7.021		829	
3500	1.95		1790		Dislocations
1750		15.6		1842	Dislocations
1750		15.84		1871	Dislocations
1750		6.85		809	
1750	2.14		819		

resulted because of the resistance change across the sample during growth. The growth rate was then determined from an equation with a form

$$\frac{\Delta U}{\Delta t} = I \cdot \frac{\Delta R}{\Delta \ell}\bigg|_T \cdot V \tag{68}$$

where ΔU is the recorded potential differential drop after being corrected for the Seebeck emf. Δt is the time interval between two consecutive measurements; I is the current and $\Delta R/\Delta \ell$ is the change of resistance along the sample with respect to unit solidified length. Typical values of U were in the range of about 10 mV for the common initial resistance, in the order of 2 ohms, across the sample and the rest of the circuit. Δt ranged from 1.8 to .02 seconds for the fastest growth rates. The value of $\Delta R/\Delta \ell$ for each sample was calculated theoretically using the reported resistivities of single crystals and liquid Ga[322] corrected for temperature and orientation, and also determined experimentally from the optical growth rate measurement in the range of 500-(1.5 - 2) x 10^3 μm/s. The agreement between the measured and calculated values was considered more than satisfactory, with a maximum difference of about ±3%. A comparison between the experimental and calculated values of $\Delta R/\Delta \ell$ for the (111) interface is shown in Fig. 21.

During each milliamp current pulse, a minimum of four rate measurements were made; the average was then taken as the growth rate at the mean of the supercoolings measured during the picoamp pulse before and after the milliamp plateau, provided that the difference between the two supercoolings was less than ±.025°C. The maximum standard deviation never exceeded 5% for the highest average resisistivity growth rates.
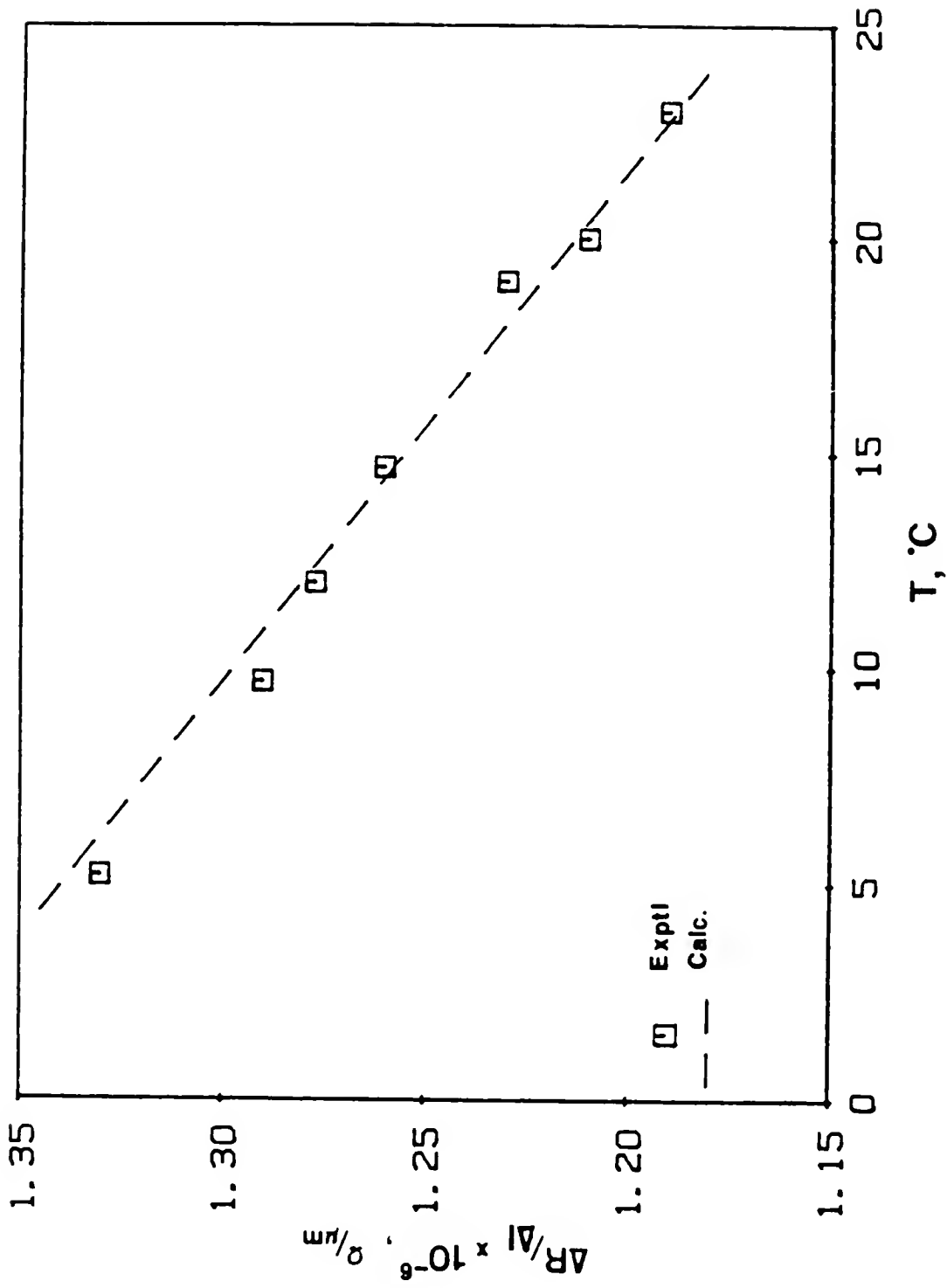
Figure 21 Experimental vs. calculated values of the resistance change per unit solidified length along the (111) orientation vs. temperature.

All measurements would stop when the interface had reached the top of the observation bath. Then, the interface was melted back all the way out of the observation bath and the procedure was repeated at a different bulk supercooling.

Experimental Procedure for the Doped Ga

The Ga-In alloys were prepared by mixing high purity Ga (99.99999% Ga) and In (99.999% In);[*] a desired amount of In in the form of grindings, weighed to four decimal places, was added to the as received polyethylene bag that contained the 25g Ga ingot.   After the bag was resealed, the ingot was melted by the heating lamp, as described earlier; liquid Ga at T_m can dissolve up to 30 wt% of In. (The Ga-In system is described in more detail in Appendix II.) Consequently, a capillary was filled with the doped liquid with a procedure similar to that of the pure Ga. The capillary was seeded for the (111) interface.   The sample was initially solidified rapidly, at a rate of about .5-1 cm/s in order to prevent macrosegregation across the sample.   The two ends of the sample were then melted and connected to the electrical circuit, as described earlier. The unused portion of the alloy was solidified and was used for chemical analysis.   The analysis of the alloys as well as the intended compositions are given in Table 5.

The preliminary procedure before the growth kinetics measurements was the same as that of the pure Ga.   The experimentally determined Seebeck coefficients for the two compositions used are given in Table 6. Note that because of the effect of In on the Seebeck coefficient, these

---

[*] As indicated by the supplier, AESAR Johnson Mathey, Inc., N.J.

Table 5. Analysis of In-Doped Ga Samples.

Sample	Intended Composition (wt% In)	Analyzed Composition[*] (wt% In)
1	.01	.012
2	.1	.12

[*] As determined by Applied Technical Services, Inc., Marietta, GA by atomic absorption technique.

Table 6.   Seebeck Coefficients of S/L In-Doped (111) Ga Interfaces.

Composition (wt% In)	$S_{s\ell}$ (μV/°C)	Comments
.01	1.72	24 hrs equilibration
	1.75	end of a run; after the interface was melted back
	1.81	after interfacial break-down
	1.628	V = 5.6 μm/s; distance solidified, x = 3500 μm[*]
	1.56	V = 21.3 μm/s; x = 2200 μm[*]
.12	1.49	24 hrs equiliation
	1.31	V = 1.9 μm/s; x = 2100[*]
	1.27	V = 2.8 μm/s; x = 3500[*]
	1.3	V = .88 μm/s; x = 2900[*]
	1.468	after breakdown

[*] $S_{s\ell}$ measured upon heating at the end of the run.

values are lower than those of the (111) interface for the pure material. Moreover, the "noise" of the Seebeck emf was higher than that of the pure and the offset emf was not as stable throughout an experimental cycle. These effects are attributed to the "non-homogeneity" of the sample caused by a) diffusion of the In towards or away from the interfaces; and b) by the solute (In) rich liquid bands entrapped along the solid portion of the sample.

In spite of these difficulties, the Seebeck emf was recorded during growth of the doped material so as to provide a continuous and in-situ detection of the interfacial conditions; it was revealed that the Seebeck technique also detects morphological instability of the interface and entrapment of second phase deposits during growth. This can be seen in Fig. 22, where the Seebeck emf generated across the S/L (111) interface of a Ga-0.01 wt% In doped sample is shown. For a low level of dopant concentration, the growth mechanism of the doped Ga is similar to that of the pure, except the growth rates are slightly lower at a particular ΔT, as discussed later. As growth proceeds, the solute build-up ahead of the interface reaches a critical profile, causing morphological instability or interfacial breakdown. During the breakdown, the interface moves faster than prior to the instability and an In-rich layer is entrapped. The abrupt changes in the interfacial conditions (V, ΔT, and C_i) are reflected in the momentary changes in the Seebeck potential. After the formation of the In-rich band, the interface becomes faceted again and the supercooling changes back to its original position.

The interfacial supercooling during growth for the doped material was calculated from the solutions of the associated heat transfer model
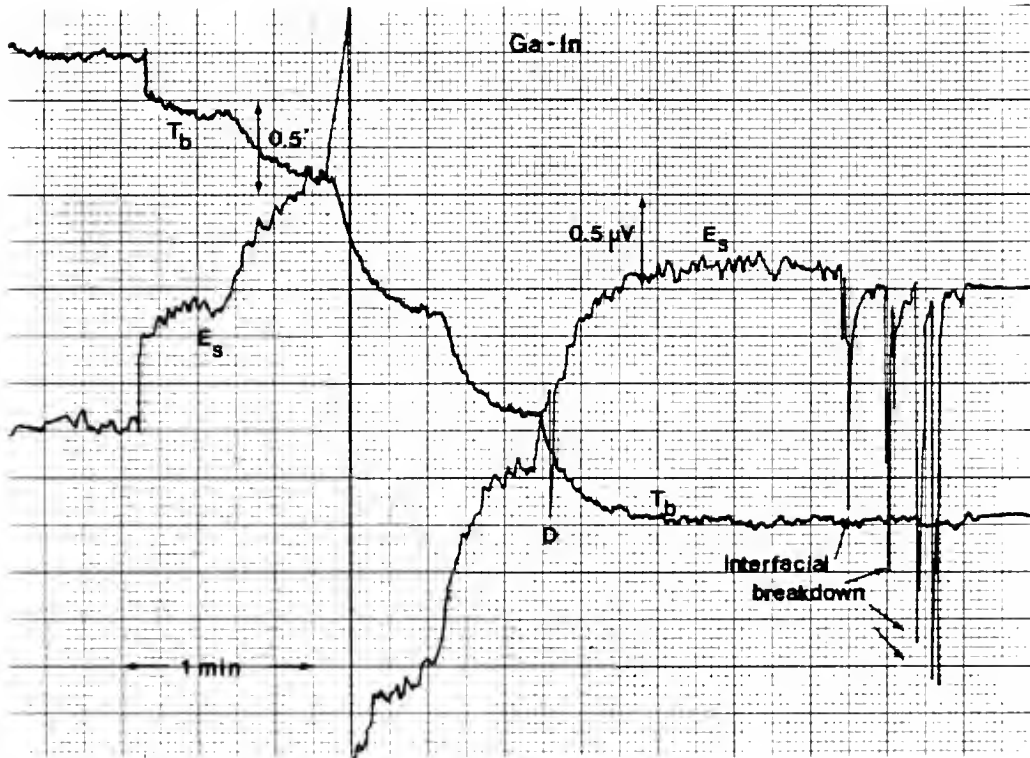
Figure 22 Seebeck emf compared with the bulk temperature as affected
by dislocation(s) and interfacial breakdown, recorded
during growth of In-doped Ga.

(see calculations in Appendix III), the validity of which has been veri-
fied for the case of pure Ga. Moreover, the interfacial supercoolings
were calculated also by the Seebeck method. The agreement then between
the two ΔT values was quite satisfactory. Furthermore, as discussed
later and in Appendix III, at low growth rates, i.e. $V \leq 10$ $\mu m/s$, the
bulk supercooling is approximately the same as the interfacial super-
cooling ($\Delta T_b/\Delta T \geq .98$). Thus, at rates less than 1 $\mu m/s$, the values of
$S_{s\ell}$ and E_{off} can be back calculated with the aid of ΔT_b. This procedure
provided an extra check in determining the ΔT values.

All the growth rate measurements were made via the optical micro-
scope. Initially, the interface, II or I, depending on whether the
growth was antiparallel or parallel to the gravity vector, was super-
cooled by .5-.7°C below the liquidus temperature; the sample was held at
this supercooling, where the interface was practically stationary, for a
period of 24-48 hours. Afterwards, the water flow was turned off and
the circulator temperature was set to a lower desired temperature. When
the temperature of the circulator had become constant, the flow was then
resumed and the rates measuring procedure started. At a given bulk
supercooling the growth rates were measured as a function of the dis-
tance solidified (i.e. the distance from the initial equilibrium posi-
tion of the interface); the latter ranged from .5-3 cm. After the com-
pletion of these measurements, the interface was melted back to about
its original position, where it was held for 24-48 hours, and the rate
measurements were repeated at another bulk supercooling. It should be
noted that the rate measurements along the parallel and antiparallel to
the gravity vector growth direction were performed on the same sample.

CHAPTER IV
RESULTS

The experimental investigation of the high purity Ga interfacial kinetics covers a range of 10^{-3} to 2×10^4 µm/s growth rates and interfacial supercoolings up to about 4.6°C, corresponding to bulk supercoolings up to 53°C. In addition, the kinetics have been determined as a function of crystal perfection (dislocation-free versus dislocation-assisted interface) and crystal orientation ([111] and [001]). On the other hand, the In-doped Ga kinetics study covers a range of 10^{-2} to 45 µm/s growth rates and interfacial supercoolings up to about 2.5°C. For the doped material the kinetics have also been determined for two initial compositions, Ga - .01 wt% In and Ga - .12 wt% In, for dislocation-free interfaces of the (111) type. Furthermore, the growth rates have been measured as a function of solidified length and growth direction with respect to the gravity force.

In this chapter the growth kinetics results are presented and, whenever it is obvious, they are qualitatively related to the earlier discussed growth theories.

(111) Interface

When the bulk supercooling[*] was less than about 1.5°C, the undisturbed (111) S/L interface was practically stationary in contact with

---

[*] It should be noted that for a motionless interface, the bulk and interface supercoolings are the same.

the supercooled liquid; for example, no motion was detected at 40X magnification (e.g. a movement of the interface by a distance of about 5-10 μm) when the interface was held at 1.5°C below the melting point for about 72 hours. On the other hand, the motionless interface would immediately start to move rapidly when the capillary tube was bent or twisted; frequently during this action several other facets moving at different rates would also form at the interface. Some of the facets (the faster moving ones) would eventually grow out of the interface, leaving only {111} interface(s). When more than one {111} facets were left, they would move one at a time for several seconds; if only one (111) facet was left, the interface would move in a steady state until it would become stationary again. On many occasions, a similar sudden motion of the stationary (111) interface was also observed after changing the water bath temperature abruptly, e.g. from 1.4°C supercooling to 0.5°C or after suddenly changing the water flow rate, which, in turn, caused strong vibrations of the glass capillary tube.

At supercoolings larger than about 1.5°C, the undisturbed (111) interface moved parallel to itself at a constant rate that was strongly dependent on the bulk supercooling. Moreover, similar to the growth behavior at lower supercoolings, disturbing the crystal by mechanical or thermal means caused the interface motion to increase abruptly and other facets (mostly {111} and {001}) to appear at the interface. The interface moved at the increased rate for a few seconds after which the rate abruptly dropped to its previous undisturbed value. As indicated by the work of Pennington et al.[99] and Abbaschian and Ravitz,[2] and as it will become apparent later, the growth of the disturbed interface corresponds

to the dislocation-assisted growth,[*][323-326] whereas that of the undisturbed interface belongs to one of the 2D nucleation and growth mechanisms. The latter is termed as dislocation-free growth in this study, as contrasted with dislocation-assisted growth.

The dislocation-free and dislocation-assisted growth rates are plotted on a linear scale versus the interface supercooling in Fig. 23. As can be seen in the supercooling range of about 1.5-3.5°C, one clearly distinguishes two growth rates for the same ΔT; one belonging to the undisturbed samples, the other belonging to the disturbed samples. At lower than 1.5°C (ΔT), the data points belong only to the latter. As indicated earlier, below this supercooling the (111) interface remained practically stationary "indefinitely"; it would advance only when the crystal was disturbed by mechanical or thermal means. The existence of the threshold supercooling and the functional relationship between the growth rates of the undisturbed samples and the interfacial supercoolings, as discussed below, are indicative of 2D nucleation-assisted growth, whereas those of the disturbed samples correspond to dislocation-assisted growth. At higher than about 3.5°C supercoolings, the two growth rates become approximately similar, and it is rather difficult to clearly differentiate them. At these high supercoolings, thermally induced dislocations also emerge and grow out of the interface very rapidly, sometimes faster than the measurement rate of 48-25 per second. Therefore, the measured rates in this range are sometimes the mixture of

---

* This growth mechanism refers only to the classical SDG mechanism and not to any other growth modes proposed for imperfect interfaces[323] and/or associated with dislocations in the bulk liquid and solid.[324-326]
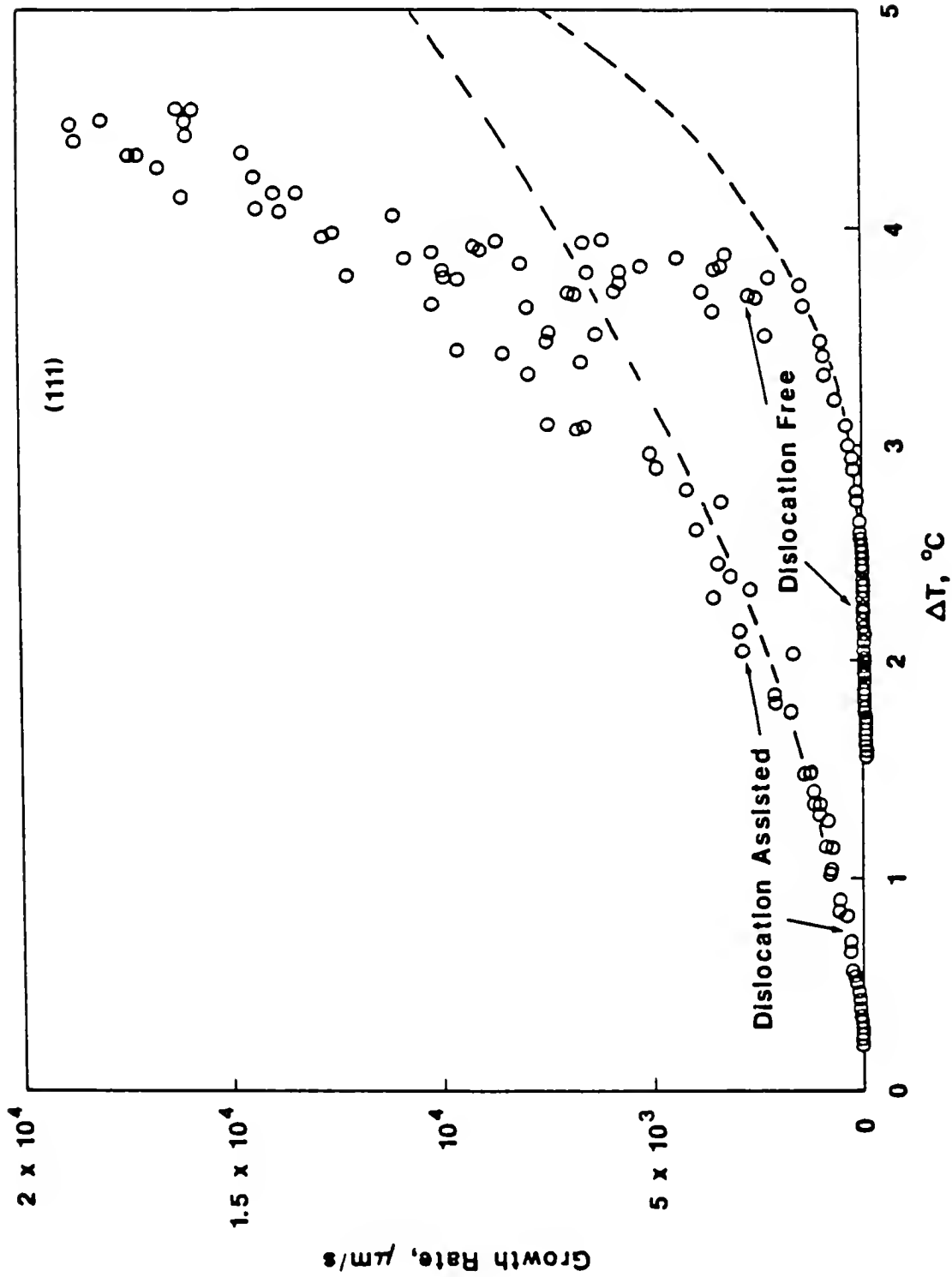
Figure 23 Dislocation-free and Dislocation-assisted growth rates of the (111) interface as a function of the interface supercooling; dashed curves represent the 2DNG and SDG rate equations as given in Table 7.

the two growth modes, which accounts for the relatively large scatter of the data points for rates higher than about 6500 μm/s.

The growth rates of the (111) interface as a function of the inter-face and bulk supercooling for several samples are shown on a linear and log-log scale in Figs. 24 and 25, respectively. As can be seen, the bulk supercooling is higher than the interfacial one at growth rates higher than about 1 μm/s; for example, for growth rates in the order of 3, 350, and 1.9 x 10^4 μm/s, the bulk supercooling is about .015, 1.6, and 45°C, respectively, larger than the corresponding interfacial super-cooling. At low growth rates, less than about 1 μm/s, the two super-coolings are nearly equal, as revealed in Figs. 24 and 25. The differ-ence between dislocation-free and dislocation-assisted kinetics is easily revealed from Fig. 26, where the growth rates are plotted on semi-log scale versus the reciprocal of the interfacial supercooling. Note that for graphical clarity the x-axis is shown in two different scales in this figure. The data are for several samples, some with cross-sectional area of A and others with 4.5A. The kinetics data for each growth mode, dislocation-free and dislocation-assisted, are pre-sented separately in more detail in the following section.

Dislocation-Free (111) Growth Kinetics

The dislocation-free data for the (111) interface, as shown in Figs. 23 and 26, represent the growth behavior of a total of 15 samples[*]

---

[*] In reality, this is the number of samples whose kinetics data extend at least two orders of magnitude in growth rates; otherwise, the num-ber of samples tested far exceeds the above mentioned one. Further-more, it should be noted that all the (111) graphs represent growth data from 15 samples, except where otherwise stated.
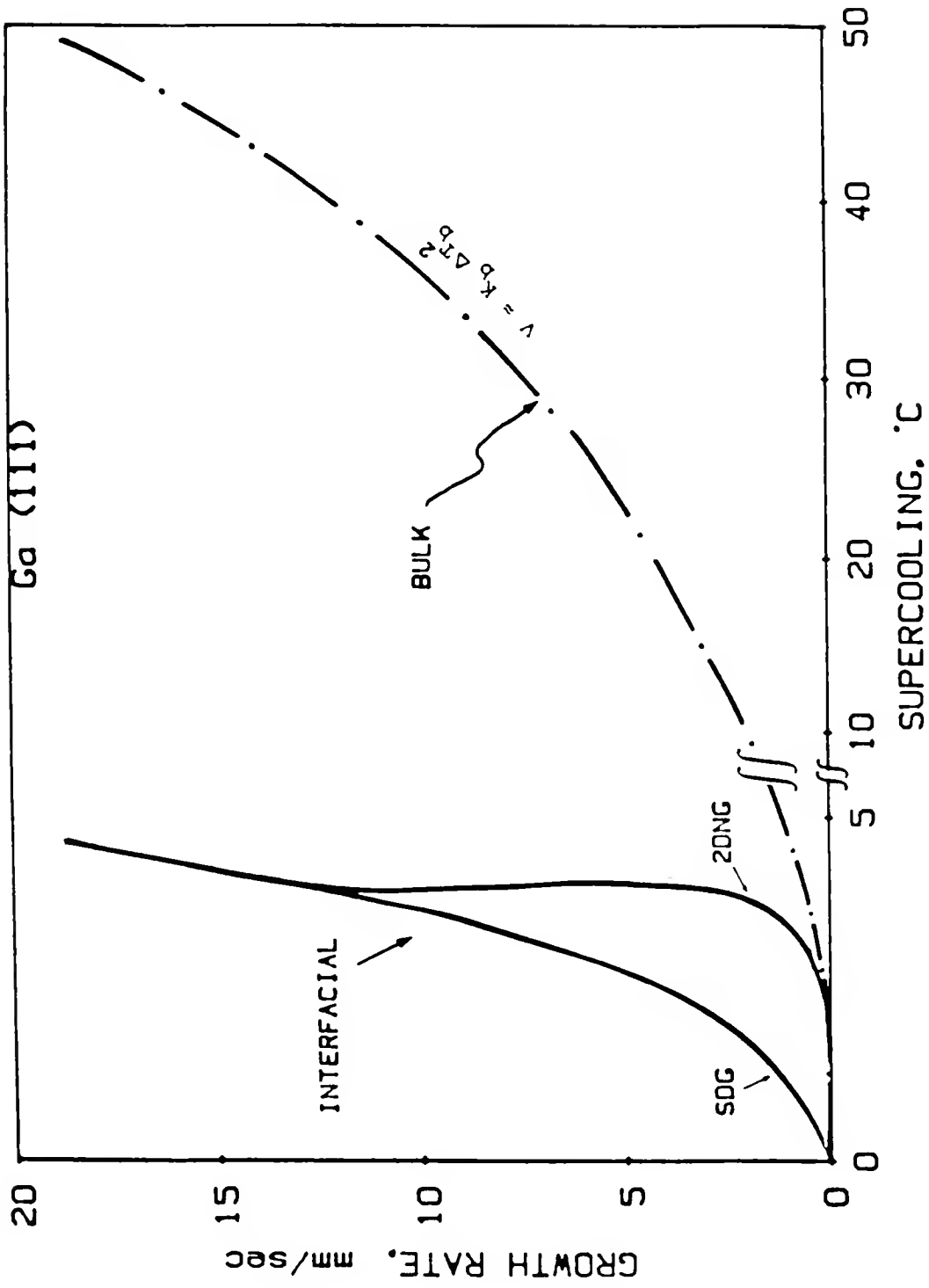
Figure 24 Growth rates of the (111) interface as a function of the interfacial and the bulk supercooling.
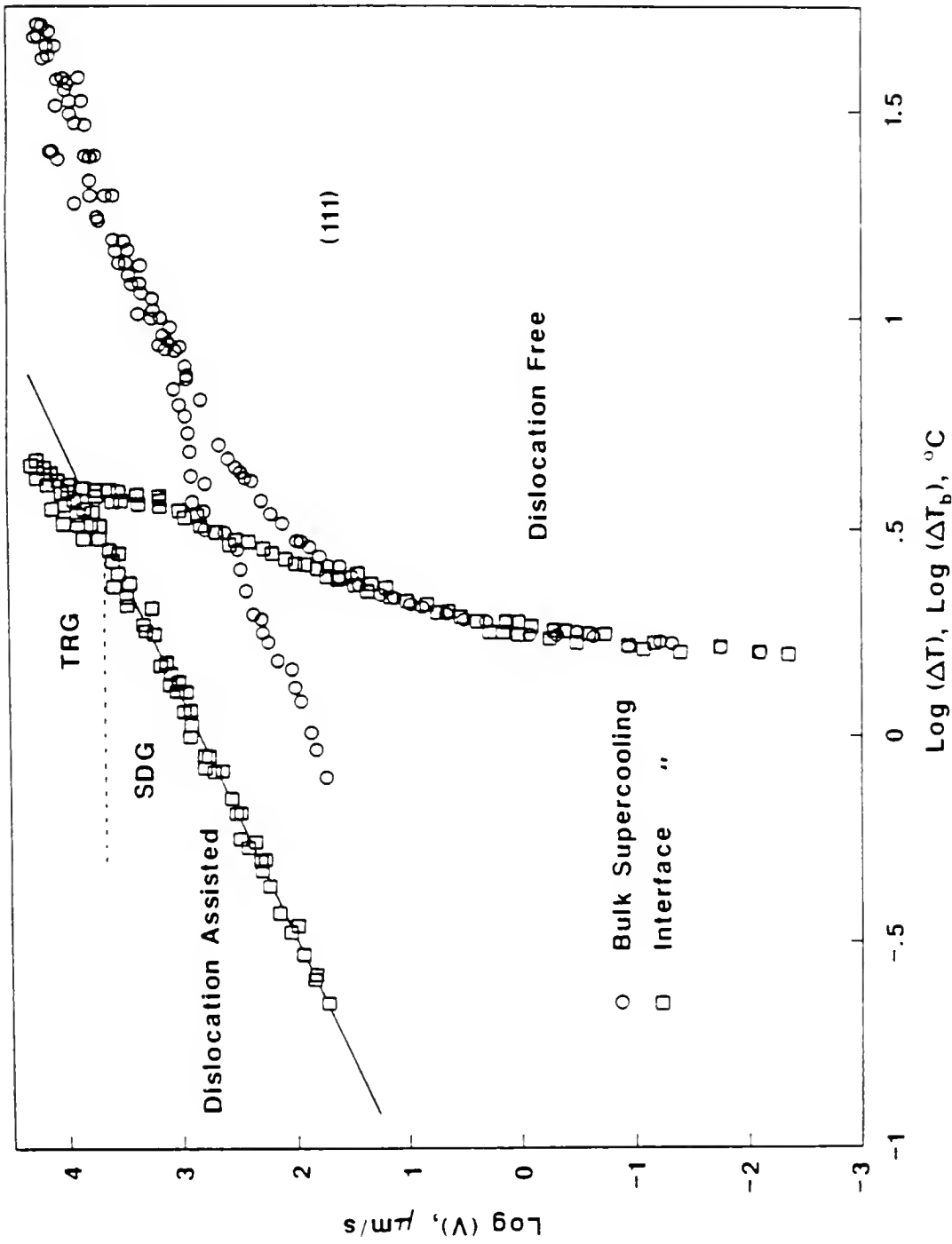
Figure 25   The logarithm of the (111) growth rates plotted as a function of the logarithm of the interfacial and bulk supercoolings; the line represents the SDG rate equation given in Table 7.
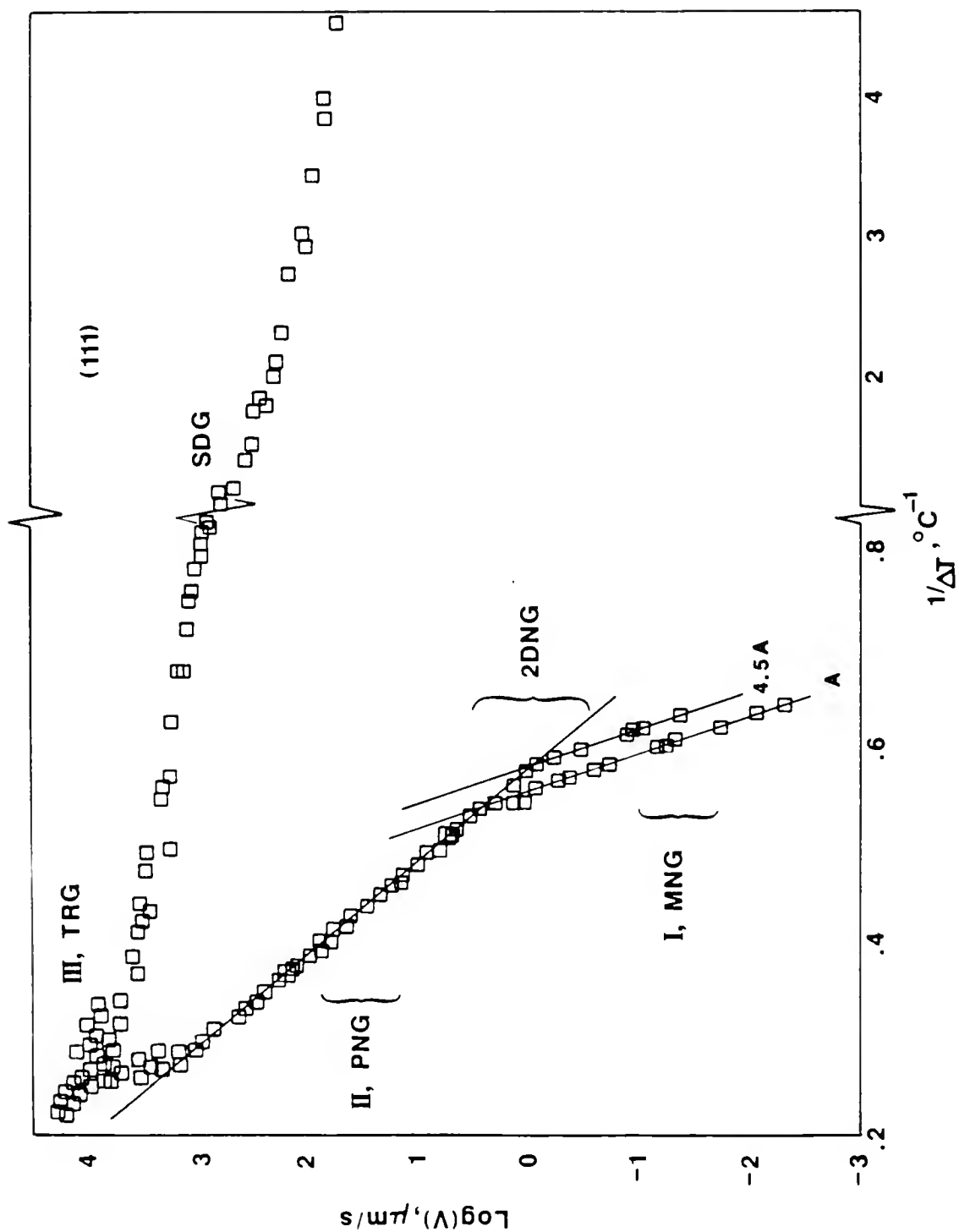
Figure 26 The logarithm of the (111) growth rates versus the reciprocal of the interfacial supercooling; A is the S/L interfacial area.

tested. By observing these figures, and particularly the semilogarithmic plot of Fig. 26, it is realized that the growth rate of the perfect interface is a strong function of the reciprocal of the interface supercooling. However, its growth behavior does not appear to be monotonically related to the supercooling within the investigated experimental range. Indeed, as can be seen in Fig. 26, the growth rates at the lower range of supercoolings increase much faster with the supercooling than those in the intermediate range, but still slower than those at supercoolings higher than 3.5°C. The latter feature is better revealed in Fig. 23. It is easily depicted from Fig. 26 that at least up to supercoolings of about 3.5°C the growth rates depend upon the interface supercooling in an Arrhenius fashion (e.g. $V \propto \exp(- 1/\Delta T)$), and at supercoolings less than about 1.9°C, the rates also depend on the sample size. As may be surmised, already these features provide a basis for "grouping" the growth behavior of the dislocation-free interface within a given range of supercoolings. Such grouping is intended for a more detailed discussion of the results, rather than identifying and/or implying kinetically distinct regions. Indeed, the dislocation-free kinetics, which have all the characteristic signs of two-dimensional nucleation assisted growth, are well expressed over the whole experimental range by the rate equation

$$V = \frac{K_1 \ A \ (\Delta T)^{1/2} \ \exp(- B/\Delta T)}{(1 + K_2 \ A^{5/3} \ \Delta T^{1/2} \ \exp(- B/\Delta T))^{3/5}} \tag{69}$$

where A is the S/L interface area. The reasoning behind the general 2DNG equation, eq. (69), as well as the magnitude of the parameters K_1, K_2, and B and their dependence upon the growth variables will be given in the following chapter.

As indicated above, the dislocation-free (111) data could be divided into three regions, as shown in Fig. 26. The first two regions, I (MNG) and II (PNG), will be discussed in detail below; the third region, III (TRC), which covers growth rates higher than about 1500 μm/s and interface supercoolings larger than 3.5°C, will be discussed in a later section. The cut-off points for each region are established by realizing a systematic deviation of data points from carefully determined regression lines representing the kinetics for the region adjacent to them. The regression lines were initially determined from data points well beyond or above (with respect to ΔT) the cut-off points. Subsequently, transitional data points would be included in the regression analysis only if their deviation from the former line was small enough so that it did not significantly affect the parameters of the rate equation. Furthermore, the population of the data points and the number of samples used, quantitatively ensures the justification for assigning a borderline supercooling between each region.

MNG region

Region I (MNG), ranges from 1.5 to about 1.9°C supercoolings and for growth rates up to about 1 μm/s. The growth rates in this region depend on the size of the capillary tube cross section. For each

capillary size, the data points fall on a straight line with a negative slope, indicating that the growth rates are exponential functions of $(-1/\Delta T)$. As discussed earlier, the mononuclear growth mechanism is likely to be observed at ΔT's just larger than a critical threshold supercooling, with growth rates that are exponential functions of $(-1/\Delta T)$ and proportional to the interface area (see eq. (40)). The predictions of the MNG model are satisfied for the low growth rates data ($<$ 1 μm/s), as shown in Fig. 27 in a log (V) vs. $1/\Delta T$ plot. Note that the data fall on two parallel lines, each corresponding to different samples with the same capillary tube inside diameter, D. The growth rate in this region is also proportional to the S/L interfacial area. The proportionality of the growth rates upon the S/L interfacial area is better illustrated in Fig. 28, where a plot of the quantity log (V/D^2) as a function of $1/\Delta T$, for all samples, results in a straight line. The equation for this line, as determined by regression, is given by

$$\log \frac{V}{D^2} = 17.132 - \frac{25.517}{\Delta T}$$

with a coefficient of determination .9991 and of correlation .9995. Thus, the growth rate equation for the MNG region is determined as

$$V = 1.731 \times 10^9 \, A \, \exp \, (- 58.759/\Delta T) \qquad (70)$$

V is the growth rate in μm/s and A is the S/L interfacial area in $μm^2$.

PNG Region

The second region, called PNG, covers the supercoolings range from about 2 to 3.5°C and growth rates in the range of $1 - 1.5 \times 10^3$ μm/s. The data points here, as shown in Fig. 26, still fall into a line, but with a smaller slope than that of Region I. Moreover, the growth rate
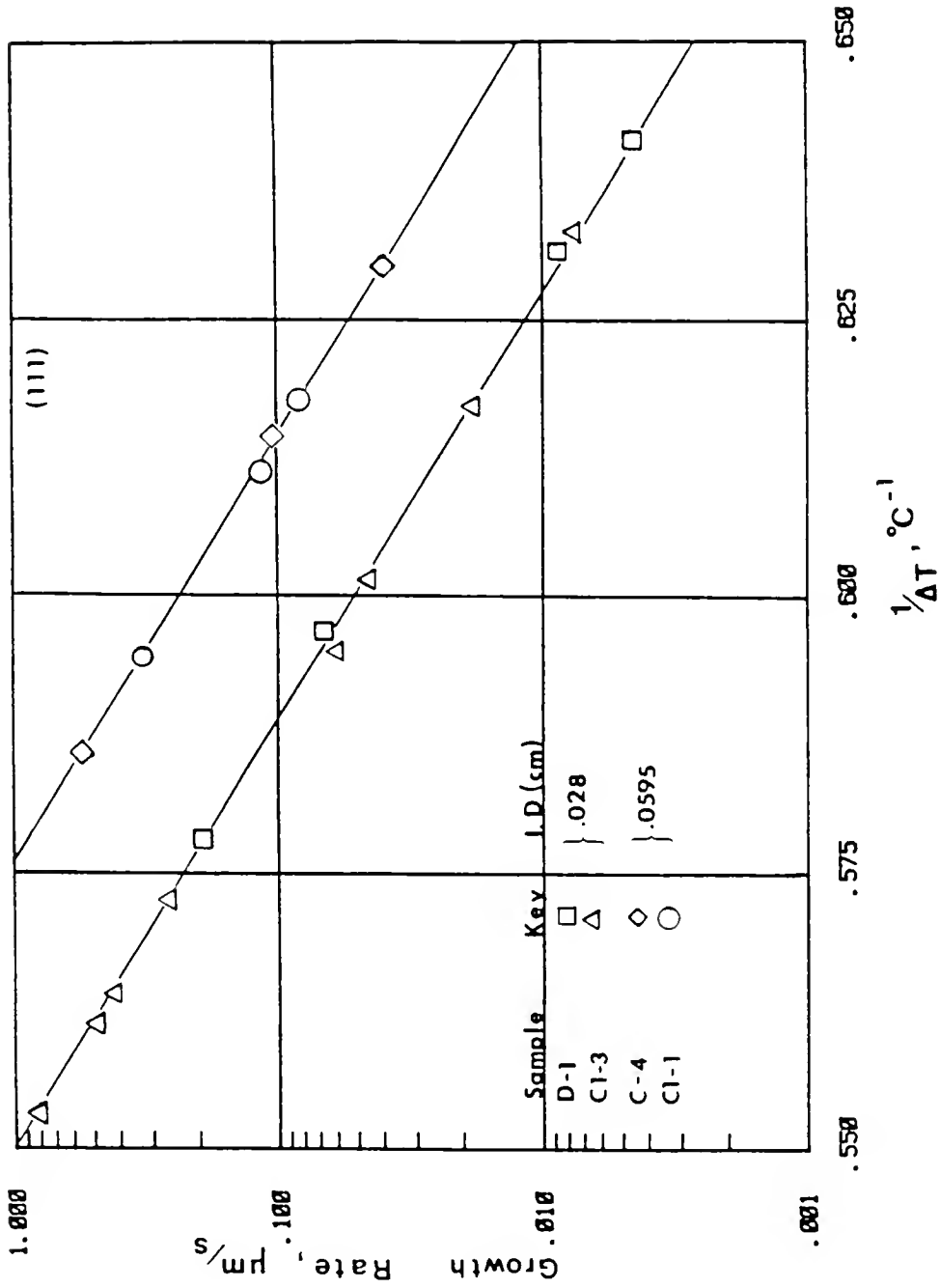
Figure 27   Dislocation-free (111) low growth rates versus the interfacial super-
cooling for 4 samples, two of each with the same capillary tube cross-
section diameter.
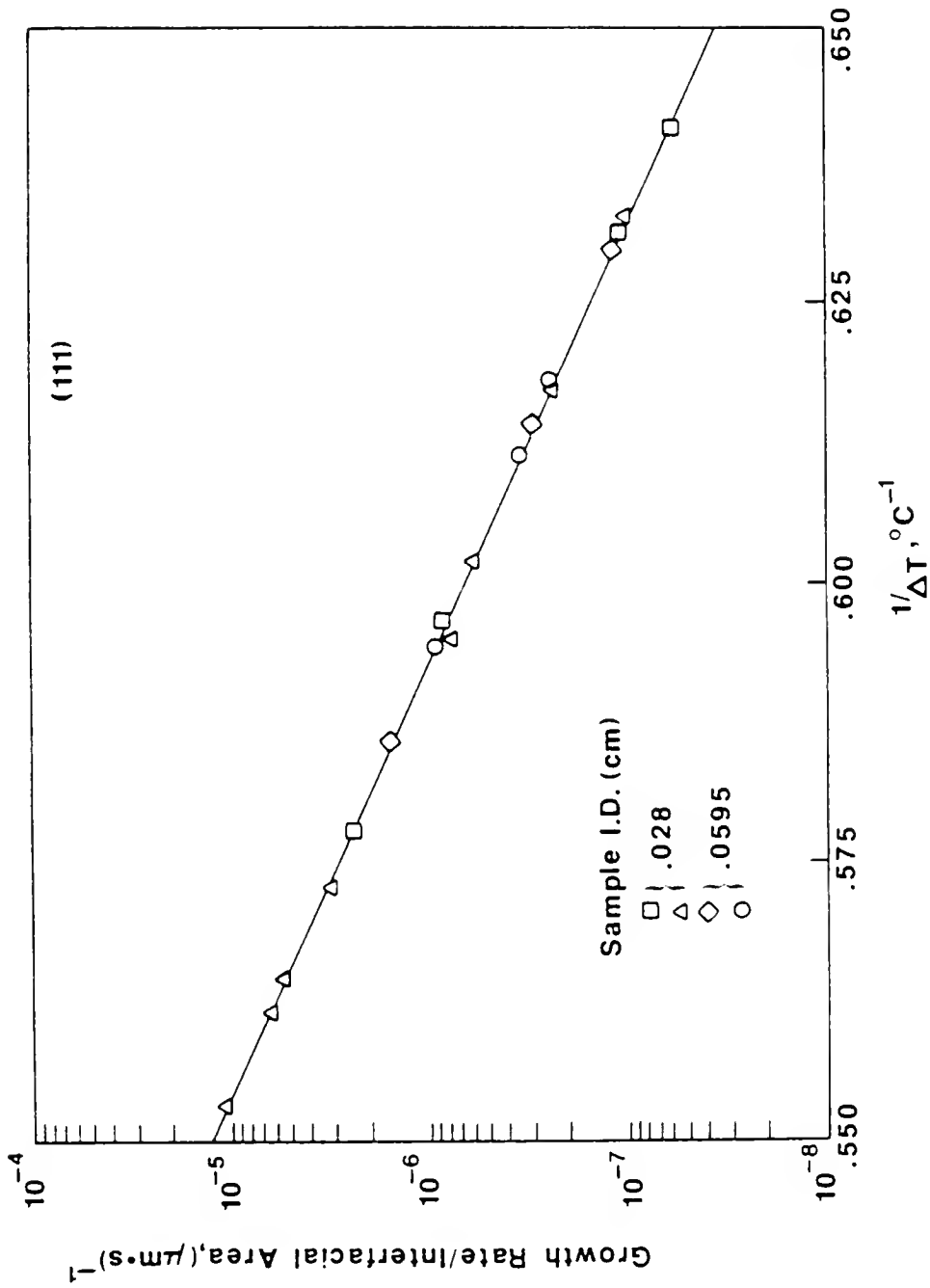
Figure 28 The logarithm of the MNG (111) growth rates normalized for the S/L interfacial area plotted versus the reciprocal of the interface supercooling.

is independent of the sample size. These are in qualitative agreement with the theoretical predictions; as indicated in the discussion of 2DN growth models, the mononuclear gradually changes to the polynuclear growth mechanism above a certain supercooling. The growth rates are still exponential functions of $(-1/\Delta T)$, and fall into a line in the log (V) vs. $1/\Delta T$ plot of Fig. 29. The equation of the regression line for data points up to interfacial supercoolings of 3.51°C and growth rates of 1455 μm/s is given as[312]

$$\log V = 5.98 - 10.42/\Delta T$$

with a coefficient of determination of .992 and a coefficient of correlation of .996. The growth rate equation for the PNG region is thus given as

$$V = 9.56 \times 10^5 \exp(-23.995/\Delta T) \qquad (71)$$

where V is the growth rate in μm/s.

Dislocation-Assisted Growth Kinetics

The dislocation-assisted (111) data seem also to be divided into two growth regions, as shown in Fig. 25. The data fall on a straight line up to interfacial supercoolings of about 2°C; this region is called the SDG region. At larger supercoolings than this, the data points deviate from the line for the lower growth rates and approach the (high supercoolings) dislocation-free growth rates.

The growth kinetics in the first region are determined for supercoolings up to about 2°C and corresponding growth rates of 2100 μm/s. The dislocation-assisted growth kinetics, like the dislocation-free kinetics, can be represented by an equation in the form of

$$V = K_D \frac{\Delta T^2}{\Delta T_c} \tanh \frac{\Delta T_c}{\Delta T} \qquad (72)$$

160
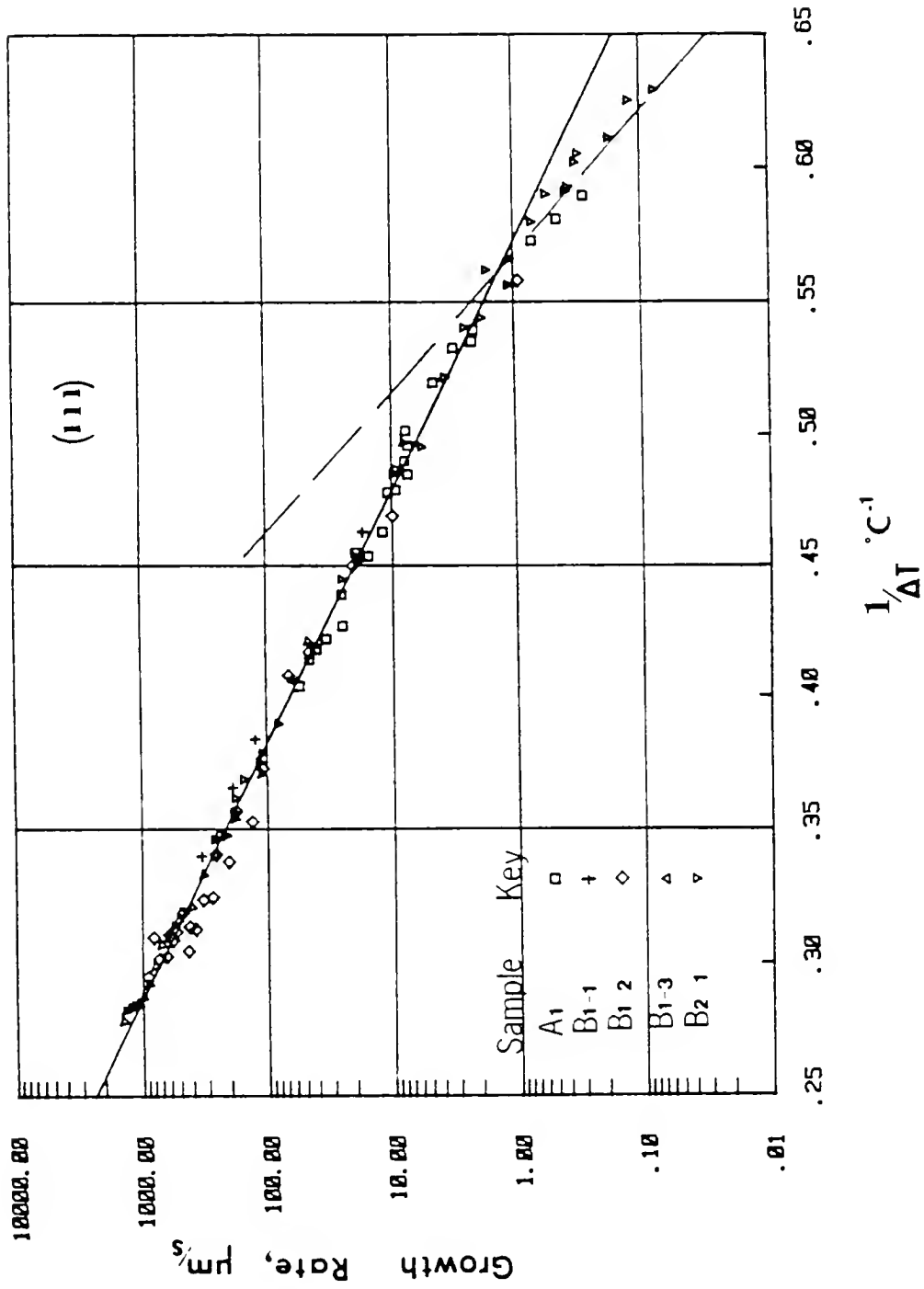
Figure 29 PNG (111) growth rates versus the reciprocal of the interface supercooling; solid line represents the PNG rate equation, as given in Table 7.

regardless of the supercooling range. In eq. (72), which represents the classical spiral growth mechanism, K_D and ΔT_c are the curve-fitting parameters related to growth and interfacial conditions; a detailed discussion about these will be given in the Discussion chapter. The rate equation, as determined from the regression analysis of the data points, as shown in Fig. 30, is given as

$$\log V = 1.73 \ \Delta T + 2.845 \ \text{or}$$

$$V = 700 \ \Delta T^{1.73} \tag{73}$$

where V is the growth rate in $\mu m/s$. The coefficients of determination and correlation are, respectively, .99 and .995.

Growth at High Supercoolings, TRG Region

The results indicate that as ΔT increases, the relationship V (ΔT) deviates from both dislocation-assisted and dislocation-free kinetic laws presented earlier, as shown in Figs. 23 and 26. The data points are for 15 samples; four of the samples were tested from growth rates 10^{-3}-10^{-2} to 1-2 x 10^4 $\mu m/s$, i.e. covering the entire experimental range. The dislocation-free and dislocation-assisted rate equations for lower growth rates are also shown in these figures. As can be seen, the deviation from the low supercoolings laws is toward higher growth rates at a given ΔT; furthermore, the deviation takes place at lower super-coolings for the dislocated interface. For the latter, the deviation starts in the range of about 2-2.5°C supercoolings, whereas for the dislocation-free interface, the transition can be approximately located at about 3.5°C supercooling. At supercoolings higher than the above mentioned ones, the two growth modes (SDG and PNG) approach each other
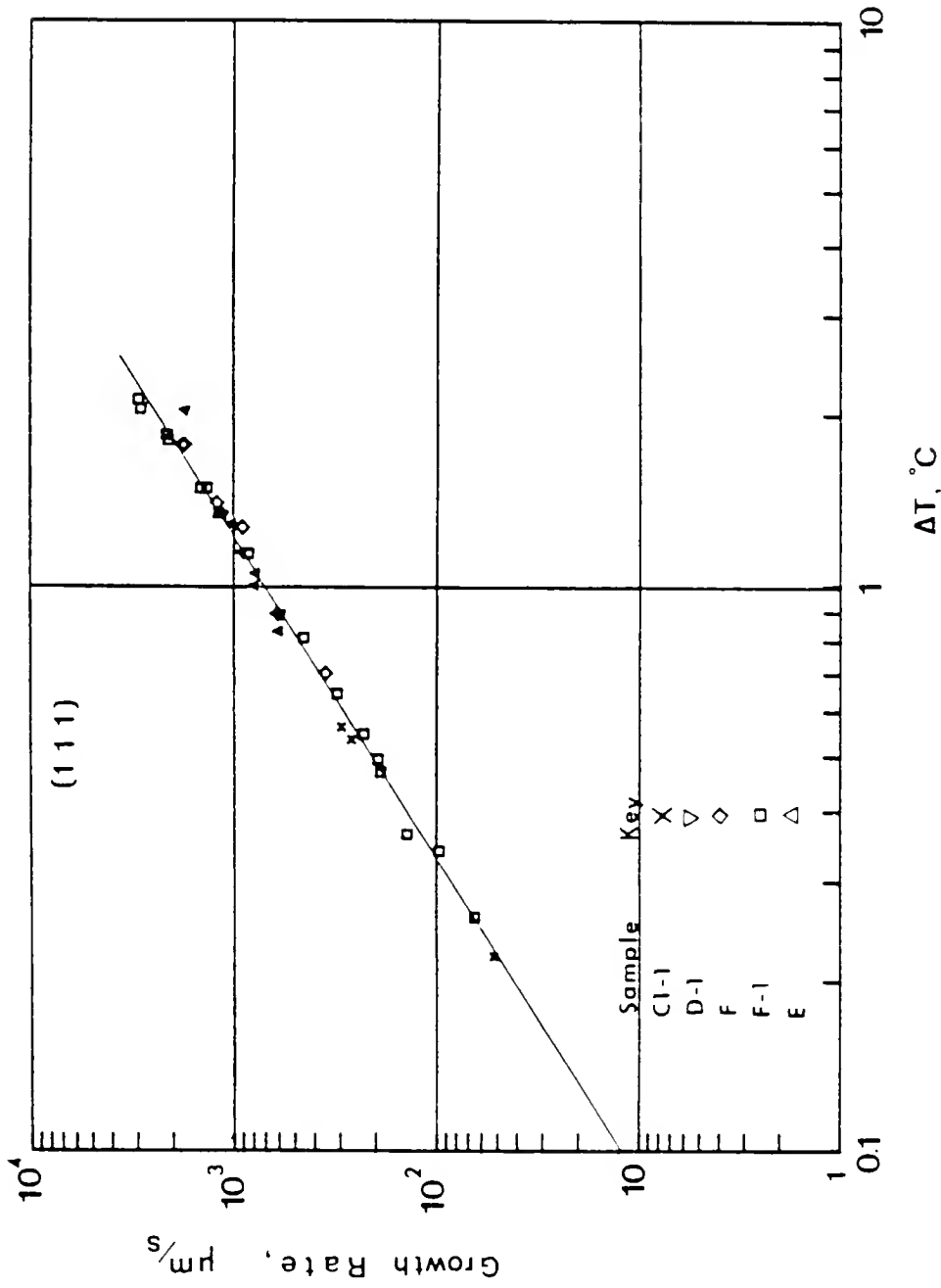
Figure 30 Dislocation-assisted (111) growth rates versus the interface supercooling; line represents the SDG rate equation, as given in Table 7.

and eventually fall under the same kinetics equation. It should also be noted that, although the dislocation-free rates seem to deviate more drastically than those of the dislocated interface in the $(V, \Delta T)$ range before they meet, the latter still moves much faster. The scatter of the $(V, \Delta T)$ points in this range is generally larger than those of the lower supercooling regions. No variations in experimental circumstances could be found which would explain this effect. The estimated errors involved in determining the data points were no more than 5% and 2.5% for the growth velocities and the supercoolings, respectively. These error limits are smaller than the observed scatter in the data. As mentioned previously, even though the growth rates were measured by the resistivity change technique, the interface was still directly observed at the high growth rates region. Nucleation ahead of the interface was never detected, even for the highest bulk supercooling. However, because of the small magnifications involved (7-10X) and the rapid rates, it cannot be claimed that the faceted character of the interface is retained for growth rates larger than about 1 cm/s.

The scatter in the data, as indicated earlier, may be attributed to the combined SDG + 2DNG growth mode or to the common sluggish behavior of transitional kinetics, as in most transformations. Linear regression analysis of data points for growth rates higher than about 6500 μm/s indicates that the data points fall between two almost parallel upper and lower boundaries. The analysis points out that they may be correlated

by a linear relationship, in contrast with a geometric ($V \propto \Delta T^n$) or parabolic relationship. The rate equation is given as

$$V \approx 9500 \ (\Delta T - 2.7), \qquad\qquad \Delta T > 3.5 \qquad\qquad (74)$$

with a coefficient of correlation of about .93.

(001) Interface

The growth behavior of the (001) interface in contact with the supercooled liquid, as shown in Fig. 31, was qualitatively similar to that of the (111) interface, except that the threshold supercooling necessary to obtain a measurable growth rate ($\sim 10^{-3}$ μm/s) for the undisturbed (001) interface was about 0.6°C; only the dislocated (001) interface was mobile below this threshold supercooling. It should be mentioned that the rate measurements for this interface were more difficult than those for the (111) interface. This is because when dislocation(s) would intersect the growth front, the (001) would frequently change into two or more {111} type interfaces or it would grow out of the interface, leaving only a (111) face. Such behavior was also very common at higher supercoolings and particularly when the initial (001) was not perfectly normal to the growth direction. This is understood since the (111) face, if dislocation-free, is immobile for supercoolings up to about 1.5°C and it moves much slower than the (001) face, as discussed later. In contrast with the earlier described growth behavior for the dislocated interfaces, restoration of the initial (001) face was rarely done by itself. Hence, in order to bring out the initial (001) interface, it was necessary to melt the sample back and allow it to grow again.
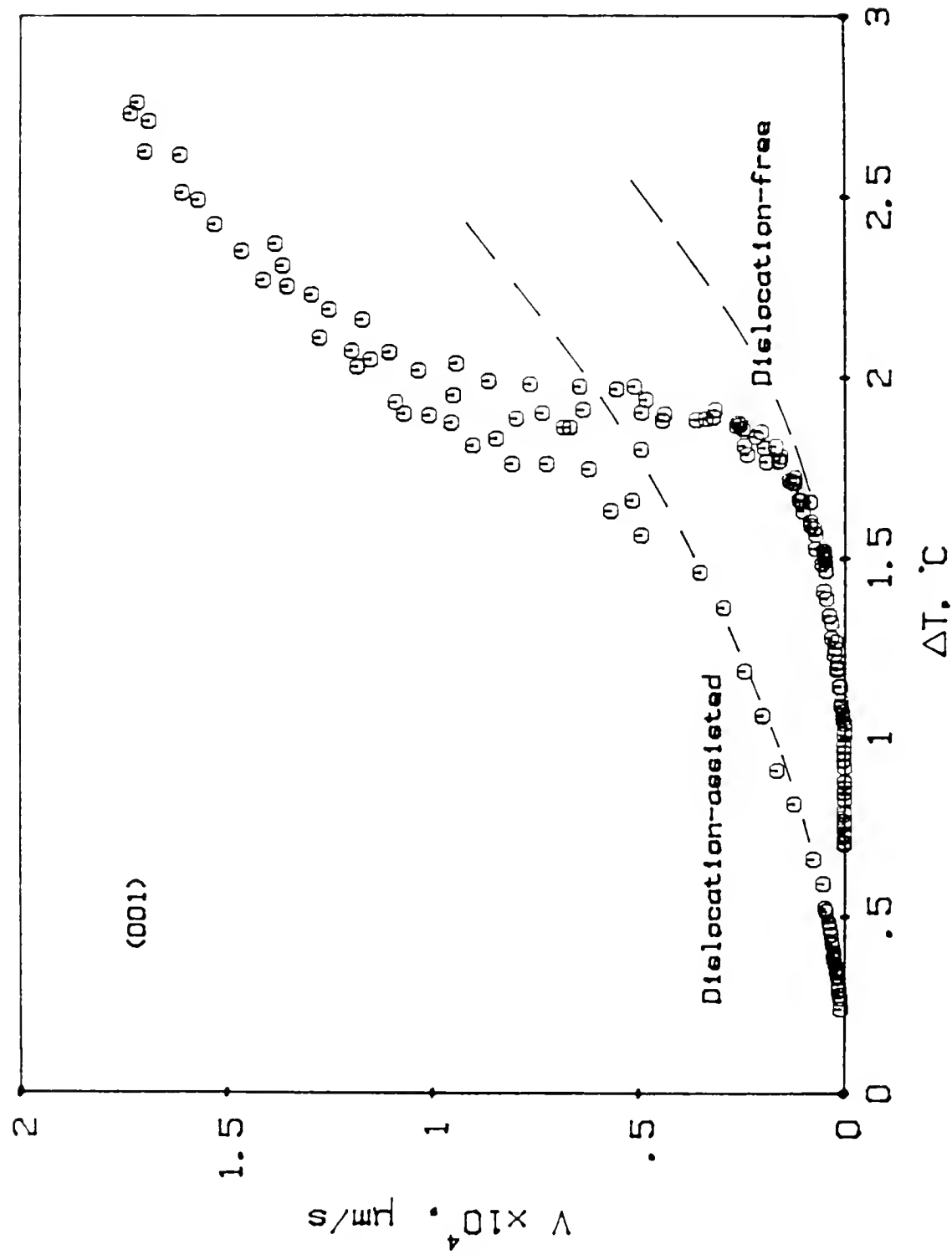
Figure 31 Dislocation-free and Dislocation-assisted growth rates of the (001) interface as a function of the interface supercooling; dashed curves represent the 2DNG and SDG rate equations, as given in Table 7.

The dislocation-free and dislocation-assisted data for the (001) interface are also shown on a log-log scale in Fig. 32. Comparing the (001) with the (111) growth rates, as shown in the composite linear plot of Fig. 33, it is realized that the (001) interface moves much faster than the (111) at any interface supercooling. For example, at $\Delta T = 1.8°C$, the dislocation-free (001) interface is growing by a factor of about 1.5×10^3 faster than the (111) interface, whereas with $\Delta T = .8°C$, the dislocation-assisted (001) interface is growing by a factor of about two faster than the (111) dislocated interface.

Dislocation-Free Growth Kinetics

The dislocation-free (001) data, similar to the (111) interface, can be well correlated up to supercoolings of about 1.5°C, by the general 2DNG equation, eq. (69), presented earlier. Similarly, for a more detailed discussion of the results, the (001) data can be divided into three regions, as shown in Fig. 34. The first region, called MNG, extends from about 0.6-0.8°C interface supercoolings and growth rates up to about 1 μm/s. The second region, PNG, covers the range of about 0.9-1.45°C supercoolings. The growth rates in these two regions are exponential functions of $(- 1/\Delta T)$. The sample size affects only the rates in Region I, but not in Region II. It should be noted that the data in Region II also fall on two separate lines. As will be discussed later, the two rate equations are not due to the effect of the interfacial area. Region III, TRG, follows region II at supercoolings larger than about 1.5°C.

MNG region

The proportionality of the low growth rates (< 1 μm/s) upon the S/L interfacial area is shown in Figs. 35 and 36. In the latter, a plot of
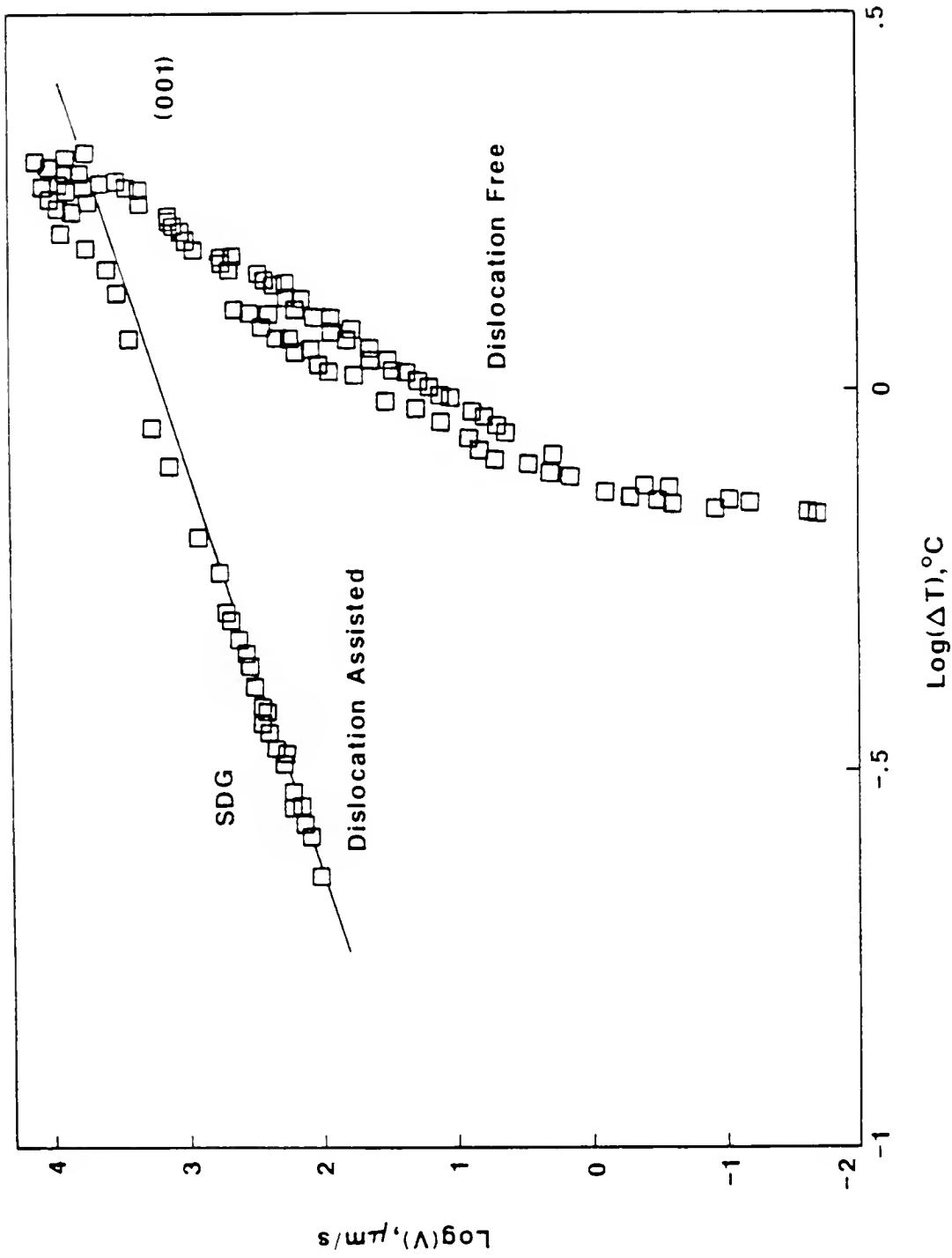
Figure 32   The logarithm of the (001) growth rates versus the logarithm of the interface supercooling; dashed line represents the SDG rate equation, as given in Table 7.
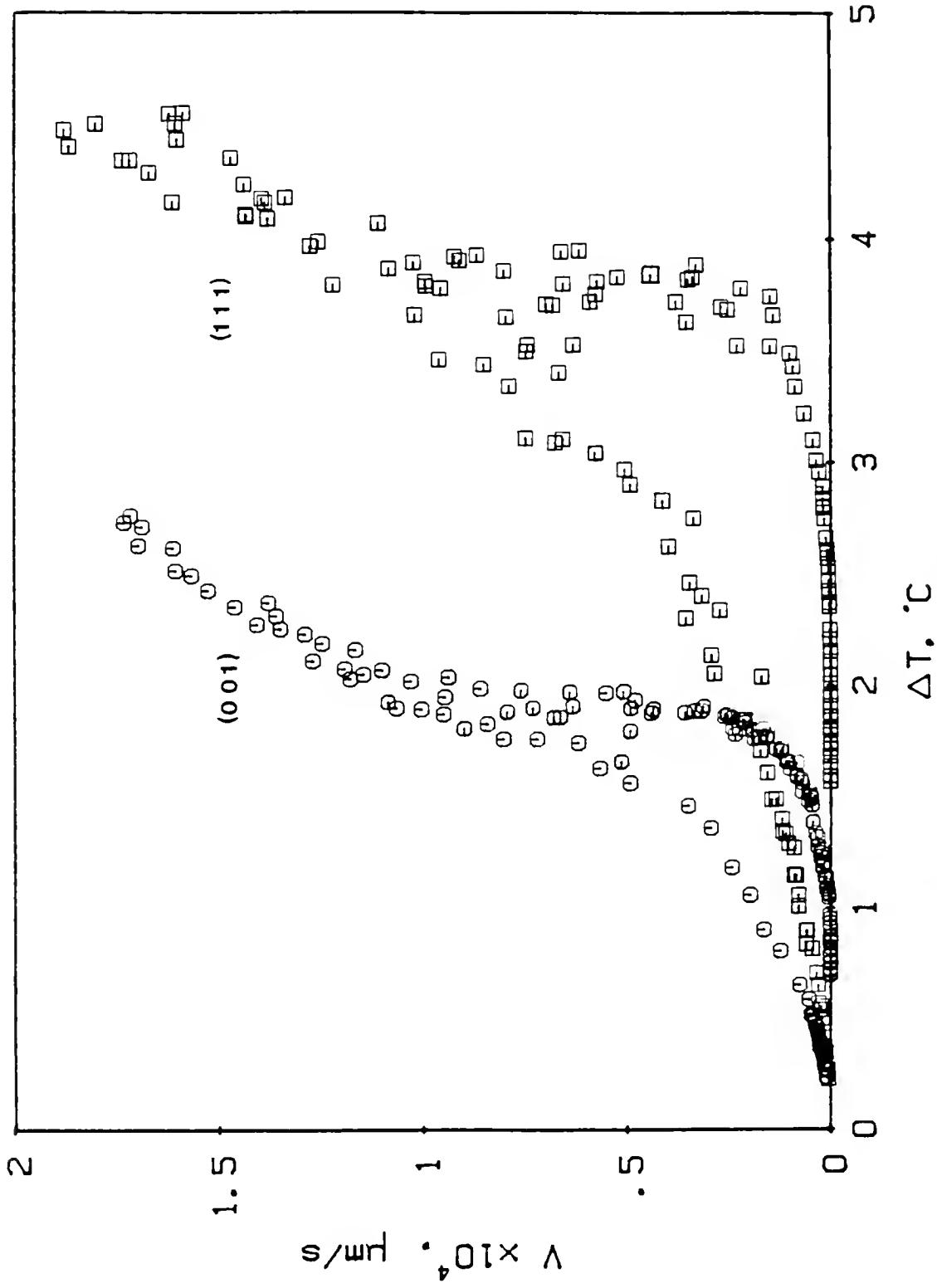
Figure 33   Growth rates of the (001) and (111) interfaces as a function of the interfacial supercooling.
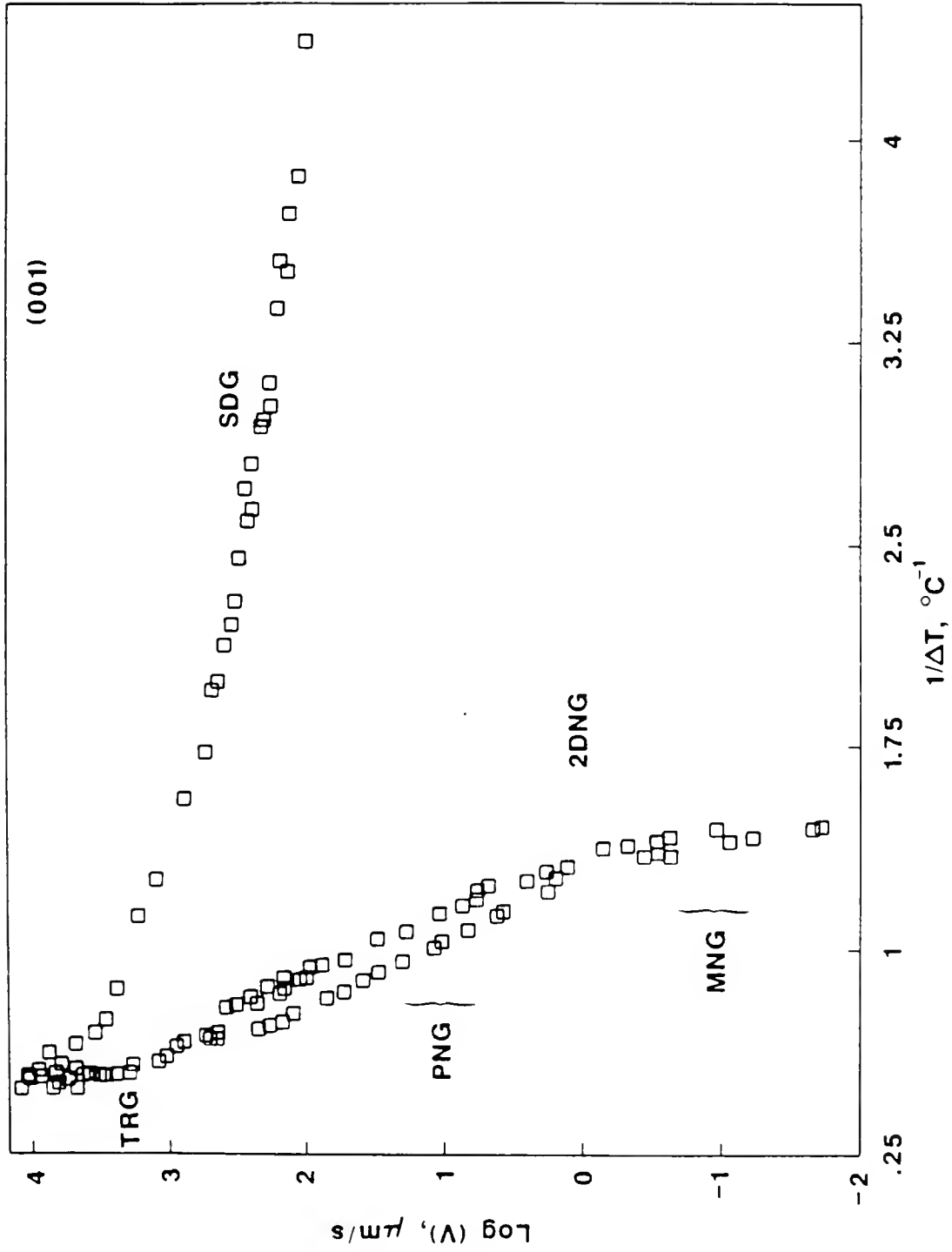
Figure 34   The logarithm of the (001) growth rates versus the reciprocal of the interface supercooling.
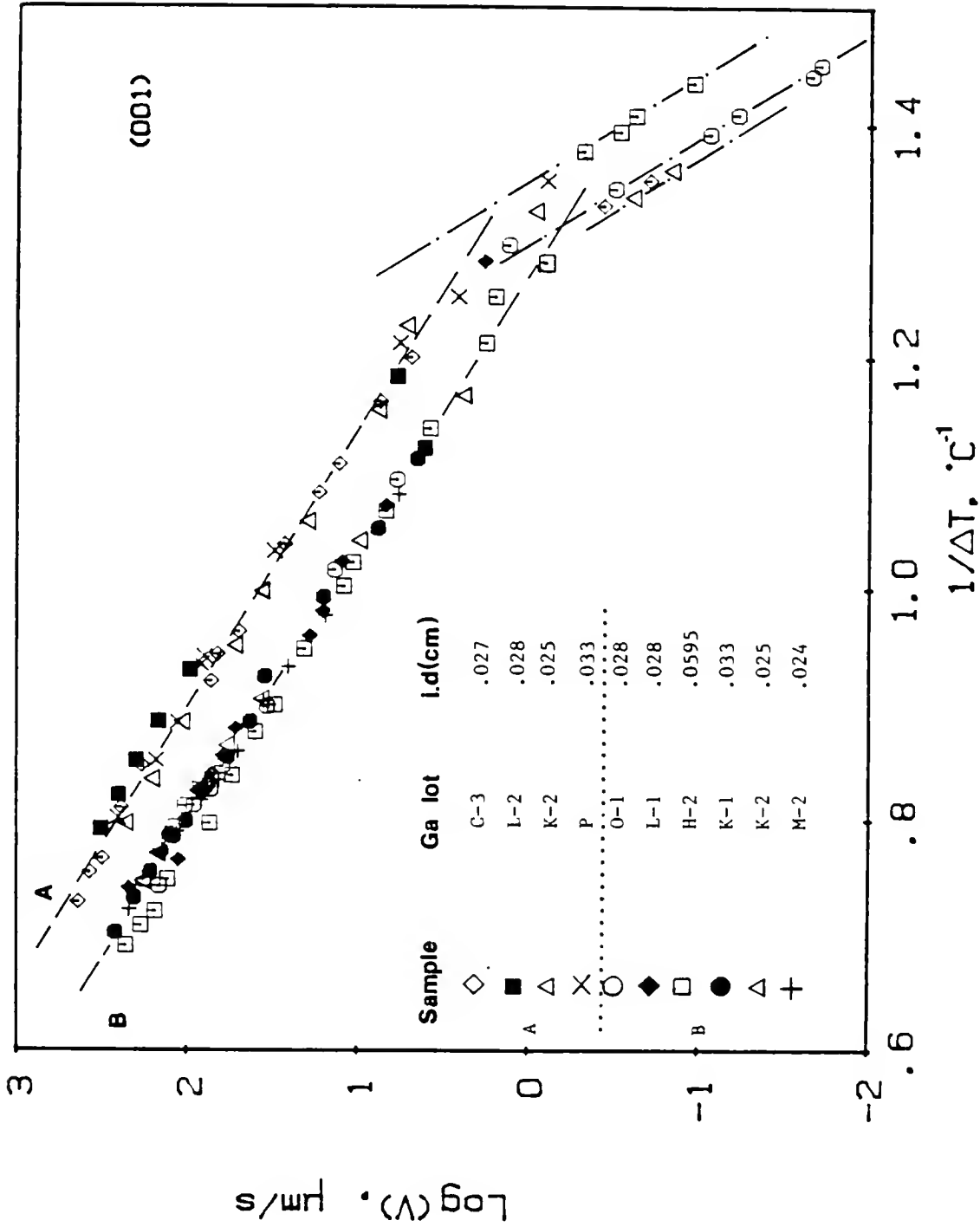
Figure 35 The logarithm of dislocation-free (001) growth rates versus the reciprocal of the interface supercooling for 10 samples; lines A and B represent the PNG rate equations, as given in Table 7.

171
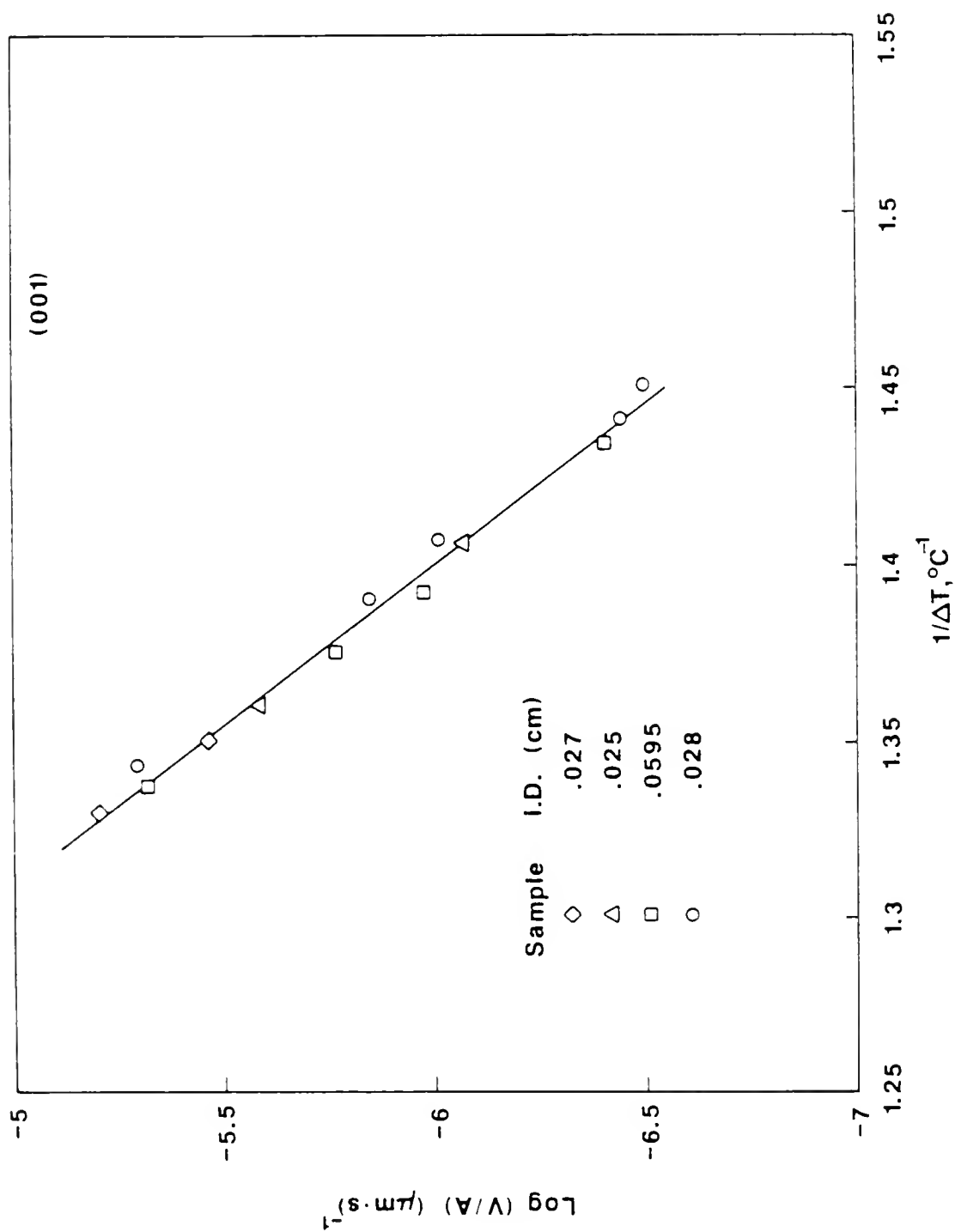
Figure 36   The logarithm of the (001) low growth rates (MNG) normalized for the S/L interfacial area plotted versus the reciprocal of the interface supercooling.

the quantity log (V/A) as a function of the $1/\Delta T$ results in a straight line for four samples with different capillary cross sections. The equation for the regression line, as determined from least square analysis, is given as

$$\log \frac{V}{A} = 17.4702 - \frac{11.0438}{\Delta T}$$

with a coefficient of determination and correlation of 0.99 and 0.995, respectively. The growth rate equation is, therefore, determined as

$$V = 2.948 \times 10^9 \, A \, \exp\left(- 25.428/\Delta T\right) \tag{75}$$

where V is the growth rate in $\mu m/s$ and A is the S/L interfacial area in μm^2. The features of this region, as well as the form of the growth rate equation, as indicated by eq. (75), show that the growth behavior of this region is in good qualitative agreement with the mononuclear growth theory.

PNG region

In this region, the data points are still exponential functions of $(-1/\Delta T)$, but with a smaller slope than that for the MNG region, as shown by the plot of log (V) vs. $1/\Delta T$ in Fig. (35). However, in contrast with the (111) PNG region, the growth data for the (001) interface of 10 samples fall onto two approximately parallel lines A and B; line A is composed from data of four samples and line B from six samples. The growth rate equation as determined from the regression analysis are

$$\text{line A:} \quad V = 6.03 \times 10^5 \, \exp\left(- 9.7/\Delta T\right)$$
$$\text{line B:} \quad V = 2.4 \times 10^5 \, \exp\left(- 9.78/\Delta T\right) \tag{76}$$

where V is the growth rate in $\mu m/s$. The coefficients of determination and correlation are, respectively, .991 and .995 for line A, and .984

and .992 for line B. It should be realized that, unlike the MNG region, the difference between the two rate equations is not due to the effect of the interfacial area; for example, each line comes from samples of different sizes (e.g. for line B max i.d. = .0595 and min i.d. = .024 cm) and samples with a given size fall on both lines. Figure 35 also designates the lot of Ga from which the samples were prepared. As can be seen, for samples prepared from the same Ga lot, the data points fell on either of the two curves. This indicates that the difference between the two lines is not due to possible differences in the residual impurities in the as received Ga lots. Futhermore, for a sample, which gave data points belonging to curve A, was melted in the capillary tube and reseeded, the data points shifted to curve B. Interestingly enough, all samples with the fastest kinetics (line A) also had higher Seebeck coefficients (about 2.5 $\mu V/°C$, see Table 3) than that for the perfectly oriented (001) interface (2.2 $\mu V/°C$), and their interface trace on the glass wall was inclined with respect to the capillary axis by 4-10°. Needless to say, the difference between B and A lines is not due to the inclination, since the actual growth rates of the latter have been corrected to account for the normal growth rates.

Dislocation-Assisted Growth Kinetics

The qualitative similarities between the growth behavior of the (111) and (001) interfaces also hold for the dislocation-assisted growth. The growth rates of the dislocated (001) interface, as shown in Fig. 31, can be fit into the general SDG rate equation, eq. (72), given earlier. The correlation parameters K_D, ΔT_C will be presented in the

next chapter. At supercoolings less than 0.8°C, the growth rates can also be correlated by a nearly parabolic equation. The rate equation, as evaluated from the regression analysis is given as

$$V = 1640 \ \Delta T^{1.93} \tag{79}$$

where V is the growth rate in μm/s. The coefficients of determination and of correlation for this analysis are .988 and .994, respectively.

Growth at High Supercoolings, TRG Region

The behavior of the (001) high supercoolings data is quite similar to that of the corresponding (111) data. This is shown in Figs. 31 and 32, where the results indicate that as ΔT increases, the kinetics deviate from both dislocation-assisted and dislocation-free kinetic laws shown as dashed curves and continuous lines in these figures. The deviation from the low supercoolings laws is in the direction of faster rates at a given ΔT. The two growth modes (SDG and PNG) approach each other as ΔT increases and finally fall under the same kinetics range for supercoolings higher than about 1.75°C. Above this supercooling, the growth rates increase very drastically with ΔT up to supercoolings of about 2°C; still, at higher supercoolings than the latter value of ΔT, the relationship $V(\Delta T)$ becomes linear, as can be seen in Fig. 31. Although this feature is also observed in the (111) V vs. ΔT linear plot (Fig. 23), it seems more pronounced for the (001) growth data. Furthermore, the scatter of the (001) data in the range of the fastest growth rates is less than that of the (111) interface. If a line is drawn from the origin of the V vs. ΔT plot through the data points with growth rates higher than 14000 μm/s, it results in a rate equation given as

$$V = 6300 \ \Delta T \qquad\qquad (78)$$

with a coefficient of correlation equal to .97.

The rate equations of the dislocation-assisted and dislocation-free growth data for both (111) and (001) interfaces up to supercoolings of about 3.5 and 1.5°C, respectively, are summarized in Table 7. The experimental growth kinetics for supercoolings higher than the above mentioned ones are quantitatively described in the Discussion chapter.

In-Doped (111) Ga Interface

The In-doped Ga growth rates have been measured as a function of distance solidified and interface supercooling for two dopant levels, 0.01 and 0.12 wt% In. In addition, the effect of growth direction, with respect to the gravity vector, was also determined by allowing the growth to proceed parallel or antiparallel to the gravity vector. For each composition, the results are presented in the next section in accord with the above mentioned order of the solidification rate variables. It should be noted that all the growth rates mentioned here are dislocation-free rates; also, unless indicated otherwise, the growth direction is antiparallel to the gravity force, $\vec{g}$.

Ga - .01 wt% In

As mentioned earlier, the growth rates of the doped Ga, unlike those of the pure Ga, were a function of the distance solidified at a constant bulk supercooling. The results for three constant but different bulk supercoolings are shown in Fig. 37. It can be seen that the growth rate decreased gradually as the interface moved along the capillary until interfacial breakdown, indicated by arrows in Fig. 37, had

Table 7. Experimental Growth Rate Equations; V in μm/sec and A in μm².

Interface	Growth Mechanism		Supercooling Range, °C	Growth Kinetics
(111)	Dislocation-free, 2DNG	MNG	1.5 - 1.9	$V = 1.7 \times 10^9 \, A \, \exp\left(-\dfrac{58.76}{\Delta T}\right)$
		PNG	2 - 3.5	$V = 9.5 \times 10^5 \, \exp\left(-\dfrac{23.9}{\Delta T}\right)$
	Dislocation-assisted, SDG		.2 - 2	$V = 700 \, \Delta T^{1.7}$
	Kinetic Roughening		> 3.5	$V \propto \Delta T$
(001)	Dislocation-free, 2DNG	MNG	.6 - .8	$V = 2.95 \times 10^9 \, A \, \exp\left(-\dfrac{25.4}{\Delta T}\right)$
		PNG	.8 - 1.45	(A) $V = 6 \times 10^5 \, \exp\left(-\dfrac{9.7}{\Delta T}\right)$ (B) $V = 2.4 \times 10^5 \, \exp\left(-\dfrac{9.78}{\Delta T}\right)$
	Dislocation-assisted, SDG		.2 - 1	$V = 1640 \, \Delta T^{1.93}$
	Kinetic Roughening		> 1.5 .	$V \propto \Delta T$
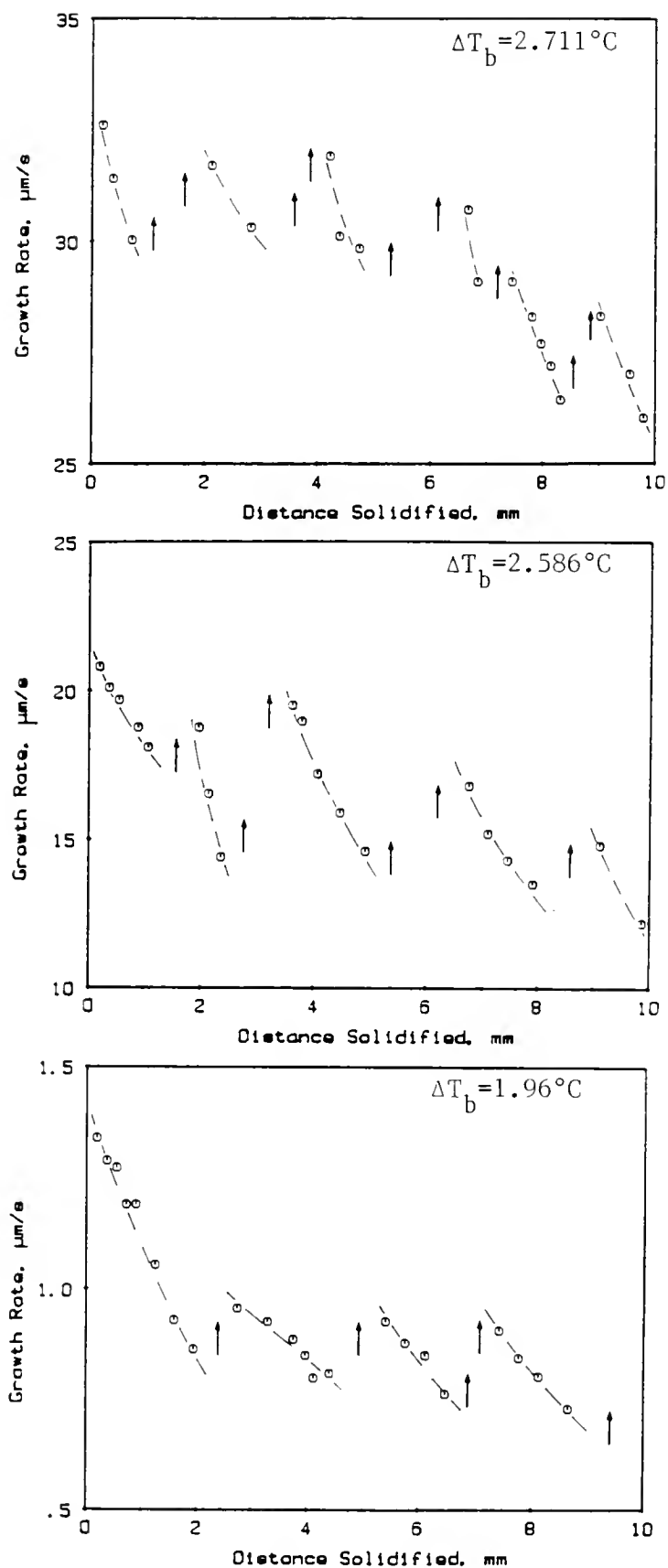
Figure 37   Growth rates as a function of distance solidified of
Ga-.01wt%In at different bulk supercoolings; (↑)
indicates interfacial breakdown.

occurred. During breakdown, the interface moved much faster than prior to it, sometimes by several orders of magnitude. At the same time, the (111) face would break into {111} and/or {001} faces rapidly and a part of the interface would spread across the capillary walls or between the solid and the glass wall entrapping a pocket(s) or a band of liquid, as shown in Fig. 38. After the entrapment, the moving interface left a liquid pocket behind, and assumed its faceted morphology as before the breakdown. The liquid bands or pockets had faceted boundaries, and remained liquid even for bulk supercoolings below the equilibrium eutectic temperature, 16.5°C (see Appendix II); their shape and size was diverse along the sample, but it can be stated empirically that their size decreased as the bulk supercooling increased. A few times the entrapped liquid would appear with boundaries nearly parallel to the (111) interface. It should also be mentioned that sometimes, particularly at large supercoolings, small liquid pockets were formed without any visually noticeable change in the growth rate and front; their detection was only possible by the Seebeck emf output (see Fig. 22).

The frequency of the interface breakdown increased as the bulk supercooling, and hence the growth rate, increased. At bulk supercoolings higher than 3°C, it was not possible to take any rate measurements because the interface appeared to break frequently, even at the beginning of growth. Proceeding the first breakdown, the S/L interface moved with a rate usually slightly higher than that before the growth disturbance, as shown in Fig. 37.
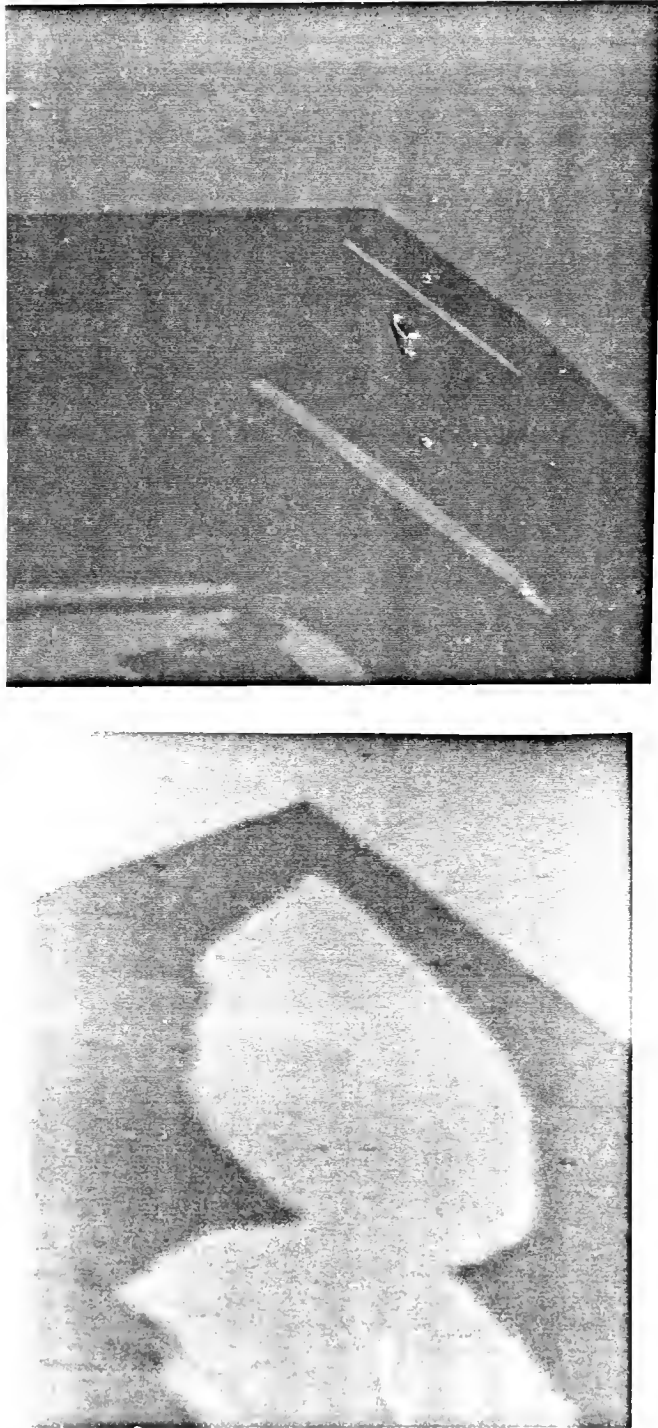
Figure 38   Photographs of the growth front of Ga doped with .01
            wt% In showing the entrapped In rich bands (lighter
            regions), X 40.

The initial growth rates versus the reciprocal of the interface supercooling are shown on a semi-log scale in Fig. 39 as solid symbols. The open symbols connected to them by the dotted curves show the effect of distance solidified on the growth rate at a given ΔT_b. The line in Fig. 39 represent the growth rate equations of the pure (111) Ga interface, as given in Table 6.

The interface supercooling was calculated based on the bulk supercooling and liquidus temperature, T_L, of the Ga-.01 wt% In as

$$\Delta T = \Delta T_b - \delta T - \delta T_s = T_L - T_b - \delta T - \delta T_s \qquad (79)$$

where δT is the heat transfer correction (see calculations and discussion in Appendix III) and δT_s is the temperature correction because of the solute build up given as

$$\delta T_s = -m (C_i - C_o)$$

As defined earlier, m is the liquidus slope, C_i is the instantaneous interface composition, and C_o is the bulk composition. As discussed in the "Segregation" section, as the doped interface grows, it rejects solute ahead of the interface (for k < 1). Hence, the interfacial composition C_i is higher than the initial bulk composition C_o. δT_s is zero at the onset of growth when $C_i = C_o$ and since m < 0, it increases with distance solidified (see eq. (62) where $C_\ell = C_i$). Therefore, δT_s, by itself, should result in a decreased interface supercooling since the interface equilibrium temperature is lower than that of the interface at
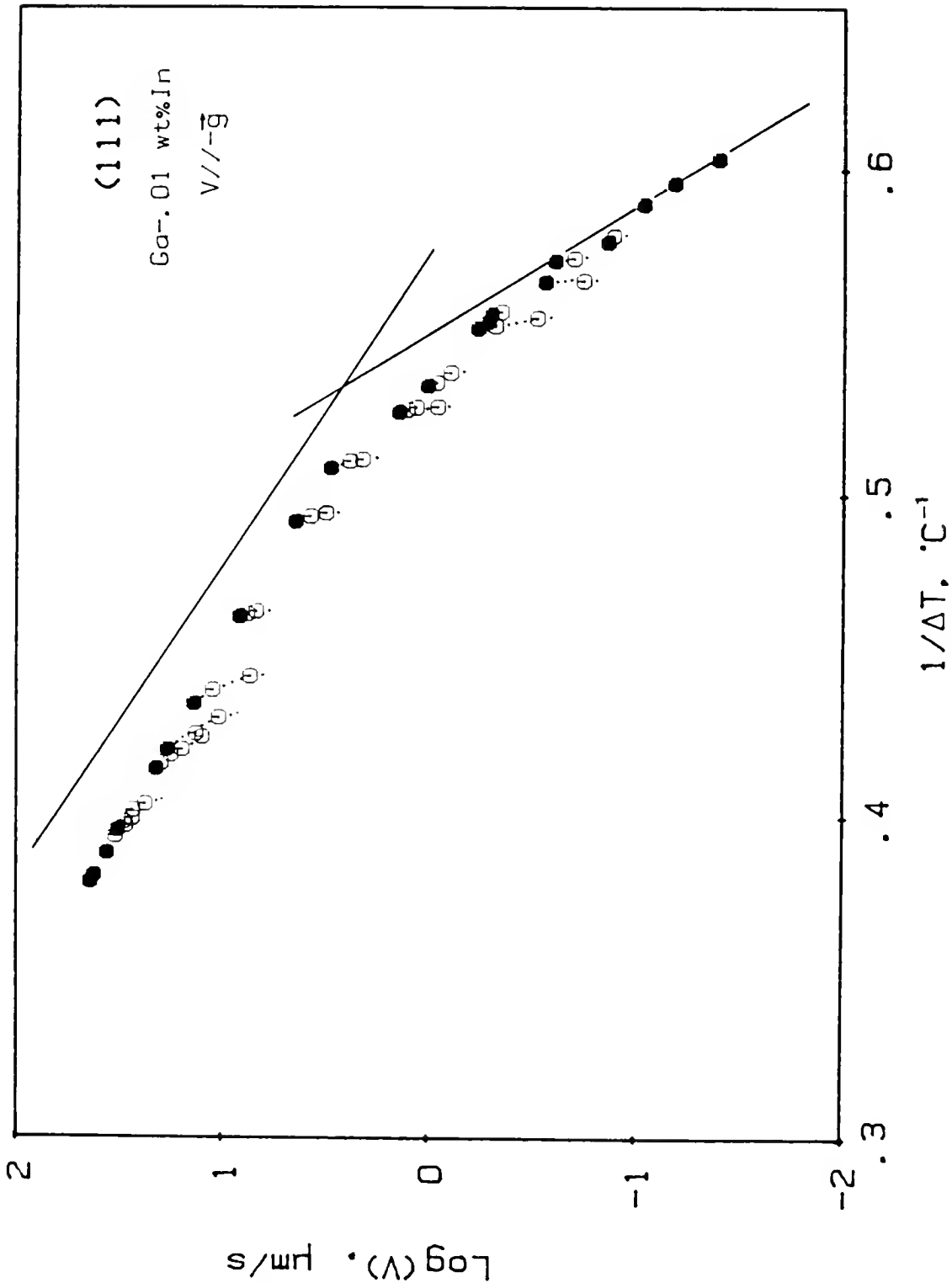
Figure 39 Initial (111) growth rates of Ga-.01 wt% In as a function of the interface supercooling; (···O···) effect of distance solidified on the growth rate, and (——) growth rate of pure Ga.

the initiation of growth. Consequently, as the interface supercooling is reduced, the growth rate decreases with distance, as shown in Fig. 37. This simple explanation for the observed behavior of the data points in the log V(x) vs. 1/ΔT plot, Fig. 39, disregards (for the moment) the effect of solute on the kinetics and the fact that δT decreases as the growth rate decreases; however, a detailed discussion of these effects, together with a more detailed explanation of the growth rate-supercooling relation will be given in the Discussion chapter.

As depicted in Fig. 39, the initial growth rates are exponential functions of 1/ΔT, and similar to those of the pure material; there is a limiting supercooling of about 1.5°C for a measurable growth rate, and the results seem to fall into two regions, i.e. the mononuclear and the polynuclear. The rate equations for the initial growth the two regions were estimated as approximately

$$\text{MNG:} \quad V = 9.96 \times 10^6 \text{ A } \exp(-50.23/\Delta T) \tag{80}$$

$$\text{PNG:} \quad V = 1.88 \times 10^5 \exp(-21.8/\Delta T) \tag{81}$$

where V is given in μm/s and A is the interfacial area in μm^2; the coefficients of correlation of the two rate equations are .999 and .994, respectively. Also note that the regression analysis for the PNG region extends up to supercoolings of about 2.55°C. In the MNG region, the growth rates are slightly lower than those of the pure Ga. On the other hand, the rate equation, eq. (80), has a slope almost the same as that

of the pure Ga. In the PNG region, the rates for the doped material are also slower; however, as the supercooling increases, the rates gradually increase and fall above the extrapolated regression line for these of the lower supercoolings. This behavior is intensified with increasing C_i, as shown in Fig. 39, for the rates as a function of the distance solidified.

The growth rate of the doped interface when growing parallel to the gravity vector, wersus the distance solidified, is shown in Fig. 40. Note that the rate decreases with distance from the onset of growth until the interface breaks, as for the interface growing upward. However, in comparing Figs. 37 and 40, it should be noted that at a given bulk supercooling, the doped interface becomes unstable less frequently when it grows downward; furthermore, for the latter growth direction, the initial growth rates are higher and seem to decrease less drastically with distance than those for upwards growth.

The growth rates of the interface growing downwards versus the interface supercooling are given in Fig. 41. In this figure, similar to Fig. 39, the effect of the distance solidified in V is also shown by dotted lines. For the parallel $\vec{g}$ growth direction, the rates also closely follow those of the pure Ga, with the latter ones still being higher. However, in comparison with the rates of the interface moving upward, it is revealed that the latter are smaller at a given interface supercooling, as shown in Fig. 42. At the lower supercoolings, the two rates are comparable. However, as the ΔT increases, the rates of the
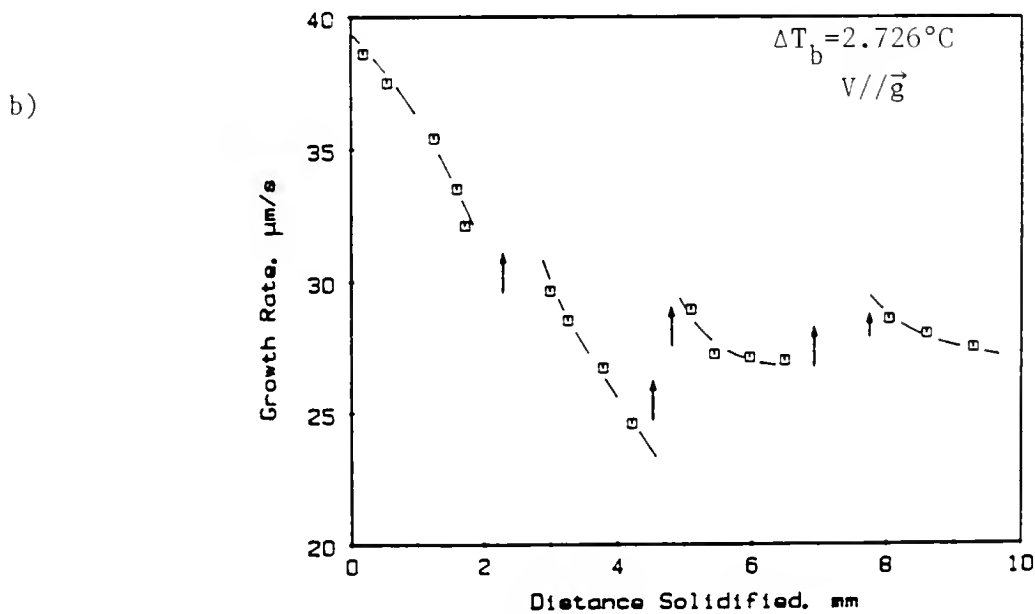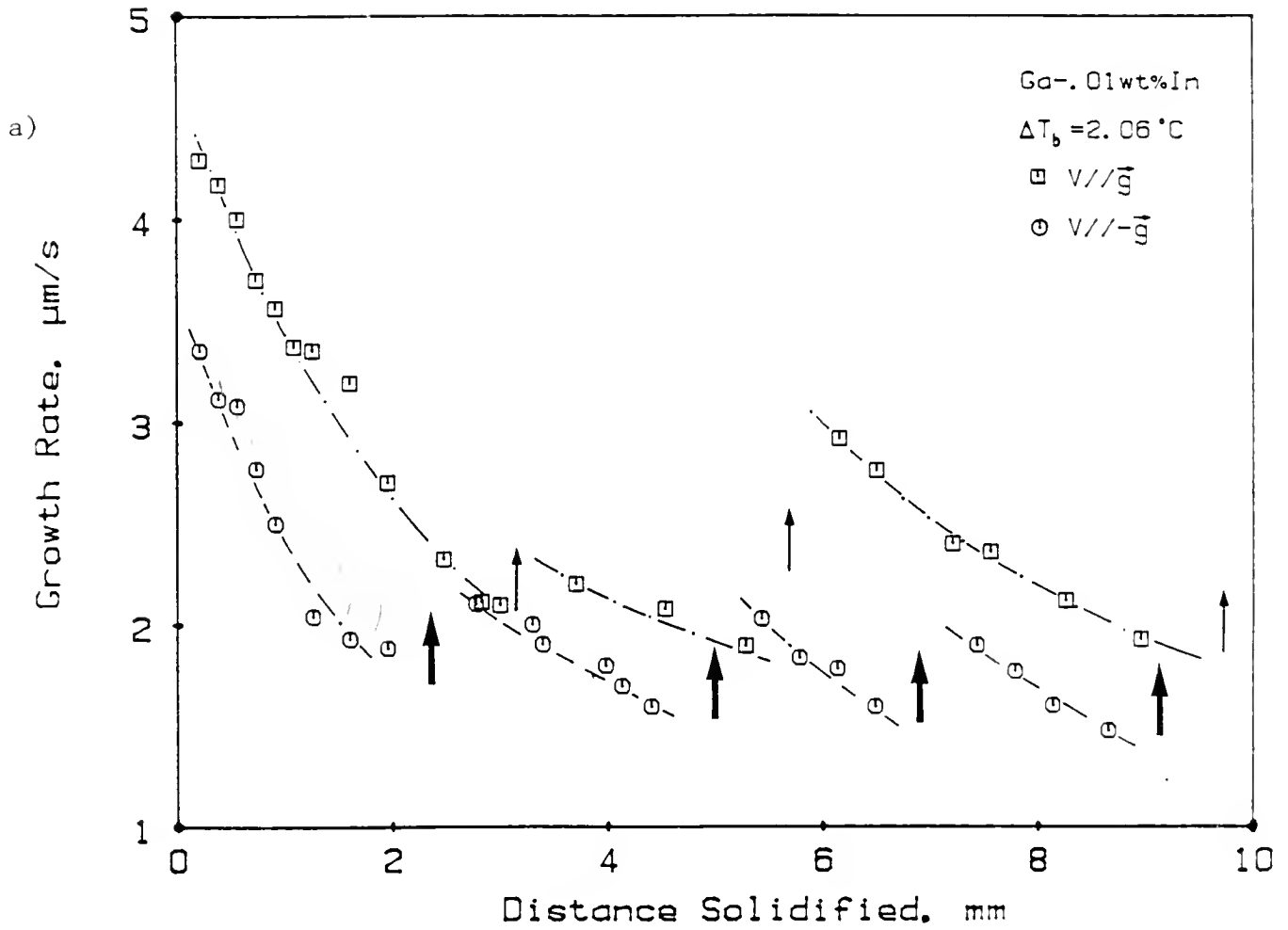
Figure 40   Effect of distance solidified on the growth rate of Ga-.01wt%In
            grown in the direction parallel to the gravity vector (a,b),
            and comparison with that grown in the antiparallel direction(a).
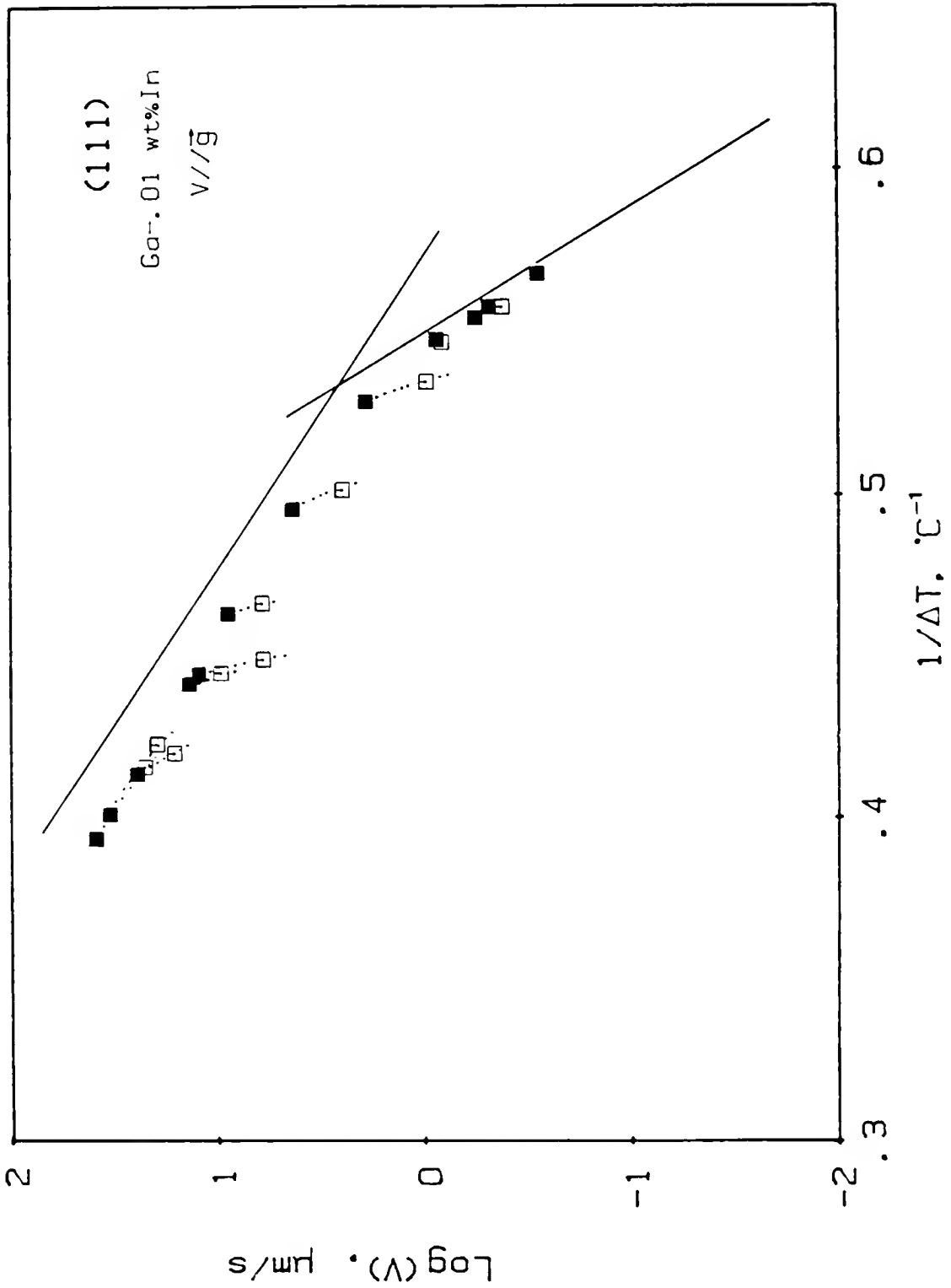
Figure 41 Initial (111) growth rates of Ga-.01 wt% In grown in the direction parallel to the gravity vector; (··□··) effect of distance solidified on the growth rate, and (——) growth rate of pure Ga.

186
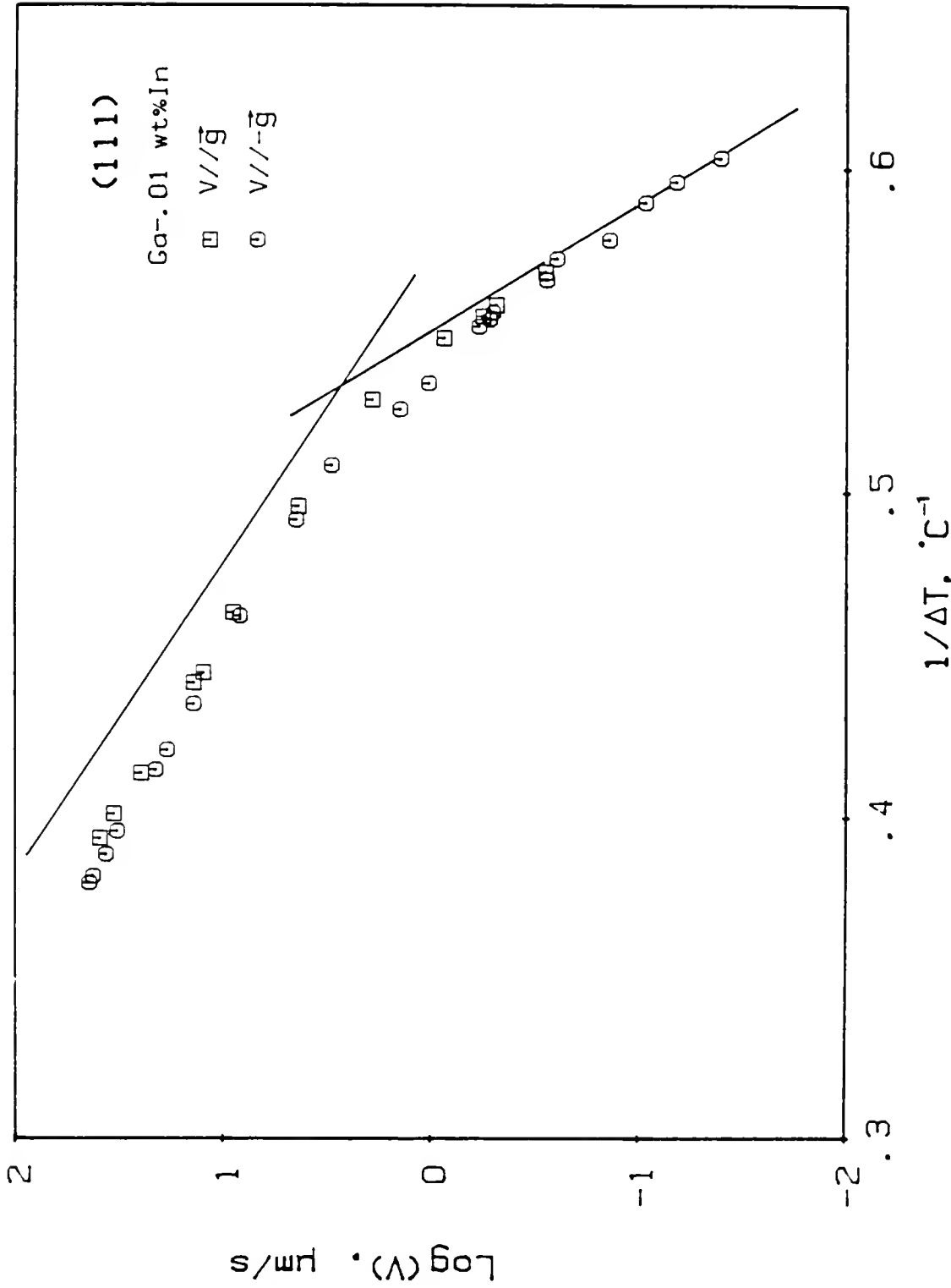
Figure 42   Comparison between the growth rates of Ga-.01 wt% In in the direction parallel (□) and antiparallel (○) to the gravity vector as a function of the interface super-cooling; line represents the growth rate of pure Ga.

interface that advances downward are higher by as much as 15% in the range of 30 μm/s growth rates.

The rate equations for the two growth regions are determined to be as

$$\text{MNG:} \quad V = 14.6 \times 10^7 \text{ A } \exp(-54.8/\Delta T) \tag{82}$$

$$\text{PNG:} \quad V = 2.217 \times 10^5 \exp(-22.019/\Delta T) \tag{83}$$

where V is in μm/s.

Ga - .12 wt% In

Increasing the In content to .12 wt% In had a similar effect on the growth kinetics, as compared with the .01 wt% In alloy, but several distinguishing features were observed. The addition of .12 wt% In to Ga caused very frequent interruptions in growth and multifacet formation at the growth front. Nevertheless, the growth behavior was similar to that of .01 wt% In; the growth rates at a constant bulk temperature were still a function of the distance solidified. Here, following the interfacial breakdown, there was always entrapped liquid, which sometimes extended as much as .5 cm along the capillary. The size of the entrapped liquid decreased with increasing supercooling, as before. The frequency of the interfacial breakdown was more for the .12 wt% In-doped Ga, as shown in Fig. 43.

The growth rates as a function of the interface supercooling for the .12 wt% In-doped (111) Ga interface are shown in Fig. 44 on a log(V) vs. 1/ΔT plot. It appeared that, over the range of supercoolings indicated, the interface retained its faceted character, and the growth
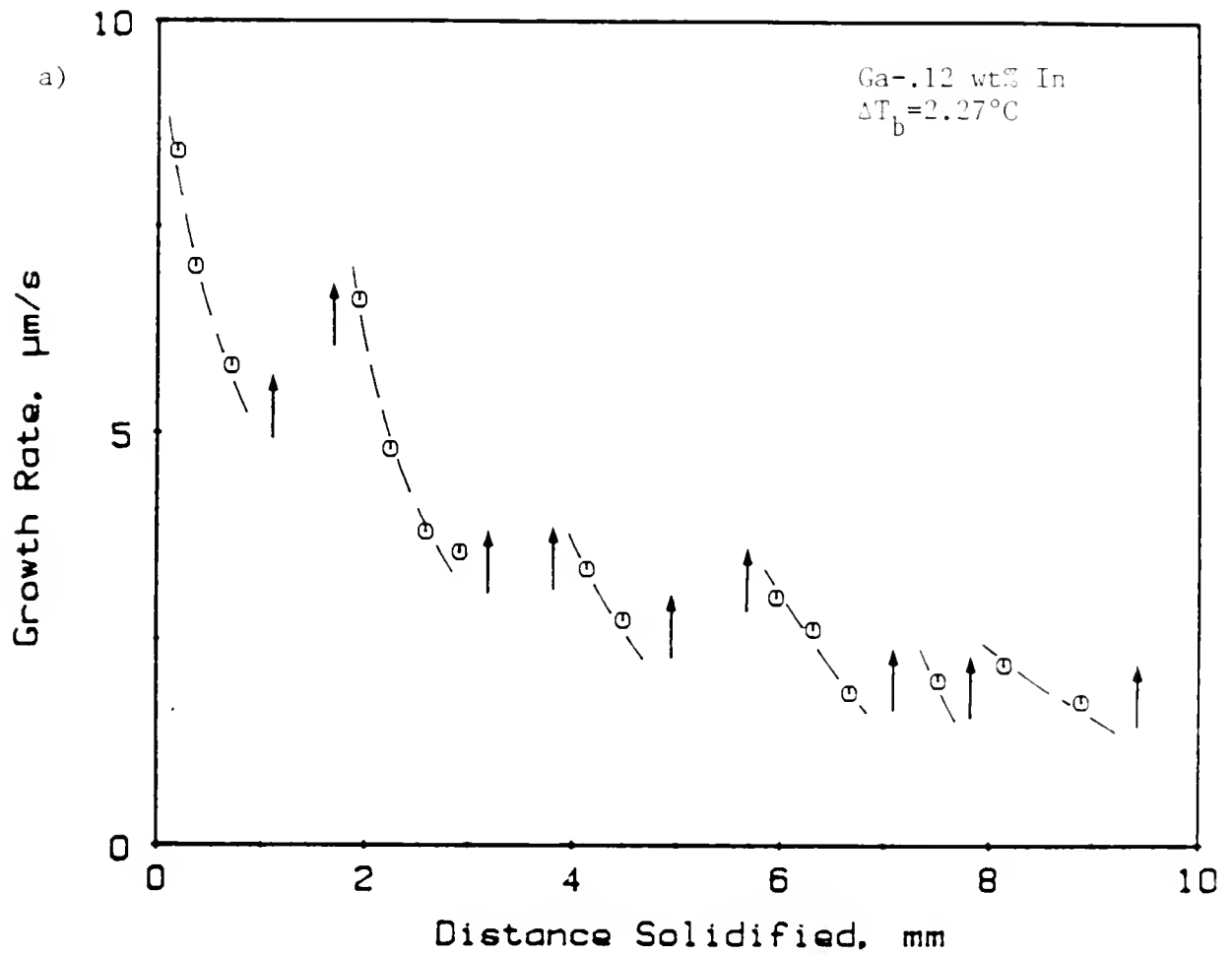
Figure 43   Growth behavior of Ga-.12 wt% In (111) interface; a) Growth
rates as a function of distance solidified, b) Growth front
X40; solid shows as darker regions
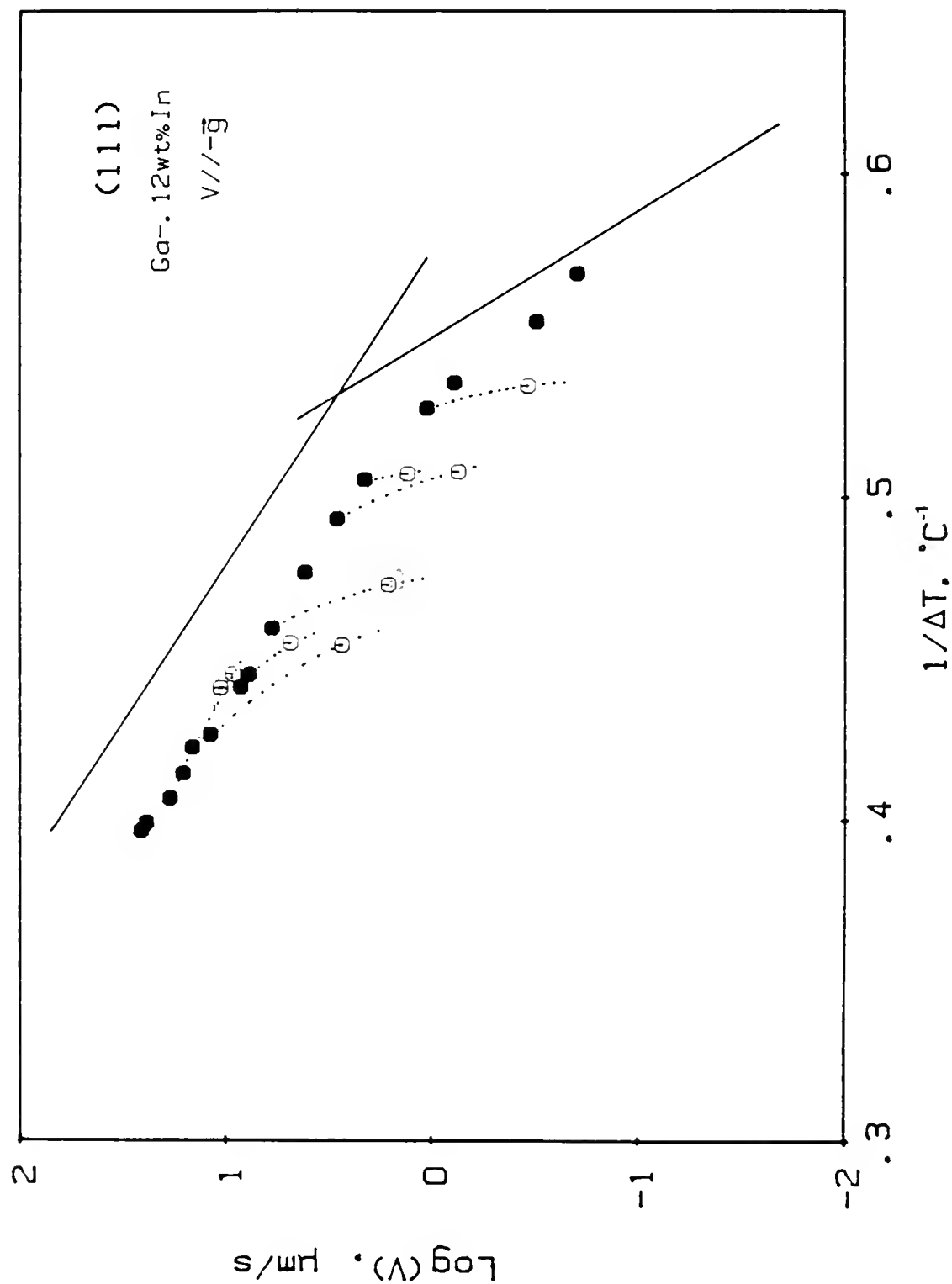
Figure 44 Initial (111) growth rates of Ga-.12 wt% In a a function of the interface super-
cooling; (·o···) effect of distance solidified on the growth rate, and (——) growth
rate of pure Ga.

kinetics had the characteristics of the 2DNG mechanism. Nevertheless, the growth rate at a given ΔT for the .12 wt% alloy is much smaller than that of the pure Ga and that of the .01 wt% alloy, as shown in Figs. 44 and 45. The data in the growth rates range of 1 to 12 μm/s are correlated with an equation in the form of

$$V = 7 \times 10^4 \exp(-20.47/\Delta T) \tag{84}$$

where V is the growth rate in μm/s.[*]

The growth rates as a function of the interfacial supercooling of the .12 wt% In sample growing in the direction parallel to the gravity vector are shown in Fig. 46. As can be seen in this plot, the growth rates at a given supercooling are higher than those of the .12 wt% In-doped Ga solidified in the antiparallel direction to $\vec{g}$. The difference with the latter is more easily depicted from Fig. 47, which gives a linear plot of the initial growth rate versus ΔT.

The rate equation for growth parallel to the gravity vector was determined from the data points for V > 2 μm/s as

$$V = 1.07 \times 10^5 \exp(-21/\Delta T) \tag{85}$$

where V is in μm/s.

---

[*] For both growth directions for the Ga-.12 wt% In sample, the number of data points for growth rates less than 1 μm/s (MNG) is too small to estimate realistic values for the rates constants.
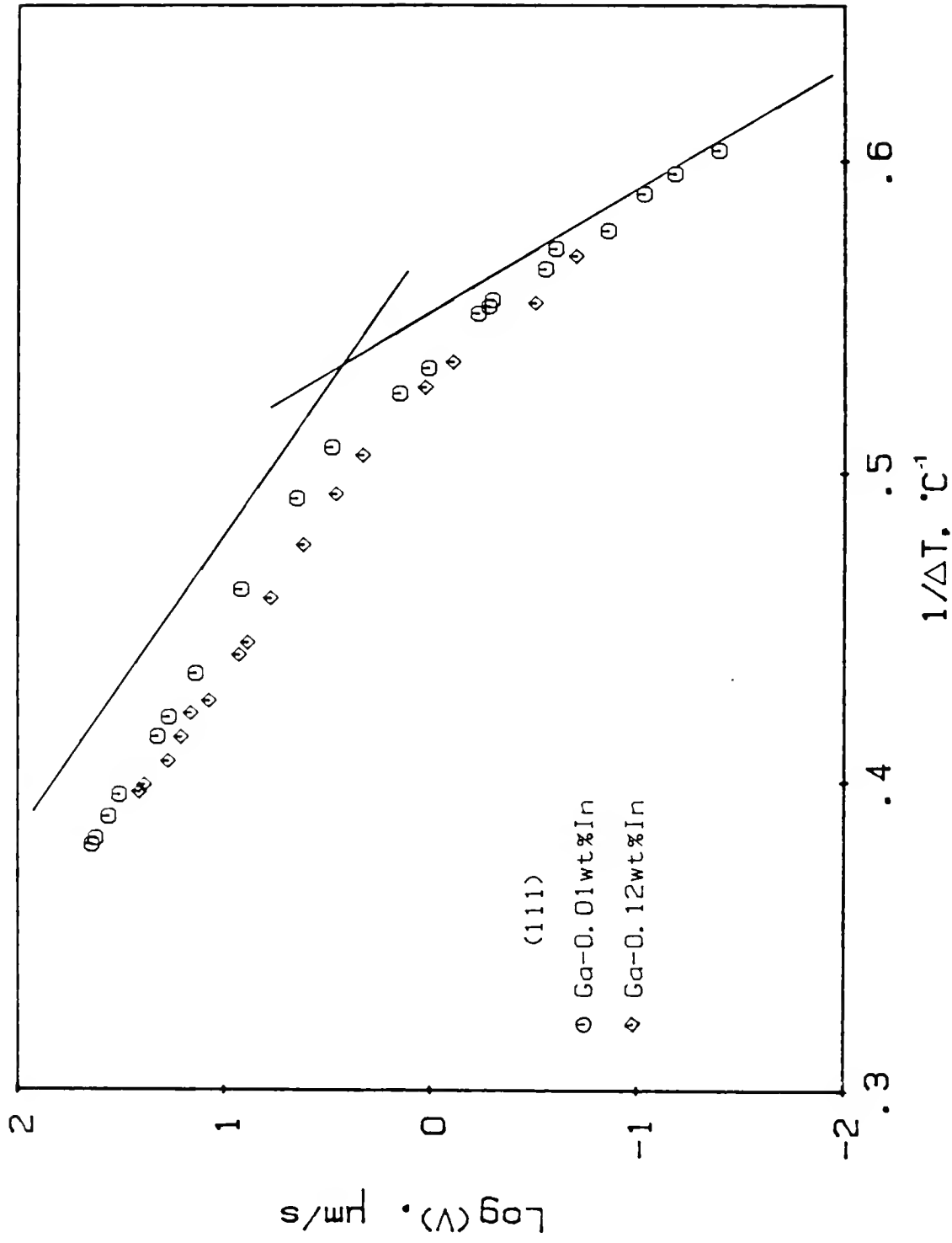
Figure 45 Initial (111) growth rates of Ga-.01 wt% In (O) and Ga-.12 wt% In (◇) as a function of the interface supercooling; line represents the growth rate of pure Ga.
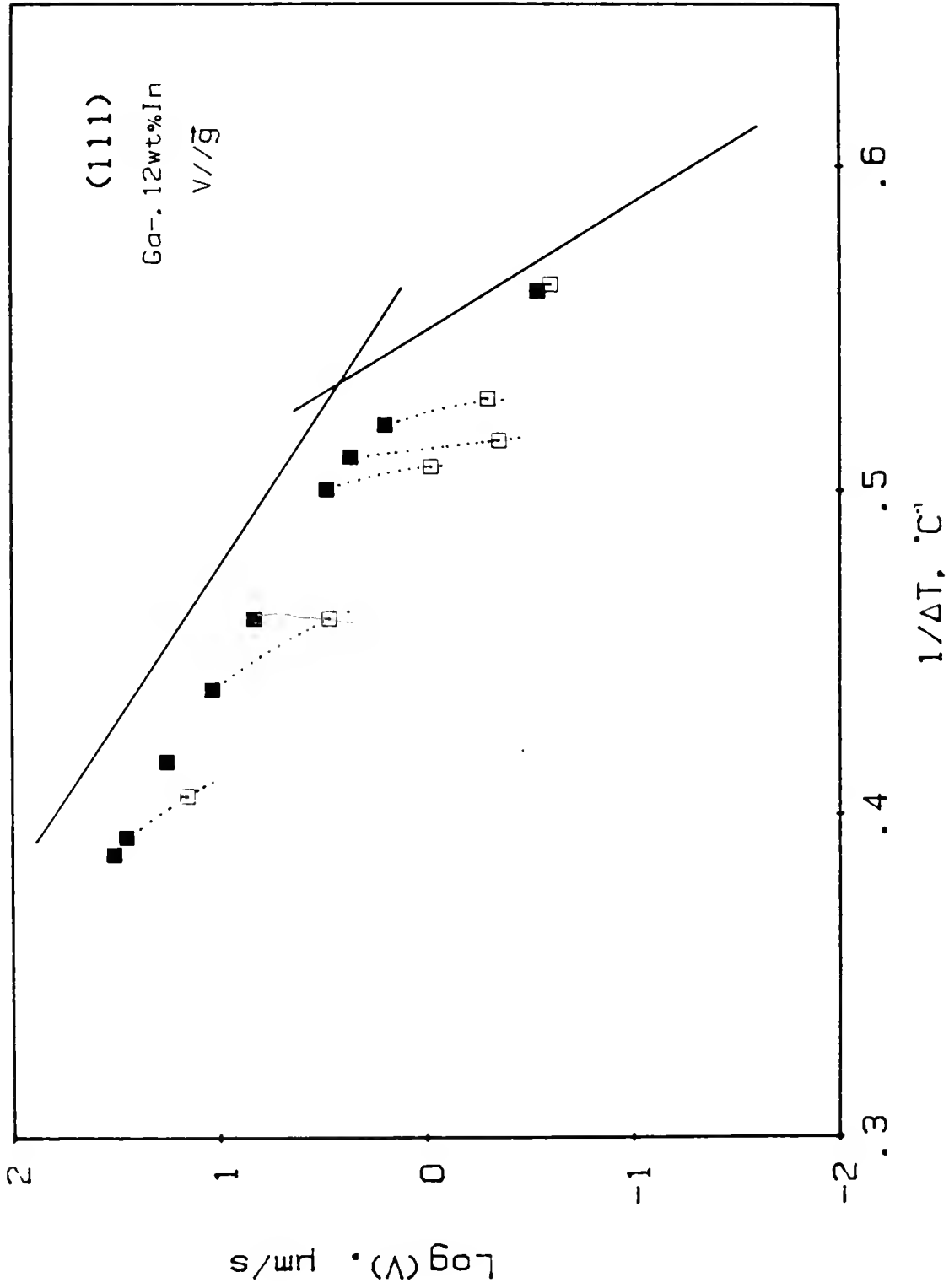
Figure 46   Initial (111) growth rates of Ga-.12 wt% In growth in the direction parallel to the gravity vector as a function of the interface supercooling; (··□··) effect of distance solidified, and (———) growth rate of pure Ga.
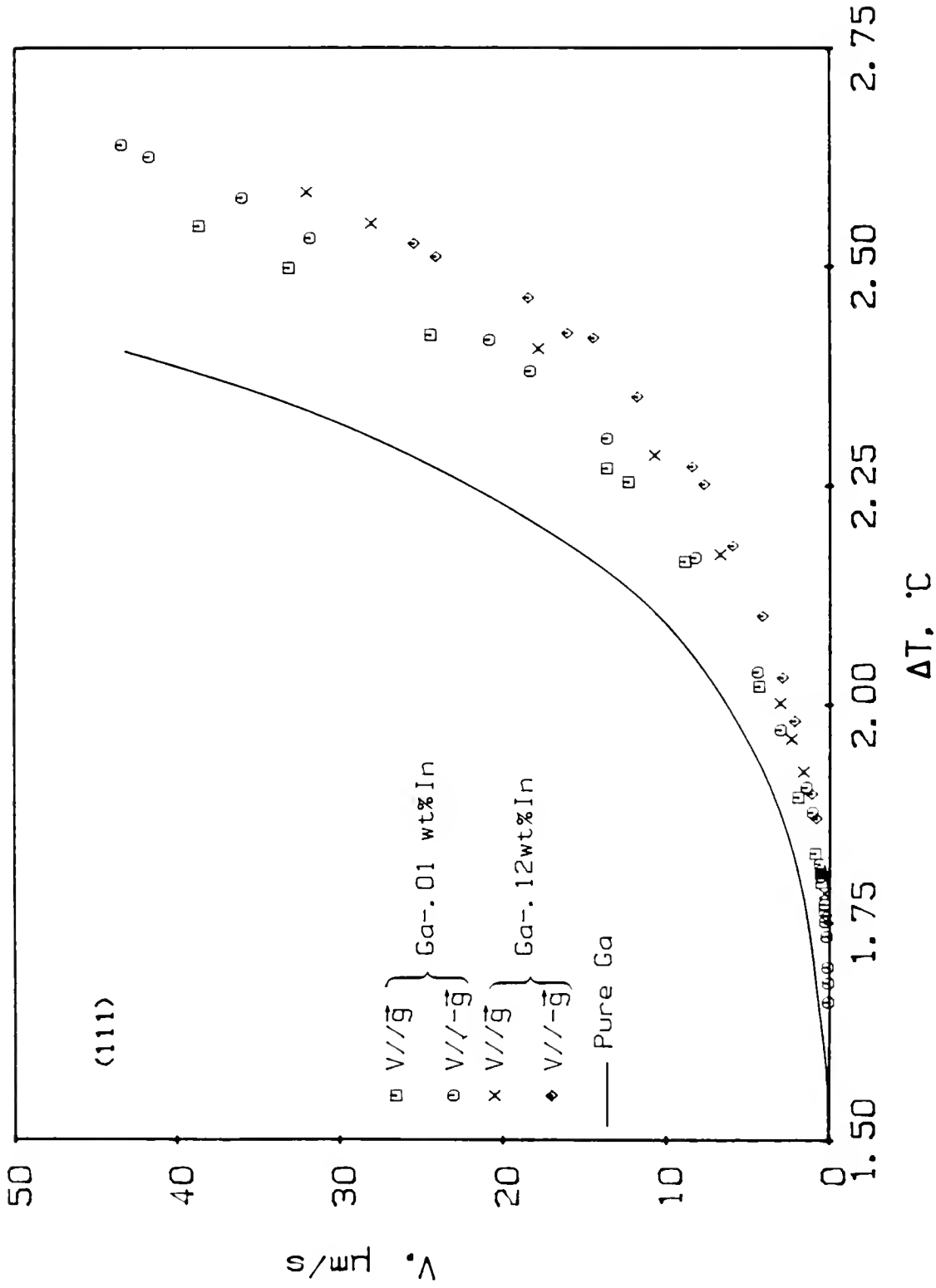
Figure 47 Initial (111) growth rates of Ga-.01 wt% In (□ , ○) and Ga-.12 wt% In (✕ , ◇) grown in the direction parallel (□ , ✕) and antiparallel (○ , ◇) to the gravity vector; continuous line represents the growth rate of pure (111) Ga interface.

CHAPTER V
DISCUSSION

Pure Ga Growth Kinetics

Interfacial Kinetics Versus Bulk Kinetics

Since the beginning of this century, when the first crystal growth mechanism was proposed,[194] the importance of the interfacial supercooling has been realized as all theoretical treatments of growth deal with the form of the relation between the growth velocity and the supercooling at the interface. The interfacial supercooling is also important in describing various aspects of solidification of undercooled melts such as, for example, morphological stability, microsegregation, and growth anisotropy. Notwithstanding, most experimental investigations, as discussed earlier, disregard the essential role of the interfacial supercooling and deal with bulk kinetics. According to the present experimental results, as shown in Fig. 24, the (111) Ga growth kinetics as a function of the bulk supercooling can be represented by

$$V = k_b \; \Delta T_b{}^2$$

where k_b is a constant dependent upon the supercoolings range; for example, in the range of 30-500 μm/s, k_b is determined as 22 (μm/s$^\circ$C^2). In view of this parabolic relationship, and in the absence of interfacial supercooling measurements, not only the true growth modes of the interface would be hidden, but also a false agreement between theoretical growth laws and the experiment could be readily concluded. This is

194

due to the fact the a $(\Delta T)^2$ growth law could arise in different ways, as indicated earlier.

Another misconception in using the bulk kinetics is that the value of the coefficient k_b depends on the heat transfer conditions, sample and interface geometry, and the specifics of the experimental set-up. This complicates interpretation of the results and may explain the contradictory conclusions reached by various investigators on the growth mode and kinetics, even for the same material (see earlier example on the growth kinetics of Sn). An example of the effect of sample size on bulk kinetics is illustrated in Fig. 48, where the interfacial and bulk kinetics for the Ga (111) interface are given for samples of different S/L interfacial areas but growth under otherwise identical conditions. The heat transfer calculations (see Appendix III) show that the interface temperature is related to the bulk temperature by an overall heat transfer coefficient h_c. The coefficient is shown to increase approximately proportionally to the interfacial area. Therefore, at a given bulk temperature, the sample with the largest diameter exhibits the highest interface temperature, and, consequently, the slowest bulk kinetics. In contrast, the interfacial kinetics (not the growth rate) are the same for both cases in this example. On the other hand, as discussed earlier, there are situations where differences in the mechanism of growth of one and the same material really exist because of the unsimilar conditions in the crystal/melt interface. The problem with using bulk kinetics in this case is that, as can be seen in Fig. 24, it is not sensitive enough to allow for detection of these growth mechanisms. In the following sections, the reliability and accuracy of the
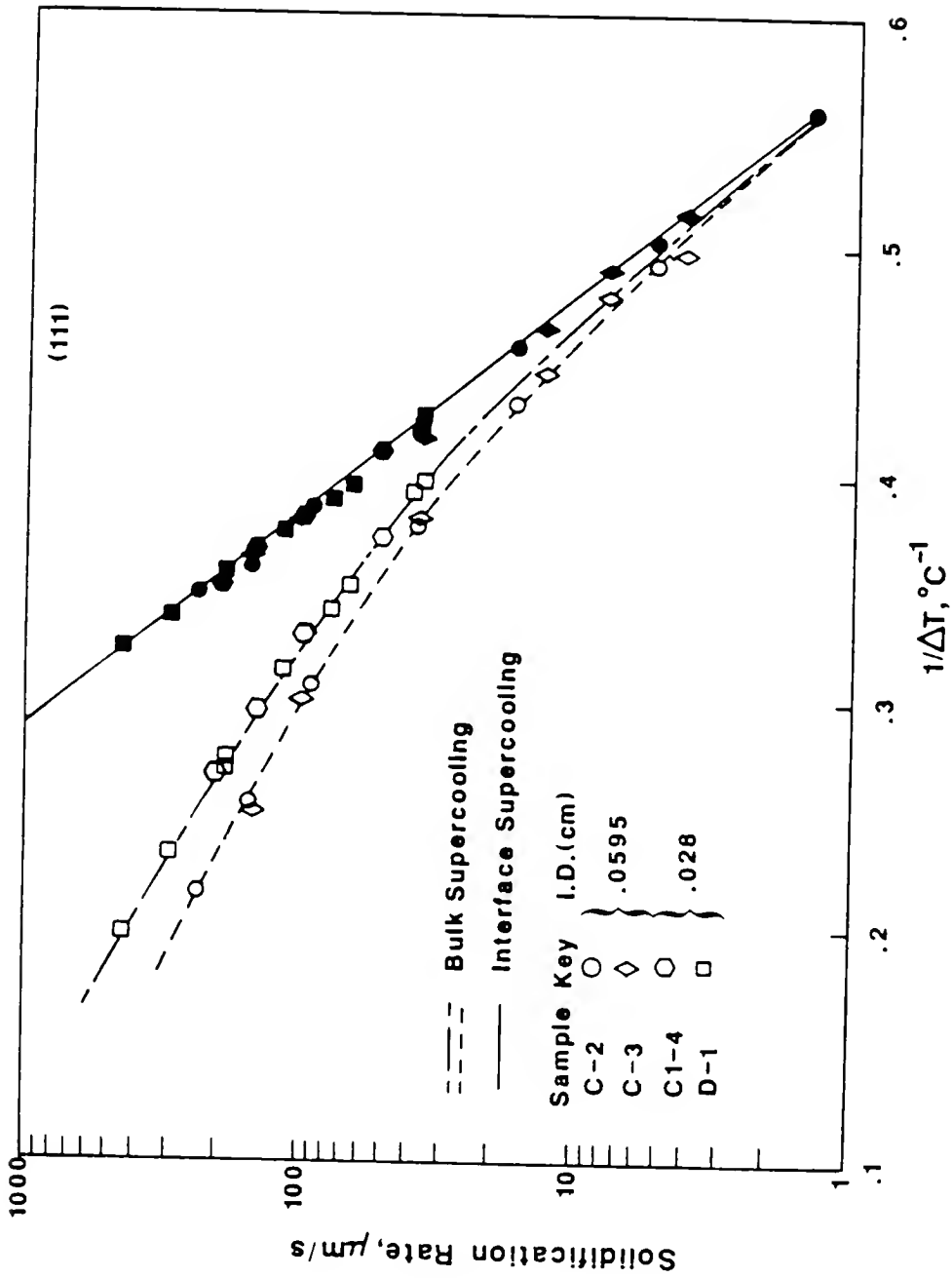
Figure 48   The logarithm of the (111) rates versus the reciprocal of the interfacial (open symbols) and bulk supercooling (closed symbols) for two sample sizes.

experimental techniques used in the present study are discussed, followed by the discussion of the results.

Evaluation of the Experimental Method

The Seebeck technique,[1,311] has been used exclusively to determine the interfacial temperature during the present growth kinetics study. This study has revealed that the Seebeck technique is very accurate, sensitive, and fast responding to very small changes in temperature. It is relatively simple since the recorded emf can be easily converted to temperature. The only experimental difficulty in using this method rather lies on the elimination of electrical noises that are troublesome for the low level Seebeck potentials (μV range). The noise, however, can be eliminated if reasonable precautions are taken into account, as demonstrated in this investigation. The recorded potential then can be easily processed so that the measuring procedure is automated and continuous. However, the greatest potential of the technique is the fact that it can be used to directly monitor the perfection of the S/L interface during growth and to detect[313] a) emergence of dislocations at the interface, b) interfacial instability, and c) solute banding. The applicability of the technique during commercial growth processes is currently being investigated. It should be mentioned that the use of the Seebeck emf to detect temperature fluctuations at the S/L interface during crystal pulling,[327] or to measure the interfacial temperature,[308,328] has also been applied by others. Notwithstanding, these investigations neither reached the level of the accuracy of the present study nor realized the full potential of the technique.

As discussed earlier, the direct measurement of the interfacial supercooling via the Seebeck principle requires the knowledge of the Seebeck coefficient of the S/L interface, $S_{s\ell}$, as a function of temperature and orientation of the solid. $S_{s\ell}$ was measured directly in this study (see also Ref. (311)); some of the determined values for the (111) and (001) interfaces were given previously in Table 3. Note that these values agree well with those calculated from the absolute Seebeck coefficients of solid and liquid Ga, according to the following relationship[1]

$$S_{s\ell}^{(111)}(T) = S_s^{[111]}(T) - S_\ell(T) = 1.86 \ \mu V/°C \text{ at } T = 29°C$$

$$S_{s\ell}^{(001)}(T) = S_s^{[001]}(T) - S_\ell(T) = 2.2 \ \mu V/°C \text{ at } T = 29°C$$

where S_s and S_ℓ are the absolute Seebeck coefficients of the Ga. S_s was determined as a function of crystal orientation and temperature, from the following equation

$$S_s^{[hkl]}(T) = S_s^{[001]}(T) \cdot \varphi_1^2 + S_s^{[010]}(T) \cdot \varphi_2^2 + S_s^{[100]}(T) \cdot \varphi_3^2 \tag{86}$$

where φ_1, φ_2, and φ_3 are the direction cosines of the crystal orientation of interest ([hkl]) with respect to the principal crystal axes. The temperature coefficients of the Seebeck coefficients were[311] .0107 and .012 $\mu V/(°C)^2$ (negative) for the (111) and (001) interfaces, respectively. Figure 49 shows the Seebeck coefficient of the liquid and solid along the principal axes as a function of temperature.

According to the theoretical background of the Seebeck technique, the recorded Seebeck emf, E_s, is related to the supercooling of the moving interface (II) as
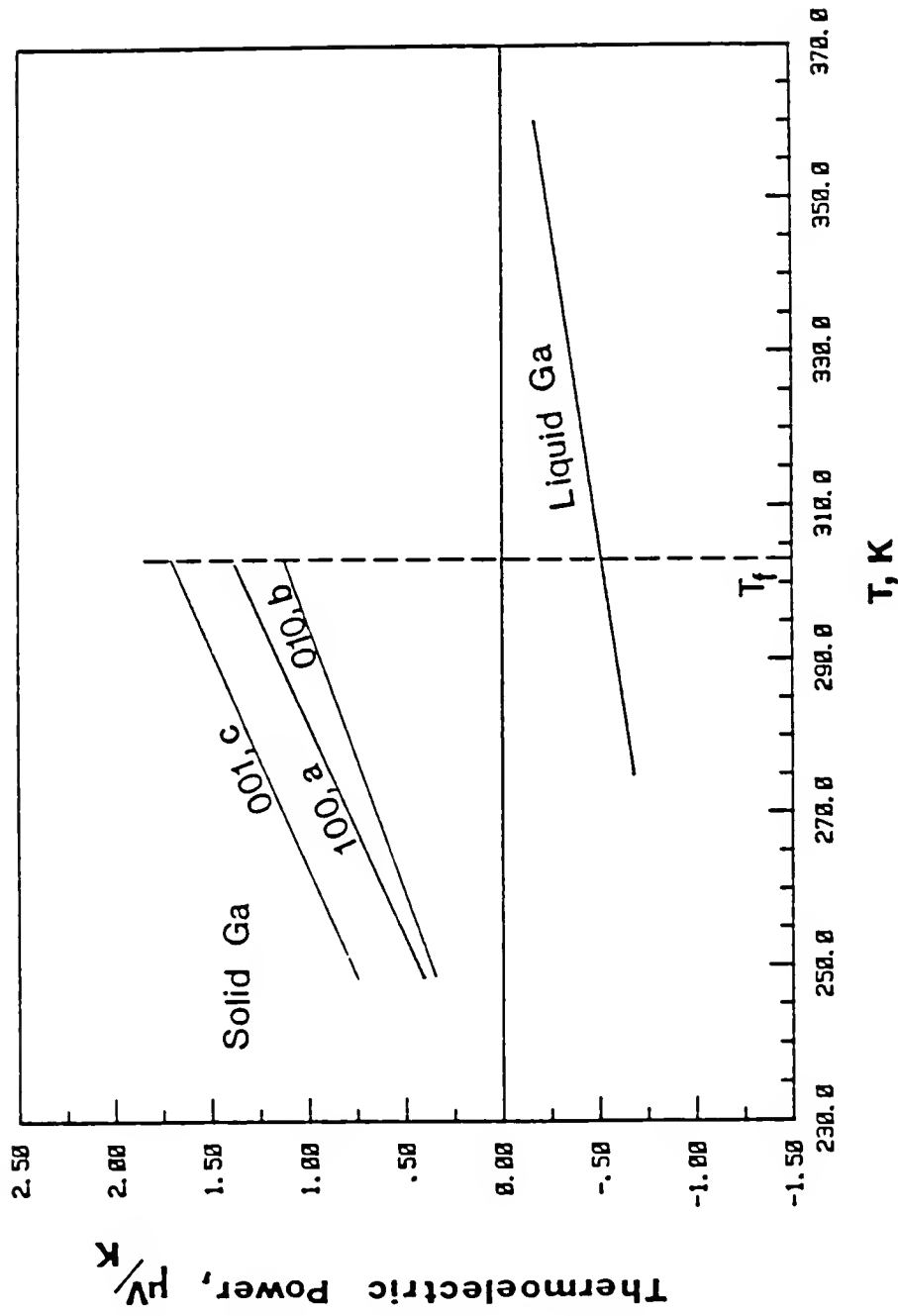
Figure 49 Absolute thermoelectric power of solid along the three principle Ga crystal axes and, liquid Ga as a function of temperature.

$$\Delta E = S_{s\ell}(T_m) \cdot T_m - S_{s\ell}(T_i) \cdot T_i \approx S_{s\ell}(T) \cdot \Delta T \qquad (87)$$

where T_i is the interface temperature. Note that eq. (87), as indicated, is an approximation since it is assumed that $S_{s\ell}(T_m) = S_{s\ell}(T_i)$; its use introduces an error in the ΔT estimate that is small at low ΔT's, for example, about .008°C for $\Delta T = 2$°C, but it increases at higher ΔT's. Therefore, the temperature coefficients of the Seebeck coefficients, $dS_{s\ell}/dT$, were taken into account so that the interfacial super-cooling was calculated from the following relation

$$\frac{dS_{s\ell}}{dT} \cdot (\Delta T)^2 - (S_{s\ell}(T_m) + \frac{dS_{s\ell}}{dT} \cdot T_m) \cdot \Delta T + \Delta E = 0.$$

The emf output of the sample was measured with an accuracy of .005 μV, which corresponds to an accuracy of about ±.003°C in supercooling. It should be noted that this accuracy is one order of magnitude better than the constancy of the bulk temperature, which was within ±.025°C at any set temperature.

The growth rate measurements, as indicated in the previous chapter, cover a range of seven orders of magnitude, i.e. from about 10^{-3} to 10^4 μm/s. Such a broad range of measurements assures not only a complete picture of the growth behavior of the interfaces, but also eliminates any possible misinterpretation of the growth kinetics. In addition, as mentioned previously, for several of the used samples, the rate measurements extended over 6-7 orders of magnitude while using the same experimental techniques, thus defying any questions regarding the "uniformity" of samples and experimental procedures.

The high growth rates ($V > .15$ cm/s) were determined by the square-wave current technique described earlier. The values of the current I were chosen so that the potential drop was stable enough to be resolved

for the lowest growth rates (.5 - 2 x 10^3 μm/s) within a time interval of about two seconds. Within the above mentioned range of growth rates, the interface velocities were also measured optically. A comparison between the latter rates and those determined via the potential drop using two different potentiometers and data acquisition programs (programs #2-4, as presented in Appendix IV) is shown in Fig. 50. The agreement between the two is very satisfactory considering the fact that the rates are determined by two independent techniques. Finally, it should be noted that the values of I and Δt (see eq. (68)) were stable within ±.01% and ±.02 - .5%, respectively. The standard deviation of the ΔR/Δℓ values at a given bulk supercooling never exceeded 5% from the mean.

On the other hand, the current value had to be kept minimum to avoid any Peltier heating (or cooling), as well as Joule heating at the interface. These effects are, however, negligible for the parameters used in this study. This is due to the fact that the Peltier coefficient of the S/L interface is rather small for Ga. The coefficient is defined from the Kelvin relations[314] as

$$P_{s\ell} = S_{s\ell} \cdot T.$$

Hence, for the (111) interface supercooled by about 3°C, $P_{s\ell}$ = 5.38 x 10^{-4} V. Based on the current densities used, about 8 A/cm^2, the Peltier heat is calculated as Q_p = .0043 W/cm^2 = .001 cal/s·cm^2. Taking into account that the heat of fusion for Ga is 119 cal/ cm^3, and the lowest growth rate of 500 μm/s, the rate of heat evolution at the interface because of solidification is Q_s = 6 cal/s·cm^2. Therefore, Q_p accounts for only about .016% of the heat evolved for the lowest growth rate. For
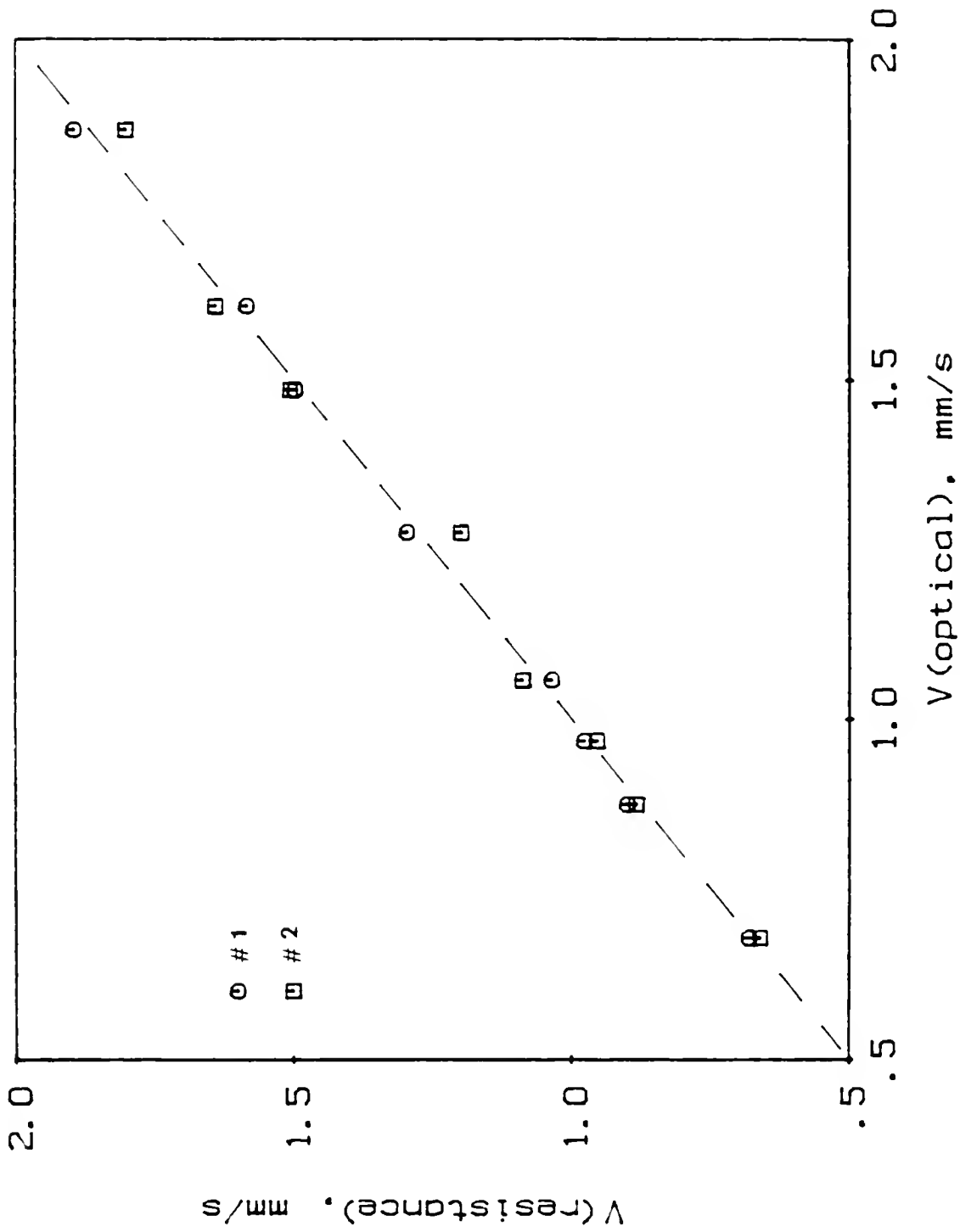
Figure 50 Comparison between optical and "resistance" growth rates; the latter were determined simultaneously by two independent ways (see programs # 2, 3 in Appendix IV).

faster rates, the Peltier heating is proportionally much smaller. Simi-
larly, the maximum Joule heating is estimated to be less than $Q_J = 6.1$ x
10^{-4} cal/s·cm^2, which is again negligible compared to Q_s. For higher
growth rates Q_s increases much faster and, therefore, the Peltier and
Joule effects are still negligible for the current densities used in
this study.

Comparison with the Theoretical Growth Models at Low Supercoolings

At low supercoolings, the faceted Ga (111) and (001) interfaces
grow by two-dimensional nucleation-assisted or screw dislocation-
assisted lateral growth mechanisms, as indicated earlier. From a theor-
etical point of view, the experimental data are of particular interest,
especially considering the lack of reliable kinetics studies for growth
from a metallic melt, because they provide accurate results against
which the existing theoretical growth models can be tested and compared.
Prior to comparing the Ga results with the predictions of the classical
models, the "α" factor as proposed by Jackson to predict the growth be-
havior of the two interfaces are considered first.

According to Jackson,[8] if α, defined as $\alpha = L\xi/KT_m$, is greater than
two, the interface should be smooth, while for values of α < 2 the
interface should be rough and normal growth should prevail. The value
of L/KT_m for Ga is about 2.2. By taking into account the bond strength
of first and second neighbors, as discussed in detail in Appendix I, ξ
is calculated to be about 0.3 for the (001) face and 0.5 for the (111)
face. The α parameters become $\alpha_{(001)} = 0.7$ and $\alpha_{(111)} = 1.1$ using the ξ
factors cited above; therefore, normal growth should be expected for

both interfaces based on Jackson's theory, in contrast to the experimental findings. This clearly illustrates that the "α" factor is not adequate to describe the nature of the interface of a "borderline" (i.e. L/KT ~ 2) material with complex structure and/or bonding. As discussed elsewhere, materials such as Si, Ge, and P_4, for example, also form facets irrespective of the "α" factor.

2DNG kinetics.

The growth behavior of the perfect interfaces was described earlier by the general 2DNG rate equation, eq. (69). However, since existing theories treat the mononuclear and polynuclear growth separately, in this section the 2DNG kinetics will be compared with them separately, preceding the discussion of the generalized 2DNG rate equation.

The qualitative features of the Ga dislocation-free growth kinetics are in excellent agreement with the predictions of the classical 2DNG models. These features are the threshold supercooling for a measurable rate and the exponential kinetics beyond this supercooling, as given in Table 7. In addition, it was shown that the rates are dependent on the S/L interfacial area at low supercoolings, but not at higher supercoolings where the slope of the log(V) vs. 1/ΔT curve was also found to be smaller. Indeed, as predicted by the theoretical models, the 2DNG kinetics are divided into regimes, the mononuclear and the polynuclear one.

In order to make a quantitative comparison of the experimental findings with the existing growth models, the pre-exponential terms, K_1 and K_2, of the MNG and PNG growth rate equations, eqs. (36) and (37), respectively, were calculated from the corresponding analytical solutions, as given in Table 8. Note that from eqs. (20), (27), (36), and

Table 8. Experimental and Theoretical Values of 2DNG Parameters.

Growth Mode	Interface	K_1 $(\mu m\ sec)^{-1}$ Exp.	K_1 Theor.	K_2 $\mu m/sec$ Exp.	K_2 Theor.	σ_e $ergs/cm^2$ Exp.	σ_{sl}	Slope ratio MNG/PNG in log(V) vs. $1/\Delta T$ Exp	Theor.
MNG	(111)	2.25×10^{10}	4.8×10^{14}			$20.3 \times f(\Delta T)$	67-40	2.45	3 or
PNG	(111)			5.2×10^7	1.6×10^8				2.5 or
MNG	(001)	6.08×10^{10}	5.9×10^{14}	6.3×10^7		$11.7 \times f'(\Delta T)$		2.6	2
PNG	(001)			2.5×10^7	1.8×10^8				

(37) these constants are given as $K_1 = chK_o^{1/3}K_E^{2/3}D$ where c is a constant of the order of unity. $K_o = (N/V_m) \cdot (L/RT_m)^{1/2}$ $3\beta/2a$ and K_E is given as $3\beta/2a$ L/RT_m; β is assumed to be one in the calculations.

The results reveal about four orders of magnitude difference between the experimental and calculated terms for the MNG and about one order of magnitude difference for the PNG kinetics. The experimental values of K_1 and K_2 were determined from careful linear regression analysis of the growth data for both growth rates and interfaces, as presented earlier. Although there is some uncertainty in the theoretical calculations concerning the constants involved, it is believed that the lack of coincidence between the experimental and theoretical values lies on the use of the liquid self-diffusion coefficient D (1.6×10^{-5} cm^2/s^{329}) in the calculations for the migration of the atoms across the interface. For the PNG region, the two values are quite close, considering the uncertainty in calculating the pre-exponential term of the nucleation rate equation. However, this discrepancy between the experimental and calculated PNG values can still be reconciled, as explained later.

The step edge free energy (σ_e) was also calculated from the exponential term

$$\exp\left(-\frac{M\sigma_e^2}{\Delta T}\right) = \exp\left(-\frac{\pi\sigma_e^2 V_m T_m}{hKT \, \Delta T}\right),$$

i.e. from the slope of the $\log(V)$ vs. $1/\Delta T$ line for the data in the MNG regime.[*] The values of σ_e per unit length of steps on the (111) and

---

[*] Properly, σ_e should be computed using the slope of $\log(V/\Delta T^{1/2})$ vs. $1/\Delta T$. However, since the ΔT range is small (from 1.5 to 1.9°C and from .6 to .8°C), and the pre-exponential factor is large, the incorporation of the $\Delta T^{1/2}$ factor has a negligible effect on σ_e.

(001) interface (see detailed discussion in Appendix I) were calculated to be 59.4 and 44.8 x 10^{-8} ergs/cm, respectively; in the calculations h is 2.9 and 3.8 Å for the (111) and (001) interfaces, respectively, while V_m is equal to 11.8 cm^3/mole. The experimentally found σ_e values per unit area of the edge of the step (i.e. σ_e/h) of 20.3 and 11.7 ergs/cm^2 are much smaller than the reported $\sigma_{s\ell}$ values of 40,[330] 56,[60] and 67[331] ergs/cm^2 from "homogeneous" nucleation experiments of Ga, and 52[87] from theoretical calculations. It should be noted, as discussed earlier, that the surface energy per unit area of the edge of the step is not necessarily the same as the S/L interfacial energies. Furthermore, the values obtained from homogeneous nucleation experiments have been subjected to broad criticism, particularly in the existence of poor wetting of the crystal by the melt which has been reported for Ga.[332]

According to the classical 2DNG models, the ratio of the slopes of the mononuclear and polynuclear kinetics in a log(V) vs. 1/ΔT plot should be either three for the case of uniform 2D cluster spreading, or two for the non-isotropic case for which the cluster area increases linearly with time (see eqs. (33) and (34), respectively). However, for both growth directions this ratio was found to be between these limits, as 2.4 and 2.6 for the (111) and (001) interfaces, respectively, indicating that the growth of clusters is controlled simultaneously by the attachment kinetics and the arrival flux of the atoms. For such a case, the growth rate is given as $V \approx c'h (Ju_e^2)^{2/5}$. Indeed, the experimental ratios of 2.4 and 2.6 are close to the value of 2.5, which is the predicted value for the PNG model (see eq. (35)) discussed earlier.

Although the (001) interface growth behavior was similar to that of the (111) interface, the former showed a unique feature that the (001)

PNG data fall on two different growth kinetics, lines A and B, shown in Fig. 35. In contrast to the growth kinetics in the MNG region, the difference between the two is not due to the effect of the interfacial area. For example, compare samples L-2, P and O-1, K-1. Similar observations were also made by Abbaschian and Ravitz[190] regarding the growth kinetics of the (001) face. They attributed their findings to the possibility of different impurities concentration in their as-received Ga lots. However, in the present investigation this possibility is excluded since data from samples from the same lot (L, K) fell on either growth curve. According to the results (see Table 7), the two rate equations differ by a factor of 2.5 in the pre-exponential terms. Since in the MNG region the kinetics are shown to be dependent only on the interfacial area, it can be assumed that a variation in the step height (h) is not the reason behind the observations. Furthermore, the difference between the two rates cannot be due to a change at the step edge free energy σ_e, because, if this was the case, then the exponential terms of the two rate equations would have been different, in contrast with the experimental results, as shown in Table 7.

As discussed in Appendix I, there are four Ga_2 molecules per cell lying symmetrically in the (010), (α-c plane), at angles of approximately $\pm 17°$ to the [001] direction. It seems then that the growth kinetics of the (001) interface are affected by the relative orientation of the Ga-Ga covalent bond with respect to the growth direction of the interfacial steps, and, consequently on σ_e. A possible reason for the different growth rates would be a change in the step velocity σ_e. Since $V(A)/V(B) = 2.5$, according to eq. (33), this would imply $\upsilon_e(A)/\upsilon_e(B) =$

1.85. The difference of the υ_e's most likely comes from dissimilarities in the elementary molecular rearrangement at the edge of the steps. Possibly, for certain orientations close to the [001] direction, the Ga_2 molecule becomes the growth unit instead of single atoms. Accordingly, the ratio of the local advancement would be equal to the ratio of the covalent bond length to the atomic radius. This ratio is about $2.4/1.3^*$ ≈ 1.84, which is equal to the ratio of the step edge velocities. This explanation for the observed differences in the kinetics along the (001) interface is further justified by the fact that the samples with faster growth rates had a few degrees misorientation with the tube axis. Although this rationale is satisfactory for the PNG region, it seems to break down at higher growth rates (>1000 μm/s) where the rates appear to become the same. However, as will be discussed later, the nature of the interface changes as the interface supercooling increases because of the kinetic roughening.

SDG kinetics.

When dislocation(s) intersect the faceted interface, the kinetic characteristics are entirely different than those of the 2DNG mechanism. The dislocated interfaces are mobile at all supercoolings and their growth rates, at a given ΔT, are several orders of magnitude higher than those of the dislocation-free interfaces. For example, at 1.5 and 2°C supercoolings the SDG rates of the (111) interface are higher than the 2DNG rates by six and three orders of magnitude, respectively. Although the growth rate equations given in Table 7 indicate a nearly parabolic relationship between the rate and the interfacial supercooling for both

the (111) and (001) interfaces, the SDG kinetics are better correlated by an equation in the form of

$$V = K_D \frac{\Delta T^2}{\Delta T_c} \tanh \left(\frac{\Delta T_c}{\Delta T}\right) \tag{88}$$

Here the parameters K_D and ΔT_c are constants, given below in Table 9, as determined by curve-fitting the SDG (111) and (001) experimental growth data in eq. (88). This rather illustrates the problem with using the parabolic law, $V \propto \Delta T^2$, over a limited experimental range to describe the SDG kinetics. As a matter of fact, most of the experimental studies on SDG kinetics conclude on relationships in teh form of $V \propto \Delta T^n$ with $1.5 < n < 2.5$, which is not surprising based on teh form of eq. (88). Certainly, the dislocation-assisted growth data can be fitted, within isolated $(V, \Delta T)$ ranges, to an equation in the form of $V = K \ \Delta T^n$ with n close to 2. Nevertheless, such an interpretation of the kinetics is of limited importance since the growth data are proportional to ΔT^2 tanh $(1/\Delta T)$ over the entire experimental range, as discussed later.

Table 9.   Experimental and Theoretical Vlaues of SDG Parameters

Interface	K_D (μm/sec·°C)		ΔT_E (°C)
	Theoretical	Experimental	
(111)	7.3×10^4	1422	1.775
(001)	5.7×10^4	1968	1.1

Based on this model, ΔT_c is given as

$$\Delta T_c = \frac{4\pi \, \sigma_e \, V_m \, T_m}{2x_s \, L}$$

Assuming σ_e to be independent of ΔT (the general case where σ_e is a function of ΔT is discussed later) and neglecting the temperature dependence of x_s within the temperature interval under consideration, ΔT_c should then be constant. From the experimental values of ΔT_c, the mean diffusion length, x_s, is estimated to be about 430 Å for both interfaces. The latter value of x_s indicates[193a] an activation energy for atomic migration in the order of 3 Kcal/mole, as compared to that one for liquid self-diffusion of about 1.85 Kcal/mole. One the other hand, if multiple dislocations are considered,[*] i.e. a number of S dislocations, the earlier calculated value of x_s reduces to x_s/S. In utilizing the other constant K_D, it is uncertain about estimating some parameters from the BCF theory. For melt growth the term before the tanh term (see eqs. (40) and (88)) could be approximated with the term

$$\frac{K_E \, D \, x_s \Delta T}{2\pi r_c \, T}$$

Accounting for the experimental value of ΔT_c, the value of K_D is calculated to be 73000 and 57000 $\mu m/s \cdot °C$, using $D = 10^{-5}$ cm^2/s. These values are about two orders of magnitude smaller than the experimental values of K_D given in Table 9. It should be noted that by replacing D with D_i, the interfacial diffusivity, in the order of 10^{-7} cm^2/s would bring the calculated values in agreement with the experimental ones. The reason

---

[*] This considers the case of an array, L length, of S dislocations that satisfies the condition $2\pi r_c > L$; the latter implies that L < 850 Å.

for using the interfacial diffusivity instead of bulk diffusion will be given later.

As realized in this section, the pioneering work of BCF has been borrowed in applying theory to practice.   Their model, which is still considered among the most elegant, is hard to apply since most of its parameters are not known but have to be estimated, particularly for melt growth. Moreover, one might legitimately question whether such a theory, that strongly depends on surface diffusion, could relate to the growth of a S/L interface.   However, as discussed earlier, only this model   could   explain   the   observed   non-parabolic growth laws. If the experimental results are "forced" to follow a parabolic law, the rate equations for the two interfaces can be represented (V in μm/s) as[*]

$$(111): \quad V = 730 \ \Delta T^2 \qquad\qquad (.2 \leq \Delta T \leq 1.9)$$

$$(111): \quad V = 1703 \ \Delta T^2 \qquad\qquad (.2 \leq \Delta T \leq 1.1)$$

with coefficients of correlation of .87 and .9, respectively. Next, the experimental growth rate coefficients are compared with the calculated ones from the parabolic law, eq. (41), of the SDG model. Substituting $\sigma_{s\ell}$ in eq. (41) with σ_e, as determined from the 2DNG kinetics and assuming that the Burgers vector $\vec{b}$ of the dislocations is equal to the step heights used earlier, the kinetic coefficients of the (111) and (001) interfaces is calculated as 72 and 124 (μm/s$\cdot$°C^2), respectively. By comparing these values with those of the experimentally determined rate equation, it is realized that the latter are greater by about a factor

---

[*] Note that the kinetic coefficient here is larger than that given in Table 7 because the largest population of data points is for ΔT's less than 1°C supercooling.

of ten for both interfaces, or, according to the diffuse interface growth model, by a factor of 10 β/g.

Generalized Lateral Growth Model

The two-dimensional nucleation assisted growth kinetics over both the mononuclear (MNG) and polynuclear (PNG) regimes (supercoolings from 1.5 to 3.5°C and .6 to 1.45°C and growth rates from 10^{-3} to 1500 μm/s and 10^{-2} to 600 μm/s for the (111) and (001) interfaces, respectively) are well expressed by the following rate equation

$$V = \frac{K_1 \ A \ (\Delta T)^{1/2} \ \exp(-\frac{B}{\Delta T})}{(1 + K_2 \ (\Delta T)^{1/2} \ A^{5/3} \ \exp(-\frac{B}{\Delta T}))^{3/5}} \tag{69}$$

Here K_1, K_2, and B are assumed, for the time being, to be independent of the growth parameters and A is the S/L interfacial area. It should be noted that B is a weak function of supercooling within the above mentioned range of supercoolings, but becomes strongly dependent on ΔT at higher supercoolings, as indicated later. The values of K_1, K_2, and B found by fitting (111) and (001) crystal growth data to the proposed eq. (69) are given in the following Table.

Table 10. Growth Rate Parameters of General 2DNG Rate Equation

(111)	$K_1 = 1.39 \times 10^{17}$	$K_2 = 7.5 \times 10^{18}$	B = 58.76	A in cm^2	V in μm/sec
(001)	$K_1 = 3.8 \times 10^{17}$	$K_2 = 4.6 \times 10^{19}$	B = 25.43		

A comparison between the experimental data and the calculated ones, by using eq. (69) in conjuction with the parameters in Table 10, is shown in Figs. 51 and 52 for the (111) and (001) interfaces,
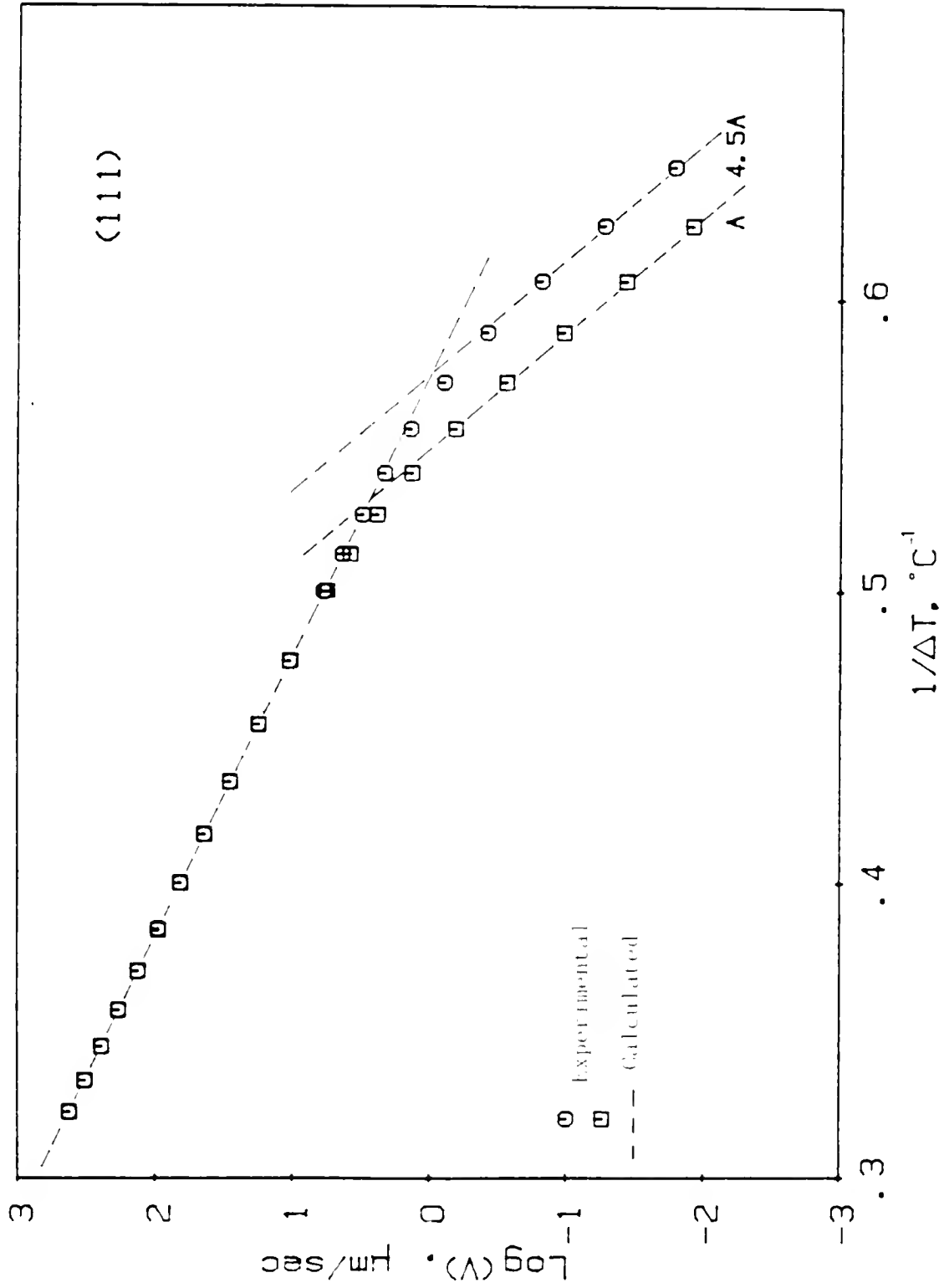
Figure 51 Comparison between the (111) experimental growth rates and calculated rates, via the general 2D&c rate equation, as a function of the supercooling.
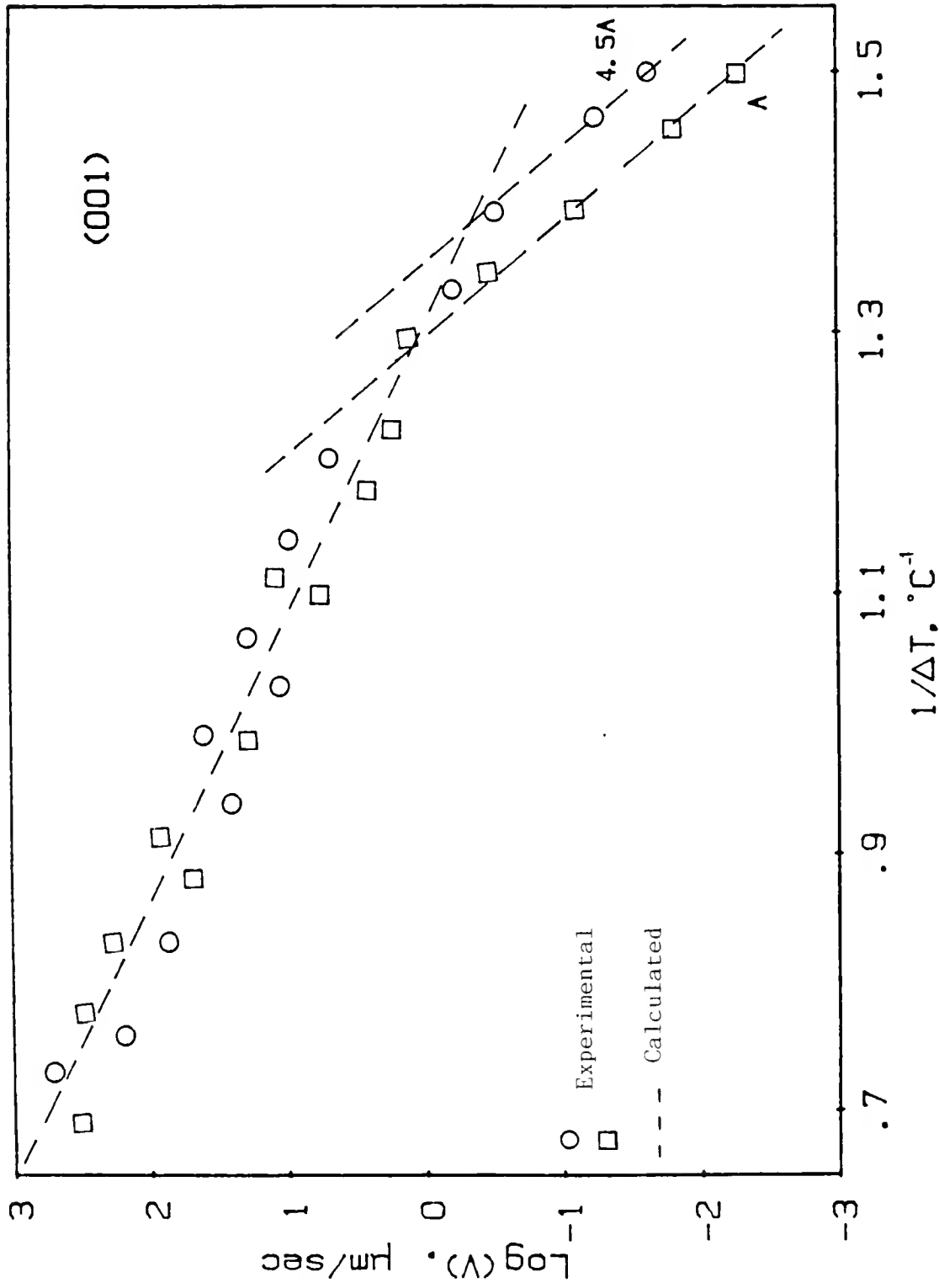
Figure 52 Comparison of the (001) experimental growth rates and those calculated using the general 2DNG rate equation, as a function of the supercooling; note that the PNG calculated rates were not formulated so as to include the two observed experimental PNG kinetics.

respectively. From these figures, it can be seen that the calculated curves agree well with the experimental data points. Indeed, the model, as formulated in eq. (69), accounts for the interfacial size dependence of the growth rate in the mononuclear region, as well as of the slope change of the kinetics from the MNG to the PNG mechanism, shown in these log(V) vs. 1/ΔT plots. These qualitative predictions of the rate equation (eq. (69)) and its quantitative representation through the parameters of Table 10 will become evident through the following discussion of the model.

As discussed earlier, the 2DNG rate equations are given in terms of a steady state 2DN rate J and a lateral spreading velocity, υ. A general 2DNG rate equation should have a form that at low supercooling reduces to the rate equation for MNG as

$$(MNG): \quad V = h \, J \, A$$

while at high supercoolings it becomes identical with the rate equation for PNG, given as

$$(PNG): \quad V = c \, h \, (J \, \upsilon_e^2)^{1/2m+1}$$

where c is a constant and m is a constant in the range of 1/2 to 1. Note that the demarkation between the mononuclear and the polynuclear growth regimes could be assumed to be predicted by the ratio

$$\frac{A^{m+1/2} \, J^m}{m^{-1} \, \upsilon_e} \underset{<}{>} 1$$

where A is the S/L interfacial area. If this ratio is less than one, mononuclear growth prevails, in contrast with the other extreme, for

which the polynuclear growth takes over. The expression satisfying these conditions can have the following form

$$V = \frac{h\,J\,A}{(1 + \frac{A^{1+1/2m}\,J}{m^{-1/m}\,\upsilon_e^{1/m}})^{2m/2m+1}}$$

(89)

According to the above discussion, at low supercoolings, when the dimensionless term in the denominator is much less than unity, eq. (89) reduces to the MNG rate equation of $V = hJA$. For the reverse case, it is realized that the general eq. (91) reduces to the form of eqs. (33)-(35) for the PNG mechanism. Assuming that $m = 3/4$, eq. (89) can be rewritten as

$$V = \frac{h\,J\,A}{(1 + \frac{A^{5/3}\,J}{1.46\,\upsilon_e^{4/3}})^{3/5}}$$

As may be surmised already, the exponent $m = 3/4$ was chosen because, as indicated earlier, this particular PNG submodel satisfactorily predicts the experimental slope ratios between the MNG and PNG kinetics for both interfaces. At first glance, after recalling the expression for the 2DN rate, J (eq. (27)), equation (89) is identical to the "fitted" one, eq. (69). In the latter, K_1 is the product of the pre-exponential term of the 2D nucleation rate and the step height (h); K_2, in turn, expresses the ratio of $K_1/1.46\,h\,\upsilon_e^{4/3}$. Generally, the edge velocity υ_e is assumed to be proportional to ΔT. Based on this assumption, K_2 should then vary as about ΔT^{-1}. However, thorough evaluation of the factors K_1 and K_2 suggests that K_2 is indeed independent of the supercooling, which implies that $\upsilon_e \propto \Delta T^{3/4}$.

Interfacial Diffusivity

In the discussion regarding the two-dimensional nucleation growth theories, it was indicated that the transport of atoms across the 2D nucleus/liquid interface is expressed by the self diffusion coefficient in the liquid. Based on this assumption, there are about four orders of magnitude difference between the experimental and calculated pre-exponential terms for the MNG and about one order of magnitude difference for the PNG kinetics. It is believed that the lack of coincidence between the experimental and theoretical values lies on the use of liquid Ga self diffusion coefficient D (1.6×10^{-5} cm^2/s) for the diffusion of the atoms across the interface.

The assumption in incorporating D in the classical equations of J and υ_e, although it has been questioned in some cases, has been used over the years. Recent experimental studies and molecular dynamic simulations, which were reviewed earlier, have measured interfacial diffusivities, D_i, that are up to four-five orders of magnitude smaller than the self diffusion coefficient of the melt. The studies also indicate that a liquid layer, with distinct properties to those of the bulk liquid and solid, exists next to the interface. Across this layer, which can be considered as arising from density or order fluctuation, one would expect a gradual transition of the average 2D properties moving from the crystalline to the fluid phase. Similar observations have been made in MD simulations of the S/L interface which indicated that the in-layer (2D) ordering gradually decreases with distance away from the top crystalline plane; however, its decay rate was found to be higher than that for the in-between planes. For a faceted interface

there should also exist a variation in the ordering of atoms within each 2D layer. The localized ordering corresponds to 2D clusters and/or islands formed during growth; the interface layer in front of these advancing steps, if not identical to the above discussed one, should also be diffuse. For a rough interface, on the other hand, the ordering within the interfacial region occurs mostly in the direction normal to the interface, with less fluctuations in ordering parallel to the interface. A rationale for this suggestion, that the 2D ordering is less extensive for rough interfaces, could be that a rough face has a lower atomic density per layer and less number of lateral bonds per atom on the plane. Moreover, because of the great number of available attachment sites, clustering in the liquid is less extensive, at least in between the solid propagating into the liquid.

Therefore, D must be replaced by a much smaller coefficient which represents the "interfacial diffusion coefficient," D_i. The magnitude of D_i, somewhere between D and D_s[333] ($D_s \sim 10^{-13}$ cm^2/s) depends, among other factors, on the location within the interfacial zone.

Based on earlier discussions, in the MNG regime where the lateral growth takes place by the spreading of a monolayer island, the ordering of the atoms should complete within 2-3 layers. Nevertheless, the island is surrounded by various size 2D and 3D clusters. The interfacial diffusivity is then expected to be in the order of 10^{-8} - 10^{-9} cm^2/s, i.e. the average of the solid and liquid self diffusion coefficients. During polynuclear growth, however, the atomistic processes occur simultaneously within several layers (estimated to be 3-4 layers

for Ga). In this case, the region next to the clusters of the top layer is more "liquid-like" than that in the first layer next to the crystal.

In the PNG region, because of dimensional arguments, nucleation events are predominant at the top layers while layer spreading is controlled by the lower layers. Also keeping in mind that D_i in the case of the PNG process could be written as the product of $(D_i^{nucl})^{1/3} \cdot (D_i^{gr})^{2/3}$, a value of about $10^{-6} - 10^{-7}$ cm^2/s can be estimated.

The above mentioned argument explains the discrepancy between the pre-exponential theoretical and experimental terms at low supercoolings. It does not explain, though, the observed transitional kinetics for both interfaces occurring at high supercoolings, as shown in Figs. 23 and 31, where the dashed lines represent the calculated rates in accord with the 2DNG models corrected for D_i. The reasoning for the observed deviation in the growth kinetics of high supercoolings is discussed next.

Step Edge Free Energy

As discussed earlier, the classical 2DNG theory assumes that the step edge free energy is independent of the interfacial supercooling. Based on this assumption, the only deviation in the growth kinetics one could expect at high supercoolings is when the free energy for the formation of a critical nucleus ΔG^* equals the thermal energy KT^* (in other words, when the exponential term in eqs. (37) and (69) diminishes). According to the experimental values of σ_e, the (111) interface should deviate from the 2DNG rate equation at supercoolings in the order of

---

* Note that this criterion, $\Delta G^* = KT$, has recently been identified with the onset of the kinetic roughening, incorrectly, as discussed later.

76°C. However, as shown earlier, the (111) kinetics deviate from those of the 2DNG theory at much lower supercoolings. The same arguement also holds for the (001) kinetics.

It is believed that the deviation from the classical rate law is due to a reduction in the 2D nucleation barrier as the driving force for growth (i.e., the supercooling) increases, thus implying that the step edge energy σ_e is decreasing with supercooling. As understood, the behavior of σ_e is closely related to the concept of kinetic roughening, which is expected to prevail at high supercoolings.

The variation of the step edge free energy with the supercooling can be determined directly from the experimental results and the general equation for two-dimensional nucleation growth (see eq. (69)).   To achieve this, the mobility of the steps, which governs the pre-exponential term in the 2DNG rate equation (eq. (37)) was assumed to have about the same order of magnitude of mobility at the lower end of the PNG regime. The σ_e values of the best fit are shown in Fig. 53 as a function of the interface supercooling. It can be seen that the step edge energy is approximately constant up to supercoolings of about 3°C.   At higher supercoolings it starts decreasing, first gradually and later rapidly with ΔT. The functional form of $\sigma_e(\Delta T)$ was found to be best expressed by an exponential relation given as

$$\sigma_e = \sigma_e^o \{1 - \exp[-2.69 \ (\Delta T_R - \Delta T)]\} \qquad (90)$$

where σ_e^o is a constant equal to 20.3 ergs/cm^2 (i.e. the step edge energy near the 2DN threshold supercooling) and ΔT_R is the supercooling at
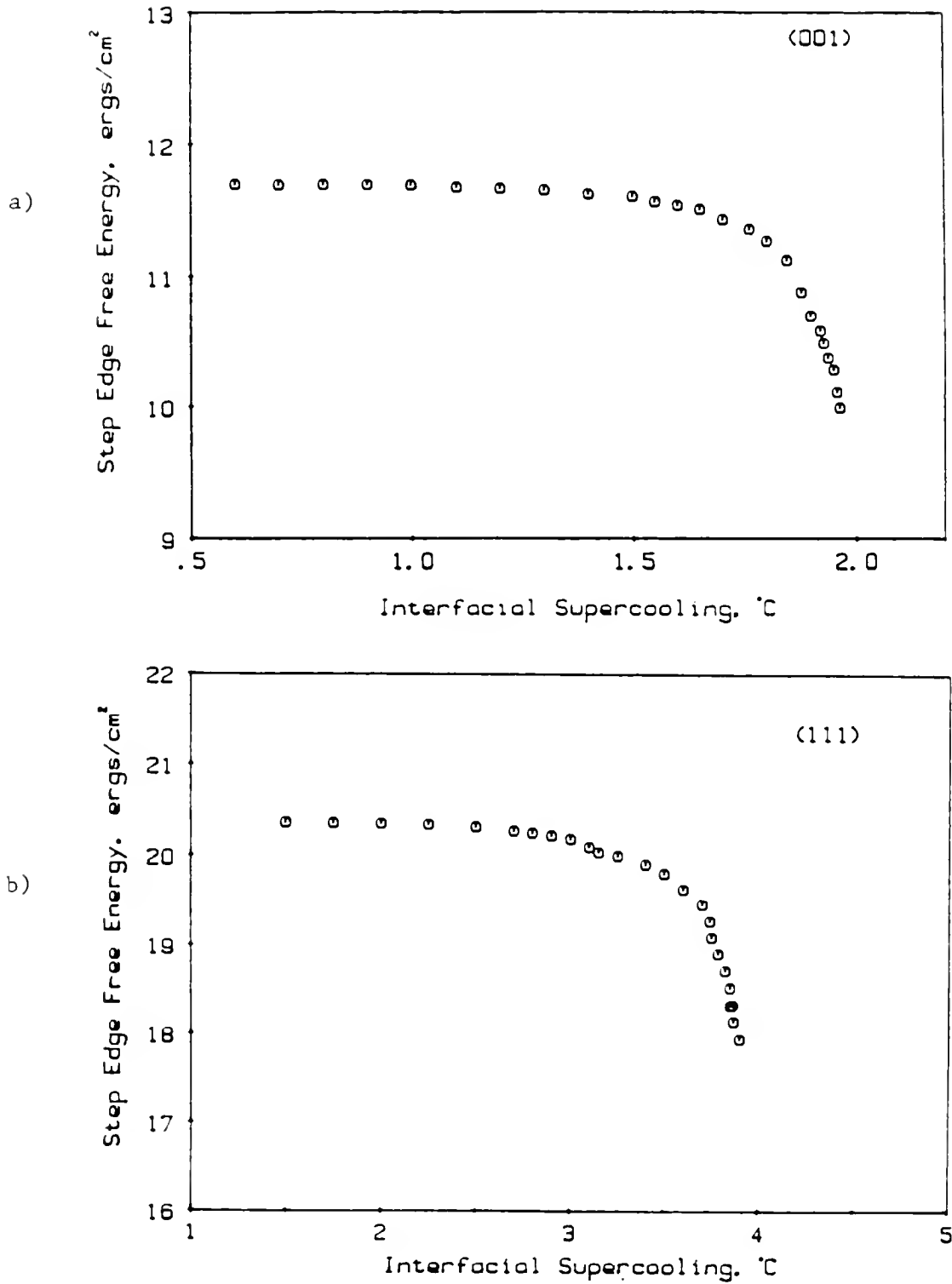
Figure 53   The step edge free energy as a function of the interfacial
supercooling.   a) σ_e (ΔT) for steps on the 001 interface
b) σ_e (ΔT) for steps on the (111) interface.

which σ_e vanishes; ΔT_R was determined as 4.75°C. Similarly, near this supercooling, it was found that σ_e approaches zero as

$$\sigma_e \propto \exp(- .736/(T - T_R)^{1/2})$$

where $T_R = T_m - \Delta T_R$. It should be indicated that attempts to quantify $\sigma_e(\Delta T)$ as a power law resulted in poor regression analysis coefficients. Furthermore, for the best fit power law behavior, ΔT_R was found to be in the order of 3.5°C. a value which is much smaller than that of the (111) experimental results.

Similarly for the (001) interface, the relation between the step edge free energy and the supercooling, shown in Fig. 53, was determined to be given as

$$\sigma_e = \sigma_e^0 \{1 - \exp[-6.36(\Delta T_R - \Delta T)]\} \qquad (91)$$

where σ_e^0 is equal to 11.7 ergs/cm^2 and ΔT_R is found to be equal to 2.28°C.

Interestingly enough, such a rapid divergence of the step energy upon approaching the roughening transition temperature is predicted by theoretical studies, as discussed earlier in Chapter 2. The exponential divergence of the step edge energy with the supercooling seems quite reasonable, since, for example in the Kosterlitz-Thouless[113] model, σ_e vanishes at T_R as $\exp(-C|(T - T_R)/T_R|^{1/2})$. However, this theoretical behavior is related to the thermal roughening of the interface and, therefore, to the temperature dependence of σ_e rather than the driving force. Similar behavior has been supported recently by a growth kinetics study of the (0001)-face of ^{4}He,[130] where the values of σ_e were deduced from a 2DNG rate equation as a function of the equilibrium temperature of the S/L ^{4}He interface.

In contrast with the above mentioned studies, σ_e was recently cal-culated[334] to be independent of T for the (110) face of napthalene grown from the solution within the range of 10-55°C of equilibrium tempera-tures; σ_e was calculated from the critical supersaturation above which the growing (001) Kossel crystal/vapor interface becomes kinetically rough according to CS results. The critical supersaturation was deter-mined by extrapolating the high supersaturation part of the growth curve down to zero growth rate. They claim that growth rates become linear at high supersaturations after kinetic roughening of the interface, thus monotonically replacing the non-linear growth at the lower supersatur-ations. This transition was believed to happen when $\Delta G^* = KT$, as dis-cussed earlier. In any case, for the SOS model, σ_e was found to de-crease with increasing T exponentially.

At the moment, an explanation of the significance of the exponen-tial type of divergence of σ_e upon increasing ΔT and approaching the kinetic roughening of the interface is still lacking. Despite the fact that qualitatively the thermal and kinetic roughening appear to be simi-lar, it has not been theoretically shown, to the author's knowledge, that these are equivalent. However, more about the kinetic roughening of the interface will be discussed later. Next, the general 2DNG rate equation (69) is corrected for a supercooling dependent step edge energy.

By incorporating in the 2DNG rate equation the effect of the super-cooling on the step edge energy or the effect of the kinetic roughening on the nature of the interface and thus on the lateral growth process, as discussed later, eq. (69) could be rewritten as

$$V = \frac{K_1 \ A \ (\Delta T)^{1/2} \ \exp[-B(f(\Delta T))^2/\Delta T]}{\{1 + K_2 \ (\Delta T)^{1/2} \ A^{5/3} \ \exp[-B(f(\Delta T))^2/\Delta T]\}^{3/5}} \qquad (92)$$

where the analytical forms of K_1 and K_2 given earlier still hold, but are corrected for D_i instead of D. B is defined as $\pi(\sigma_e^o)^2 h \ V_m \ T_m / L \ K \ T$ and $f(\Delta T)$ is equal to $\sigma_e(\Delta T)/\sigma_e^o$ as expressed in eqs. (90) or (91) depending on the interface under consideration. The calculated growth rates using the parameters given in Table 10 and eqs. (90) and (91) are presented in Fig. 54. As can be seen, the calculated rates agree very well with the experimental dislocation-free results over about the entire experimental range for the (111) interface, but up to supercoolings of about 2.1°C for the (001) interface. The (001) growth kinetics beyond this supercooling will be described later.

Similarly, for the dislocation-assisted growth kinetics accounting for a supercooling dependent step edge energy, the SDG rate equation (88) could be rewritten as

$$V = K_d \ \frac{\Delta T^2}{f(\Delta T)} \ \tanh(\frac{\Delta T_c \ f(\Delta T)}{\Delta T}) \qquad (93)$$

where K_d is equal to $K_D/\Delta T_c$, and the analytical forms of $f(\Delta T)$, K_D, and ΔT_c were given previously. From the curve-fitting parameters for the (111) dislocation-assisted growth data, shown in Fig. 55, ΔT_c is evaluated to be in the order of 3 and 10 at ΔT's higher than about 3°C supercooling. Accordingly, $x_s S = 250$ or 80 Å (or about 185 and 60 Å assuming that the spiral steps are polygonized instead of circular); a possible combination of parameters for $\Delta T_c = 10$ is $S = 20 \ x_s = 4$ Å. The latter value of x_s is close to that calculated based on the assumption that $x_s = a \ \exp(L/4 \ K \ T)$ where a and L are the interatomic distance and heat of
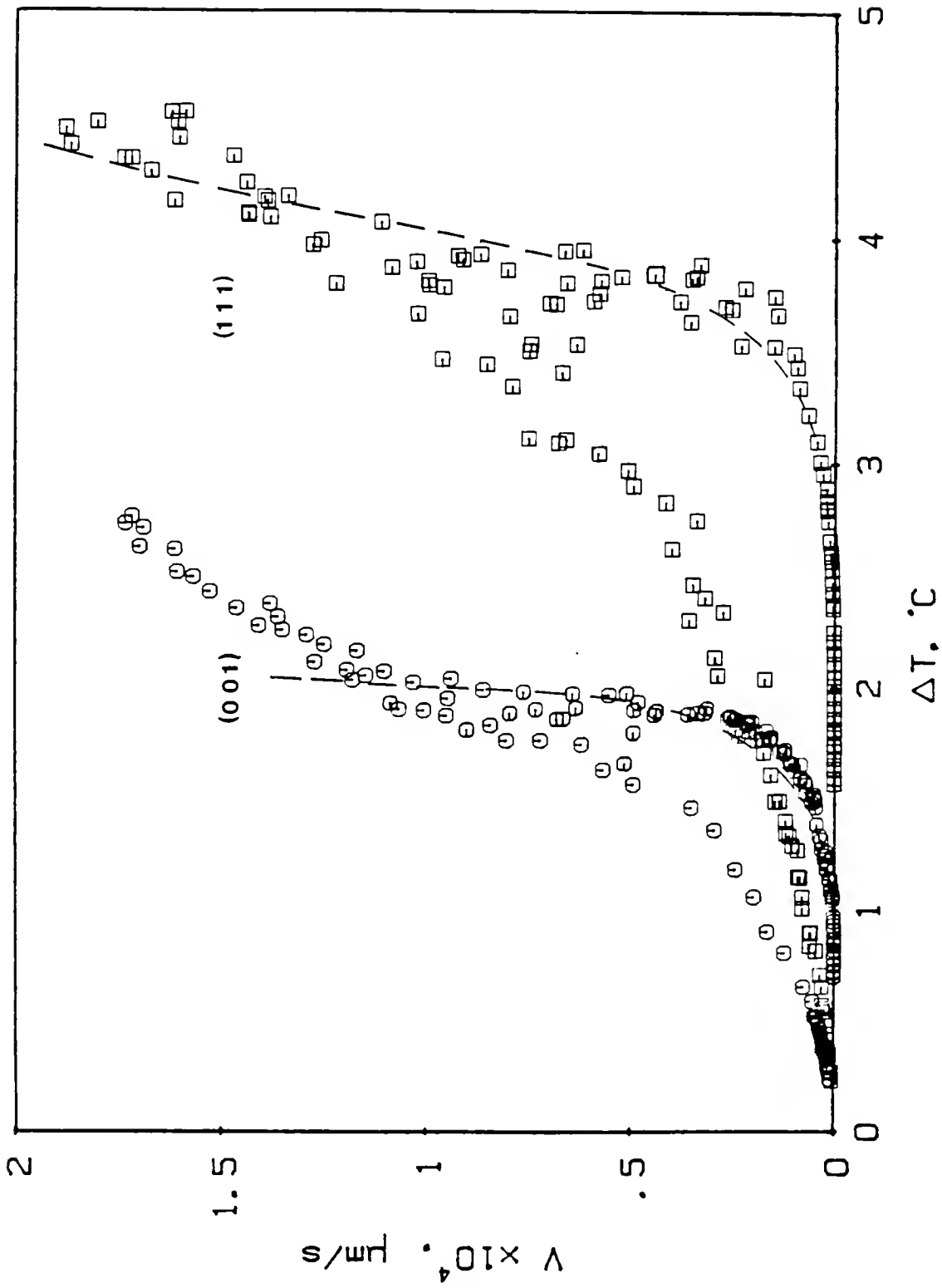
Figure 54   The (111) and (001) growth rates as a function of the interfacial supercooling. The dashed lines are calculated in accord with the general 2DNG rate equation "corrected" for D_i and supercooling dependent σ_e.
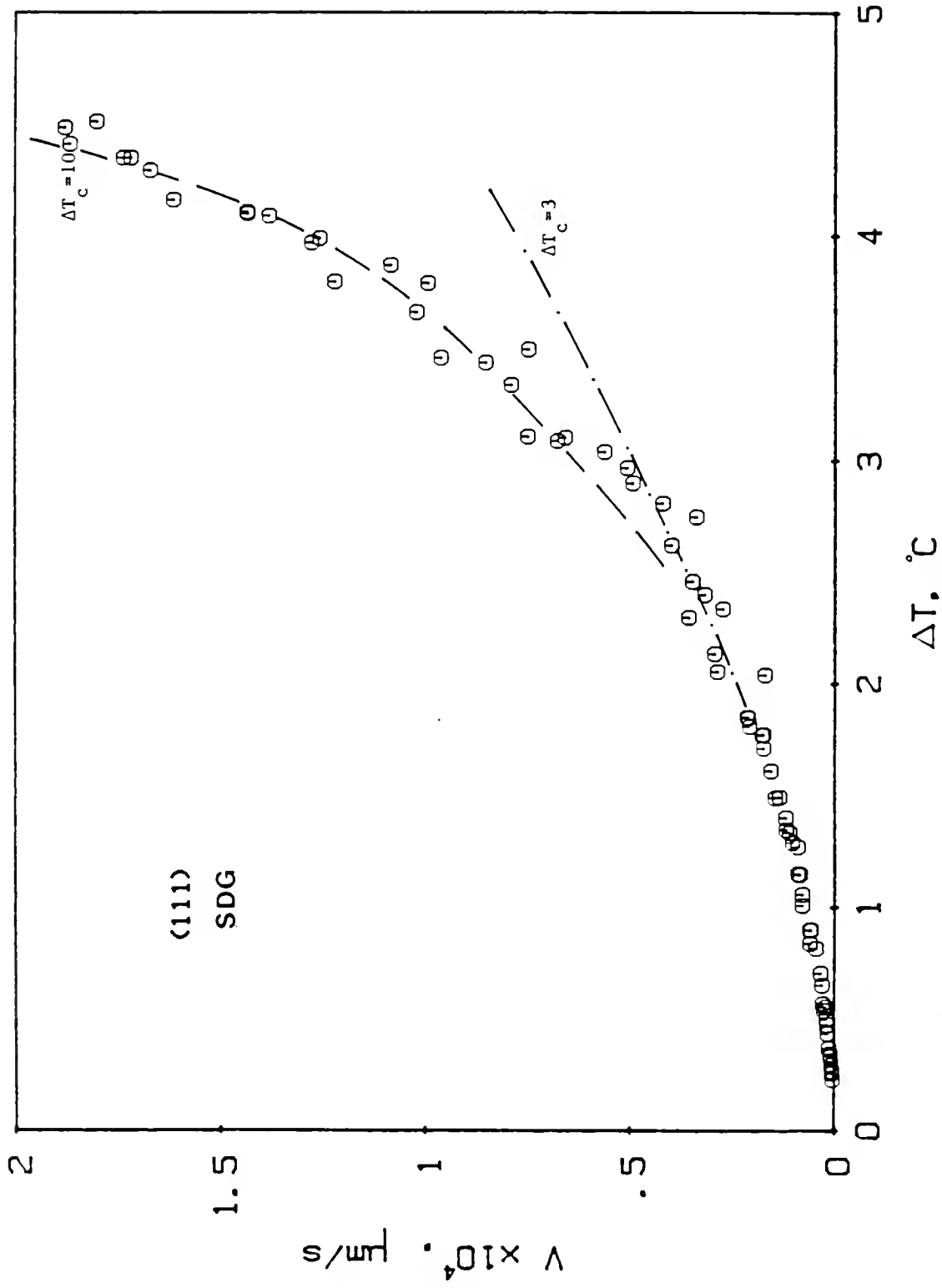
Figure 55   Comparison between the (111) dislocation-assisted growth rates and the SDG Model calculations shown as dashed lines.

fusion, respectively. Note that even the largest value of $x_s = 81$ Å is still larger than the spiral step spacing which is estimated to be about 280 Å at 4°C supercooling. The reason why ΔT_c increases from 3 to 10 at high supercoolings could be due either to a different distribution of dislocations (i.e. on S) at higher supercoolings or to a 2DN contribution to the spiral growth process. On the other hand, K_d is evaluated as 746 μm/s·°C which, together with the above mentioned value of ΔT_c (e.g. $\Delta T_c = 0$), implies that the kinetic coefficient of the step lateral spreading rate is about .75 cm/s. The latter value in turn indicates that D_i is about 3×10^{-7} cm^2/s (or about 10^{-8} cm^2/s for $\Delta T_c = 3$), which agrees with the earlier estimates of D_i. Extending the calculations for the (001) dislocation-assisted growth data shown in Fig. 56, using eqs. (91) and (93), ΔT_c and K_d are evaluated as 9 and 1840, respectively. These values indicate that $x_s S = 47$ Å and $D_i = 6 \times 10^{-7}$ cm^2/s.

All of the above mentioned parameters, besides the fact that they are reasonable as far as numerical values are concerned, they are "consistent" between interfaces and growth mechanisms, and most importantly, they point out consistently that a) the growth rate equations (92) and (93) describe the results well, b) $D_i < D$, and c) σ_e is a function of the supercooling.

These conclusions will be further strengthened later, where it is shown that several proposed "hypotheses" for explaining the high growth rates kinetics fail to describe the present results. Next, the kinetic roughening of the interface is discussed.
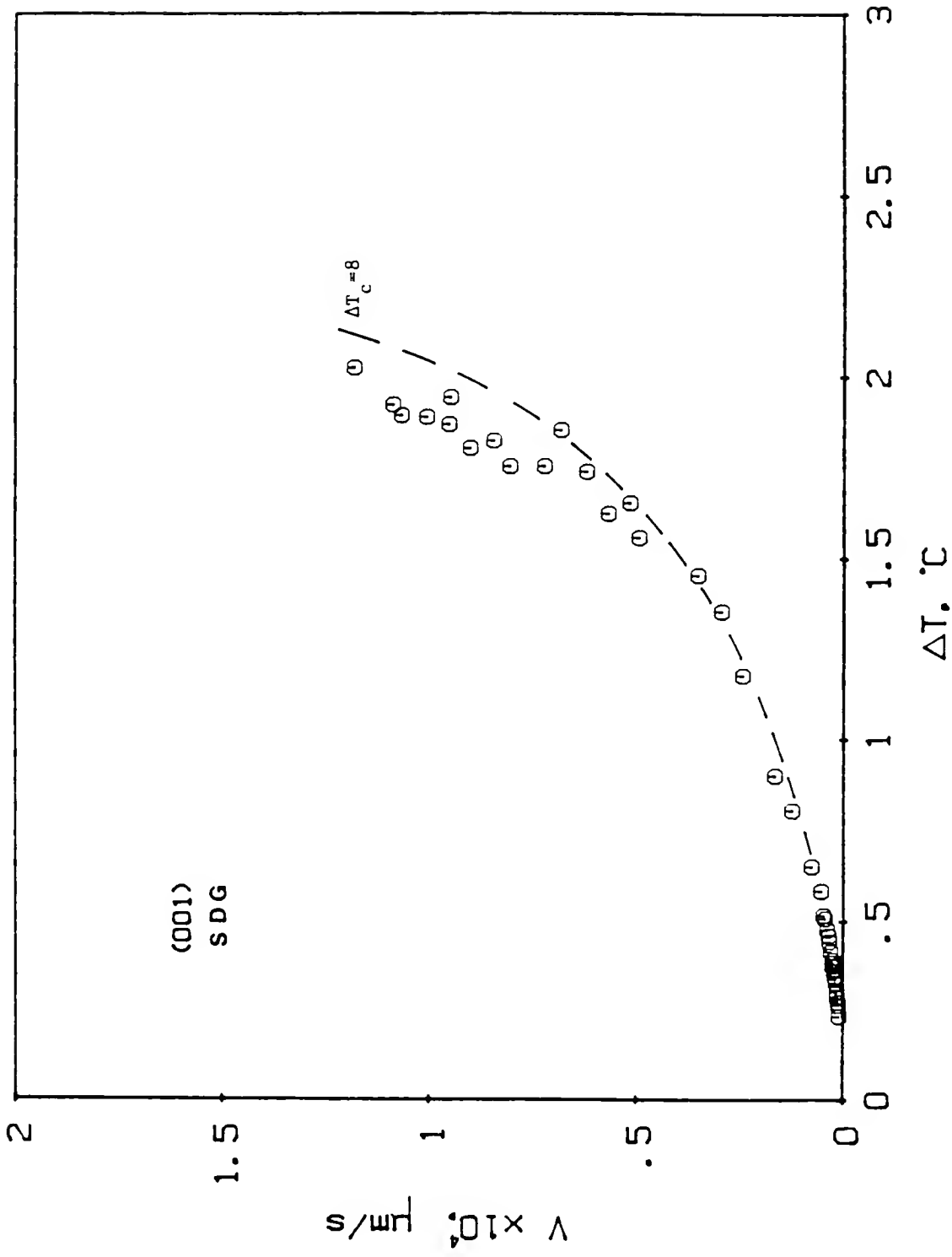
Figure 56 Experimental (001) dislocation-assisted growth rates as compared to the SDG Model calculated rates (dashed lines) as a function of the interface supercooling.

Kinetic Roughening

When a smooth interface is growing at a temperature below T_R, but at a driving force which is larger than a certain value, it will become rough and the non-linear $V(\Delta T)$ relation (i.e. lateral growth mechanism) will be replaced by a linear one. This phenomenon, as discussed earlier, is known as kinetic roughening. In comparison with the thermal roughening transition, little attention has been paid to the characterization of the former.

From a theoretical point of view, the transition could be best related to the conditions where the necessity for interfacial steps (in order for the smooth interface to grow) ceases to exist and, therefore, the two-dimensional nucleation barrier diminishes and dislocations have no effect on the growth rate. The nucleation barrier is meaningless either when thermal fluctuations result in a vast number of critical nuclei or when the step edge free energy becomes zero. The former implies a critical supercooling ΔT_k at which the free energy for forming a critical 2D nucleus ΔG^* becomes equal to the thermal energy KT; on the other hand, the latter indicates a supercooling dependent step edge energy. From the experimental point of view ΔT_k is relatively small only when σ_e is small to begin with. For example, assuming that the (111) interface kinetically roughens at $\Delta T = 4°C$ by satisfying the condition $\Delta G^* = KT$, σ_e is estimated to be about 5.32 ergs/cm^2; this is about 25% of the measured σ_e via the MNG rate equation. It is possible to rationalize a smaller σ_e value assuming that the 2D clusters are anisotropic. For example, if it is assumed that the nuclei are parallelogram-like (instead of circular) with the two sides r_1 and r_2 such that

the anisotropy $\delta = r_2/r_1$ is about .1, σ_e is calculated for the (111) interface to be about 6 ergs/cm^2 at $\Delta T = 1.5°C$. Nevertheless, since σ_e is assumed to be independent of supercooling, the criterion $\Delta G^* = KT$ is only satisfied at supercoolings much higher than 10°C. In conclusion, based on the experimentally determined exponential terms of the 2DNG (111) and (001) rate equations, the criterion $\Delta G^* = KT$ fails to explain the observed deviation in the growth kinetics.

The case of a supercooling dependent edge free energy was examined earlier. It was shown that as ΔT increases σ_e decreases and finally becomes zero in a fashion analogous to that for the thermal roughening transition. At first glance, such behavior seems to be in the opposite direction from what one would expect; since T_R is expected to be not very far from T_m (but larger), σ_e should increase with decreasing T_i, or at least it should remain constant. However, this idea abandons the dynamic morphology of the interface because of the lateral growth process, as well as the state of the liquid near the spreading steps. At high supercoolings, an interface that is growing by any of the stepwise mechanisms (2DNG or SDG) is not only covered by of 2D clusters and therefore of heavily kinked edges, but also extends itself over several atomic planes regardless of its diffuseness. While the former is due to the increased 2DN rate, the latter is because of the nature of the lateral growth processes. Therefore, the top layers of the interface would "look" alike to the MC simulations computer drawings of Fig. 6 as well as the resultant growth kinetics, as shown in Fig. 57. Under such conditions, an interfacial step, which is a rather unique feature in the background of the interface at small supercoolings, cannot be
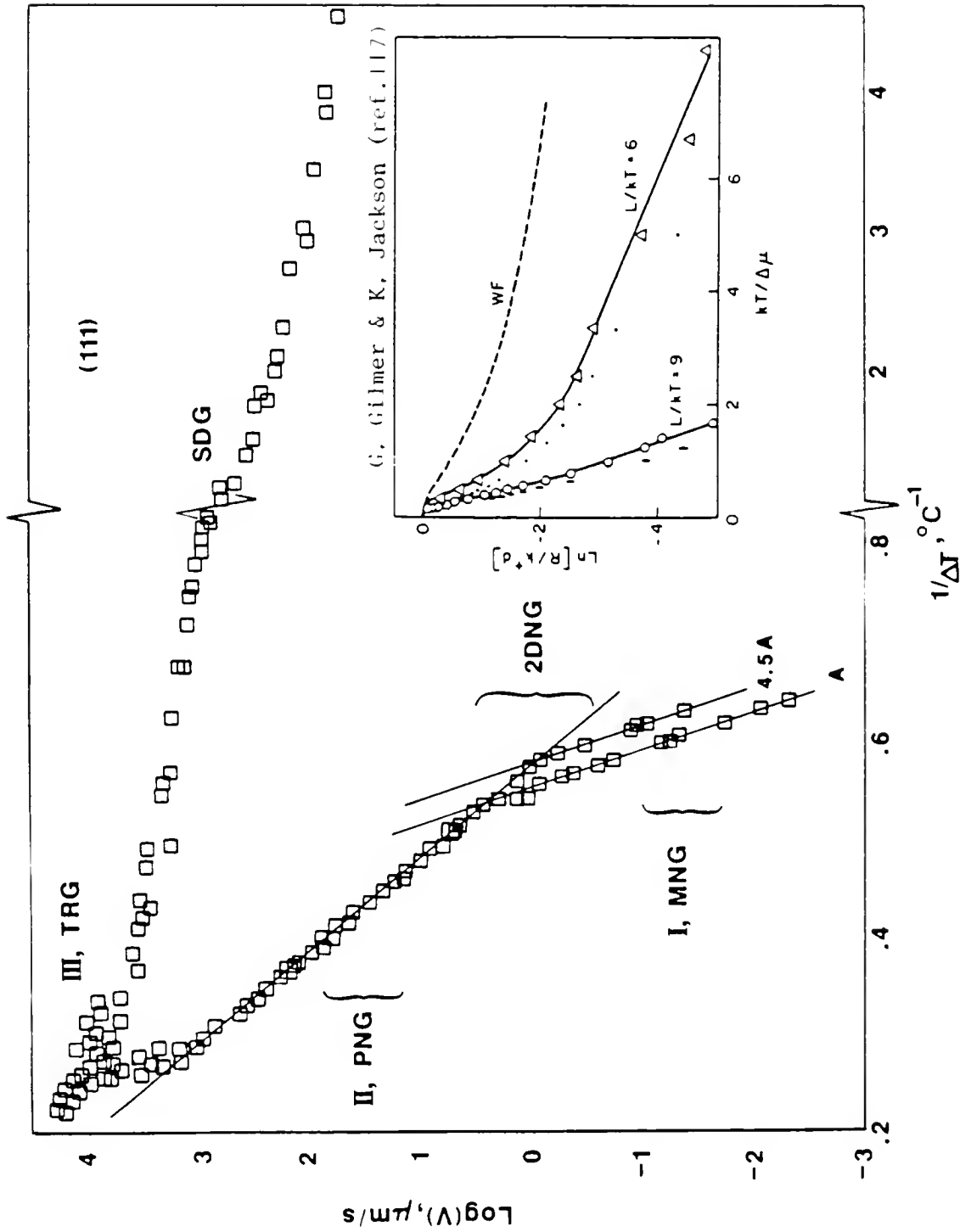
Figure 57　The (111) growth rates versus the interface supercooling compared to those determined from CS on the solid/vapor interface (Ref. (117)).

distinguished from its many similar neighbors whose effect can also be thought as a "catalytic" one. Similarly, the addition of the peripheral area of a new cluster on the multistepped interface would hardly alter its total energy.

Furthermore, from the diffuseness point of view, the liquid is extensively clustered in both directions normal and parallel to the interface, which would result in steps of quite large width, and, therefore, of negligible step edge energy.

As shown earlier, it was found that σ_e goes to zero at supercoolings of 4.75 and 2.2°C for the (111) and (001) interfaces, respectively. The present experimental results were described well in the previous section by taking into account the kinetic roughening of the interfaces (i.e. assuming that σ_e depends on ΔT). It was also shown that approaching the roughening transition, the dislocation-assisted growth rates become comparable to the dislocation-free. Such a behavior cannot be explained otherwise; for example, assuming that the high ΔT's growth rates are the sum of the 2DNG and SDG rates determined from the lower supercoolings.[335] This comparison is shown in Fig. 58 for the (111) interface, where it is realized that the actual growth rates are higher than the calculated ones, shown as the dashed line in this figure.

At supercoolings below that of the kinetic roughening (TRG region), the mixed (2DNG/SDG) rates depend approximately linearly on the supercooling, as shown in Figs. 23 and 31 and as discussed earlier. This linear growth curve extrapolates to the right of the origin on the supercooling axis. It should be noted, however, that this linear (V, ΔT) curve neither implies a different growth mechanism nor can be
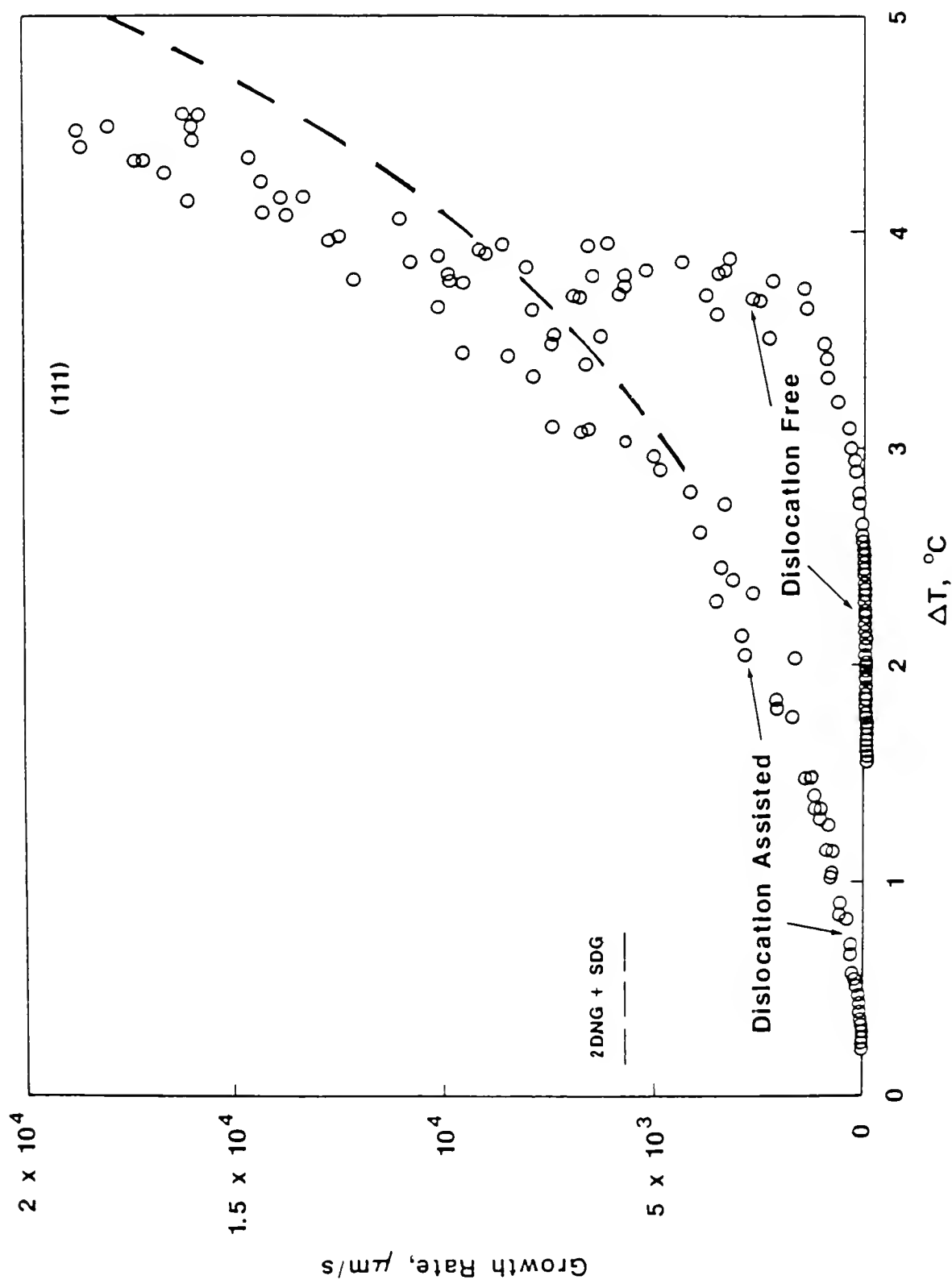
Figure 58   The (111) growth rates versus the interface supercooling compared to the combined mode
of 2DNG + SDG growth rates (dashed line) at high supercoolings.

associated with the kinetic roughening recently described[334] for the growth of naphthalene from solution. This is because, as shown before, the growth data in this region can still be expressed via a 2DNG or SDG mechanism. Moreover, dislocations in this region, yet appear to effect although in a minor way, the growth rates as clearly shown for the (111) interface in Fig. 23. This is expected since for the (111) interface the highest growth rates are for supercoolings in the range of 4.5-4.6°C, which is below the estimated roughening supercooling of 4.75°C.

The (001) growth kinetics beyond the roughening supercooling (~2.2°C) are different than those of the TRG regions for both interfaces, as can be seen in Fig. 31. Indeed, the linear growth curve for V > 1.4 cm/s, if extrapolated to zero growth rates, essentially passes through the origin. On the other hand, the determined kinetic coefficient of .63 cm/s·°C seems to be in excellent agreement with that of the continuous growth theory, as discussed later.

Disagreement Between Existing Models for High Supercoolings Growth Kinetics and the Present Results

As it was discussed earlier, the growth rates at high supercoolings deviate from the rate equations expressing both the spiral and bi-dimensional growth mechanisms at lower supercoolings. Nevertheless, as shown in the previous section, the kinetics are well described by a general lateral growth model based on the classical ideas, but corrected for D_i and $\sigma_e(\Delta T)$.

Several features of the experimental growth data curve, as shown in Fig. 59, are in qualitative agreement with the diffuse interface theory[25] such as: i) lateral growth at low supercoolings regardless of the values of "α" factor for each interface, ii) the growth curve at
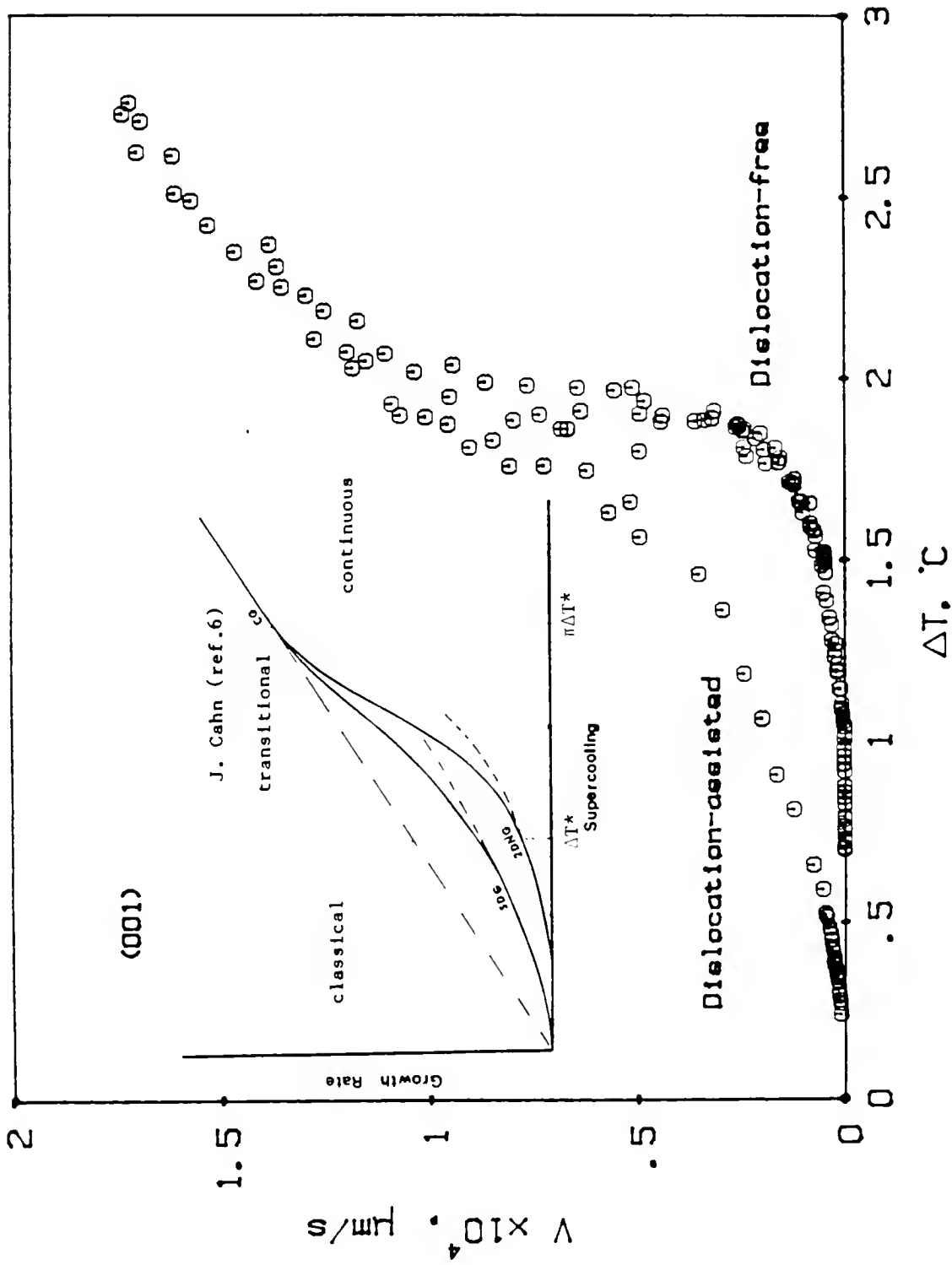
Figure 59 Comparison between the (001) growth curves and those predicted by the diffuse interface model[6].

higher supercoolings deviates from the classical equations in the direction of the faster growth rates, and iii) dislocations affect the growth only below the transition. However, for a complete comparison, the two phenomenological parameters of the theory, β and g, have to be computed from the experimental data through the proposed equations. The value of g is expected to be in the order of one, if the interface is sharp and much less than one if the interface is diffuse. The theory gives several relationships to evaluate g for a given material. One of the relationships relates $\sigma_{s\ell}$, σ_e, and g as follows.

$$\sigma_e/h = \sigma_{s\ell} \sqrt{g} \qquad (38)$$

Substituting the experimental values of σ_e/h (see Table 8) and 67 or 40 ergs/cm^{2*} for $\sigma_{s\ell}$ the calculated value of g for each face are given in Table 11. The theory gives another relationship to estimate the value of g as

$$g = \frac{50 \text{ K L } \Delta T_t}{\pi \sigma_{s\ell}^2 \text{ h } V_m} \qquad (94)$$

where ΔT_t is the threshold supercooling for a measurable growth rate by the 2DNG mechanism. Substituting the experimental values of ΔT_t as 1.5°C (111) and 0.6°C (001), the calculated values of g, as given in Table 11, range from .12 to .34 for the (111), and .04 to .1 for the (001) interface. Note that eq. (94) was derived based on the assumption that the onset of the detectable growth occurs at a value of ΔT_t for which

---

* The values of 67, 40 cover the range of the existing theoretical and experimental values for $\sigma_{s\ell}$ of Ga in the literature.

Table 11. Calculated Values of g.

Interface	Equation (38)		Equation (94)		Equation (49)	
	$\sigma_{s\ell}=67$	$\sigma_{s\ell}=40$	$\sigma_{s\ell}=67$	$\sigma_{s\ell}=40$	$\sigma_{s\ell}=67$	$\sigma_{s\ell}=40$
(111)	.09	.26	.12	.34	.025	.04
(001)	.03	.085	.04	.1	.013	.022

$$\Delta G_t = 50KT$$

If, instead of 50KT, 40KT is assumed, then the calculated g values from eq. (94) are in agreement with those calculated via eq. (38).

The critical supercooling at which the transition off the lateral growth (i.e. for both 2DNG and SDG mechanisms) occurs, can be used to calculate g from the previously derived equation (eq. 49) as

$$\Delta T^* = \frac{\sigma_{s\ell} \, g \, V_m \, T}{h \, L} \tag{49}$$

Assuming that ΔT^* is the supercooling for which the deviation from the low supercoolings 2DNG rate equations is observed (i.e. $\Delta T^*(111) = 3.5°C$ and $\Delta T^*(001) = 1.5$), the latter equation yields estimated g values as .02 to .04, and .01 to .02 for the (111) and (001) interface, respectively. These values of g are less than those calculated previously from the step edge free energy and from ΔT_t. It should be mentioned that ΔT^* is assumed to be such that the thickness of the interface becomes equal to the 2D critical nucleus radius. It is interesting to note that, although the theory implies that σ_e should approach zero in the transitional regime, it does not predict any quantitative decrease in the g parameter (i.e. increased diffuseness) with supercooling. The prediction of the onset for the transition from lateral to continuous growth at a supercooling such that the width of the nucleus exceeds its radius seems to be correct, since it implies that the step will loose its "identity" in the background of the interface following the transition. The estimated g values indicate a one to two layer S/L interface, as expected for a faceted interface. However, these values, as shown previously, are not quantitatively self-consistent with the proposed tests of the theory.

The second parameter β of the theory, which rather meant to "modify" the liquid self-diffusion coefficient for interfacial transport, can be obtained from the continuous growth rate equation as

$$\beta = \frac{h \ RT^2 V_c}{LD \ \Delta T} \tag{95}$$

where V_c is the growth rate in the continuous regime. However, since the theory assumes that continuous growth prevails above the break point in the growth rate curve (at $\Delta T \simeq 3\Delta T^{*}$) and that the product $V\eta$ should be linear with ΔT in this regime, then the present (111) data should be still in the transitional regime. Thus, a lower limit to the quantity β can be obtained as

$$\beta \geq \frac{Vh}{D} \frac{RT^2}{L\Delta T}$$

where V is the actual growth rate. For the (111) interface at $\Delta T = 4°C$, the measured rate is about 1.25 cm/s. Thus, β must be at least .08 according to the above inequality. It is expected that for symmetrical molecules β should be in the order of ten. If this is the case, then the kinetic coefficient of the linear growth in the order of about 40 cm/s would be an almost acceptable high value. An upper limit for β could be estimated from the slope of the experimental high growth data linear equation, assuming that the continuous growth predicted by the theory should pass through the origin of a V vs. ΔT plot. Then

$$\frac{\beta \ D_L \ L}{h \ RT^2} \leq .98 \quad \text{or} \quad \beta \leq .25$$

Indeed, this upper value of β agrees well with the previously calculated values of interfacial diffusivity. Furthermore, if β is calculated via eq. (95) for the (001) interface, utilizing the experimental kinetic

coefficient of the (001) normal growth $V_c/\Delta T$ = .63 cm/s·°C (see Results chapter) a value of β = .205 is found. Note that this value, being consistent with that of the upper limit calculated for the (111) interface and the interfacial diffusivity values, could indicate, according to the diffuse interface model, that the (001) linear growth at the highest supercoolings is due to a continuous growth mechanism. This was, anyhow, expected since the (001) interface at this range of supercoolings ($\Delta T > 2.2$°C) is rough, as indicated from the fact that σ_e is zero at this range.

In conclusion, despite the fact that the experimental data are in qualitative agreement with most of the diffuse theory's predictions, the lack of quantitative agreement makes one to believe that the theory does not explain the magnitude of the observed transition from the lateral growth; an agreement could be possible if the model would allow for a supercooling dependent interfacial diffuseness, g. On the other hand, the estimated β values agree well with the experimental results and support the conclusions of this study that the interfacial diffusivity is smaller than the Ga liquid self-diffusion coefficient.

The possibility of morphological breakdown of the planar interface (changing to a cellular or dendritic form) was also investigated using the morphological stability criteria to determine the conditions under which the interface may become unstable, as discussed in detail in Appendix IV. The analysis indicates that the (111) S/L interface, for example, should be stable up to about .8 cm/s if the perturbation wavelength is equal to the interface diameter; for smaller perturbations the interface should be stable at higher rates. Therefore, since the

deviation from the classical laws takes place at lower growth rates, it is believed that the kinetics transition, for both interfaces, is not due to the interfacial breakdown. However, since the analysis indicated that a possible breakdown of the interface might have occurred at rates in the order of .8 cm/s, it is appropriate as a last check to compare the growth data with that of the dendritic growth theory.

Figure 60 shows the (111) growth data as plotted in a normalized growth velocity (V_n) vs. the normalized supercooling (ΔT_n) plot. V_n is defined as[336]

$$V_n = \frac{V}{2\alpha} \cdot d_o = \frac{V}{2\alpha} \cdot \frac{T_m \, \sigma_{s\ell}}{\Delta \cdot C_p}$$

where V is the actual growth rate, α is the thermal diffusivity, C_p is the specific heat, and Δ is the unit supercooling defined as L/C_p. The normalized supercooling is given as

$$\Delta T_n = \frac{\Delta T_b}{\Delta}$$

where ΔT_b is the bulk supercooling. The physical parameters used for the growth parameters are given in Appendix I.

The experimental points as shown in Fig. 60 fall into a single line with a slope of about 1.45, as compared with that of 2.65 for the universal dendritic growth law rate equation[336] (continuous line in Fig. 60).

Furthermore, at normalized supercoolings larger than .2, it is predicted that the power of the growth law should increase from 2.65.

Results of Previous Investigations

Alfintsev et al.[104,215] first studied the growth of single crystals of Ga placed between two glass plates. The growth rates were measured
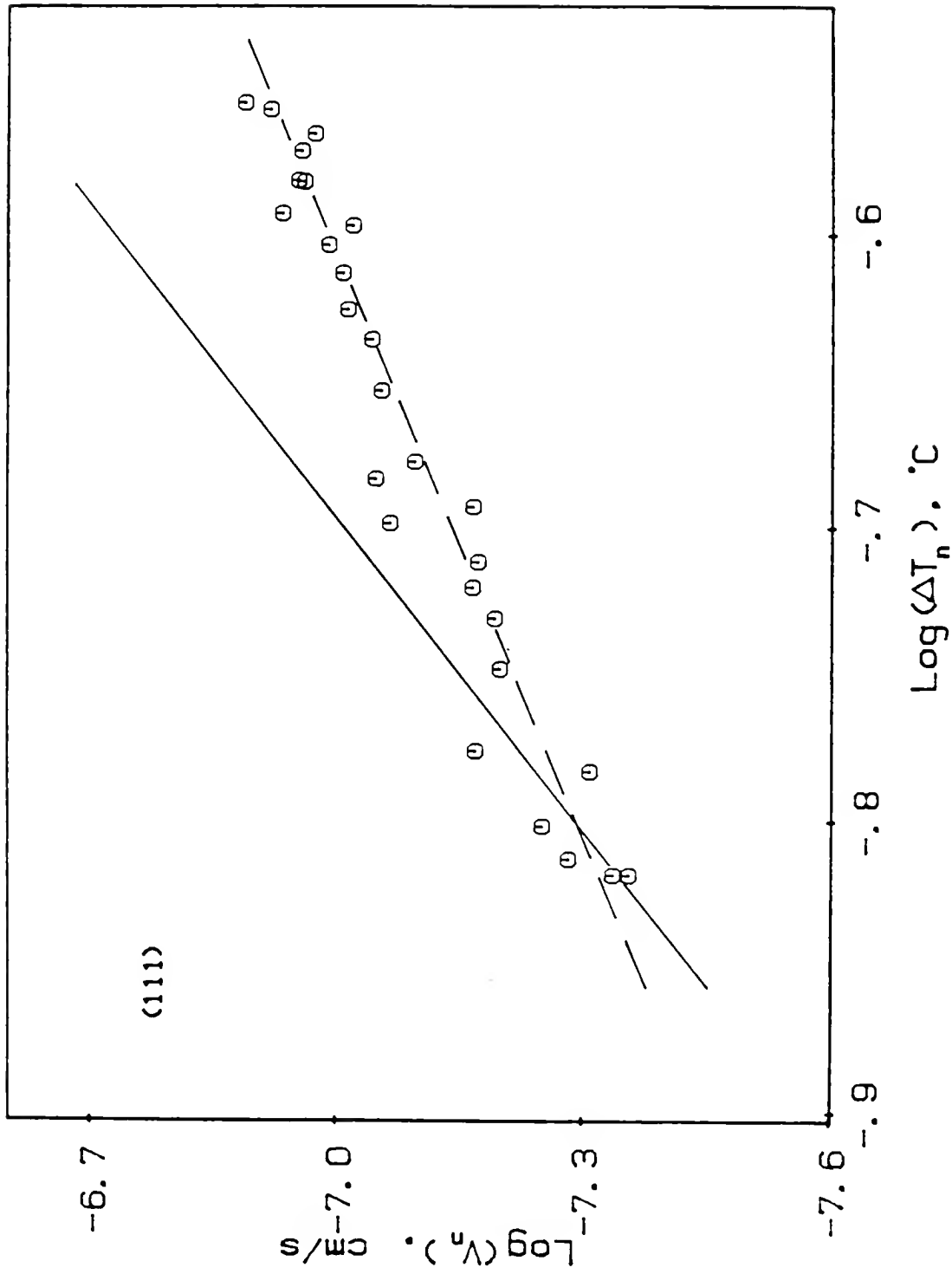
Figure 60   Normalized (111) growth rates as a function of the normalized supercooling for interface supercoolings larger than 3.5°C; continuous line represents the universal dendritic law growth rate equation (ref. 33).

optically, whereas the interfacial supercooling was assumed to be equal to the bulk supercooling at low growth rates. At higher rates, the interface temperature was determined by a thermocouple. They reported that the growth of perfect crystals is characterized by 2DNG kinetics and that of the imperfect crystals by the SDG mechanism. Although their results are in qualitative agreement with the present ones, a quantitative comparison between the two is not possible. This is because their growth rates extend in a small range (2-4 µm/s for the dislocation-free and 10-280 µm/s for the dislocated interfaces), and the data points are plotted in small linear graphs. Semiquantitatively, however, their results are in fair agreement with those of the present study. Another difficulty in comparing their data to the present ones is that their growth rate equations, given by the authors in references (104) and (215), are not consistent with each other. They relate the discrepancies to the differences between the experimental conditions of each experiment.

Kinetics of solidification of dislocation-free and dislocated single crystals of Ga, grown in glass capillaries, were also studied by Abbaschian et al.[2,99] The growth rates (up to 2500 µm/s) were measured optically and the interface supercoolings were determined from a heat transfer model. Their (111) results are in good agreement with those of the present experiments, up to growth rates of about 500-600 µm/s. Above these rates, the present results show slightly higher growth rates (about +7% in the range of 600 µm/s only). This is believed to be due to the limited accuracy of the heat transfer model used to determine the interface supercooling at high growth rates (see more about it in their

discussion[2] and in Appendix III). The authors have cautioned the use of heat transfer calculations at high rates, since the calculations become very sensitive to the errors involved in the thermo-physical property values and assumptions of the calculations. Based on the numerical calculations and the present direct measurements, the analytical solution underestimates the supercooling at rapid rates, as discussed in Appendix III. For the (001) interface there is a difference, up to about 15%, between the growth rate parameters for the PNG and SDG kinetics. Abbaschian et al.[2] have also showed that their dislocation-free and assisted data for both interfaces approach each other at high supercoolings and that for the (001) interface they meet at about 1.6°C interface supercooling. They also reported that, for dislocation-assisted growth at minute supercoolings (<0.1°C), the growth kinetics could be interpreted by a linear relationship in the form of $V = K \Delta T$. At larger than about 0.05°C ΔT, the kinetics of the dislocated interface followed a ΔT^n relationship with n around 1.7. The linear growth can be explained, assuming that growth was due to S dislocations (of the same sign) arranged in an array of length L so that $L > 2\pi r_c > L/S$. Accordingly, the rate is then proportional to $\upsilon_e S/L$ (see earlier discussion in Chapter II) and, therefore, linearly dependent on ΔT. In order for the linear law to extend to ΔT's as low as .005°C, a possible combination of parameter values required is for example $L = 200$ μm and $S = 50$, which imply that $x_s \ll 4$ μm and υ_e about 1.6 cm/s (based on the 40 μm/s·°C^2 experimental kinetic coefficient), which appear to be quite reasonable.

Borisov et al.[216,337] reported solidification data of Ga thin layers with growth rates up to 200 cm/s and corresponding supercoolings

up to 35°C. The growth direction, and the perfection of the crystals, were not specified. In their view, the lateral type of growth for Ga, reported in the above mentioned investigations,[2,99,104,215] was caused by impurities. They claim that the observed linear rate equation (V = 5.3 ΔT cm/s) agrees satisfactorily with their own theory of normal growth mechanisms. Based on their explanation, Ga should not behave as a facet forming material and should grow continuously at any supercooling. Their inaccuarate results have been attributed to the rather heuristic experimental conditions used,[338a] which produced very strained crystals. Finally, Gutzow and Pancheva[338b] have reported that solidification of Ga single crystals, growth by the capillary technique, was of the faceted type.

In-Doped Ga Growth Kinetics

The kinetic results presented earlier indicate that the growth rate of the (111) interface of Ga doped with In up to .12 wt% depends on the supercooling, In content, distance solidified, and growth direction with respect to the gravity vector. Furthermore, it is shown that the faceted interface breaks down as the growth process proceeds; the frequency of which depends on the In content and the supercooling. The effects of each parameter on the growth kinetics are discussed in the following sections.

Solute Effects on the 2DNG Kinetics

The inital growth rates of the Ga-.012 wt% In samples versus the interfacial supercooling, as shown in Figs. 39 and 41, compared with the 2DNG kinetics of pure Ga indicate that at growth rates less than .5

μm/s, the solute has no appreciable effect on the rates. At higher rates, however, the addition of the solute decreases the growth rates. Based on the experimental growth rate equations (eqs. (78) and (80)), the pre-exponential term for doped Ga is smaller than that for the MNG rate equation of the pure Ga (eq. (69)) by 1-2 orders of magnitude. In the PNG region, this difference (compare the pre-exponential terms of eqs. (79) and (81) versus eq. (70)) reduces to less than one order of magnitude. The solute effect on the pre-exponential term of the 2DNG rate equations might be due to the interaction of adsorbed solute atoms on the interface with the lateral spreading process, i.e. the edge spreading rate υ_e and/or the change of the kinetic factor K_n of the 2DN rate equation (eq. (28)).

The edge free energy of the steps on the (111) Ga interface decreases slightly, about 3-4% by the addition of In. The In additions decrease σ_e, and thus the size of the critical nucleus, reducing the activation free energy of the 2DN process. Nevertheless, the overall nucleation rate seems to be decreased, as depicted from the lower growth rates, in comparison to those of the pure Ga in the mononuclear regime. Therefore, only a minute amount of an impurity is necessary to drastically decrease K_n, while its effect on σ_e is still negligible. This is because adsorption takes place mostly at the growth sites of the clusters and decreases the molecular kinetics across the cluster/bulk interface. Regarding the solute effect on the step edge velocity, one has to distinguish whether the In molecules adsorb separately on the surface or in the kinks and steps. Although such a distinction is rather impossible since the S/L interface cannot be investigated directly, it can be

assumed that the most preferred sites should be the most energetic ones, i.e. the kinks. At higher concentrations, adsorption should take place at less energetic sites. In any case, υ_e is expected to decrease either because of the reduction of kinks or because of the decrease in the step spreading process. For example, if a step tries to pass through two adsorbed In molecules, this would be possible only if their distance d is less than $2r_c$. If this condition is satisfied, the step can bow out and pass the impurities. However, then its curvature will increase and, therefore, its velocity will decrease (see eq. (22)). Thus, the interaction of the In molecules with the 2DNG processes becomes more pronounced at higher supercoolings, as shown in these experiments. For example, the decrease in the growth rate at supercoolings 1.8 and 2.3°C accounts for up to about 28 and 50%, respectively.

Increasing the In concentration to .12 wt% results in a more effective decrease of the growth rates of the (111) doped Ga interface relative to those of the pure Ga, as shown in Figs. 44 and 45. The 2D nucleation rate further decreases as shown in Fig. 45. At growth rates higher than about 15 μm/s, the rates start deviating in the direction of faster growth rates, i.e. towards the pure Ga and Ga-.012 wt% In growth curves. The reasoning for this behavior is that, at these supercoolings and decreased values of σ_e, the critical nucleus becomes quite small so that the interface possibly starts roughening.

By observing the crystal growth of the In-doped Ga samples, it was revealed that liquid rich bands were entrapped by the growth front, as shown in Fig. 38, which had faceted boundaries. This is believed to happen due to a non-uniform solute distribution across the S/L inter-

face.[209] The part of the interface with the lower In concentration will move ahead of the rest since it is more supercooled; however, when the top of the protuberance reaches an adjacent region of liquid with low In concentration, it will then spread across, entrapping the solute rich strip. At high supercoolings (>5°C), the inner surfaces of these bands developed several protuberance-like cells, indicating that the growth inside these bands is rather purely diffusive because of the high In content.

Next, the effect of the interfacial segregation process on the growth kinetics is discussed in relation to the fluid flow effects associated with the growth direction with respect to the gravity vector.

Segregation/Convection Effects

As shown earlier, the initial growth rates for the parallel to gravity growth direction were higher than those for the antiparallel at a given interface supercooling. A possible cause for this finding could be due to differences in the nature and magnitude of convection in the liquid. The convection could be caused either by density inversion of the liquid and/or by the contact forces between the glass wall and the melt. When a Ga-In alloy is solidified upwards, a solute boundary layer is built up ahead of the S/L interface where the solute concentration decreases exponentially with the distance from the interface. Hence, the density of the liquid is higher at the interface and decreases with the distance from the S/L interface, x'. Thus, based on the previous discussion about convection in Chapter II, the composition gradient does not result in a solutally driven convection. On the other hand, the negative temperature gradient (see Appendix III) acts in the opposite

direction to the solute concentration gradient with respect to the density of the liquid, and could cause convection. The exact opposite situation prevails when growth takes place downwards. Here, the solute concentration gradient results in a positive density gradient, i.e. unstable for convection, which is opposite to that caused by the positive thermal gradient. Therefore, in both growth directions the density gradient may be statically stable or unstable depending on its relative magnitude due to the temperature gradient, $(d\rho/dx)_T$, and that due to the solute concentration gradient, $(d\rho/dx')_C$.

For the solute distribution at the initial transient state (see eq. (62)) with a planar S/L interface $(d\rho/dx')_C$ is given as

$$(\frac{d\rho}{dx'})_C = \frac{d\rho}{dC_\ell} \frac{dC_\ell}{dx'} = \frac{d\rho}{dC_\ell} \frac{C_o V}{D} \frac{k-1}{k} \exp[1 - \exp(-\frac{kVx}{D})] \exp(-\frac{Vx'}{D})$$

$$\leq \frac{d\rho}{dC_\ell} \frac{VC_o}{D} \frac{k-1}{k} \exp[1 - \exp(-\frac{kVx}{D})]$$

(96)

where $d\rho/dC_\ell$ is the solutal density coefficient and x is the distance from the onset of growth. As noted from eq. (96), it is assumed that the solute has not yet reached the steady state value. This is because the steady segregation region is expected to take place at distances greater than about 1700 μm from the onset of solidification for the highest growth rates of 40 μm/s. This distance (in the order of D/kV) is much larger than the distance, about 175 μm, where the initial growth rate measurement was taken. The density gradient caused by the thermal field is given as

$$(\frac{d\rho}{dx'})_T = \frac{d\rho}{dT} \cdot \frac{dT}{dx'} = \frac{d\rho}{dT} G_L$$

(97)

where $d\rho/dT$ is the thermal density coefficient. The necessary condition to suppress the convection is expressed by the following inequality.

$$\frac{d\rho}{dx'} = \left(\frac{d\rho}{dx'}\right)_T + \left(\frac{d\ell}{dx'}\right)_C < 0 \qquad (98)$$

Using $d\rho/dc = 7.95 \times 10^{-3}$ g/cm^3·wt% In and $d\rho/dT = -9.7 \times 10^{-4}$ g/cm^3·°C (see Appendix II), eqs. (96) and (97) are calculated on the basis of the experimental conditions and the results of the heat transfer model (see Appendix III) for $C_O = .012$ wt% In, as shown in Table 12. In these calculations, both the temperature and the concentration gradients have been estimated at $x' = 7$ µm, which is smaller than the characteristic decay distance (D/V) of G_c. According to Table 12, $|(d\rho/dx')_C|$ were greater than $|(d\rho/dx')_T|$ up to about sixty times at the highest growth rates. The results of Table 12 are also schematically shown in Fig. 61.

For growth in the upward direction $d\rho/dx$ was negative in the region between the S/L interface and at a minimum distance of about 34 µm for the highest growth rate. At a further distance away than this, the liquid could be statically unstable, since $d\rho/dx$ becomes positive. However, because of the very small thermal gradients in these experiments (e.g. $G_L = 2.5$°C/cm at V = 40 µm/s, $x' = 7$ µm) and the fact the G_L in these experiments decreases fast with x' (see Appendix III), it is believed that convection does not occur during upwards growth. On the other hand, when the growth direction was parallel to the gravity vector, $d\rho/dx'$ was positive in the interfacial liquid up to a minimum distance D/V away from the S/L interface. Therefore, it can be considered that the In-doped Ga grown downwards had been solidified under the unstable conditions for convection. Nevertheless, one can still account for a purely diffusive layer of thickness δ near the interface in accord

Table 12. Solutal and Thermal Density Gradients (x' = 7 μm).

V, x 10^{-4} cm/s	$-/+^{*}$ $(d\rho/dx')_C$, g/cm^3/cm	$+/-^{*}$ $(d\rho/dx')_T$, g/cm^3/cm
.5	2.2×10^{-5}	1.07×10^{-6}
1	8.98×10^{-5}	2.12×10^{-6}
5	2.2×10^{-3}	2.7×10^{-4}
10	8.8×10^{-3}	6.1×10^{-4}
15	.0198	8.9×10^{-4}
20	.0351	1.16×10^{-3}
25	.0544	.00143
30	.0779	.00177
35	.1054	.00211
40	.137	.00237

* Top and bottom signs apply for growth in the upward and downward direction, respectively.
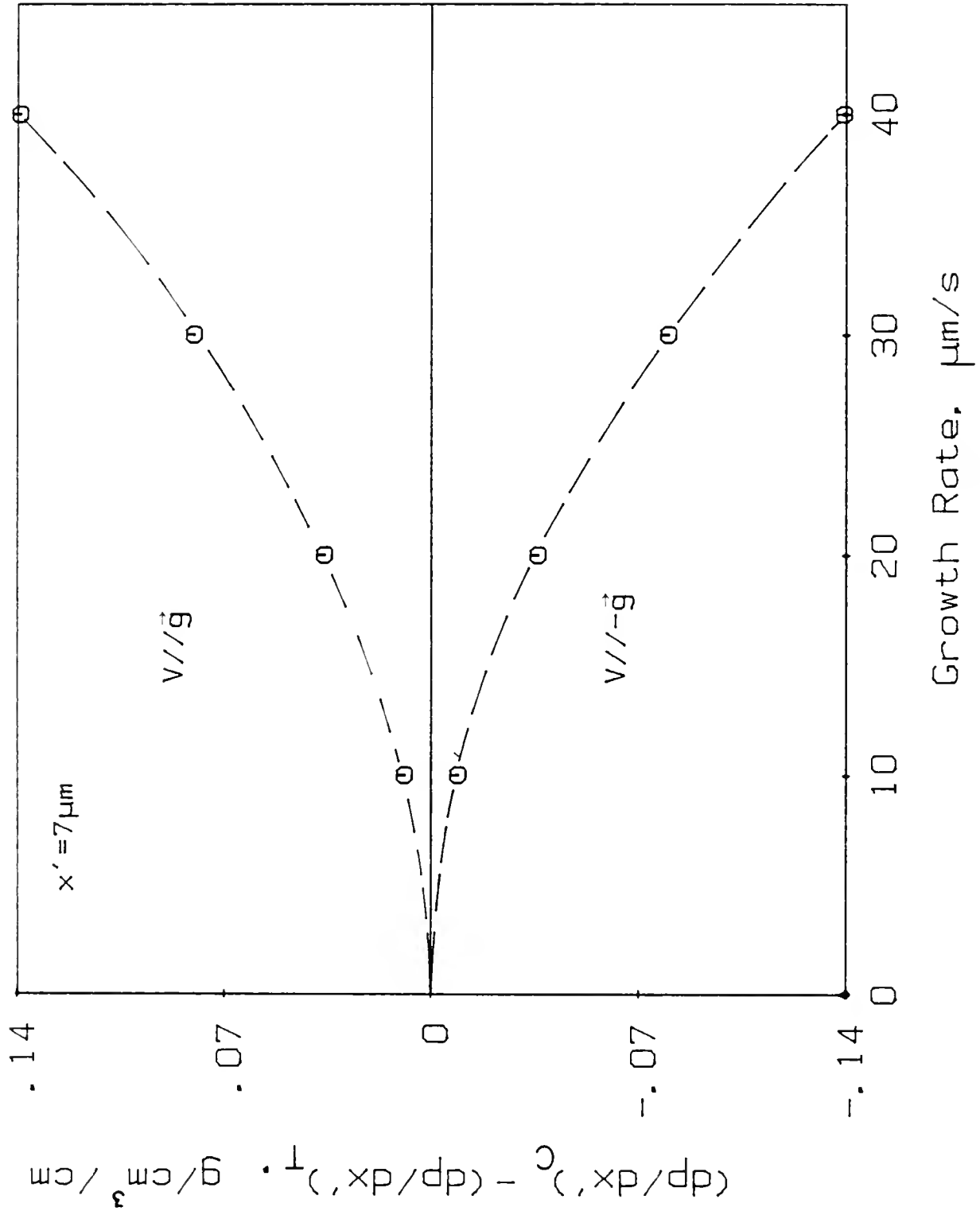
Figure 61   Density gradients as a function of growth rate.

with the "stagnant film model," regardless of the amount of convectional flows; at the S/L interface diffusion-advection fluxes will always dominate over the convection fluxes.

The same discussion applies for the .12 wt% In-doped Ga sample. In addition, because of the ten-fold increase in C_O in comparison with the .012 wt% alloy, $(d\rho/dx')_C$ is ten times larger than those given in Table 12. Accordingly, this sample should have grown under more stable and unstable conditions for the convection in the upwards and downwards growth directions, respectively. However, regardless of the dopant (In) level, the convection cannot be confirmed directly in these samples. Nevertheless, if convection was present near the S/L interface during growth in the downwards direction, the observed differences in the growth kinetics for the two growth directions can be explained as follows. During growth in the direction parallel to the gravity vector, the interfacial liquid seems to be mixed by convective flows, the pattern of which is likely to be, for example to the right of the capillary axis, such that liquid from near the wall is brought to the interface in a clockwise motion. Accordingly, liquid from the lower temperature and solute concentration region transfers to the interface. Therefore, at a given bulk supercooling and initial solute (In) concentration, the growth rate in this direction should be higher than that for upwards growth because the advancing interface "sees" a liquid which has less In content than that for the interface grown under quiescent but otherwise similar conditions. Since the higher the In content the slower the Ga growth kinetics become, as discussed earlier, it is understood then why the growth rates parallel to $\vec{g}$ are higher than these antiparallel to $\vec{g}$.

Low concentrations for the onset of solutal convection during growth have been predicted theoretically.[295] For example, during growth of Pb-Sn under solutally unstable conditions, at a growth rate of 1 μm/s and a temperature gradient of 50°C/cm, solutal convection will occur at all compositions above 1×10^{-4} wt% Sn; at smaller gradients the critical concentration is predicted to be even less.

However, a surprising feature of the solutal convection is the fact that the small (.028 cm) tube diameter seems to be unable to suppress convection. Since the length (D/V) is the characteristic scale of compositional inhomogeneities in the liquid, the solute Rayleigh number is based on this length for the prediction of solutal convection. However, D/V is smaller than the radius of the tubes used in this study only for growth rates larger than 9 μm/s.

The absence of convection during upwards growth appears obvious. The solutal convection is eliminated and hence the solute diffusion process is not interrupted. On the other hand, the very small thermal gradient (G_L < 2.5°C/cm) near the interface does not promote thermal convection. For typical parameters of the present experiments[*] a thermal Rayleigh number $R_t = a\ g\ G_L\ r^4/\nu\kappa$ for this geometry, where a is the thermal expansion coefficient, g the acceleration of gravity, r the tube radius, ν the kinematic viscosity, and κ the thermal diffusivity. The Rayleigh number is less than 68, which is the predicted value for critical Rayleigh number for tubes of finite length and of aspect ratios greater than 22.[339,340] For smaller aspect ratios, R_t^{cr} is larger than

---

[*] $\alpha = 1.58 \times 10^{-3}$°C^{-1}, g = 980 cm/s^2, $\nu = 3.46 \times 10^{-3}$ cm^2/s, D = 1.35 $\times$ 10^{-5} cm^2/s; see more also in Appendix II.

68. For the present experiment, the aspect ratio is larger than 200, and R_t is smaller than 3.

Whether or not convection is steady during growth is a question of interest. In order to answer this question, the stagnant boundary layer δ has to be evaluated as a function of the growth conditions. In doing so, one could adopt the following scheme: a) find out the interfacial composition C_i necessary to match the parallel to $\vec{g}$ growth data points $V(\Delta T, C_i)$ with those $V(\Delta T, C_i')$ for the antiparallel direction and b) by knowing c_i and V, one can back-calculate with the aid of eqs. (62) and (63). However, such a procedure would lack quantitative sense because 1) of the approximations in the calculations involved; 2) the differences in the resultant interfacial temperature by using k_{eff} instead of k in the determination of C_i are very small. For example, asssuming δ = 100 µm, this difference is in the order of .008°C for a growth rate of 30 µm/s and c_o = .012 wt%; for δ = 300 µm and V = 40 µm/s, the difference becomes .03°C, which is the order of the temperature measurements accuracy. For smaller δ and V this difference gets even smaller. Finally, 3) as discussed earlier, it is assumed that growth takes place under the initial transient conditions as far as segregation is concerned. However, under diffusive-convective conditions in the liquid, the initial transient distance is much shorter than the corresponding diffusion-only case. It is given as[341]

$$x = \frac{50}{V} \frac{1}{.25 + (m_l/b)^2}$$

where b = $\delta V/D$ and m_l is a constant in the order of unity which depends on k and b. For example, assuming that δ = 100 µm/s, V = 10 µm/s, and k = .019, x is calculated as 218 µm, which is 30 times smaller than the

corresponding distance (~7000 μm) under the diffusive conditions only. Similarly, for $\delta = 50$ μm, x is calculated as about 44 μm. Therefore, depending on the conditions, it is uncertain whether the solute temperature correction should be evaluated from the transient or steady state solute profiles.

It seems that detailed quantitative work would obviously require a compositional analysis along the solidified length; although the latter does not assure the former (see, for example, the conclusions of references (297) and (298), which are just qualitative), it still provides valuable information concerning the convection process.

CHAPTER VI
SUMMARY AND CONCLUSIONS

A novel technique based on thermoelectric principles was developed to determine directly the S/L interfacial supercooling during unidirectional and unconstrained growth of Ga single crystals from the supercooled melt. The method utilizes the Seebeck emf generated across the moving S/L interface with respect to a stationary S/L interface, together with its thermoelectric power, to measure accurately, within .005°C, the interface temperature. The Seebeck technique also detects, in-situ, the emergence of dislocation(s) at the crystallization front; furthermore, during growth of doped materials it also allows for the detection of the interfacial instability and breakdown.

The crystal growth kinetics of faceted interfaces of high purity Ga, and In-doped Ga as a function of the interface supercooling have been studied using the Seebeck technique. The growth rates were measured optically and/or by utilizing the resistance change across the sample upon growth. The investigation of the Ga interfacial kinetics covers a range of 10^{-3} to 2×10^4 μm/s growth rates at interface supercoolings from 0.2 to 4.6°C, corresponding to bulk supercoolings of about 0.2 to 53°C. In addition, the kinetics have been determined as a function of crystal perfection, dislocation-free versus dislocation-assisted interface, and crystal orientation, [111] and [001]. The In-doped Ga kinetics study covers a range of 10^{-2} to 45 μm/s growth rates

and interfacial supercoolings up to about 2.5°C. For the doped material the kinetics of two initial compositions, Ga-.01 wt% In and Ga-.12 wt% In, have also been determined for dislocation-free interfaces of the (111) type. Furthermore, the growth rates have been measured as a function of solidified length and growth direction with respect to the gravity force. The concluding remarks of this study are given below.

1) The capabilities of the Seebeck technique make it unique for in-situ and continuous monitoring of the perfection and chemical homogeneity of the growing crystal. The applicability of the technique, which can be easily automated, during commercial growth processes would likely result in valuable benefits of great technical importance.

2) The experimental results obtained with respect to the interfacial and bulk supercooling have clearly shown the difficulties and misinterpretations which may arise in utilizing the bulk kinetics to describe the interfacial growth process. In order to understand the macroscopic transport (heat flow) effects on the growth process and differentiate them from the interfacial kinetics effects, it was shown that the interfacial temperature has to be measured directly.

3) The faceted (111) and (001) Ga interfaces grow at low supercoolings with either of the lateral growth mechanisms, two-dimensional nucleation (2DNG) or screw dislocation-assisted (SDG), depending on the perfection of the interface. The "α" factor model fails to predict the lateral growth mode of the Ga faceted interfaces. Furthermore, the classical theories regarding the growth kinetics of smooth interfaces inadequately describe the results quantitatively.

4) A quantitative justification of the experimental results for both 2DNG and SDG mechanisms is possible by removing the existing assumptions which treat the interfacial atomic migration as the liquid bulk diffusion process and the step edge energy as independent of the supercooling.

5) Based on the above mentioned, the diffusion coefficient within the interfacial layer, D_i, was found to be up to about 3-4 orders of magnitude smaller than the liquid Ga self-diffusion coefficients (10^{-5} cm^2/s).

6) At higher supercoolings, the results show that the faceted interfaces gradually become kinetically rough as the supercooling increases. The step edge free energy, which as indicated should be treated as a function of the supercooling, was shown to diverge exponentially with the supercooling at the faceted-nonfaceted transition. The roughening supercooling was found to be smaller for the faster growing (001) interface.

7) A lateral growth model, which includes the interfacial diffusivity and supercooling dependent step edge free energy, was found to describe well the growth kinetics of both interfaces up to the supercoolings marking the kinetic roughening transition.

8) At supercoolings higher than that of the transition dislocations, which at lower supercoolings enhance the growth rate of the perfect interface by several orders of magnitude, do not affect the growth rate. Furthermore, beyond the transition the growth rates are linearly

dependent on the supercooling, which implies that the growth mode changes from lateral to normal.

9) The growth of the In-doped Ga, similar to the dislocation-free growth of pure Ga, takes place by the two-dimensional nucleation assisted mechanism.

10) The small additions of In reduce the growth rate of Ga but do not effect the growth mode. In as a dopant decreases the step edge free energy, but slows down the transport kinetics and decreases the lateral step spreading rate, particularly at high dopant levels.

11) The growth rate at a given bulk temperature decreases with distance solidified because of the solute build-up at the interface.

12) The faceted In-doped interface breaks down as growth proceeds, because of the solute enriched boundary layer at the interface. Upon breakdown, In-rich bands are entrapped by the advancing crystal. The frequency of these breakdowns and size of the bands increases and decreases, respectively, as the In concentration and the supercooling increase.

13) For a given In dopant level and bulk temperature, the growth rates in the direction parallel to the gravity vector were found to be higher than those in the antiparallel direction. Furthermore, in the parallel direction, the growth rate decayed, as a function of distance solidified at a slower rate and the frequency of interfacial breakdowns was less than that for the antiparallel growth direction. These differences are explained based on the convection effects in the interfacial solute boundary layer.

14) During growth of the In-doped Ga in the direction parallel to the gravity vector, gravitationally induced convection takes place because of the solutal gradient.

Physical Properties of Gallium

Gallium, which was discovered in 1875 and was named from Gallia in honor of its discoverer's homeland,[341] is a unique element in many ways. Although the solid has the characteristic silvery (slightly bluish) appearance of a metal, the liquid is more white than silver, with a shiny surface that resembles Hg to a great extent; it has some very particular properties uncharacteristic of metals. For example, it has an extremely low melting point, 29.78°C, and a very high boiling point, about 2370°C; it has the second longest range of all the elements. Its vapor pressure is very low even at elevated temperatures, and it expands upon solidification (3.2%) — a property shared by only three other elements: Ge, Bi, and Sb. Its crystal structure, as discussed later in this appendix, is unusual for a metal; black P, Br, and I have the same structure. Furthermore, it displays marked anisotropy on its electrical, thermal, and mechanical properties. For instance, the ratio between its largest and smallest electrical conductivity is about 7, the highest value among all metals.[342] Most of its unusual properties and strong anisotropy are usually attributed to the existence of Ga_2 molecules and the combined metallic and covalent bonding in the crystal.

Current applications for Ga are primarily in compound form, mostly III/V compounds (GaAs, GaP), used in optoelectronic devices, coherent

electroluminescence, photovoltaic conversion, Schottky barrier switching, magnetic bubbles, and superionic conduction. Since its vapor pressure is so low at high temperatures, it is particularly suited as a sealant in high temperature manometers. A new use of Ga is as a thermoelectric standard and in the form of a chloride solution for neutrino radiation measurements. Ga is also useful as an alloying agent. Table A-1 summarizes important physical properties of Ga, together with the relevant references.

Ga, a member of the B-Al family, is very active chemically; at a given temperature, liquid Ga is believed to be the most corrosive substance to almost any metal.[351] Only W, Nb, and Ta show good resistance to Ga up to temperatures of about 500°C. Liquid Ga penetrates very quickly into the crystal structure of certain metals, thus having a hazardous embrittling property, particularly for aluminum. It scarcely reacts with water and glass at low temperatures,[345] but it is easily oxidized by such oxidizing agents as aqua regia and H_2SO_4 when it is hot. It also readily reacts with halogens upon heating. Ga wets almost all surfaces, especially in the presence of oxygen, which promotes the formation of a fine Ga suboxide film (by which it is protected from air oxidation at ambient temperatures); the oxide film causes the loss of its mirror-like surface appearance and it can be removed by treating the oxidized metal with dilute HCl or simply by draining the metal through a capillary tube. When it is free of oxides, it no longer wets glass and other surfaces, as experienced during this study.

Table A-1.
Physical Properties of Gallium

reference #

Atomic number	31	
Atomic weight	69.72	
Electronic structure	$3d^{10}4s^24p^1$	
Isotopes	^{69}Ga (60.2%)	
(12 unstable mass 63-76)	^{71}Ga (39.8%)	
Melting point (°C)	29.78	344
Boiling point (°C)	2403	
Density (g/cm^3)		
solid (29.6°C)	5.904	345
liquid (29.8°C)	6.095	346
(-16.3°C)	6.136	
Latent heat of fusion (cal/g)	19.15	347
Solidification expansion	3.2%	
Linear coefficient of thermal		
expansion of solid (/°C)		348
a — Axis (-50-0°C)	1.65×10^{-5}	
b — Axis	1.15×10^{-5}	
c — Axis	3.2×10^{-5}	
Vapor pressure (mm Hg)		
600°C	4.4×10^{-9}	
1800°C	21	
Specific heat (cal/g°C)		349
solid (80-302 K)	.0902	
liquid (250-600 K)	.097	
Thermal conductivity (cal/cm·s·°C)		348
liquid (29.8°C)	.08	
solid: a — Axis (20°C)	.0975	
b — Axis (20°C)	.211	
c — Axis (20°C)	.0382	
Resistivity (μΩ·cm)		322
liquid (0°C)	25.2	
solid: a — Axis (20°C)	17.3	
b — Axis (20°C)	7.85	
c — Axis (20°C)	55.5	
Viscosity, poises		350
29.78°C	.0213	
0°C	.0259	
Spectra lines (strong) Å	2874	
	2944	
	4033	
	4172	
Ionic radius Å	.62	
Covalent radius Å	1.25	
Atomic radius Å	1.22	
Fermi energy (eV)	10.6	

High purity Ga supercools very easily and can frequently be held for a long time at a temperature of 0°C without solidifying. By dividing Ga into small droplets, it has been possible to supercool the liquid by more than 150°C.[330,352,353] The marked tendency of Ga to supercool has been discussed as a result of the suggested persistence of the Ga_2 molecules in the liquid state.[354] The latter, however, is contrasted by other works which believe that the covalent binding is destroyed upon melting, resulting in more metallic-like properties for the liquid.[355] Amorphous Ga has also been prepared by vapor deposition onto He-cooled substrates;[356] however, calorimetric and DTA measurements on single droplets down to 150K have shown no signs of any glass transition.[357] When solid Ga, or even ice, comes in contact with the supercooled liquid, crystallization takes place rapidly. In this manner several grams of Ga can be converted to nicely defined orthorhombic crystals. This was routinely done in this study, where it was also realized that, by increasing the supercooling, the geometry of the crystal changed from trapezoid to pyramid (also, see Ref. 322c).

Some metastable phases at atmospheric pressure are obtained from supercooled Ga or by solid-solid phase transitions.[358-362] Two phases are formed only at high pressures.[363,364] The most important of these phases and some of their physical properties are listed in Table A-2. It should be noted that only normal Ga (α or I) expands upon solidification.

There are several studies on Ga and its physical properties, mainly because of its peculiar character and of its growing importance, particularly in the electronics industry. However, review of all of them is

Table A-2.
Metastable and High Pressure Forms of Ga.

Property	Metastable Forms at Normal Pressure		
	β	δ	γ
melting point, °C	-16.3	-19.4	-35.6
density at T_m, g/cm^3	6.22	6.21	6.2
crystal structure	monoclinic	trigonal	orthorhombic

	High Pressure Forms	
	II	III
pressure atmosphere	28	26
crystal structure	cubic	tetragonal

beyond the scope of this study. Briefly reviewed below are some of the aforementioned studies which might provide some insight into its properties and behavior related to this work.

A contradictory aspect of the solid to liquid transition of Ga is the premelting phenomenon.[365] For example, the abrupt rise of the specific heat (c_p) near T_m[366] of Ga thin samples was explained by a surface melting model.[367] The thickness of the premelted surface liquid layer was estimated to be in the range of 10-80 nm, an extremely large value, and to be dependent upon the differences in the interfacial surface energies ($\sigma_{sv} - \sigma_{s\ell} - \sigma_{\ell v}$).[368] The temperature of the premelting transition and the crystal orientation of the samples were not specified. Although the model explained the observed rise in the c_p, the magnitude of its parameters and their physical relevance cannot be explained. Premelting phenomena in Ga, very close to T_m, were also associated with premonitory effects observed in a thermoelectric study of Ga single crystals.[318] However, the premonitory emf anomaly is believed to be within the experimental error range of the investigation.[369] In contrast to these studies, premelting effects could not be detected up to temperatures of 10^{-4}°C close to the melting temperature,[370] during an anomalous x-ray transmission study of Ga perfect crystals (<010>).

Interfacial free energies for the liquid/vapor and solid/vapor Ga interfaces have been measured by several investigators. The former ranges from 700-900 ergs/cm^2,[371-373] while the latter is about 780-850 ergs/cm^2.[374,375] Based on these values and those for the S/L interface (40-70 ergs/cm^2), it can be shown that the Young's condition for perfect wetting ($\sigma_{sv} \geq \sigma_{s\ell} + \sigma_{\ell v}$) is most likely satisfied. However, this in

contrast with two other studies where it was found that the liquid does not perfectly wet the solid and the contact angle between the solid and the liquid was estimated to be about 7°,[332a,b] while it is supported by another study[332c] which concluded that the S/L contact angle is 0°.

The self diffusion coefficient in liquid Ga has been studied experimentally by using ^{72}Ga isotope and three independent techniques.[329,376,377] The Arrhenius parameters of the diffusion coefficient equation ($D = D_o \exp(-Q/RT)$) are $D_o = 3.45 \cdot 10^{-4}$ cm^2/s and $Q = 1.85$ Kcal/mol in the range of 280-680 K. Self diffusion in Ga crystals has also been measured using ^{67}Ga[337a] and ^{72}Ga.[337b] In both investigations it was found that the process is characterized by very low self diffusion coefficients, about 10^{-15}[338] and 10^{-13}[337] cm^2/s at 20°C, in crystal orientations [100], [010], and [001]. A certain degree of anisotropy of the activation energy for self diffusion is also indicated.

Crystal Structure of Gallium

Like the rest of its properties, the crystal structure of Ga is quite unusual for a metal; Ga crystallizes in the base centered orthorhombic system in a complex manner and is very anisotropic. The latter property, as well as most of its other unique characteristics, is attributed to the coexistence of metallic and directed non-metallic (covalent) binding within the crystal.

The crystal structure of Ga was first reported incorrectly as tetragonal.[378] Later, it was shown that the structure is orthorhombic, with eight atoms in the unit cell, although, as in the earlier work, it was considered that two of the crystal axes were approximately equal.[379]

The orthorhombic structure was verified by Bradley,[380] who showed that all three axes were different in length and gave more precise values of the atomic position parameters. Subsequent redeterminations of the lattice constants and of the positional parameters by the use of more extensive diffraction studies were made.[381-384] The results of the above mentioned works are summarized in Table A-3.

It is realized from the lattice constants that the α and b^* axes are very nearly equal, with the c axis longer than the α and b axes. Not only is the cell almost tetragonal, but c/α is nearly $\sqrt{3}$, so that it is also pseudohexagonal. Furthermore, the inequality $c > \alpha$ holds throughout the temperature range,[383] in agreement with the thermal expansion coefficients reported[385] as being in the ratio of 1:0.7:1.9 for the $c:\alpha:b$ axes.

The Ga atoms form a network of regural hexagons parallel to the (010) plane at heights x = 0 and x = 1/2 and are distorted in the plane. In addition, the pseudohexagonality of the structure is revealed by another set of atomic hexagons which are perpendicular to the α axis being buckled normal to their planes; the structure can be thought of as consisting of a stacking of these distorted hexagonal close packed layers, as shown in Figs. A-1, A-2, and A-3, which show projections of the structure on the (100), (010), and (001) planes, respectively. A Ga atom has seven nearest neighbors, with the shortest Ga-Ga bond being considered as covalent or that the closest pair of atoms form Ga_2 molecules.[386] This would reduce the structure alternatively to four

---

* In some of the recent work on Ga, the new setting Cmca has been used; however, in this work the old designation is used whenever reference is made to the crystal structure.

Table A-3. Crystallographic Data of Gallium (α-Ga).

	Old Designation Abma, V_n^{18}	New Designation Cmca, D_{2h}^{18}	Laves[379] (1933) (T_{room})	Bradley[380] (1935) (T=18°C)	Swanson & Fuyat[381] (1953) (T=25°C)	Reference Sharma & Donohue[382] (1962) (T_{room})	Barrett Spooner[383] (1965) (T=24°C)	Donohue[384] (1972) (T_{room})
Space Group								
Lattice Constants in Å	a	c	4.515	4.5258	4.524		4.5258	4.5258
	b	α	4.515	4.5198	4.523		4.5186	4.5192
	c	b	7.657	7.6602	7.661		7.657	7.6586
Positional Parameters	p (z)	y	.159 or .153	.1525		.1549		.1539
	m (x)	z	.08	.0785		.081		.0798

Atomic Coordinates in the Unit Cell (8 Atoms)

$(m, 0, p)$
$(m + 1/2, 1/2, \bar{p})$
$(m + 1/2, 1/2, p)$
$(\bar{m}, 0, \bar{p})$
$(m, 1/2, p + 1/2)$
$(m + 1/2, 0, \bar{p} + 1/2)$
$(\bar{m} + 1/2, 0, p + 1/2)$
$(\bar{m}, 1/2, \bar{p} + 1/2)$

Each Ga atom at (mOp) or at (Oyz) has seven nearest neighbors

(Ref. 380)	(Ref. 381)	(Ref. 384)
1 at 2.437 Å, (d_1)	1 at 2.484 Å	1 at 2.465 Å
2 at 2.706 Å, (d_2)	2 at 2.691 Å	2 at 2.7 Å
2 at 2.736 Å, (d_3)	2 at 2.73 Å	2 at 2.735 Å
2 at 2.795 Å, (d_4)	2 at 2.788 Å	2 at 2.792 Å

The next closest neighbors are at 3.727 Å

The next closest neighbors are at at 3.753 Å

'y' coordinates
○ 0
● .5
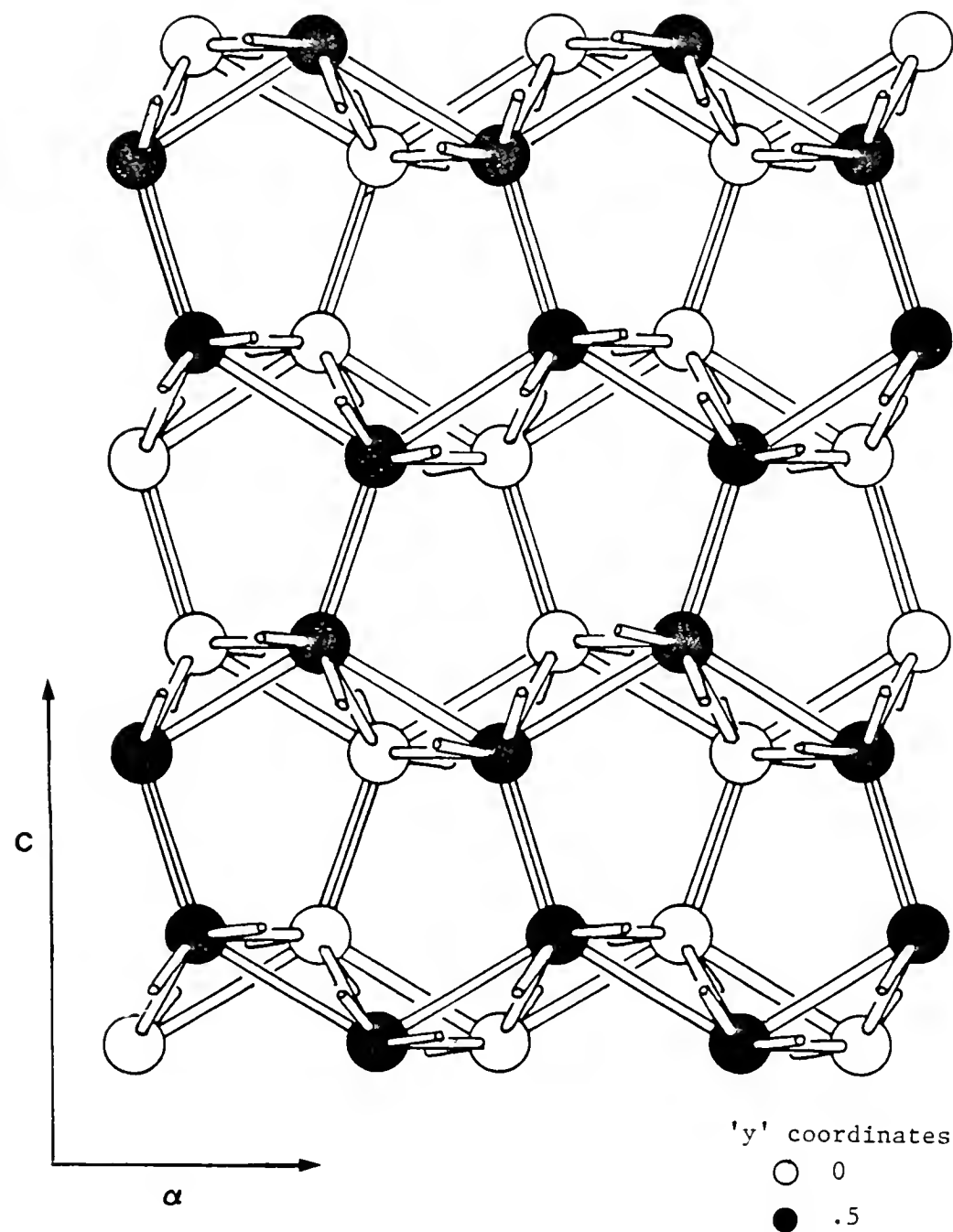
Figure A-1   The Gallium structure(four unit cells) projected on the (010)
plane; triple lines indicate the covalent(Ga_2) bond.

'x' coordinates

○	.08
⊗	.42
⊘	.58
●	.92
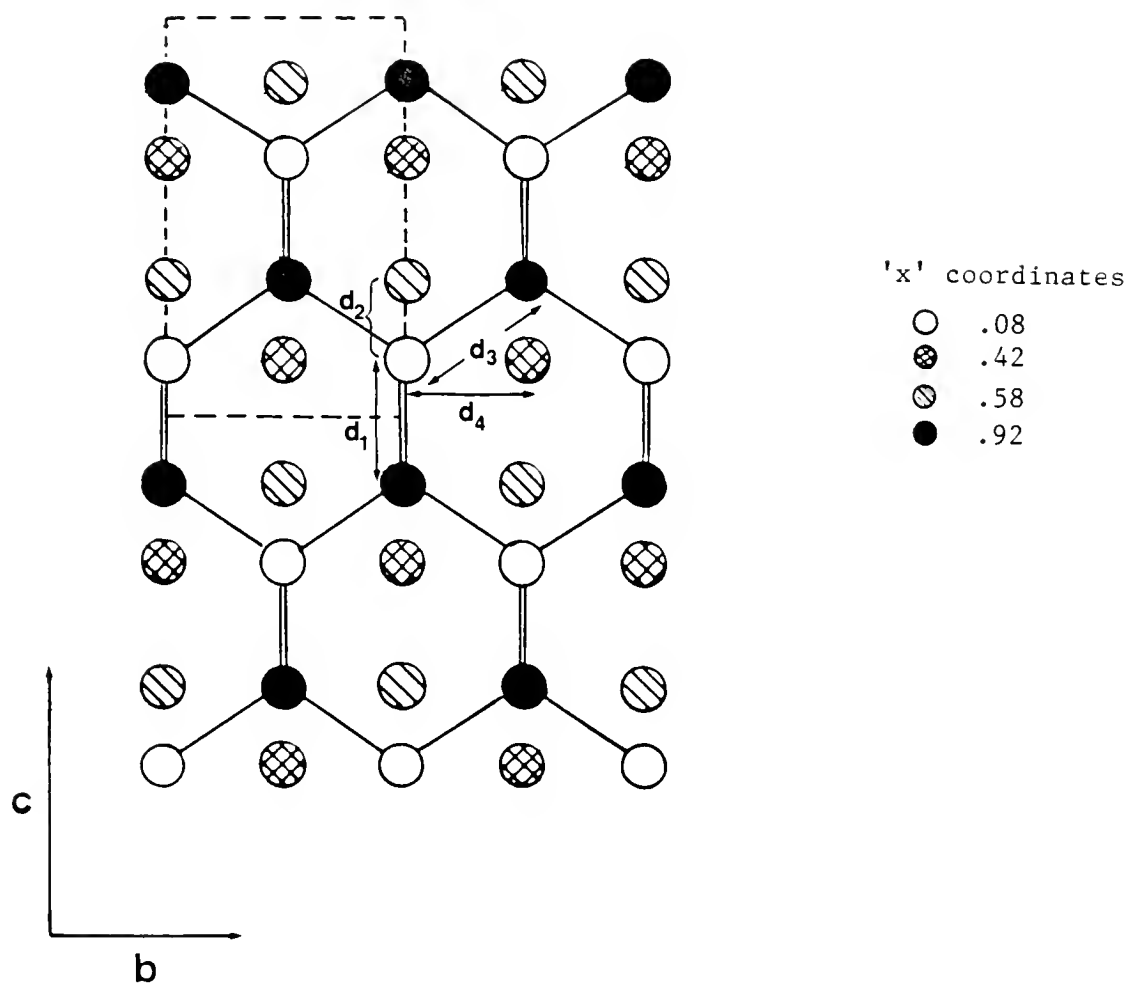
Figure A-2   The Gallium structure projected on the (100) plane;
double lines indicate the short(covalent) bond distance
d_1. Dashed lines outline the unit cell.
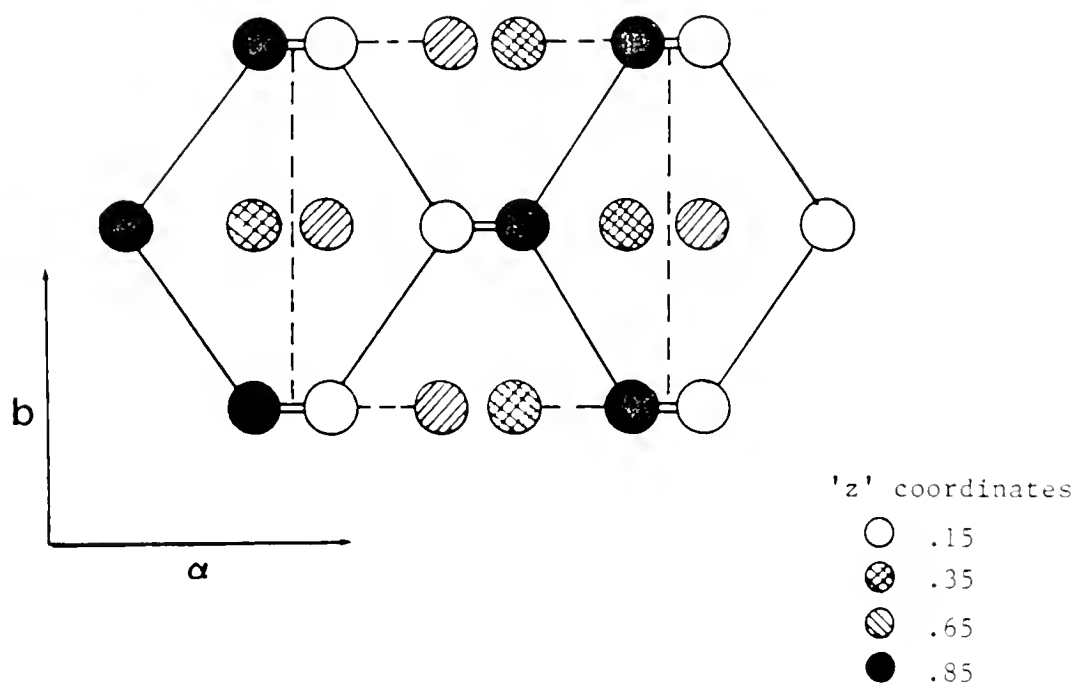
Figure A-3   The Gallium structure projected on the (001) plane;
            double lines indicate the covalent bond and dashed
            lines outline the unit cell.

such molecules per unit cell, sitting symmetrically on the a-c (010) plane at angles of about ±17° to the [001] direction; the spacing of their planes being b/2. From a geometrical point of view, the pseudo-hexagonality of the structure along the c axis is also revealed as a packing of these molecules into an FCC structure which has been pulled out in the two directions to accommodate the elongated shape of these molecules. These strongest bonds join the rumpled hexagonal layers of Ga atoms with the bonds in the layers being considerably weaker in an order of approximately 1/3. In particular, the assigned bond numbers are 1.21, 0.43, 0.38, and 0.31 to the four respective kinds of short distance.[387] It has been indicated that the tendency of Ga to form diatomic molecules may explain its low melting point; presumably it could melt into diatomic molecules.[388]

The complexity of the structure as regards axial ratios, nearest neighbors, and covalency effects has been theoretically tested from various points of view,[389] and it was indeed found that the observed qualitative features of the structure "make sense." The covalency was evaluated to amount to about 27 Kcal/g-atom.

The speculated existence of covalent bonding in the crystal is also intensified by the plastic deformation behavior and anisotropic mechanical properties of Ga single crystals.[390-392] Slip in Ga at room temperature is confined to these systems: (001) [010], (102) [010], and (011) [011].[390] Slip takes most easily on a (001) plane because it is among the very few "flat" low indices planes in the unit cell with a high density of atoms. However, as a slip direction, the [010] is always observed[57] on the expense of the equally probable, from atom

packing considerations, [100] direction; this is understood based on the explanation that slip along the [100] would disrupt the strong covalent bonds. Twinning occurs readily in Ga with compression along [100], by transforming the a and b axes of the matrix to the b and a axes of the twin; it is believed to be associated with the rotation of the Ga_2 molecules about the c axis.[393] Based on the results of the deformation study,[390] a standard (001) stereographic projection for Ga was prepared.[394]

Upon melting, the low symmetry Ga structure changes into a state with 9-10 nearest neighbors, about 2.8 Å apart from each other[395], arranged in somewhat loose close packing.[396] This pronounced change in short range order upon the melting point is reflected in the anomalous density increase of 3.2%, whereas most metals show a density decrease of 2-6%.

As far as the structural form of the interfaces under consideration is concerned, the (001) appears to be very flat, because the centers of its atoms lie on the plane. There are two Ga atoms per unit face area (αxb). If the crystal is sliced along this plane, it is realized that each atom is missing four nearest neighbor bonds, two of the d_2 type and two of the d_4 type. On the other hand, the (111) plane, in contrast with the (001), is not flat, but appears to have a zig-zag like structure composed of flat stripes which are part of the (211) plane. On the plane each Ga atom has three neighbors of the d_1, d_2, and d_3 kind.

In the calculation of the geometric factor ξ (one of the parameters included in the Jackson's model "a" factor), which is the ratio of the

bonds parallel to the interface under consideration over that in the bulk, the binding with the first, second, and third nearest neighbors were taken into account. In particular, the bond strength of each neighbor to that of the closest one was normalized as the inverse of the cube of their respective bond lengths ratio, given as

$$\frac{\phi_2}{\phi_1} = (\frac{d_1}{d_2})^3 = .7518, \quad \frac{\phi_3}{\phi_1} = (\frac{d_1}{d_3})^3 = .7244, \text{ and } \frac{\phi_4}{\phi_1} = (\frac{d_1}{d_4})^3 = .68.$$

Accordingly, the bulk bond strength, assuming seven nearest neighbors, is given as

$$B_b = 1 + (2 \times .7518) + (2 \times .7244) + (2 \times .68) = 5.3124$$

Since each Ga atom on the (001) phase is bonded to two neighbors, each with a strength of ϕ_3, the factor ξ is then calculated to be as

$$\xi_{(001)} = \frac{1.448}{5.313} = .28$$

Similarly, for the (111) face, ξ is calculated to be given as

$$\xi_{(111)} = \frac{2.432}{5.312} \approx .46$$

Nearly equal values of $\xi_{(111)}$ by less accurate determinations have been determined by other investigations.[179,326]

APPENDIX II
Ga-In SYSTEM

The Ga-In phase diagram has been studied through several investigations,[397-400] as compiled by Hansen.[401] Unfortunately, however, the Ga-rich side, as shown in detail in Fig. A-4, has not been investigated thoroughly. The eutectic temperature and composition and solid solubility[215] of In in Ga indicated on the diagram apparently represent available data.[402] The calculated values of the equilibrium partition coefficient k and the liquidus slope m are:

liquidus slope, m_L = -.5755 wt%/°C

partition ratio, k = .01918

Several other important physical properties of the Ga-In system (Ga-rich) that have been used in this study are given below:

density of In at T_m (156.6°C),[250] ρ = 7.31 g/cm^3

diffusivity of In in liquid Ga,[403] D = 2.1 x 10^{-4} exp (-1640/RT) cm^2/s

density of eutectic alloy at T_E,[404] ρ = 6.312 g/cm^3

density of eutectic alloy at T_m (Ga),[404] ρ = 6.285 g/cm^3

solute density coefficient, dρ/dc(In) = 7.947 x 10^{-3} g/cm^3·wt%

ρ = 6.09029 + 7.947 x 10^{-3} (C), (T = T_m, C ≤ 24.5 wt% In)

thermal density coefficient,[405,406] dρ/dT = -9.69 x 10^{-4} g/cm^3·°C (C ≤ 24.5 wt% In, 15.7°C < T < T_m)

crystal structure of In: tetragonal
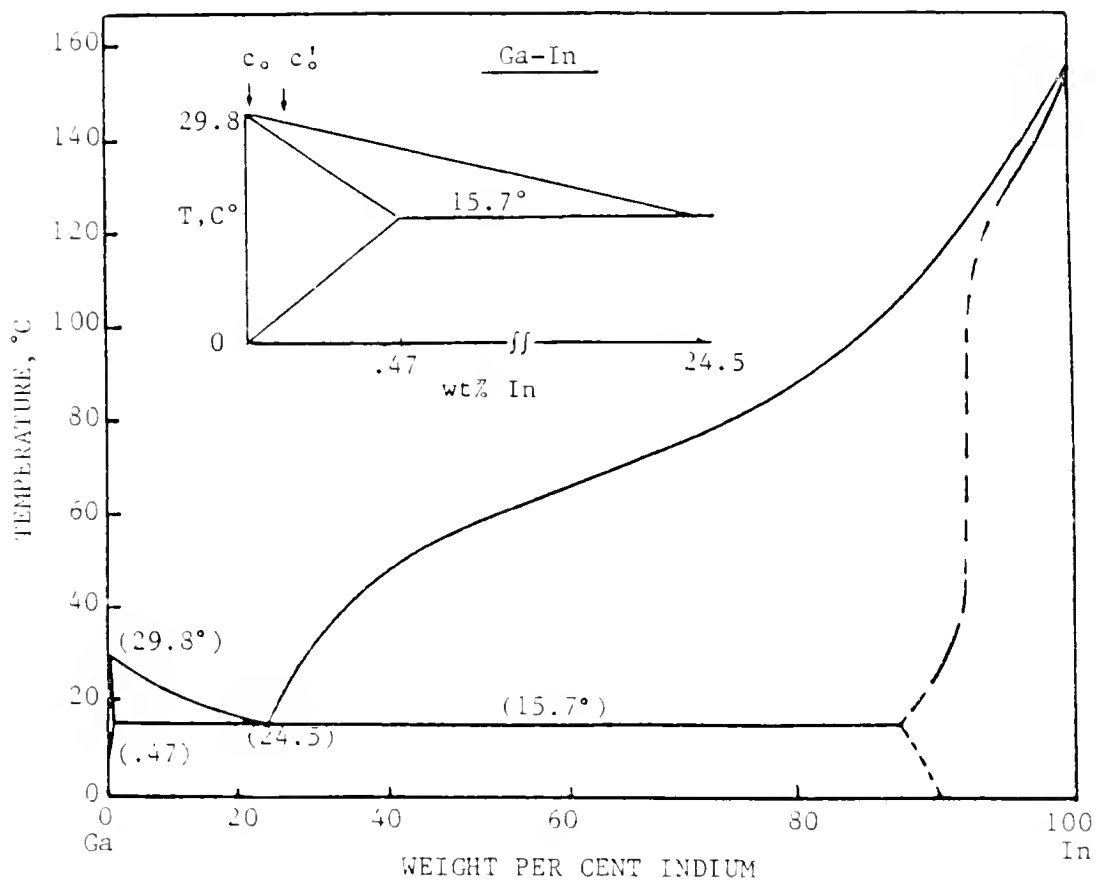
Figure A-4 Ga-In phase diagram; c_o and c_o' indicate the two alloy compositions investigated.

APPENDIX III
HEAT TRANSFER AT THE SOLID/LIQUID INTERFACE

Heat transfer problems during solidification processes are characterized by the existence of a moving S/L interface. The advancing of the interface is accompanied by the release of the heat of fusion, which in turn raises the temperature at the interface so that the latter is warmer than any other point in the system for growth into a supercooled melt. Except for a few idealized situations, exact solutions are not available.[407,408] The difficulty in solving this kind of problem either numerically or analytically lies mainly in simulating the thermal effect of releasing the heat of fusion.[409] The treatment of the moving interface as a heat source by the application of Greens' function[410] and the replacement of temperature by enthalpy as the dependent variable,[411] the so called enthalpy model, represent two approaches that have been developed during the past decade. However, both methods have some problems, among them being the determination of the time step-size.[412]

For the case of unidirectional solidification, the analysis requires values of at least two of the three parameters: interface shape, interface composition, and interface velocity. In the present experiments, for which the growth is unconstrained, the modified problem is employed which utilizes the interface shape and velocity and calculates the interface temperature (or, in reality, the difference, δT, between the temperature of the coolant medium, T_b, and the actual temperature of the interface, T_i).

This Appendix deals with the heat transfer problem during steady-state unconstrained growth into a supercooled melt. Its basic concept is that the heat evolved at the interface (in proportion to the growth rate) must be transported away from and into the heat sink (coolant) via a thermal resistance; the latter, as shown in Fig. A-5, consists of the Ga, the wall of the capillary tube, and a cooling fluid boundary layer surrounding the tube. The analytical model is based on the original formulation[*] of Michaels et al.[181] for their experiments on the growth kinetics of the (0001) ice/water interface in capillary tubes. It was later modified by Abbaschian and Ravitz,[2] who used it to determine the interface supercooling during a previous Ga growth kinetics study. Both analyses have been augmented with the assumption that solids and liquids have the same thermal properties, equal to the average properties of the two, as discussed in more detail later. In the present calculations, this assumption was removed and the calculated results at various growth rates have been compared with the actual interface temperature measurements obtained by the Seebeck technique.

Analytical Model for Heat Flow Calculations

The geometry of the system used for the heat transfer analysis is shown in Fig. A-5. It is assumed that the S/L interface is planar and normal to the axis of the capillary tube and that it advances into the

---

[*] Actually, the original analysis was given by Hillig,[178] who assumed that the temperature of the outer wall of the capillary was equal to T_b. Michaels et al.[181] removed this assumption by introducing the heat transfer coefficient between the tube surface and the bulk of the cooling bath; the latter is available for certain geometries such as for a cylinder in cross-flow.[413]
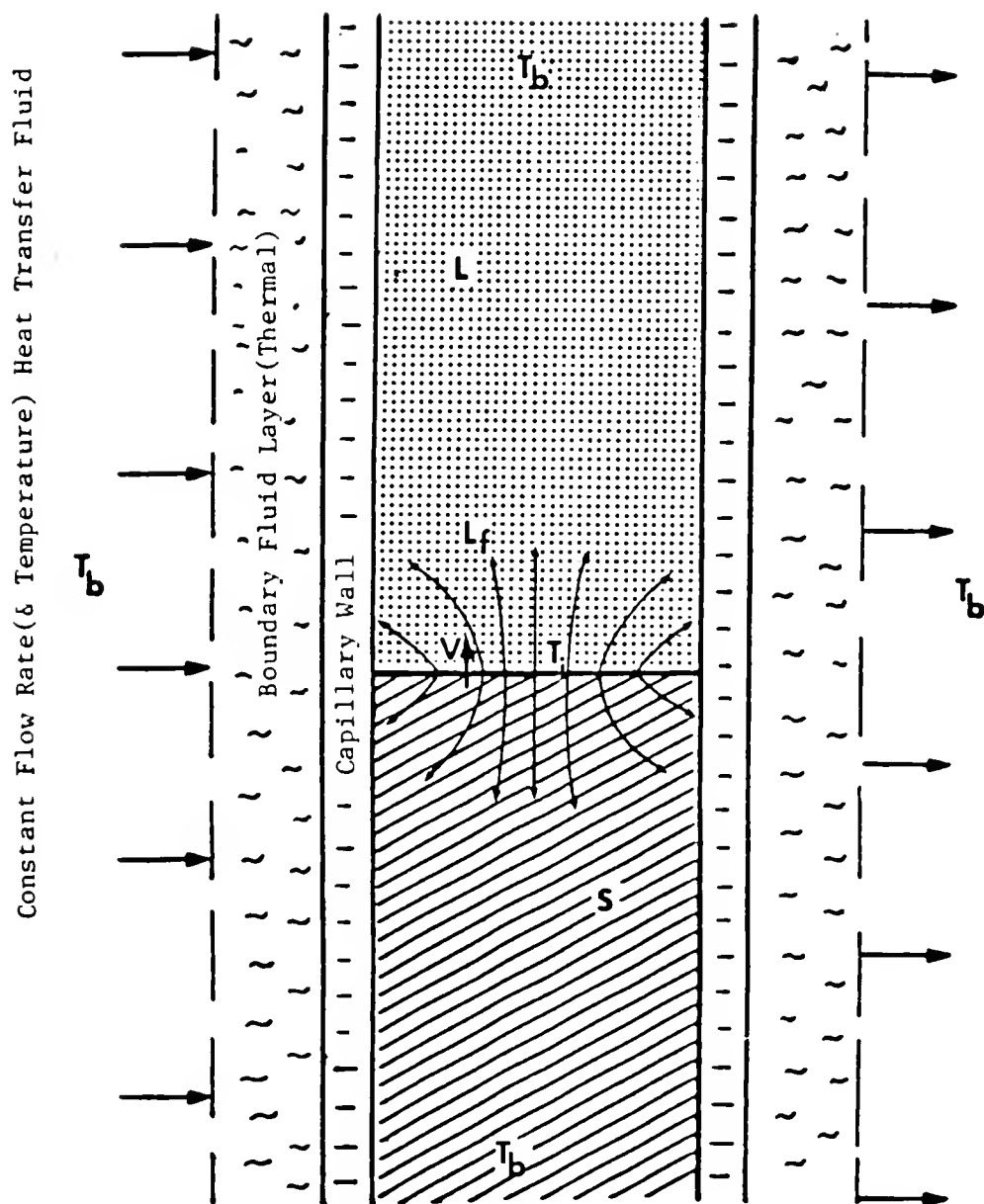
Figure A-5 Geometry of the interacial region of the heat transfer
analysis; L_f is the heat of fusion.

supercooled liquid Ga at a constant velocity V. The capillary with an inside radius r_i and wall thickness x_g is assumed to be of infinite extent in axial direction z on both sides of the interface. Under these assumptions, the temperature distribution in the system is described by the following equations and boundary conditions:

Heat conduction in the solid region,

$$(\partial^2 T_s/\partial r^2) + (1/r)(\partial T_s/\partial r) = (V/\kappa_s)(\partial T_s/\partial z_s) - (\partial^2 T_s/\partial z_s^2) \quad (A1)$$

Heat conduction in the liquid region,

$$(\partial^2 T_L/\partial r^2) + (1/r)(\partial T_L/\partial r) = (V\rho_s/\kappa_L \rho_L)(\partial T_L/\partial z_L) - (\partial^2 T_L/\partial z_L^2) \quad (A2)$$

Boundary conditions:

(1) Far away from S/L interface condition,

$$T_L = T_s = T_b \quad \text{as} \quad z_L \text{ or } z_s \to \infty, \ 0 \le r \le r_i \quad (A3)$$

(2) Symmetry condition,

$$(\partial T_L/\partial r) = (\partial T_s/\partial r) = 0 \text{ at } r = 0, \text{ for } 0 \le z_L, z_s \le \infty \quad (A4)$$

(3) Condition at the inner wall of capillary tube

$$-K_L (\partial T_L/\partial r)_{r=r_i} = U_i[(T_L)_{r=r_i} - T_b], \ 0 \le z_L \le \infty \quad (A5)$$

$$-K_s (\partial T_s/\partial r)_{r=r_i} = U_i[(T_s)_{r=r_i} - T_b], \ 0 \le z_s \le \infty \quad (A6)$$

where U_i is the overall heat-transfer coefficient of the glass wall and the boundary layer; it is assumed to be the same for the solid and the liquid region and is given by

$$1/U_i = (1/h)(r_i/r_o) + (x_g/K_g)(r_i/r_{\ell m}) \quad (A7)$$

In the above expression, K_g is the thermal conductivity of the capillary, $r_{\ell m}$ is the mean logarithmic radius, and h is the heat transfer

coefficient across the tube-coolant boundary. The latter is given by the following empirical equation[413]

$$h = Nu_d K_b / 2r_o \qquad (A8)$$

where Nu_d is the Nusselt number for the tube and K_b is the thermal conductivity of the coolant fluid.

(4) Condition at the S/L interface

$$T_s = T_L \text{ at } z_L = z_s = 0, \text{ for } 0 \le r \le r_i \qquad (A9)$$

(5) Heat balance condition at the interface

$$-V\rho_s L = -K_L \left(\partial T_L / \partial Z_L\right)_{z_L=0} - K_s \left(\partial T_s / \partial Z_s\right)_{z_s=0} \qquad (A10)$$

Introducing the following dimensionless variables,

$$- \theta_{s,\ell} = (T_{s,L} - T_b)/(T_m - T_b), \ z_{s,\ell} = z_{s,L}/r_i, \text{ and } r' = r/r_i \ (A11)$$

equations (A1) - (A10) become dimensionless. Assuming that the solutions to equations (A1) and (A2) in the dimensionless form have the following forms

$$\theta_s(r', z'_s) = R_s(r') \cdot Z(z'_s) \qquad (A12)$$

$$\theta_\ell(r', z'_\ell) = R_\ell(r') \cdot Z_\ell(z'_\ell) \qquad (A13)$$

the heat conduction equations (A1) and (A2) become

$$(\ddot{R}_s/R_s) + (\dot{R}_s/r'R_s) = (Vr_i/\kappa_s) \ (\dot{Z}_s/Z_s) - (\ddot{Z}_s/Z_s) \qquad (A14)$$

and

$$(\ddot{R}_\ell/R_\ell) + (\dot{R}_\ell/r'R_\ell) = -(Vr_i/\kappa_L) \ (\rho_s/\rho_L) \ (\dot{Z}_\ell/Z_\ell) - (\ddot{Z}_\ell/Z_\ell) \quad (A15)$$

Since the right hand sides and the left hand sides of the above equations are functions of different variables, the only way they can be equal is for the expressions of either side of both equations to be equal to some constants. To assure real solutions for the radial parts of the two equations these two constants must be negative.

Thus, for the solid region:

$$(\ddot{R}_s/R_s) + (\dot{R}_s/r'R_s) = - \gamma_s^2 \qquad (A16)$$

$$(Vr_i/\kappa_s)(\dot{Z}_s/Z_s) - (Z_s/Z_s) = - \gamma_s^2 \qquad (A17)$$

and for the liquid region

$$(\ddot{R}_\ell/R_\ell) + (\dot{R}_\ell/\kappa_L R_\ell) = - \gamma_\ell^2 \qquad (A18)$$

$$(Vr_i/\kappa_\ell)(\dot{Z}_\ell/Z_\ell) - (\ddot{Z}_\ell/Z_\ell) = - \gamma_\ell^2 \qquad (A19)$$

General solutions of the above equations are

$$\begin{aligned} Z_s = C_1 &\exp\{[(Vr_i/2\kappa_s) + ((Vr_i/2\kappa_s)^2 + \gamma_s^2)^{1/2}]z_s'\} \\ &+ C_2 \exp\{[(Vr_i/2\kappa_s) - ((Vr_i/2\kappa_s)^2 + \gamma_s^2)^{1/2}]z_s'\} \end{aligned} \qquad (A20)$$

$$R_s = C_3 J_o(\gamma_s r') + C_4 Y_o(\gamma_s r') \qquad (A21)$$

and

$$\begin{aligned} Z_\ell = C_5 &\exp\{[-(Vr_i\rho_s/2\kappa_L\rho_L) + ((Vr_i\rho_s/2\kappa_L\rho_L)^2 + \gamma_\ell^2)^{1/2}]z_\ell'\} \\ &+ C_6 \exp\{[-(Vr_i\rho_s/2\kappa_L\rho_L) - ((Vr_i\rho_s/2\kappa_L\rho_L)^2 + \gamma_\ell^2)^{1/2}]z_\ell'\} \end{aligned} \qquad (A22)$$

$$R_\ell = C_7 J_o(\gamma_\ell r') + C_8 Y_o(\gamma_\ell r') \qquad (A23)$$

where J_o and Y_o are Bessel functions of the first and second kind, respectively, and C_1, C_2, ... C_7 are constants to be determined next. Boundary condition #1 implies that

$$C_1 = C_5 = 0 \qquad (A24)$$

Also, since $Y_o \rightarrow \infty$ as $r' \rightarrow 0$,

$$C_4 = C_8 = 0 \qquad (A25)$$

The remaining part of the solutions automatically satisfy B.C #2. The third B.C is satisfied if the following equations

$$\gamma_s J_1(\gamma_s) - (U_i r_i/K_s) J_o(\gamma_s) = 0 \qquad (A26)$$

$$\gamma_\ell \, J_1(\gamma_\ell) - (U_i r_i / K_L) \, J_0(\gamma_\ell) = 0 \qquad (A27)$$

are satisfied. By assigning the roots of the above equations to be γ_{sn} and $\gamma_{\ell n}$, the temperature distribution in the solid and liquid region have the following forms

$$\theta_s = \sum_{n=1}^{\infty} A_n \, J_0(\gamma_{sn} r') \, \exp\{[(Vr_i/2\kappa_s) - ((Vr_i/2\kappa_s)^2 + \gamma_{sn}^2)^{1/2}]z_s'\} \quad (A28)$$

and

$$\theta_\ell = \sum_{n=1}^{\infty} B_n \, J_0(\gamma_{\ell n} r') \, \exp\{[(Vr_i\rho_s/2\kappa_L\rho_L) - ((Vr_i\rho_s/2\kappa_L\rho_L)^2 + \gamma_{sn}^2)^{1/2}]z_\ell'\}$$

$$(eq. \; (A29))$$

Values of γ_s and γ_ℓ that satisfy the above equations can be found in table form,[407] whereas the values of the coefficients A_n and B_n can be obtained from the remaining two boundary conditions, equations (A9) and (A10). Truncating equations (A28) and (A29) at Nth terms and inserting them into equations (A9) and (A10), yields

$$\sum_{n=1}^{N} A_n \, J_0(\gamma_{sn} r') = \sum_{n=1}^{N} B_n \, J_0(\gamma_{\ell n} r') \qquad (A30)$$

$$\frac{V\rho_s L r_i}{T_m - T_b} = - K_s \sum_{n=1}^{N} A_n \, J_0(\gamma_{sn} r') \, [\frac{Vr_i}{2\kappa_s} - ((\frac{Vr_i}{2\kappa_s})^2 + \gamma_{sn}^2)^{1/2}]$$

$$(A31)$$

$$- K_L \sum_{n=1}^{N} B_n \, J_0(\gamma_{\ell n} r') \, [\frac{Vr_i\rho_s}{2\kappa_L\rho_L} - ((\frac{Vr_i\rho_s}{2\kappa_L\rho_L})^2 + \gamma_{\gamma n}^2)^{1/2}]$$

Since the above equations must be satisfied for all values of r', one can randomly chooses N values of r' between 0 and 1 and insert them into equations (A30) and (A31); this results into 2N equations with 2N un-knowns and unique solutions of A_n and B_n of any order are thus assured. By inserting the solutions back into equations (A28) and (A29), the axial

and radial temperature profiles can be determined. Furthermore, the temperature correction δT can be calculated from any of equations (A28) or (A29) after setting z_s' or z_ℓ' equal to zero. Accordingly, then

$$\theta_i = \frac{T_i - T_b}{T_m - T_b} = \frac{\delta T}{T_m - T_b} = \sum_{n=1}^{N} A_n \, J_o(\gamma_{sn} r')$$ (A32)

Before proceeding, the differences of the present analysis from the former two[2,181] are briefly explained. First, both of the previous analyses assume that the thermal properties and densities of the solid and the liquid are equal; for the conductivities it is assumed that

$$K_s = K_L = \frac{K_s + K_L}{2} = \bar{K}.$$

Hence, equations (A26) and (A27) become identical, which implies that $\gamma_{sn} = \gamma_{\ell n} = \gamma_n$. Consequently, from equation (A30) it is concluded that $A_n = B_n$; the latter can then be obtained from equation (A31) and, if substituted into equation (A32), yields δT. Michaels et al.[181] had shown in their work the parameter $Vr_i/2\kappa$ is much smaller than γ_n (this is true for small growth rates and high values of $Ur_i/\bar{K}$) so that the right hand side of equation (A31) is drastically simplified. Abbaschian and Ravitz,[2] who solved the problem without incorporating the later assumption, found that the two analyses yield temperature corrections that are essentially the same for Vr_i less than 4×10^{-3} cm^2/s, but not at high growth rates where the calculations of Michaels et al.[181] were shown to overestimate δT.[177]

Results and Discussion

In order to compare the numerical solution with the experimental results obtained by the Seebeck technique, as described in the Experimental chapter, a computer program based on the above mentioned analysis was

written.[414] Parameters that are used in these calculations are given in Table A-4 and in the print-out of the program (#5) involved in Appendix V. In the calculations of the infinite series solutions, eqs. (A38) and (A39) were truncated at n=6 term. The ratios A_6/A_1 and B_6/B_1 of the coefficients in these calculations were found to be less than 0.2%. This, in addition to the fact that A_1, $B_1 < 10$, indicates that the truncation error is negligible. The results of the present calculations, designated as numerical, as compared to those of the earlier analytical analysis,[2] are summarized in Figs. A-6 through A-8.

Figures A-6 and A-7 show linear plots of the temperature correction (δT) for the (111) and (001) interfaces as a function of Vr_i at different values of $U_i r_i$. The difference between the numerical and analytical results, for the same heat transfer conditions ($U_i r_i$), is denoted by the hatched areas. As noted from these figures, the two results are approximately the same at low growth rates but become appreciably different at high growth rates (i.e. $Vr_i > 5 \times 10^{-3}$ cm^2/s). For the (001) interface, this difference is larger (by a factor 2.7) than that for the (111) interface. This is expected since $|K_L - K_S|$ is much larger for the (001) interface. Accordingly, the analytical solution based on the assumption that the liquid and solid have the same thermal properties underestimates and overestimates the temperature correction during growth along the (111) and (001) interfaces, respectively. For example, for the (111) interface the difference between the numerically and analytically calculated δT, if it were to be used at growth rates of .075, .4, and 1 cm/s is .07, .324, and 1.4°C, respectively, for conditions such that $U_i r_i = .02\bar{K}$. On the other hand, for the (001) interface under similar conditions

Table A-4.

Thermal Property Values Used in Heat Transfer Calculations

Ref. #

Liquid Ga

thermal conductivity, cal/sec·cm·°C	$K_L = .08$	348
density, g/cc	$\rho_L = 6.09$	346
thermal diffusivity, cm^2/s	$\kappa_L = .1376$	415
heat of fusion, cal/g	$L = 19.15$	347

Solid Ga

thermal conductivity, cal/sec·cm·°C	(111) $K_s = .0978$	348
	(001) $K_s^s = .0382$	348
density, g/cc	$\rho_s = 5.9$	345
thermal diffusivity, cm^2/s	(111) $\kappa_s = .1864$	416
	(001) $\kappa_s^s = .0728$	

Coolant

a) Water

thermal conductivity, cal/sec·cm·°C	$K_b = .00145$	417
viscosity, poise	$n_b = .0089$	417
specific heat, cal/g·°C	$C_p = .998$	417

b) Water-Ethylene glycol solution

thermal conductivity, cal/sec·cm·°C	30%, $K_b = .0012$	418
	40%, $K_b = .00108$	418
specific heat, cal/g·°C	30%, $C_p = .9$	418
	40%, $C_p = .84$	418
viscosity, poise	30%, $n_b = .019$	417
	40%, $n_b = .025$	417

Capillary Tube

| thermal conductivity, cal/sec·cm·°C | $k_g = .0025$ | 417 |
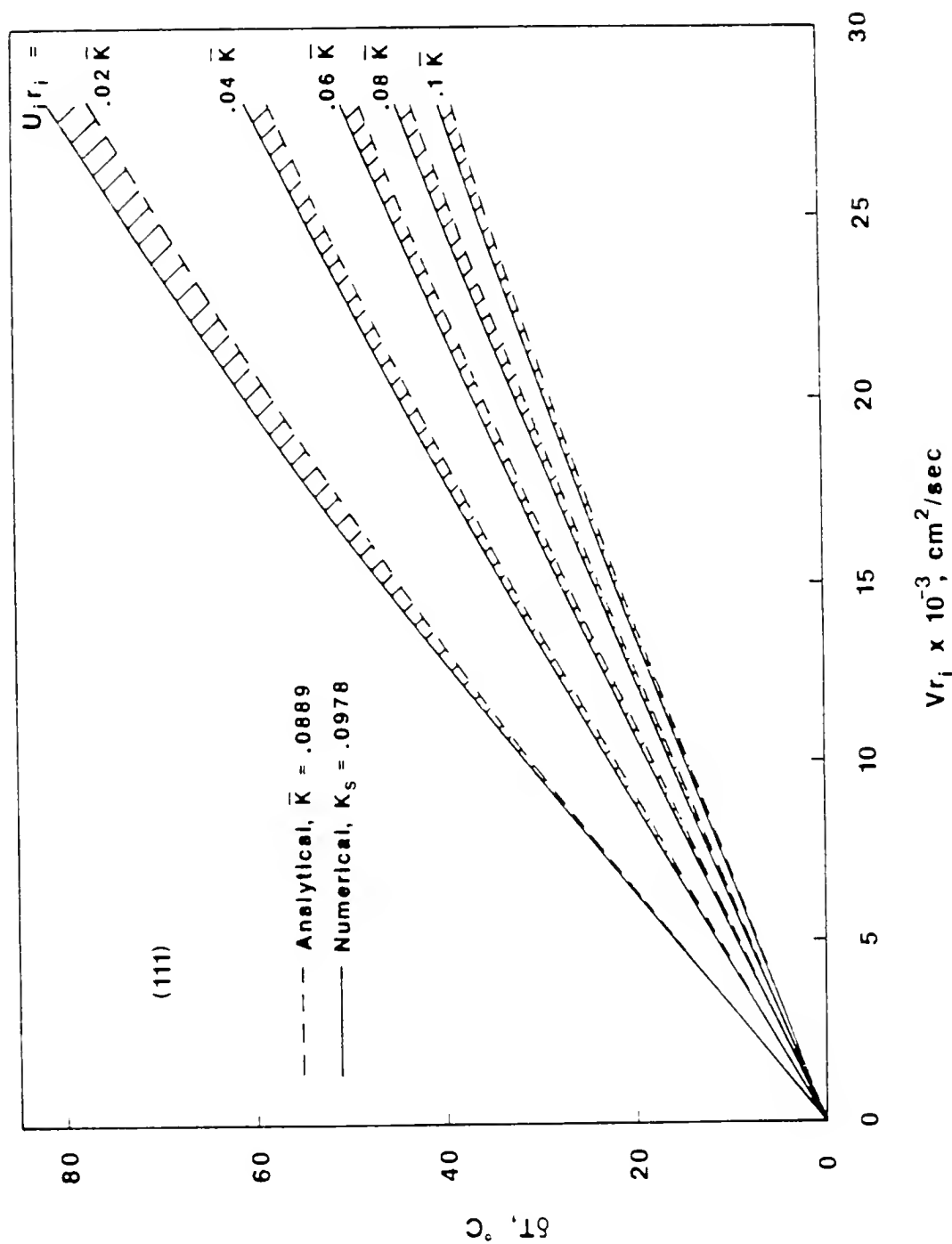
Figure A-6 Temperature correction, δT, for the (111) interface as a function of Vr_i for different heat-transfer conditions, $U_i r_i$; --- Analytical calculations ($K_L = K_s = \overline{K}$), —— Numerical calculations.
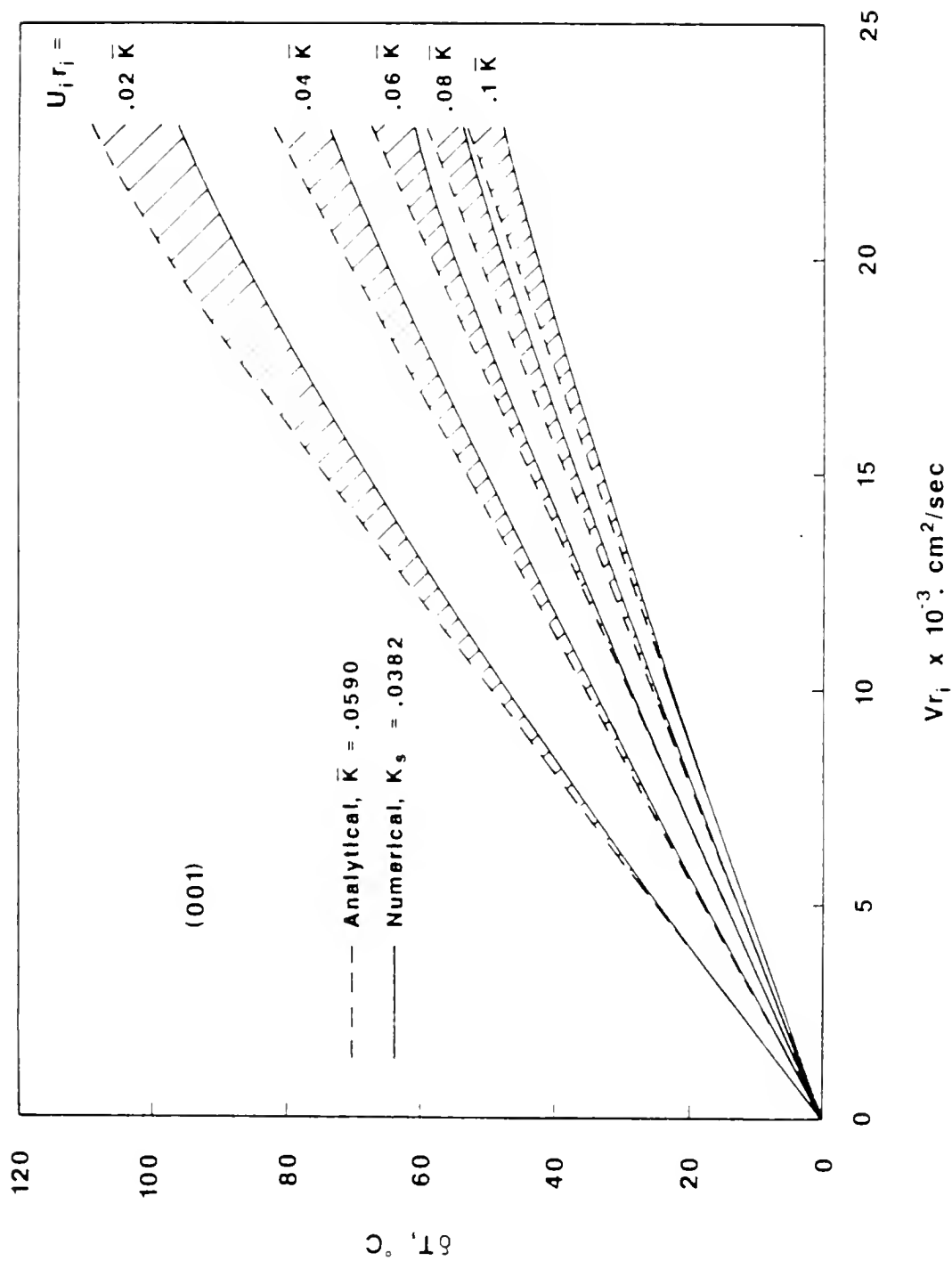
Figure A-7 Temperature correction, δT, for the (001) interface as a function of Vr_i for different values of $U_i r_i$; --- Analytical, —— Numerical calculations.
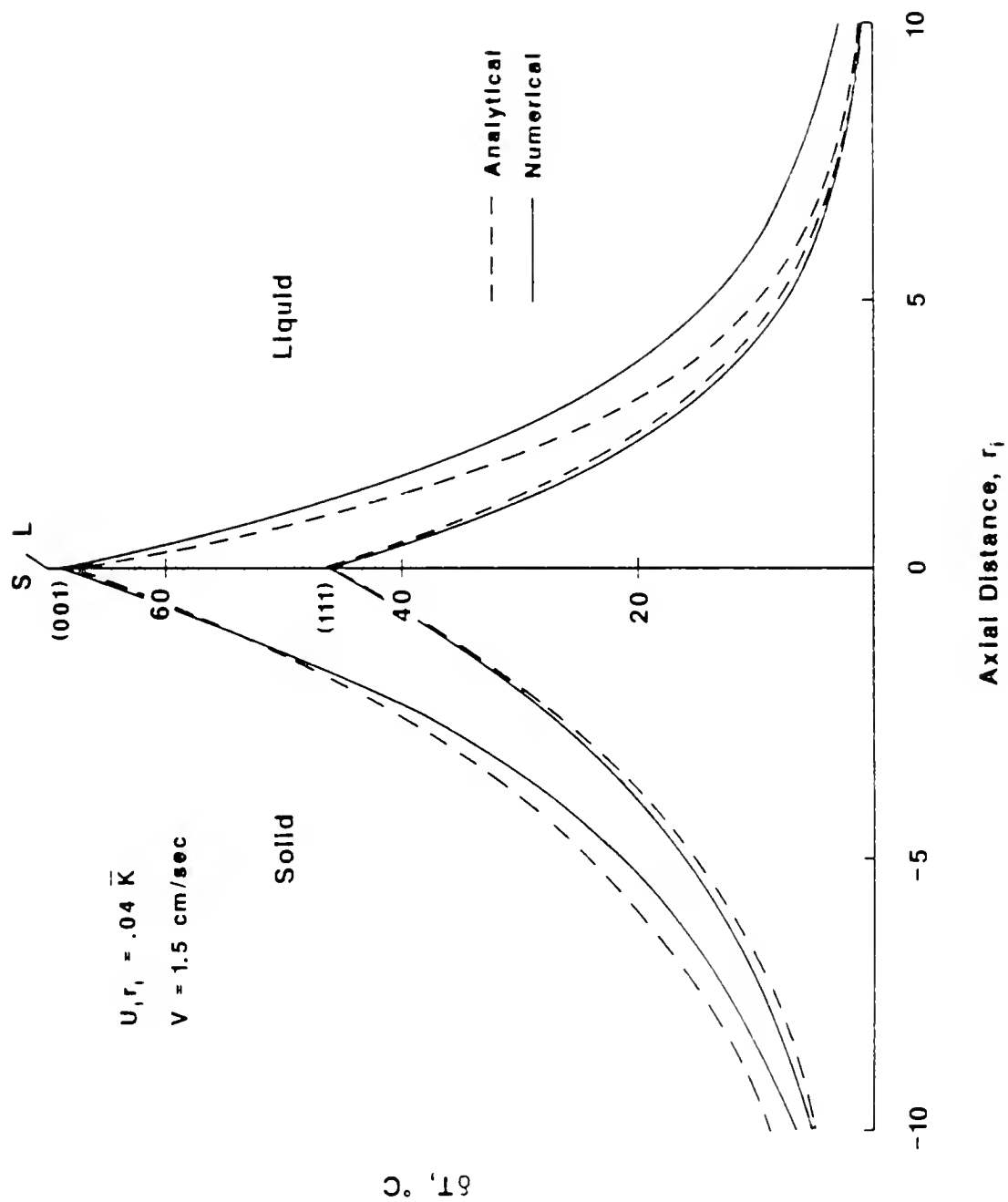
Figure A-8 Temperature distribution across the S/L (111) and (001) interfaces as a function of the interfacial radius; --- Analytical model calculations, — Numerical calculations.

and growth rates of .01, .6, and 1 cm/s, the difference between the numerical and analytical results is .03, 1.917, and 10.36°C, respectively.

Figure A-8 shows temperature distribution in the solid and liquid sides with respect to the axial distance from the S/L interface in terms of the inside radius r_i. The calculations for both (001) and (111) interfaces were performed for the heat transfer conditions, as indicated in Fig. A-8, and for a growth rate of 1.5 cm/s. The estimate of the thermal gradients at these high growth rates was important for the interfacial stability calculations, as discussed in the next Appendix. It should be noted that the temperatures on both sides of the interface fall steeply with distance away from it. For the (111) interface, for example, the liquid at a distance $10r_i$ from the growth front has about the same temperature with the bulk liquid. Figure A-9 shows the ratio of the temperature correction at any point along the interface to that of the edge (inner capillary wall) for different values of $U_i r_i / K_s$ of the (111) interface. According to these calculations, the edge of the interface is cooler than its center by 2-4.5%, depending on the $U_i r_i / K_s$ value.

Figures A-10 and A-11 compare the experimental results with the analytical and numerical for the (111) interface at low (V ≤ .2 cm/s) and high growth rates, respectively. As can be seen, the experimental results are in very good agreement with the numerical and analytical calculations. The observed slight deviation of the experimental results from the calculations towards higher δT corrections at large $V r_i$ (see Fig. A-11) could be explained as follows: the calculations are done using as a reference temperature for the properties of the coolant (30% water-ethylene glycol solution) that of 25°C. At high bulk supercoolings ($T_b <$

(111)

Tube Wall →

$\frac{U_i r_1}{K_s} = .0908$

$\frac{U_i r_1}{K_s} = .0727$

← Tube Center

$\frac{U_i r_1}{K_s} = .0363$

Radial Distance, r′

$\delta T (r′) / \delta T (r′=1)$
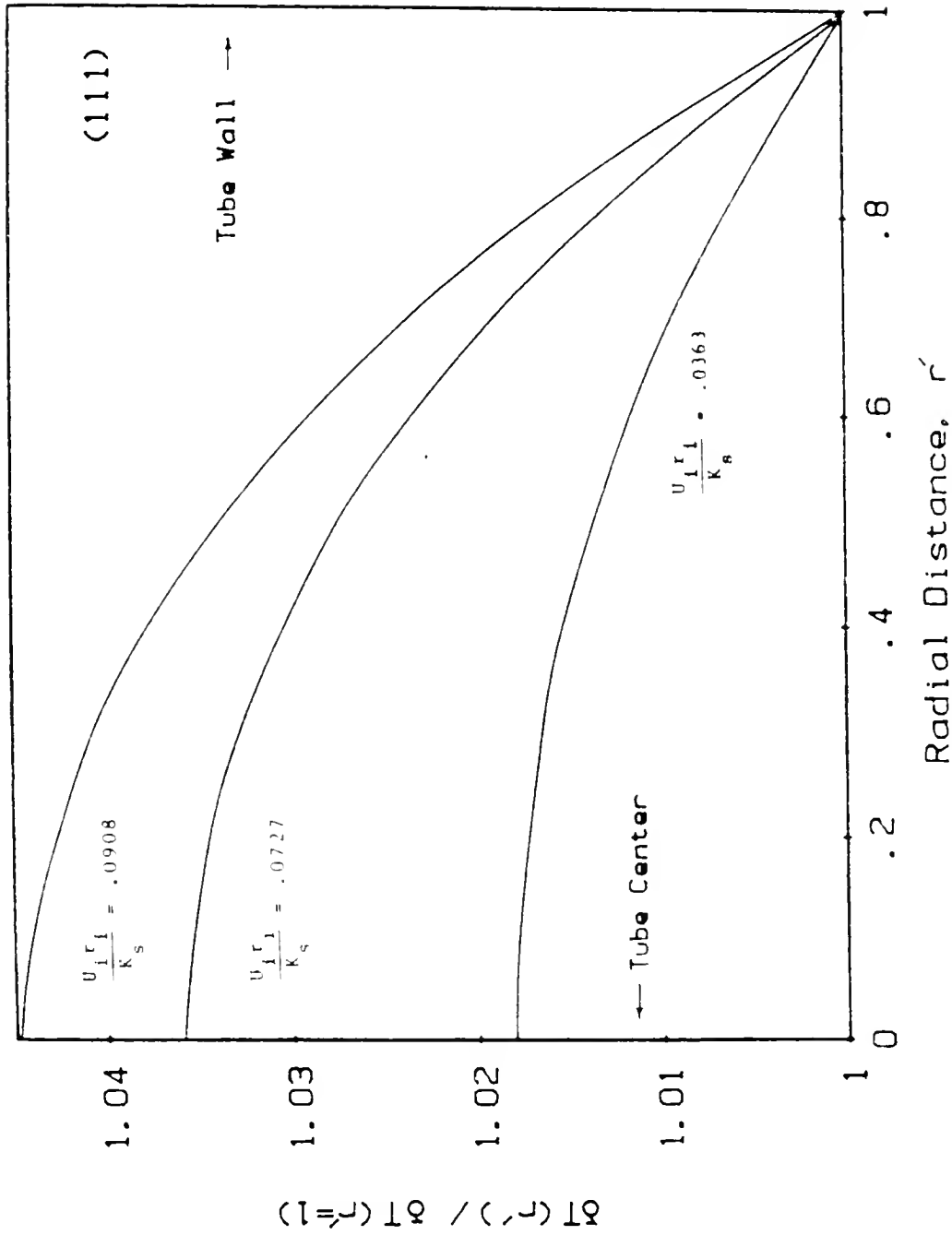
Figure A-9   Ratio of the Temperature correction(δT) at any point of the interface to that at the edge as a function of r′(r′=r/r_i) for different values of $U_i r_i / K_s$.

295
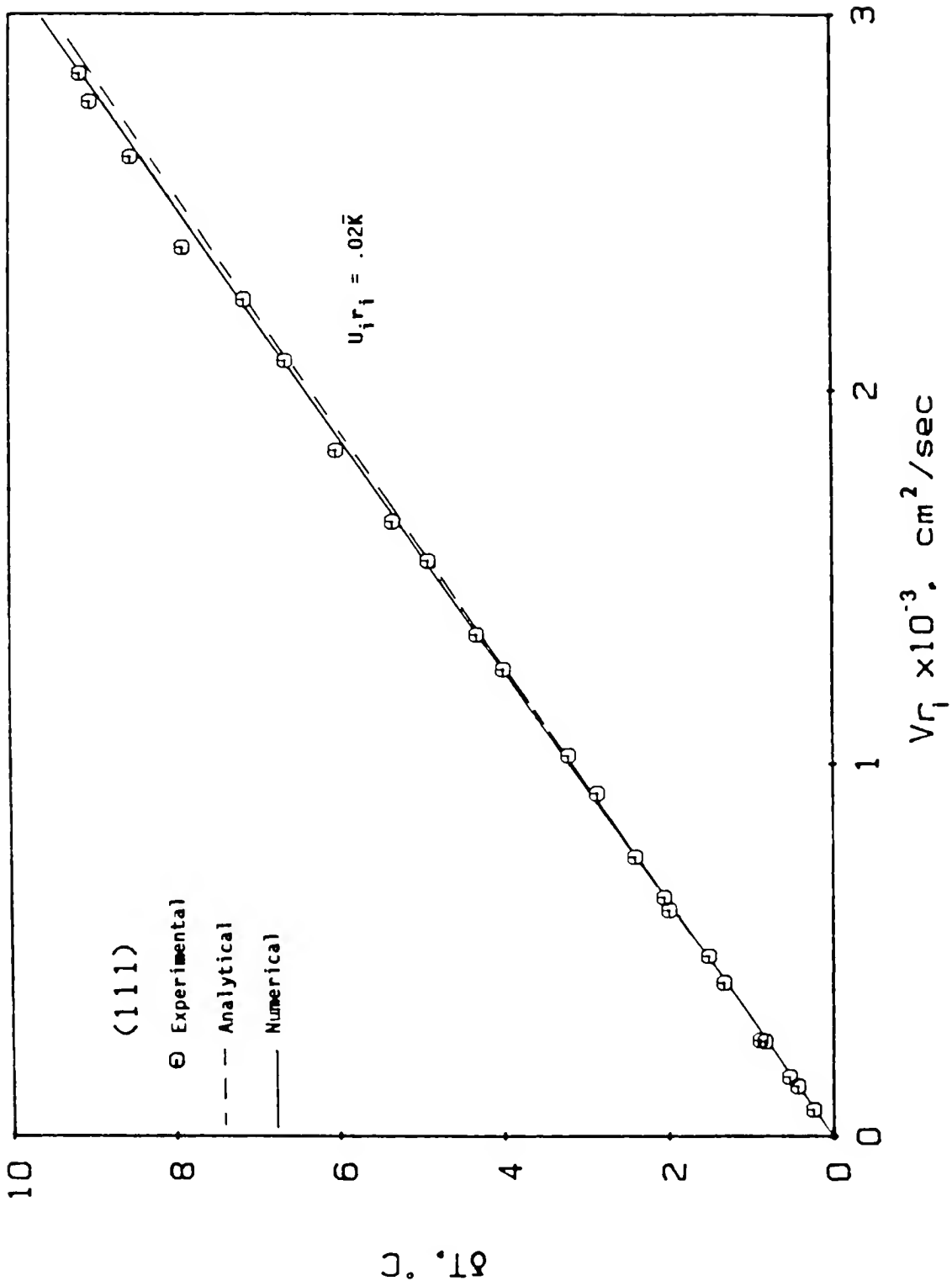
Figure A-10   Comparison between the (111) Experimental results (O) and the model (---- Analytical, —— Numerical) calculations at low growth rates (V < .2 cm/s).
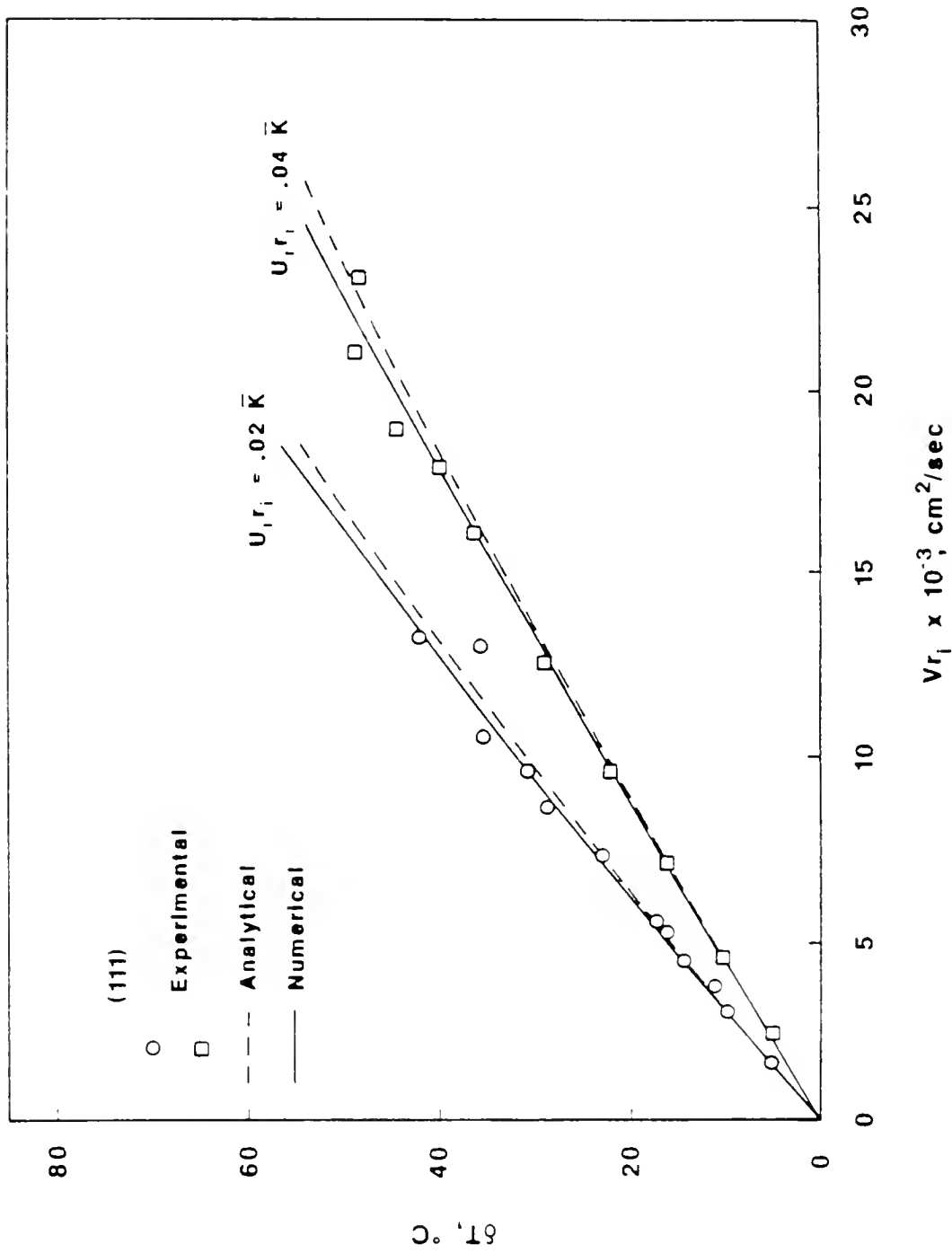
Figure A-11 Comparison between the (111) Experimental results (○, □) and the Model
(--- Analytical, —— Numerical) calculations as a function of Vr_i for
given growth conditions.

0°C) the above mentioned assumption will introduce some error. Indeed, if one recalculates the case of $U_i r_i = .02\overline{K}$ using the thermal parameters of the fluid for 0°C, it is found that these conditions correspond to $U_i r_i = .0193\overline{K}$. The latter value, as understood from Fig. A-11, would result in slightly higher δT values than the previous ones. Finally, Fig. A-12 shows the comparison between experimental and calculated results for the (001) interface. The agreement between the two is quite satisfactory, as shown in Fig. A-12; similar to the (111) interface, the experimental results for the (001) interface are slightly lower than the numerical at $V r_i$ values larger than $.01 \text{ cm}^2/\text{s}$.

The present numerical calculations have shown to be in excellent agreement with the experimental results, determined directly via the Seebeck technique. The above conclusion assures the reliability of the heat transfer model if no assumptions are made regarding the conduction of heat to the solid and the liquid phase. The assumption that the liquid and the solid have the same thermal properties (as made in the earlier calculations[2,181]) will introduce errors, particularly for the (001) interface at high growth rates. The numerical results can be used to estimate the thermal gradients at the interface and the interfacial temperature, whenever the Seebeck technique is not feasible.
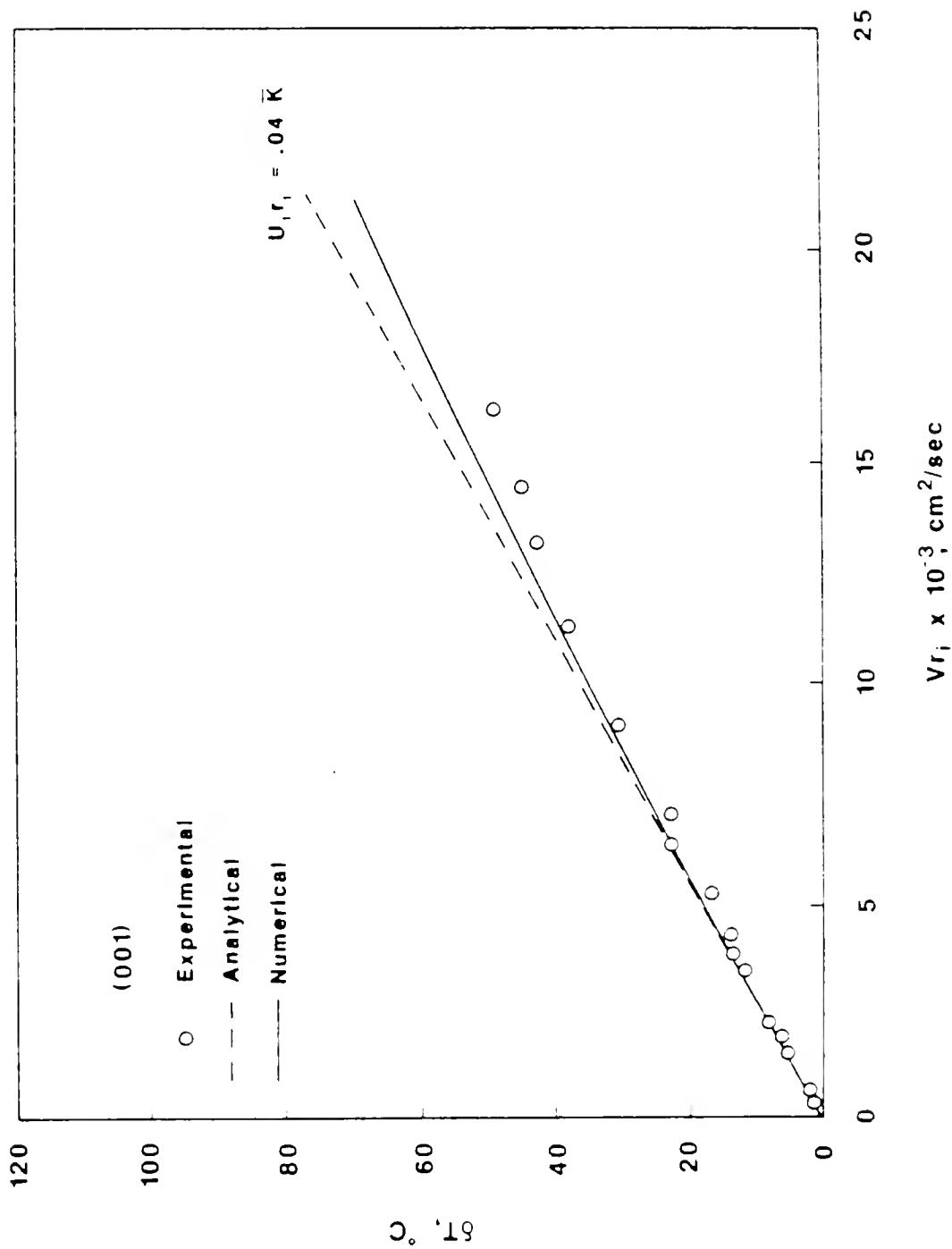
Figure A-12 Comparison between the (001) Experimental results (○) and the Model (--- Analytical, — Numerical) calculations as a function of Vr_i for given growth conditions.

APPENDIX IV
INTERFACIAL STABILITY ANALYSIS

The morphological stability of the S/L Ga interface is discussed in this Appendix. The analysis follows the linear perturbation theory formulated by Coriell and Sekerka[245,253] and includes non-local equilibrium conditions at the interface (i.e. kinetics). Calculations have been performed based on the Ga growth data; the thermal gradients have been calculated from the heat transfer analysis presented in Appendix III. The stability criterion in terms of the real part of the time constant, σ (see eq. (54) of the text), for the amplitude of a perturbation for a pure material is given as

$$\sigma = \frac{V \left\{ \left[-K_L G_L \left(\alpha_L - \frac{V}{\kappa_L} \right) - K_s G_s \left(\alpha_s + \frac{V}{\kappa_s} \right) \right] U_A - 2\bar{K} T_m \Gamma \omega^2 \bar{\alpha} \right\}}{L_V V U_T} \tag{A33}$$

with

$$U_A = 1 - \mu_A / \mu_T$$

$$U_T = 1 - \frac{\mu_A}{\mu_T} + \frac{2\bar{K} \, \bar{\alpha}}{L_V \mu_T}$$

The other parameters involved in eq. (A33) have been described previously, except for μ_T and μ_A, which are defined below. The extra terms in eq. (A33), as compared to the criterion for the dilute binary alloy (eq. (54)), account for the interfacial kinetics. Assuming that the growth rate can be expressed as $V = f(T_i, \Delta T)$, the coefficients μ_T and μ_A are given as

$$\mu_T = \frac{\partial f}{\partial(\Delta T)} \quad \text{and} \quad \mu_A = \frac{\partial f}{\partial T_i}$$

Substituting U_A and U_T into eq. (A33), we obtain

$$\sigma = \frac{[-K_L G_L(\alpha_L - \frac{V}{\kappa_L}) - K_s G_s(\alpha_s + \frac{V}{\kappa_s})](\mu_T - \mu_A) - \mu_T 2\bar{K}T_m\Gamma\omega^2\bar{\alpha}}{L_V(\mu_T - \mu_A) + 2\bar{K}\bar{\alpha}} \tag{A34}$$

Remembering that the interface is stable when $\sigma < 0$, eq. (A34) leads to results that are qualitatively similar to the previously discussed general case, as long as $\mu_T - \mu_A > 0$ (provided $\mu_T > 0$). For the opposite case, i.e. $\mu_T - \mu_A < 0$, further analysis is required since the sign of the denominator and that of the numerator depend on whether or not the liquid is supercooled (i.e. $G_L < 0$). In determining the sign of $\mu_T - \mu_A$, one has to consider a particular kinetic law and examine its properties with increasing ΔT. For example, in the case of continuous growth kinetics, $\mu_T - \mu_A > 0$ for small supercoolings and $\mu_T - \mu_A < 0$ at high supercoolings because of the increased melt viscosity at low temperatures (see also discussion in earlier chapters). For the case of 2DNG kinetics (PNG), the growth rate can be expressed as

$$V = \mu_o \Delta T^n \exp(-\frac{B}{T_i \Delta T})$$

where μ_o, B are constants and n is about one. Then

$$\mu_T = \frac{\partial V}{\partial(\Delta T)} = \mu_o \Delta T^{n-1} \exp(-\frac{B}{T_i \Delta T}) (n + \frac{B}{T_i \Delta T}) > 0$$

$$\mu_A = \frac{\partial V}{\partial T} = \mu_o \Delta T^n \exp(-\frac{B}{T_i \Delta T}) (n + \frac{B}{T_i^2}) > 0 \quad \text{and}$$

$$\mu_T - \mu_A = \mu_o \Delta T^{n-1} \exp(-\frac{B}{T_i \Delta T}) (n + \frac{B}{T_i \Delta T} - \frac{B}{T_i^2})$$

For small ΔT or high T_i $\mu_T - \mu_A > 0$. However, for practical purposes, as for the Ga growth kinetics experimental range, it can be assumed that the growth rate is only a function of supercooling. Accordingly, then

$$\mu_T = \mu_o \, \Delta T^{n-1} \, \exp(- \frac{B'}{\Delta T}) \, (n + \frac{B'}{\Delta T}) \, (\frac{cm}{sec \cdot {}^\circ C})$$

Therefore, eq. (A34) can be rewritten as

$$\sigma = \frac{[-K_L G_L(\alpha_L - \frac{V}{\kappa_L}) - (K_s G_s(\alpha_s + \frac{V}{\kappa_s})]\mu_T - \mu_T 2\overline{K}T_m \Gamma \kappa \omega^2 \overline{\alpha}}{L_V \mu_T + 2 \, \overline{K} \, \overline{\alpha}} \qquad (A35)$$

The stability/instability demarcation can be obtained by letting $\sigma \to 0$, provided that the thermal steady state approximation ($\omega \gg V/2\kappa_{L,s}$) is valid. The largest meaningful perturbation wavelength $\lambda = 2\pi/\omega \leq d_i$ where d_i is the interfacial area diameter. Since, in the present experiment, $d_i = .014$ cm, ω then is given as $\omega > 224.3$ cm^{-1}. Since for Ga $\kappa_L = .1376$ and $\kappa_s^{(111)} = .1862$ cm^2/s the condition $\omega > V/2\kappa_L$ holds, even for velocities up to about 60 cm/s. Thus, for growth rates involved in this investigation ($V < 2$ cm/s), it can be safely assumed that $\omega > V/2\kappa_{L,s}$. Based on this assumption, then α_L, α_s, and $\overline{\alpha} = \omega$ (see eq. (54) of the text and analytical forms of coefficients therein). Therefore, eq. (A35) can be written as

$$0 = \frac{\omega\{(-K_L G_L - K_s G_s)\mu_T - \mu_T \overline{2}KT_m \Gamma \omega^2 \}}{L_V \mu_T + 2\overline{K}\omega} \qquad (A36)$$

or that the interface is unstable when

$$\frac{-K_L G_L - K_s G_s}{2\overline{K}} > T_m \Gamma \omega^2 \qquad (A37)$$

Based on the morphological stability criterion, as expressed in eq. (A37), the conditions under which the planar (111) interface may become

unstable were determined. The calculations are summarized in Figs. A-13 and A-14; Fig. A-13 is a plot of the growth rate versus the critical wavelength defined as

$$\lambda_{cr}^{-1} = (\frac{-K_L G_L - K_s G_s}{4\pi\overline{K}\ T_m\ \Gamma})^{1/2}$$

Note that for $\lambda > \lambda_{cr}$ the interface is unstable. On the other hand, Fig. A-14 is a linear plot of the stability $R(\omega)$, given as

$$R(\omega) = \frac{-(K_L G_L - K_s G_s)}{2\overline{K}} - T_m\Gamma\omega^2$$

as a function of the perturbation wavelength, λ, and the growth rate. Note that here the interface is stable for conditions such that $R(\omega) < 0$. The calculations, as shown in these figures, were performed based on actual experimental data. The thermal fields within the sample were determined with the aid of the heat transfer model, which was discussed earlier in Appendix III.

The analysis indicates that the S/L interface should be stable at growth rates up to about .8 cm/s if the perturbation wavelength is equal to the interface diameter. For smaller perturbations, the interface should be stable even at higher growth rates.
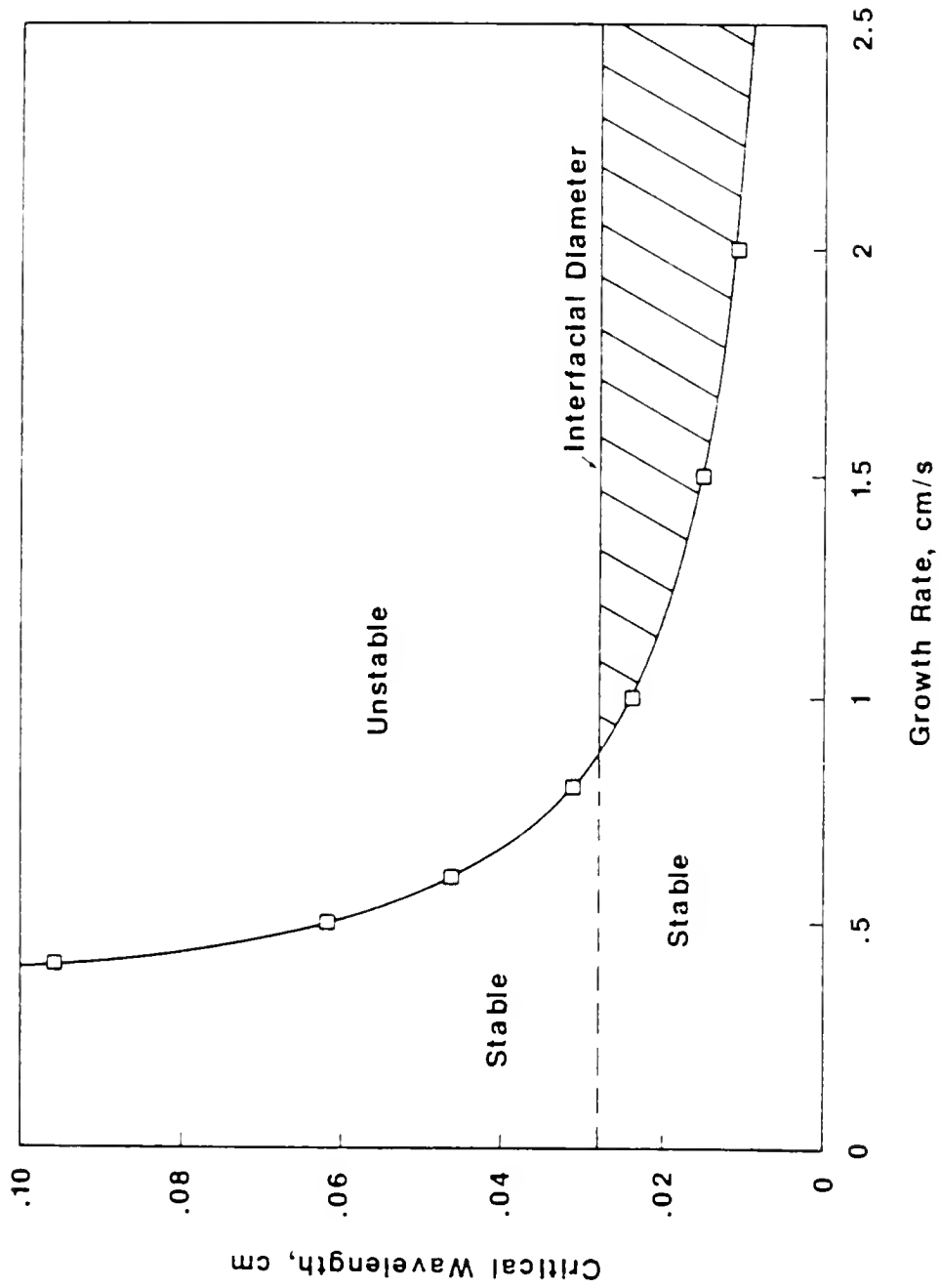
Figure A-13 The critical wavelength λ_{cr} at the onset of the instability as a function of growth rate; hatched area indicates the possible combination of wavelengts and growth rates that might lead to an unstable growth front for the given sample size(i.d.=.028cm).
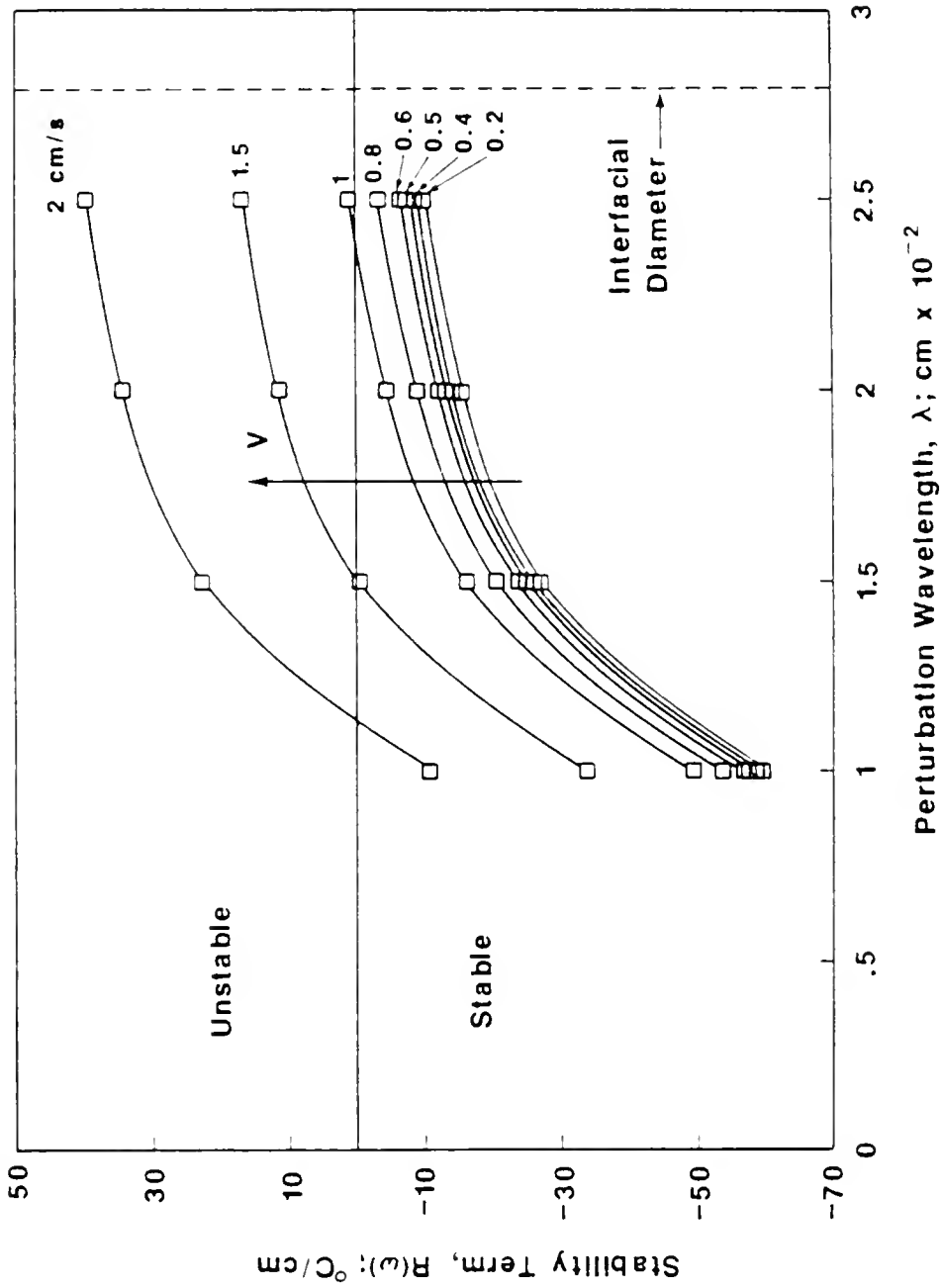
Figure A-14 The stability term R(ω) as a function of the perturbation wavelength and the growth rate.

APPENDIX V
PRINTOUTS OF COMPUTER PROGRAMS

Program #1

```
1   REM  * THIS PROGRAM RECORDS THE BULK TEMPERATURE WITH
        THE HP-VOLTMETER 3456A AND THE SEEBECK EMF WITH THE
        KEITHLEY-NANOVOLTMETER 181.
5   DIM V1(500),V2(500),T(1000)
6   DIM V1$(500),V2$(500)
10  N = 2000
30  PRINT "MAKE DATA(1) OR SAVE DATA(2)";: INPUT K
40  IF K = 1 THEN  GOTO 65
50  IF K = 2 THEN  GOTO 410
60  GOTO 30
65  Z$ =  CHR$ (26)
66  D$ = " ": REM  D$=<CTRL-D>
67  REM ****************************
68  REM  * IN THE NEXT SECTION OF THE PROGRAM THE DATA AR
        E REITREVED FROM THE ABOVE MENTIONED INSTRUMENTS.
70  PR# 3
80  IN# 3
90  PRINT "SC1"
100  PRINT "RA"
110  PRINT "LL"
120  PRINT "LF1"
130  PRINT "WTX";Z$;"R1X"
140  PRINT "WT6";Z$;"F1R2"
160  IF  PEEK ( - 16286) > 127 THEN  GOTO 180
170  GOTO 160
180 NUM = NUM + 1
184  REM ****************************
185  REM  * THE NEXT STATEMENT SETS THE FREQUENCY OF THE
        MEASUREMENTS.
190  FOR P = 1 TO N: NEXT
200  PRINT "WTX";Z$
210  PRINT "RDE";Z$;: INPUT V1$(NUM)
230  PRINT "RDV";Z$;: INPUT V2$(NUM)
240  IF  PEEK ( - 16287) > 127 THEN  GOTO 260
250  GOTO 180
260  PRINT "LA"
270  PRINT "UT"
280  PR# 0
290  IN# 0
295  REM ****************************
296  REM  * THE FOLLOWING STATEMENTS SET-UP THE PRINTER A
        ND PRINT THE DATA.
300  PR# 1
310  PRINT  CHR$ (9);"120N"
320  PRINT  CHR$ (27);"Q"
330  FOR I = 1 TO NUM
340 V1(I) =  VAL ( MID$ (V1$(I),5,15)) * 1000000
350 V2 =  VAL (V2$(I)) * 1000
360 T(I) = 4.67174E - 3 + 25.39249 * V2 - .43769 * V2 ^ 2
        + .0492097 * V2 ^ 3
```

Program #1 continued

```
370    PRINT I,T(I),V1(I)
380    NEXT I
390    PR# 0
400    GOTO 30
405    REM ************************
406    REM  * THE NEXT STATEMENTS STORE THE DATA ON A DISK
       UNDER THE FILENAME "FITDATA".
410 CD$ =   CHR$ (4):F$ = "FITDATA"
420    PRINT CD$;"OPEN";F$: PRINT CD$;"WRITE";F$
430    PRINT NUM * 2: REM  NUMBER OF DATA VALUES
440    FOR I = 1 TO NUM
450    PRINT T(I)
460    PRINT V1(I)
470    NEXT I
480    PRINT CD$;"CLOSE";F$
490 NUM = 0: GOTO 30
```

Program #2

```
5   REM   * THIS PROGRAM TAKES A SEEBECK EMF READING WITH T
        HE KEITHLEY-181 NANOVOLTMETER WHEN THE CURRENT SOURC
        E IS OFF; TURNS ON THE KEITHLEY-220 CURRENT SOURCE A
        ND RECORDS THE POTENTIAL ACROSS THE SAMPLE WITH THE
        HP-3456A VOLTMETER.
20  N = 300
25  M = 300
30   DIM V1$(M),V2$(M),V3(500),DV(500)
35   DIM V1(500),V2(500)
40  Z$ =   CHR$ (26)
50  D$ = "": REM   D$=<CTRL-D>
55   REM *************************
56   REM  * THE NEXT STATEMENTS SET-UP THE INSTRUMENTS.
60   PR# 3
70   IN# 3
80   PRINT "SC1"
90   PRINT "RA"
100   PRINT "LL"
110   PRINT "LF1"
120   PRINT "WT%";Z$;"R2X"
130   PRINT "WT6";Z$;"F1R2"
140   PRINT "WT6";Z$;"+100E-1STI"
142   PRINT "WT,";Z$;"ROP1FOX";"I5E-3";"V1";"X"
150   IF  PEEK ( - 16286) > 127 THEN  GOTO 170
160   GOTO 150
170  NUM = NUM + 1
175   REM *************************
176   REM   STATEMENTS 180,210 SET THE READINGS INTERVAL.
180   FOR P = 1 TO N: NEXT
185   REM *************************
186   REM  NEXT THE SEEBECK EMF IS RETREIVED.
190   PRINT "WT%";Z$
200   PRINT "RDE";Z$;: INPUT V1$(NUM)
203   REM *************************
204   REM  NEXT THE CURRENT SOURCE OPERATES.
205   PRINT "WT,";Z$;"F1X"
210   FOR P = 1 TO M: NEXT
215   REM *************************
216   REM  NEXT THE POTENTIAL DROP ACROSS THE SAMPLE IS RE
        CORDED
220   PRINT "RDV";Z$;: INPUT V2$(NUM)
221   REM  *************************
222   REM  NEXT THE CURRENT IS OFF
225   PRINT "WT,";Z$;"FOX"
230   IF  PEEK ( - 16287) > 127 THEN  GOTO 250
240   GOTO 170
245   REM  *************************
246   REM  * FOLLOWING THE DATA ARE PRINTED (CODED FORM) O
        N THE APPLE IIe SCREEN
250   PRINT "LA"
```

Program #2 continued

```
260    PRINT "UT"
270    PR# 0
280    IN# 0
284    REM *************************
285    REM  THE PRINTER IS SET-UP AND THE DATA ARE PRINTED
       IN THE NEXT STATEMENTS.
290    PR# 1
300    PRINT  CHR$ (9);"120N"
301    PRINT  CHR$ (27);"Q"
310    FOR I = 1 TO NUM
320 V1(I) =  VAL ( MID$ (V1$(I),5,15))
330 V2(I) =  VAL (V2$(I))
333 V3(I) = V2(I) - V1(I)
335    IF I = 1 THEN DV(I) = 0
340    IF I > 1 THEN DV(I) = V3(I) - V3(I - 1)
345    PRINT I,V1(I),V2(I),V3(I),DV(I)
350    NEXT I
360    PR# 0
380 NUM = 0: GOTO 60
```

Program #3

```
1   REM  * THIS PROGRAM RECALLS THE SEEBECK EMF AND POTENT
      IAL STORED READINGS FROM THE INTERNAL MEMORY OF THE
      3456A HP-VOLTMETER.
5   DIM V$(350)
6   DIM V1(350),X(350),Y(350)
8 CR = 0.1
9 DT = 0.1:DRDL = 0.1
10 Z$ = ""
30   PR# 3
40   IN# 3
50   PRINT "SC1"
60   PRINT "RA"
70   PRINT "LL"
80   PRINT "LF1"
90 A$ = "T4RS1"
100 B$ = "STR"
101   PR# 1
103   PRINT "NUM.        VALUE"
104   PR# 3
105   FOR NUM = 1 TO 350
106 C$ =   STR$ (NUM)
107 D$ = A$ + C$ + B$
108   PRINT "WT6";Z$;D$
109   PRINT "WT6";Z$;"RER"
115   PRINT "RDV";Z$;: INPUT V$(NUM)
116 V1(NUM) =   VAL (V$(NUM))
117   REM  ***********************
118   REM  * NEXT THE STORED VALUES ARE PRINTED
119   PR# 1
120   PRINT NUM,V1(NUM)
121   PR# 3
122   NEXT NUM
130   PRINT "LA"
140   PRINT "UT"
170   PR# 1
175   PRINT "END OF DATA"
```

Program #4


```
5    REM  * THIS PROGRAM READS THE SEEBECK EMF OR THE POTEN
        TIAL ACROSS THE SAMPLE (DEPENDING WHETHER OR NOT CUR
        RENT PASSES THROUGH THE SAMPLE) WITH THE KEITHLEY 18
        1-NANOVOLTMETER (20 mV RANGE).
10   DIM A$(20),B$(20),A(1000),C(1000)
15 Z$ =  CHR$ (26):B$ = "R2X"
20   PRINT "TAKE DATA(1) OR SAVE DATA(2)";: INPUT K
30   IF K = 1 THEN  GOTO 70
40   IF K = 2 THEN  GOTO 180
50   GOTO 20
60   REM  ************************
65   REM  * FOLLOWING THE DATA ARE RETREIVED FROM THE K-18
        1
70   PR# 3
80   IN# 3
90   PRINT "RA"
100   PRINT "WT%";Z$;A$
105   PRINT "LF1"
110   PRINT "RDE";Z$;: INPUT "";A$
111   REM  ************************
112   REM  * NEXT THE DATA ARE PRINTED ON THE APPLE IIe SC
        REEN
113   PRINT "UT"
115   PR# 0
117   IN# 0
130 NUM = NUM + 1
140   PRINT NUM,A$
145 A(NUM) =  VAL ( MID$ (A$,5,15))
150 OA =  PEEK ( - 16287)
160   IF OA > 127 THEN  GOTO 20
170   GOTO 70
175   REM  ************************
176   REM  * NEXT THE DATA ARE PRINTED
180   PR# 1
185   FOR I = 1 TO NUM
187 C(I) = A(I) - A(I - 1)
190   PRINT  CHR$ (9);"80N";(I),A(I),C(I)
195   NEXT I
200   PR# 0
205 NUM = 0
210   GOTO 20
```

Program #5

```
C     XXXXXXXXXXXXXXXXXXXXXXXXXXXXXXXXXXXXXXXXXXXXXXXXXXXXXXXXXXXX
C     X THIS PROGRAM SOLVES A(SUB N) AND B(SUB N) OF EQ.(30) OF THE  X
C     XANALYTICAL MODEL BY TRUNCATING THE INFINITE SERIES AT 6TH TERMX
C     XAND SOLVING EQS.(30) AND (31) SIMULTANEOUSLY AT 6 VALUES OF R X
C     XR+N/5*RADIUS,N=0,1,...,5.                                    X
C     XXXXXXXXXXXXXXXXXXXXXXXXXXXXXXXXXXXXXXXXXXXXXXXXXXXXXXXXXXXXXXX
C     XXXXXXXXXXXXXXXXXXXXXXXXXXXXXXXXXXXXXXXXXXXXXXXXXXXXXXXXXXXXXXX
C     X INPUT PARAMETER DESCRIPTION                                 X
C     X NOTE; USE CGS UNIT : CM,GM,SEC......                        X
C     X KLS=K(SUB L)/K(SUB S) ; RATIO OF LIQUID AND SOLID HEAT COND X
C     X                         TIVITIES                           X
C     X ASL=KAPPA(SUB S)/KAPPA(SUB L); RATIO OF THERMAL DIFFUSIVITIES X
C     X RSL=DENSITY OF SOLID/DENSITY OF LIQUID                      X
C     X VW=INTERFACE VELOCITY                                       X
C     X HCT=HEAT OF FUSION/BATH SUPERCOOLING/HEAT CAPACITANCE SOLID X
C     X Z= AXIAL LENGTH OF GA WHERE TEMP. DISTRIBUTION ARE TO BE    X
C     X    CALCULATED/I.R. OF CAPILLARY TUBE                        X
C     X TB= BATH TEMPERATURE IN DEG. CENTIGRADE                     X
C     X ASRI=KAPPA(SUB S)/I.RADIUS OF CAPILLARY TUBE                X
C     X GAMAS AND GAMAL ARE VALUES OF GAMA (SUB S) AND GAMA(SUB L)  X
C     X EVALUATED FROM EQ.(26) AND EQ.(27) WITH TABLE FROM 'CONDUC  X
C     X TION HEAT TRANSFER' BOOK                                    X
C     XXXXXXXXXXXXXXXXXXXXXXXXXXXXXXXXXXXXXXXXXXXXXXXXXXXXXXXXXXXXXXX
C     XXXXXXXXXXXXXXXXXXXXXXXXXXXXXXXXXXXXXXXXXXXXXXXXXXXXXXXXXXXXXXX
C     X OUTPUT OF THIS PROGRAM CONTAINS A LIST OF INPUT PARAMETERS  X
C     X AND THE MATRIX FOR SOLVING A(SUB N) AND B(SUB N), THE COEFFICX
C     X IENTS A(SUB N) AND B(SUB N) AND TEMPERATURE DISTRIBUTION IN X
C     X BOTH SIDES OF THE INTERFACE ACROSS THE CAPILLARY TUBE       X
C     XXXXXXXXXXXXXXXXXXXXXXXXXXXXXXXXXXXXXXXXXXXXXXXXXXXXXXXXXXXXXXX
      DIMENSION A(12,12),B(12),WKAREA(160),TS(10,100),TL(10,100)
      COMMON /GAMMA/GAMAS(6),GAMAL(6),Y1(6),Y2(6)
      REAL KLS
      M=1
      IA=12
      IDGT=0
      N=12
      IDX=0
  999 CONTINUE
      IDX=IDX+1
      READ(5,10)KLS,ASL,RSL,VW,HCT,Z
      READ(5,10)TB,ASRI
      WRITE(6,16)KLS,ASL,RSL,VW,HCT,Z,TB,ASRI
      READ(5,10)(GAMAS(I),I=1,6)
      READ(5,10)(GAMAL(I),I=1,6)
      WRITE(6,17)GAMAS
      WRITE(6,18)GAMAL
   15 FORMAT(5X,'CASE  NO. ',I5)
   16 FORMAT(5X,'INPUT PARAMETERS; KLS,ASL,RSL,V,HCT,Z,TB,ASRI',
     1/9X,8E13.6)
   17 FORMAT(5X,'GAMAS ',6E13.6)
   18 FORMAT(5X,'GAMAL ',6E13.6)
      V=VW
```

Program #5 continued

```
   21 FORMAT(5X,'VELOCITY ',E13.6)
      DO 20 I=1,6
      II=6+I
      B(I)=0
      A(1,II)=-1
      A(1,I)=1
   20 CONTINUE
C     XXXXXXXXXXXXXXXXXXXXXXXXXXXXXXXXXXXXXXXXXXXXXXXXXXXXXXXX
C     X FORMING COEFFICIENT MATRIX A(I,J) AND B(I) ACCORDING TO  X
C     X EQS.(30) AND (31)                                        X
C     XXXXXXXXXXXXXXXXXXXXXXXXXXXXXXXXXXXXXXXXXXXXXXXXXXXXXXXX
      DO 30 I=2,6
      DO 40 J=1,6
      JJ=J+6
      X=.2*(I-1)*GAMAS(J)
      Y=.2*(I-1)*GAMAL(J)
C     XXXXXXXXXXXXXXXXXXXXXXXXXXXXXXXXXXXXXXXXXXXXXXXXXXXXXXXX
C     X FUNCTION BESSEL USE INFINITE SERIES EXPRESSION OF    X
C     X BESSEL FUNCTION TO DETERMINE VALUE OF BESSEL FUNCTIONX
C     XXXXXXXXXXXXXXXXXXXXXXXXXXXXXXXXXXXXXXXXXXXXXXXXXXXXXXXX
      A(I,JJ)=-BESEL(Y)
      A(I,J)=BESEL(X)
   40 CONTINUE
   30 CONTINUE
      W=V*ASL*RSL
      DO 50 I=1,6
      II=I+6
      B(II)=V*HCT
      GML=ASRI*GAMAL(I)
      GMS=ASRI*GAMAS(I)
      Y2(I)=.5*W+(.25*W**2+GML**2)**.5
      A(7,II)=KLS*Y2(I)
      Y1(I)=-.5*V+(.25*V**2+GMS**2)**.5
   50 A(7,I)=Y1(I)
      DO 60 I=8,12
      DO 60 J=1,6
      JJ=J+6
      X1=.2*(I-7)*GAMAS(J)
      X2=.2*(I-7)*GAMAL(J)
      A(I,J)=Y1(J)*BESEL(X1)
   60 A(I,JJ)=Y2(J)*BESEL(X2)*KLS
      WRITE(6,19)((A(I,J),J=1,12),I=1,12)
      WRITE(6,19)B
   19 FORMAT(5X,'MATRIX',/(5X,12E10.3))
C     XXXXXXXXXXXXXXXXXXXXXXXXXXXXXXXXXXXXXXXXXXXXXXXXXXXXXXXX
C     X LEQT2F IS SUBROUTINE FROM LIBRARY                        X
C     X LIBRARY NAME IS IMSL.SP                                  X
C     X PLEASE CHECK WITH CIRCA FOR MORE INFORMATION             X
C     XXXXXXXXXXXXXXXXXXXXXXXXXXXXXXXXXXXXXXXXXXXXXXXXXXXXXXXX
```

Program #5 continued

```
      CALL LEQT2F(A,M,N,IA,B,IDGT,WKAREA,IER)
      WRITE(6,70)(B(I),I=1,6)
      WRITE(6,80)(B(I),I=7,12)
    1 FORMAT(5X,I5)
   10 FORMAT(2X,6F10.6)
   70 FORMAT(5X,'COEFFICIENT A(N) ',/(10X,E13.6))
   80 FORMAT(5X,'COEFFICIENT B(N) ',/(10X,E13.6))
      I=1
C     XXXXXXXXXXXXXXXXXXXXXXXXXXXXXXXXXXXXXXXXXXXXXXXXXXXXXXXXXXX
C     X SUBROUTINE TEMP USE EQS.(28) AND (29) TO CALCULATE THE   X
C     X TEMPERATURE DISTRIBUTION IN BOTH SOLID AND LIQUID REGION X
C     XXXXXXXXXXXXXXXXXXXXXXXXXXXXXXXXXXXXXXXXXXXXXXXXXXXXXXXXXXX
      CALL TEMP(B,I,TS,Z,TB,ASRI)
      I=2
      CALL TEMP(B,I,TL,Z,TB,ASRI)
      WRITE(6,90)((TS(I,J),I=1,10),J=1,100)
      WRITE(6,100)((TL(I,J),I=1,10),J=1,100)
 1100 CONTINUE
      IF(IDX.LT.ICASE)GO TO 999
 1000 CONTINUE
   90 FORMAT(5X,'TEMPERATURE DISTRIBUTION',/7X,'SOLID REGION',//(5X,10
     1E.12.5))
  100 FORMAT(/7X,'LIQUID REGION',//(5X,10E12.5))
      STOP
      END
```

```
   SUBROUTINE TEMP(B,I,T,Z,TB,ASRI)
   COMMON/GAMMA/GAMAS(6),GAMAL(6),Y1(6),Y2(6)
   DIMENSION T(10,100)
   DIMENSION B(12)
   DO 10 L=1,100
   ZZ=(L-1)*Z/99
   DO 10 M=1,10
   T(M,L)=0.
   RR=(M-1)/9.
   DO 5 N=1,6
   IF(I.EQ.1)GO TO 20
   NN=N+6
   Y=-Y2(N)*ZZ/ASRI
   GAMA=GAMAL(N)*RR
   GO TO 30
20 NN=N
   Y=-Y1(N)*ZZ/ASRI
   GAMA=GAMAS(N)*RR
30 CONTINUE
   IF(Y.EQ.0.)Y=0.000001
 5 T(M,L)=T(M,L)+B(NN)*BESEL(GAMA)*EXP(Y)
10 T(M,L)=T(M,L)*(29.7-TB)+TB
   RETURN
   END
```

. . . .

```
   FUNCTION BESEL(X)
   AO=1.
   X2=X**2
   BESEL=1.
   IF(X.EQ.O. )GO TO 30
   DO 10 I=1,30
   I2=I**2
   AN=-AO*X2/4./I2
   AO=AN
   ANN=ABS(AN)
   IF(ANN .LE.0.00001)GO TO 30
10 BESEL=BESEL+AN
30 CONTINUE
   RETURN
   END
```

SUPERSATURATION AND SUPERCOOLING

The supersaturation σ during vapor growth is defined as

$$\sigma = \alpha - 1, \quad \alpha = P/P_0 \tag{A38}$$

where P is the actual vapor pressure, P_0 is the equilibrium pressure, and α is called the saturation ratio. In the case of solution growth, the saturation ratio is given as $\alpha = C/C_e$, where C is the actual concentration of the solution and C_e is the concentration in equilibrium at the temperature T. Note that α can also be written as $\alpha = 1 + \Delta C/C_e$ or $\alpha = 1 + \Delta P/P_0$ where $\Delta C = C - C_e$ and $\Delta P = P - P_0$.

In growth from solution,

$$\ln\alpha = \frac{L_s (T_e - T)}{KT_e T} \tag{A39}$$

where L_s is the enthalpy of solution. For small saturations ($\alpha < 1.1$), also note that $\ln\alpha = \alpha - 1 = \sigma$.

Correspondingly, in growth from the melt

$$\ln\alpha = \frac{L (T_m - T)}{K T_m T} = \frac{L \Delta T}{KT_m T} \tag{A40}$$

where L is the heat of fusion per atom. In this case, for small supercoolings the supersaturation σ is proportional to $\Delta T/T_m$. An example of correspondence between supersaturation and supercooling is given next. As mentioned earlier, the critical 2D radius for vapor growth is given as

$$r = \frac{h\gamma}{KT\ln\alpha} \tag{A41}$$

316

where γ is the step edge energy per molecule. By substituting eq. (A40) into eq. (A41), one gets the familiar expression of r_c (see eq. (48)) for melt growth.

For more information regarding σ and ΔT, see Ref. (193a).

REFERENCES

1. J. Alvarez, S. D. Peteves, and G. J. Abbaschian, in: Thin Films
   and Interfaces II, J. E. E. Baglin, D. R. Campbell, and W. K. Chu,
   eds. (Elsevier, New York, 1984), p. 345.

2. G. J. Abbaschian and S. F. Ravitz, J. Cryst. Growth, 44 (1978) 453.

3. E. A. Flood, The Solid-Gas Interface, Vol. 1 (Marcel-Dekker, New
   York, 1967).

4. A. Bonissent, in: Interfacial Aspects of Phase Transformations, B.
   Mutaftschiev, ed. (D. Reidel Publ. Co., Dordrect, Netherlands,
   1982), p. 143.

5. See for example: H. Bethge, Interfacial Aspects of Phase Trans-
   formations, B. Mutaftschiev, ed. (D. Reidel Publ. Co., Dordrect,
   Netherlands, 1982), p. 669.

6. J. W. Cahn, Acta Met., 8 (1960) 554.

7. D. E. Temkin, in: Crystallisation Processes, N. N. Sirota, F. K.
   Gorskii, and V. M. Varikash, eds. (Consultants Bureau, New York,
   1966), p. 15.

8. K. A. Jackson, in: Liquid Metals and Solidification, (ASM,
   Cleveland, OH, 1958), p. 174.

9. K. A. Jackson, in: Growth and Perfection of Crystals, R. H.
   Doremus, B. W. Roberts, and D. Turnbull, eds. (J. Wiley, New York,
   1958), p. 319.

10. W. K. Burton, N. Cabrera, and F. C. Frank, Phil. Trans. R. Soc.
    London, A243 (1951) 299.

11. F. C. Frank, in: Growth and Perfection of Crystals, R. H. Doremus,
    B. W. Roberts, and D. Turnbull, eds. (J. Wiley, New York, 1958), p.
    304.

12. C. Herring, in: Structure and Properties of Solid Surfaces, R.
    Gomer and F. S. Smith, eds. (Univ. of Chicago Press, Chicago, IL,
    1953), p. 1.

13. P. Hartman and W. G. Perdok, Acta Cryst., 8 (1955) 49; 521.

14. G. Wulff, Z. Krist., 34 (1901) 449.

15. C. Herring, Phys. Rev., 82 (1951) 87.

16. L. E. Murr, Interfacial Phenomena in Metals and Alloys (Addison-Wesley, Reading, MA, 1975), p. 165.

17. M. C. Flemmings, Solidification Processing (McGraw-Hill, New York, 1974).

18. M. Ohara and R. C. Reid, Modeling Crystal Growth Rates from Solution (Prentice Hall, Englewood Cliffs, NJ, 1973).

19. J. Christian, The Theory of the Transformations in Metals (Pergamon, New York, 1965).

20. J. W. Gibbs, The Scientific Papers of J. W. Gibbs, Vol. 1 (Dover, New York, 1961).

21. B. Mutaftschiev, in: Interfacial Aspects of Phase Transformations (D. Reidel Publ. Co., Dordrect, Netherlands, 1982), p. 63.

22. D. A. Porter and K. E. Easterling, Phase Transformations in Metal Alloys (Van Nostrand, UK, 1981), p. 110.

23. D. C. Mattis, The Theory of Magnetism (Harper-Row, New York, 1965); C. Kittel and J. K. Golt, Solid State Phys., 28 (1958) 258.

24. J. W. Cahn and J. E. Hillard, J. Chem. Phys., 28 (1958) 258.

25. J. W. Cahn, W. B. Hillig, and G. W. Sears, Acta Met., 12 (1964) 1421.

26. K. A. Jackson, D. R. Uhlmann, and J. D. Hunt, J. Cryst. Growth, 1 (1967) 1.

27. D. P. Woodruff, The Solid-Liquid Interface (Cambridge Univ., London, 1973).

28. C. Domb and M. S. Green, Phase Transitions and Critical Phenomena (J. Wiley, New York, 1972).

29. J. E. Hillard and J. W. Cahn, Acta Met., 6 (1958) 772.

30. B. Widom, J. Chem. Phys., 43 (1965) 3892.

31. J. Meunier and D. Langevin, J. Physique Lett., 43 (1982) 185.

32. J. W. Cahn and J. E. Hillard, J. Chem. Phys., 31 (1959) 688.

33. J. W. Cahn, J. Chem. Phys., 42 (1965) 93.

34. J. C. Brice, The Growth of Crystals from Liquids (North-Holland, Amsterdam, 1973), p. 117.

35. T. L. Hill, An Introduction to Statistical Thermodynamics (Addison-Wesley, Reading, MA, 1960).

36. W. K. Burton and N. Cabrera, Disc. Faraday Soc., 5 (1949) 33.

37. A. Ookawa, in: Crystal Growth and Characterization, R. Ueda and J. B. Mullin, eds. (North-Holland, Amsterdam, 1975), p. 5.

38. D. Nason and W. A. Tiller, J. Cryst. Growth, 10 (1971) 117.

39. K. Huang, Statistical Mechanics (J. Wiley, New York, 1963).

40. J. R. O'Connor, J. Electrochem. Soc., 110 (1963) 338.

41. J. D. Ayers, R. J. Schaeffer, and M. E. Glicksman, J. Cryst. Growth, 37 (1977) 64.

42. J. E. Lennard-Jones and A. F. Devonshire, Proc. Roy. Soc., A169 (1938) 317.

43. J. D. Bernal, Proc. Roy. Soc., A280 (1954) 299.

44. A. Bonissent, in: Modern Theory of Crystal Growth, A. S. Chernov and H. Muller-Krumbhaar, eds. (Springer-Verlag, Berlin, 1983), p. 1.

45. A. Bonissent and B. Mutaftschiev, Phil. Mag., 35 (1977) 65.

46. F. Spaepen, Acta Met., 23 (1975) 731.

47. A. J. C. Ladd and L. V. Woodcock, Chem. Phys. Let., 51 (1977) 155; J. Phys. C., 11 (1978) 3565.

48. S. Toxvaerd and E. Praestgaard, J. Chem. Phys., 11 (1977) 5291.

49. A. Bonissent, E. Gauthier, and J. L. Finney, Phil. Mag., B39 (1979) 49.

50. J. W. Broughton, A. Bonissent, and F. F. Abraham, J. Chem. Phys., 74 (1981) 4029.

51. D. W. Oxtoby and A. D. J. Haymet, J. Chem. Phys., 76 (1982) 12.

52. F. F. Abraham and Y. Singh, J. Chem. Phys., 67 (1977) 2384.

53. A. D. J. Haymet and D. W. Oxtoby, J. Chem. Phys., 74 (1981) 2559.

54. U. Landman, C. L. Cleveland, C. S. Brown, and R. N. Barnett, in: Nonlinear Phenomena at Phase Transitions and Instabilities, T. Riste, ed. (Plenum, New York, 1981), p. 379.

55. C. L. Cleveland, U. Landman, and R. N. Barnett, Phys. Rev. Lett., 49 (1982) 790.

56. J. W. Cahn and R. Kikuchi, Phys. Rev., B31 (1985) 4300.

57. R. Kikuchi and J. W. Cahn, Acta Met., 27 (1979) 1337.

58. K. A. Jackson, J. Cryst. Growth, 24/25 (1974) 130.

59. S. T. Chui and J. D. Weeks, Phys. Rev., B14 (1976) 4978.

60. D. Turnbull, J. Appl. Phys., 21 (1950) 1022.

61. B. C. Lu and S. A. Rice, J. Chem. Phys., 68 (1978) 5558.

62. N. Eustathopoulos and J. C. Joud, in: Current Topics in Materials Science, Vol. 4, E. Kaldis, ed. (North-Holland, Amsterdam, 1980), p. 281.

63. D. E. Ovsienko and G. A. Alfintsev, in: Crystals, Vol. 2, H. C. Freyhardt, ed. (Springer-Verlag, Berlin, 1980), p. 119.

64. A. A. Chernov, Modern Crystallography III; Crystal Growth (Springer-Verlag, Berlin, 1984).

65. R. Strickland-Constable, Kinetics and Mechanisms of Crystallization (Academic, London, 1968).

66. M. E. Glicksman and C. L. Vold, Acta Met., 17 (1969) 1.

67. S. R. Coriell, S. C. Hardy, and R. F. Sekerka, J. Cryst. Growth, 11 (1971) 53; S. C. Hardy, Phil. Mag., 35 (1977) 471.

68. R. J. Scaeffer, M. E. Glicksman, and J. D. Ayers, Phil. Mag., 32 (1975) 725.

69. B. Mutaftschiev and J. Zell, Surf. Sci., 12 (1968) 317.

70. G. Grange, R. Landers, and B. Mutaftschiev, J. Cryst. Growth, 49 (1980) 343.

71. G. F. Bolling and W. A. Tiller, J. Appl. Phys., 31 (1960) 1345.

72. E. Arbel and J. W. Cahn, Surf. Sci., 66 (1977) 14.

73. W. A. Miller and G. A. Chadwick, The Solidification of Metals, Publ. 110 (Iron and Steel Institute, London, 1968).

74. C. S. Smith, Trans. AIME, 175 (1948) 15.

75. J. D. Ayers and R. J. Schaefer, Scripta Met., 139 (1969) 225.

76. N. Eustathopoulos, Int. Metals Rev., 28 (1983) 189.

77. D. Turnbull, J. Appl. Phys., 20 (1949) 817; J. Chem. Phys., 20 (1952) 411.

78. R. E. Reed-Hill, Physical Metallurgy (D. Van. Norstrad, New York, 1973).

79. D. Turnbull and R. E. Cech, J. Appl. Phys., 21 (1950) 804.

80. W. A. Miller and G. A. Chadwick, Acta Met., 15 (1967) 607.

81. See for example: a) M. J. Stowell, Phil. Mag., 22 (1970) 1; b) J. H. Perepezko, B. A. Mueller, and K. Ohsaka, in: Undercooled Alloy Phases, C. C. Koch and E. W. Collings, eds. (1986 TMS-AIME Annual Spring Meeting, N. Orleans, LA), to be published; c) J. Schade, A. McLean, and W. A. Miller, in: Undercooled Alloy Phases, C. C. Koch and E. W. Collings, eds. (1986 TMS-AIME Annual Spring Meeting, N. Orleans, LA), to be published.

82. J. Zell and B. Mutaftschiev, J. Cryst. Growth, 3/4 (1968) 535.

83. P. Tsakiropoulos, J. Cryst. Growth, 69 (1984) 449.

84. A. S. Skapski, Acta Met., 4 (1956) 576.

85. S. N. Zadumkin, Fiz. Met. Metalloved., 13 (1962) 24.

86. R. H. Ewing, J. Cryst. Growth, 11 (1971) 221.

87. Y. Waseda and W. A. Miller, Trans. Jpn. Met., 19 (1978) 546.

88. T. E. Faber, Theory of Liquid Metals (Cambridge, England, 1972) p. 93.

89. L. D. Landau and E. M. Lifshitz, Statistical Physics (Pergamon, London, 1958), p. 260.

90. A. Voronel, I. Paperno, S. Rabinovich, and E. Lapina, Phys. Rev. Lett., 50 (1983) 247.

91. Y. Saito and H. Muller-Krumbhaar, J. Chem. Phys., 74 (1981) 721.

92. O. N. Mesquita, D. G. Neal, M. Copic, and H. Z. Cummins, Phys. Rev., B29 (1984) 2846.

93. A. Mauger and D. L. Mills, Phys. Rev., B27 (1983) 7736.

94. H. Guttinger, J. H. Bilgram, and W. Kanzig, Phys. Rev., A28 (1983) 2953.

95. P. Boni, J. H. Bilgram, and W. Kanzig, J. Phys. Chem. Solids, 40 (1979) 55.

96. R. A. Brown, J. Kelzer, U. Steiger, and Y. Yeh, J. Phys. Chem., 87 (1983) 4135.

97. U. Durig, J. H. Bilgram, and W. Kanzig, Phys. Rev., A30 (1984) 946.

98. D. Elwell, AACG Newsletter, 15 (1985) 9.

99. P. R. Pennington, S. R. Ravitz, and G. J. Abbaschian, Acta Met., 18 (1970) 943.

100. J. C. Brice and P. A. C. Whiffin, Solid State Electron., 7 (1964) 183.

101. J. A. M. Dikhoff, Solid State Electron, 1 (1960) 202.

102. T. F. Ciszek, J. Cryst. Growth, 10 (1971) 263.

103. J. H. Walton and R. C. Judd, J. Phys. Chem., 18 (1914) 722.

104. G. A. Alfintsev and D. E. Ovsienko, in: Crystal Growth, H. S. Peiser, ed. (Pergamon, Oxford, 1967), p. 757; Dokl. Akad. Nauk. SSSR, 156 (1964) 792.

105. M. Toda, R. Kubo, and N. Saito, Statistical Physics I (Springer-Verlag, Berlin, 1983), p. 118.

106. L. Onsager, Phys. Rev., 65 (1944) 117.

107. H. Muller-Krumbhaar, in: 1976 Crystal Growth and Materials, E. Kaldis and H. J. Scheel, eds. (North-Holland, Amsterdam, 1977), p. 116.

108. J. P. van der Eerden, P. Bennema, and T. A. Cherepanova, Prog. Crystal Growth Charact., 1 (1978) 219, and references therein.

109. H. J. F. Knops, Phys. Rev. Lett., 49 (1977) 776.

110. H. Van Beijeren, Phys. Rev. Lett., 38 (1977) 93.

111. J. D. Weeks, in: Ordering in Strongly Fluctuating Condensed Matter Systems, T. Riste, ed. (Plenum, New York, 1980), p. 293.

112. H. J. Leamy, G. H. Gilmer, and K. A. Jackson, in: Surface Physics of Materials, J. B. Blakely, ed. (Academic, New York, 1975), p. 121.

113. J. M. Kosterlitz and D. J. Thouless, J. Phys. C6 (1973) 1181.

114. C. Jayaprakash and W. F. Saam, Phys. Rev., B30 (1984) 3916.

115. R. H. Swendsen, Phys. Rev., B17 (1978) 3710.

116. H. J. Leamy and G. H. Gilmer, J. Cryst. Growth, 24/25 (1974) 499.

117. G. H. Gilmer and K. A. Jackson, in: 1976 Crystal Growth and Materials, E. Kaldis and H. J. Scheel, eds. (North-Holland, Amsterdam, 1977), p. 79.

118. G. H. Gilmer and P. Bennema, J. Appl. Phys., 43 (1972) 1347.

119. H. Muller-Krumbhaar, in: Current Topics in Materials Science, Vol. 1, E. Kaldis, ed. (North-Holland, Amsterdam, 1978), p. 1.

120. W. Kossel, Nachr. Ges. Wiss. Gottingen, Math-Physik, Kl (1927) 135.

121. See for example: L. Coudurier, N. Eustathopoulos, P. Desre, and A. Passerone, Acta Met., 26 (1978) 465.

122. K. A. Jackson, in: Progress in Solid State Chemistry, Vol. 4, H. Reiss, ed. (Pergamon, London, 1967), p. 53.

123. D. Nenov and V. Stoyanova, J. Cryst. Growth, 46 (1979) 779.

124. A. Pavlovska and D. Nenov, J. Cryst. Growth, 12 (1972) 9.

125. K. A. Jackson and C. E. Miller, J. Cryst. Growth, 40 (1977) 169.

126. A. Pavlovska and D. Nenov, J. Cryst. Growth, 8 (1971) 209.

127. A. Pavlovska, J. Cryst. Growth, 46 (1979) 551.

128. T. Ohachi and I. Taniguchi, J. Cryst. Growth, 65 (1983) 84.

129. D. Balibar and B. Castaing, J. Physique Lett., 41 (1980) 329.

130. P. E. Wolf, F. Gallet, S. Balibar, E. Rolley, and P. Nozieres, J. Physique, 46 (1985) 1987; also, see references herein.

131. A. Passerone and N. Eustathopoulos, J. Cryst. Growth, 49 (1980) 757.

132. A. Passerone, R. Sangiorgi, and N. Eustathopoulos, Scripta Met., 14 (1980) 1089.

133. See for example: H. J. Human, J. P. Van der Eerden, L. A. M. J. Jetten, J. G. M. Oderkerken, J. Cryst. Growth, 51 (1981) 589.

134. C. Rottman, M. Wortis, J. C. Heyraud, and J. J. Metois, Phys. Rev. Lett., 52 (1984) 1009 and references therein.

135. L. D. Landau, Collected Papers, D. Terhaar, ed. (Gordon-Breach, New York, 1965), p. 540.

136. A. F. Andreev, Sov. Phys. JETP, 53 (1981) 1063.

137. C. Rottman, M. Wortis, Phys. Rev., B29 (1984) 328.

138. C. Jayaprakash, W. F. Saam, and S. Teitel, Phys. Rev. Lett., 50(1983) 2017.

139. V. L. Pokrovsky and A. L. Talapov, Phys. Rev. Lett., 42 (1979) 65.

140. E. E. Gruber and W. W. Mullins, J. Phys. Chem. Solids, 28 (1967) 875.

141. M. Jaubert, A. Glachant, M. Bienfait, and G. Boato, Phys. Rev. Lett., 46 (1981) 1679.

142. J. Metois and J. C. Heyraud, J. Cryst. Growth, 57 (1982) 487.

143. J. C. Heyraud and J. J. Metois, Surf. Sci., 128 (1983) 334.

144. D. S. Fisher and J. D. Weeks, Phys. Rev. Lett., 50 (1983) 1077.

145. J. D. Weeks and G. H. Gilmer, Adv. Chem. Phys., 40 (1979) 157.

146. J. P. Van der Eerden, C. van Leeuwen, P. Bennema, W. L. van der Kruk, and B. P. Th. Veltman, J. Appl. Phys., 48 (1977) 2124.

147. C. E. Miller, J. Cryst. Growth, 42 (1977) 357.

148. J. R. Green and W. T. Griffith, J. Cryst. Growth, 5 (1969) 171.

149. W. T. Griffith, J. Cryst. Growth, 47 (1979) 473.

150. T. Watanable, J. Cryst. Growth, 50 (1980) 729.

151. M. E. Glicksman and R. J. Schaefer, J. Cryst. Growth, 1 (1967) 297.

152. W. B. Hillig and D. Turnbull, J. Chem. Phys., 24 (1956) 914.

153. D. Turnbull, J. Chem. Phys., 66 (1962) 609.

154. D. Turnbull, Solid State Phys., 3 (1956) 279.

155. A. G. Walton, in: Nucleation, A. C. Zettlemoyer, ed. (Marcel-Dekker, New York, 1969), p. 245.

156. D. Froschhammer, H. M. Tensi, H. Zoller, and V. Feurer, Met. Trans., B11 (1980) 169.

157. R. Becker, Disc. Faraday Soc., 5 (1949) 45.

158. R. Becker and W. Doring, Ann. Physik (Leipzig), 24 (1935) 719.

159. R. Kaischev and I. M. Stranskii, Z. Phys. Chem., A170 (1934) 295.

160. M. Volmer and M. Marder, Z. Phys. Chem., A154 (1931) 97.

161. J. B. Zeldovich, Acta Physicocima, USSR, 18 (1943) 1.

162. J. L. Katz, in: Interfacial Aspects of Phase Transformations, B. Mutaftschiev, ed. (D. Reidel Publ. Co., Dordrect, Netherlands, 1982), p. 261.

163. B. Lewis, J. Cryst. Growth, 21 (1974) 29.

164. W. B. Hillig, Acta Met., 14 (1966) 1808.

165. J. P. Hirth, Acta Met., 7 (1959) 755.

166. A. M. Ovrutskii, Sov. Phys.-Cryst., 26 (1981) 242.

167. V. V. Voronkov, in: Modern Theory of Crystal Growth, A. S. Chernov and H. Muller-Krumbhaar, eds. (Springer-Verlag, Berlin, 1983), p. 75.

168. A. E. Nielsen, Kinetics of Precipitation (Pergamon, New York, 1964), p. 46.

169. A. N. Kolmogorov, Izv. Akad. Nauk, SSSR, Ser. Math., 3 (1937) 355.

170. M. Hoyashi, J. Phys. Soc. Japan, 35 (1973) 614.

171. V. Bertocci, Surf. Sci., 159 (1969) 286.

172. M. S. Viola, K. A. Van Wormer, and G. D. Botsaris, J. Cryst. Growth, 47 (1979) 127.

173. G. H. Gilmer, J. Cryst. Growth, 49 (1980) 465.

174. G. H. Gilmer, J. Cryst. Growth, 42 (1977) 3.

175. D. Kashchiev, J. Cryst. Growth, 40 (1977) 29.

176. C. Van Leeuwen and J. P. Van der Eerden, Surf. Sci., 64 (1977) 237.

177. G. J. Abbaschian, Ph.D. Thesis, Univ. of California-Berkeley (1971).

178. W. B. Hillig, in: Growth and Perfection of Crystals, R. H. Doremus, B. W. Roberts, and D. Turnbull, eds. (John Wiley, New York, 1959), p. 350.

179. A. M. Ovrutskii and T. M. Mal'chenko, Sov. Phys. Cryst., 23 (1978) 374.

180. V. V. Voronkov, Sov. Phys. Cryst., 17 (1972) 807.

181. A. S. Michaels, P. L. T. Brian, and P. R. Sperry, J. Appl. Phys., 37 (1966) 4649.

182. V. Bostanov, W. Obretenov, G. Staikov, D. K. Roe, and E. Budevski, J. Cryst. Growth, 52 (1981) 761.

183. F. C. Frank, Disc. Faraday Soc., 5 (1949) 48.

184. G. W. Sears, J. Chem. Phys., 23 (1955) 1630.

185. F. C. Frank, J. Cryst. Growth, 51 (1981) 367.

186. P. Bennema, J. Cryst. Growth, 69 (1984) 182.

187. W. J. Barnes and F. P. Price, Polymer, 5 (1964) 283.

188. N. Cabrera and M. M. Levine, Phil. Mag., 1 (1956) 450.

189. K. A. Jackson, in: Crystal Growth: A Tutorial Approach, W. Bardsley, D. T. J. Hurle, and J. B. Mullin, eds. (North-Holland, Amsterdam, 1979), p. 139.

190. E. Budevski, G. Staikov, and V. Bostanov, J. Cryst. Growth, 29 (1975) 316.

191. A. A. Chernov, Sov. Phys. Usp., 4 (1961) 116.

192. I. Sunagawa and P. Bennema, J. Cryst. Growth, 53 (1981) 490.

193. See for example: a) B. Lewis, J. Cryst. Growth, 21 (1974) 40; b) P. Bennema, in: Crystal Growth, H. S. Peiser, ed. (Pergamon, Oxford, 1967), p. 43.

194. H. A. Wilson, Philos. Mag., 50 (1900) 238.

195. J. Frenkel, Phys. Z. Sowjetunion, 1 (1932) 438.

196. K. A. Jackson and B. Chalmers, Can. J. Phys., 34 (1956) 473.

197. K. A. Jackson, Mat. Sci. Engr., 65 (1984) 7.

198. W. Ruhl and P. Hilsch, Z. Phys., B26 (1977) 161.

199. F. Spaepen and D. Turnbull, in: Laser-Solid Interactions and Laser Processing, S. D. Ferris, H. J. Leamy, and J. M. Poate, eds., AIP Conf. Proc., 50 (1979) 73.

200. S. R. Coriell and D. Turnbull, Acta Met., 30 (1982) 2135.

201. J. L. Walker, results cited in: Principles of Solidification, B. Chalmers (Wiley, New York, 1964), p. 114.

202. J. Q. Broughton, G. H. Gilmer, and K. A. Jackson, Phys. Rev. Lett., 49 (1982) 1496.

203. J. Q. Broughton and G. H. Gilmer, J. Chem. Phys., 79 (1983) 5119.

204. F. Rosenberger, in: Interfacial Aspects of Phase Transformations, B. Mutaftschiev, ed. (D. Reidel, Dordrect, Netherlands, 1982), p. 315.

205. K. A. Jackson, private communication.

206. J. D. E. McIntyre and W. F. Peck, Jr., J. Electrochem. Soc., 123 (1976) 1800.

207. J. M. Cases and B. Mutaftschiev, Surf. Sci., 9 (1960 57.

208. V. V. Voronkov, Sov. Phys.-Cryst., 19 (1974) 296.

209. G. J. Abbaschian and R. Mehrabian, J. Cryst. Growth, 43 (1978) 433.

210. E. A. Brener and D. E. Temkin, Sov. Phys.-Cryst., 30 (1985) 140.

211. M. J. Aziz, Appl. Phys. Lett., 43 (1983) 552.

212. R. Kern, in: Growth of Crystals, Vol. 8, N. N. Sheftal, ed. (Consultants Bureau, New York, 1969), p. 3.

213. R. Boistelle, in: Industrial Crystallization, J. W. Mullin, ed. (Plenum Press, New York, 1976), p. 203.

214. B. Simon and R. Boistelle, J. Cryst. Growth, 52 (1981) 779.

215. N. V. Stoichev, G. A. Alftintsev, and D. E. Ovsienko, Sov. Phys.-Cryst., 20 (1976) 504.

216. V. T. Borisov and Y. E. Matveev, Sov. Phys.-Cryst., 14 (1970) 765; 16 (1971) 207.

217. M. J. Aziz, in Undercooled Alloy Phases, E. W. Collings and C. C. Koch, eds. (TMS-AIME Spring 1986 Meeting, New Orleans, LA), to be published.

218. H. Beneking, W. Vits, in: Proc. 2nd Int. Symp. on GaAs, Inst. Phys. Soc. Conf. Ser. No. 7, p. 96.

219. See for example: a) F. Rosenberger, Fundamentals of Crystal Growth I (Springer-Verlag, Berlin, 1979); b) R. L. Parker, Sol. State Phys., 25 (1970) 151.

220. S. D. Peteves and G. J. Abbaschian, in: Undercooled Alloy Phases, E. W. Collings and C. C. Koch, eds., TMS-AIME Symp. Proc., 1986 Spring Meeting (New Orleans, LA), to be published.

221. P. Bennema, Phys. Stat. Sol., 17 (1966) 555.

222. See for example reviews in Refs. (25) and (26); for recent example see: a) K. F. Kobayashi, M. I. Kumikawa, and P. H. Shingu, J. Cryst. Growth, 67 (1984) 85.

223. G. A. Colligan and B. J. Bayles, Acta Met., 10 (1962) 895.

224. J. J. Kramer and W. A. Tiller, J. Chem. Phys., 42 (1965) 257.

225. D. A. Rigney and J. M. Blakely, Acta Met., 14 (1966) 1375.

226. G. T. Orrok, Ph.D. Thesis, Harvard University, 1958.

227. A. Rosenberg and W. C. Winegard, Acta Met., 21 (1954) 342.

228. G. J. Abbaschian and M. E. Eslamloo, J. Cryst. Growth, 28 (1975) 372.

229. G. L. F. Powell, G. A. Colligan, V. A. Surprenant, and V. Urquhart, Met. Trans., A8 (1977) 971.

230. V. V. Nikonova and D. E. Temkin, in: Growth and Imperfections of Metallic Crystals, D. E. Ovsienko, ed. (Consultants Bureau, New York, 1967), p. 43.

231. J. J. Favier and M. Turpin, presentation at I.C.C.G.5, Boston, MA, July 17-22, 1977.

232. R. T. Delves, in: Crystal Growth, Vol. 1, B. R. Pamplim, ed., (Pergamon Press, Oxford, 1974), p. 40.

233. R. F. Sekerka, in: Crystal Growth: An Introduction, P. Hartman, ed. (North-Holland, Amsterdam, 1973), p. 403.

234. D. J. Wollkind, in: Preparation and Properties of Solid State Materials, Vol. 4, W. R. Wilcox, ed. (M. Dekker, New York, 1979), p. 111.

235. J. S. Langer, Rev. Mod. Phys., 52 (1980) 1.

236. A. A. Chernov, Sov. Phys.-Cryst., 16 (1972) 734.

237. W. Rutter and B. Chalmers, Can. J. Phys., 35 (1953) 15.

238. W. A. Tiller, K. A. Jackson, J. W. Rutter, and B. Chalmers, Acta Met., 1 (1953) 428.

239. W. W. Mullins and R. F. Sekerka, J. Appl. Phys., 34 (1963) 323.

240. W. W. Mullins and R. F. Sekerka, J. Appl. Phys., 35 (1964) 444.

241. V. V. Voronkov, Sov. Phys. Solid State, 6 (1965) 2378.

242. R. T. Delves, Phys. Stat. Sol., 16 (1966) 621.

243. R. F. Sekerka, in: Crystal Growth, H. S. Peiser, ed. (Pergamon, Oxford, 1967), p. 691.

244. R. F. Sekerka, J. Appl. Phys., 36 (1965) 264.

245. S. R. Coriell and R. F. Sekerka, J. Cryst. Growth, 61 (1983) 499.

246. F. C. Frank, Proc. Roy. Soc., A201 (1950) 56.

247. S. R. Coriell and R. L. Parker, J. Appl. Phys., 37 (1966) 1548.

248. J. W. Cahn, in: Crystal Growth, H. S. Peiser, ed. (Pergamon Press, Oxford, 1967), p. 681.

249. S. R. Coriell and R. L. Parker, in: Crystal Growth, H. S. Peiser, ed. (Pergamon Press, Oxford, 1967), , p. 703.

250. S. R. Coriell and R. L. Parker, J. Appl. Phys., 36 (1965) 632.

251. G. R. Kotler and W. A. Tiller, in: Crystal Growth, H. S. Peiser, ed. (Pergamon Press, Oxford, 1967), p. 721.

252. S. R. Coriell and S. C. Hardy, J. Appl. Phys., 40 (1969) 1652.

253. S. R. Coriell and R. F. Sekerka, in: Rapid Solidification Processing: Principles and Technologies II, R. Mehrabian, B. H. Kear, and M. Cohen, eds. (Claitor's, Baton Rouge, LA, 1980), p. 35.

254. J. W. Cahn, S. R. Coriell, and W. J. Boettinger, in: Laser and Electron Beam Processing of Materials, C. W. White and P. S. Peercy, eds. (Academic Press, New York, 1980), p. 89.

255. W. H. Boettinger, S. R. Coriell, and R. F. Sekerka, Mat. Sci., Engr., 65 (1984) 27.

256. A. A. Chernov. J. Cryst. Growth, 24/25 (1974) 11.

257. R. G. Seidensticker, in: Crystal Growth, H. S. Peiser, ed. (Pergamon Press, Oxford, 1967), p. 709.

258. L. A. Tarshis and W. A. Tiller, in: Crystal Growth, H. S. Peiser, ed. (Pergamon Press, Oxford, 1967), , p. 733.

259. S. R. Coriell and R. F. Sekerka, J. Cryst. Growth, 34 (1976) 157.

260. C. M. Lawrence and D. Elwell, J. Cryst. Growth, 34 (1976) 316.

261. S. R. Coriell, M. R. Cordes, W. J. Boettinger, and R. F. Sekerka, J. Cryst. Growth, 49 (1980) 13.

262. S. R. Coriell and R. F. Sekerka, J. Cryst. Growth, 46 (1979) 479.

263. S. R. Coriell, R. F. Boisvert, R. G. Rehm, and R. F. Sekerka, J. Cryst. Growth, 54 (1981) 167.

264. S. C. Hardy and S. R. Coriell, J. Cryst. Growth, 3/4 (1968) 569; 5 (1969) 329; 7 (1970) 147; J. Appl. Phys., 39 (1968) 3505.

265. D. E. Holmes and H. C. Gatos, J. Appl. Phys., 52 (1981) 2071.

266. K. M. Kim, J. Cryst. Growth, 44 (1978) 403.

267. T. Sato and G. Ohira, J. Cryst. Growth, 40 (1977) 78.

268. K. Shibata, T. Sato, and G. Ohira, J. Cryst. Growth, 44 (1978) 419.

269. T. Sato, K. Ito, and G. Ohira, Trans. Jap. Inst. of Metals, 21 (1980) 441.

270. S. O'Hara and A. F. Yue, J. Phys. Chem. Solids, 28 (1967) 2105.

271. D. T. J. Hurle, J. Cryst. Growth, 5 (1969) 162.

272. J. J. Favier, J. Berthier, Ph. Arragon, Y. Malmejac, V. T. Khryapov, and I. V. Barmin, Acta Astronautica, 9 (1982) 255.

273. J. Narayan, J. Cryst. Growth, 59 (1982) 583.

274. W. J. Boettinger, D. Schechtman, R. J. Schaeffer, and F. S. Biancaniello, Met. Trans., A15 (1984) 55.

275. K. G. Davis and P. Fryzuk, J. Cryst. Growth, 8 (1971) 57.

276. J. P. Dismukes and W. M. Yim, J. Cryst. Growth, 22 (1974) 287.

277. J. C. Baker and J. W. Cahn, in: Solidification (ASM, Metals Park, OH, 1970), p. 23.

278. K. A. Jackson, G. H. Gilmer, and H. J. Leamy, in: Laser and Electron Beam Processing of Materials, C. W. White and P. S. Peercy, eds. (Academic, New York, 1980), p. 104.

279. M. J. Aziz, J. Appl. Phys., 53 (1982) 1158.

280. A. A. Chernov, Sov. Phys.-Uspekhi, 13 (1970) 101.

281. M. J. Aziz, in: Rapid Solidification Processing Principles and Technologies III, R. Mehrabian, ed. (NBS, Gaithersburg, MD, 1982), p. 113.

282. G. J. Gilmer, Mat. Sci. Engr., 65 (1984) 15.

283. R. N. Hall, Phys. Rev., 88 (1952) 139.

284. M. J. Aziz, in: MRS Symp. Proc., Vol. 23, J. C. C. Fan and N. M. Johnson, eds. (Elsevier, New York, 1984), p. 369.

285. W. A. Tiller, K. A. Jackson, J. W. Rutter, and B. Chalmers, Acta Met., 1 (1953) 428.

286. V. G. Smith, W. A. Tiller, and J. W. Rutter, Can. J. Phys., 33 (1955) 723.

287. J. A. Burton, R. C. Prim, and W. P. Slichter, J. Chem. Phys., 21 (1953) 1987.

288. J. R. Carruthers, in: Preparation and Properties of Solid State Materials, Vol. 3, W. R. Wilcox and R. A. Lefever, eds. (Marcel-Dekker, New York, 1977), p. 1.

289. W. R. Wilcox, in: Preparation and Properties of Solid State Materials, Vol. 1, W. R. Wilcox and R. A. Lefever, eds. (Marcel-Dekker, New York, 1977), p. 41.

290. D. T. J. Hurle, in: Crystal Growth 1971, R. A. Laudise, J. B. Mullin, and B. Mutaftschiev, eds., (North-Holland, Amsterdam, 1972), p. 39.

291. J. S. Turner, Buoyancy Effects in Fluids (Cambridge Univ. Press, Cambridge, England, 1973).

292. F. K. Moore, Theory of Laminal Flows (Princeton Univ. Press, Princeton, NJ, 1964).

293. I. G. Currie, Fundamental Mechanics of Fluids (McGraw-Hill, New York, 1974).

294. W. R. Lindberg and R. D. Haberstroh, AIChE Journal, 18 (1972) 243.

295. S. R. Coriell, M. R. Cordes, W. J. Boettinger, and R. F. Sekerka, J. Cryst. Growth, 49 (1980) 13.

296. J. D. Verhoeven, K. K. Kingery, and R. Hofer, Met. Trans., B6 (1975) 647.

297. K. Shibata, T. Sato, and G. Ohira, J. Cryst. Growth, 44 (1978) 435.

298. R. M. Sharp and A. Hellawell, J. Cryst. Growth, 8 (1970) 29; J. Cryst. Growth, 12 (1972) 261.

299. R. G. Pirich, in: Materials Processing in the Reduced Gravity Environment of Space, G. E. Rindone, ed. (Elsevier, New York, 1982), p. 593.

300. G. J. Galvin, M. O. Thompson, J. W. Mayer, R. B. Hammond, N. Paulter, and P. S. Peercy, Phys. Rev. Lett., 48 (1982) 33.

301. J. J. Kramer and W. A. Tiller, J. Chem. Phys., 37 (1962) 841.

302. W. A. Tiller, Acta Met., 14 (1966) 1383.

303. D. A. Rigney and J. M. Blakely, Acta Met., 14 (1966) 1384.

304. R. F. Sekerka, J. Chem. Phys., 43 (1967) 2344.

305. R. J. Schaefer and M. E. Glicksman, Acta Met., 16 (1968) 1009.

306. See for example: a) W. G. Pfann, K. E. Benson, and J. H. Werick, J. Electron., 2 (1957) 597. b) M. J. Wargo and A. F. Witt, J. Cryst. Growth, 66 (1984) 289. c) R. P. Silbestein, D. R. Larson, Jr., and B. Dressler, Met. Trans., A15 (1984) 2147.

307. J. D. Werhoeven and E. D. Gibson, J. Cryst. Growth, 5 (1969) 235.

308. J. J. Favier, D. Sc. Thesis, Grenoble University, France (1977).

309. D. E. Temkin, Sov. Phys.-Dokl., 5 (1960) 609.

310. M. Hansen and K. Anderko, Constitution of Binary Alloys (McGraw-Hill, New York, 1958).

311. J. Alvarez, M.S. Thesis, University of Florida, 1984.

312. S. D. Peteves, J. Alvarez, and G. J. Abbaschian, in: Rapidly Solidified Metastable Materials, B. H. Kear and B. C. Giessen, eds. (Elsevier, New York, 1984), p.15.

313. S. D. Peteves, J. A. Sarreal, and G. J. Abbaschian, in: Semiconductor on Insulator/Thin Film Transistor Technology, A. A. Chiang, et al., eds. (MRS 1985 Fall Meeting, Boston, MA), to be published.

314. D. K. C. Macdonald, Thermoelectricity — An Introduction to the Principles (John Wiley, New York, 1962).

315. P. J. Blatt, P. A. Schroeder, and C. L. Foiler, Thermoelectric Power of Metals (Plenum, New York, 1974), p. 1.

316. D. I. Finsch, in: Temperature, Its Measurement and Control in Science and Industry, Vol. 3(2), C. M. Herzfeld, ed. (Reinhold, New York, 1962), p. 3.

317. J. E. Bauerle, P. H. Sutter, and R. W. Ure, Jr., in: Thermoelectricity — Science and and Engineering, R. R. Heikes and R. W. Ure, eds. (Interscience, New York, 1961), p. 285.

318. A. R. Ubbelohde, Proc. Roy. Soc., A293 (1966) 291.

319. J. E. Nye, Physical Properties of Crystals, Their Representation by Tensors and Matrices (Oxford University Press, London, 1976), p. 215.

320. C. A. Domenicali, Phys. Rev., 92 (1953) 293.

321. J. Tauc, Photo and Thermoelectric Effects in Semiconductors (Pergamon, New York, 1962), p. 179.

322. For the liquid Ga: a) M. C. Bellissent-Funel, R. Bellissent, andG. Taurand, J. Phys. F: Metal Phys., 11 (1981) 139. b) M. Pokorny and H. U. Aström, J. Phys. F: Metal Phys., 6 (1976) 559. For single crystals of Ga: c) M. Olsen-Bar and R. W. Powell, Proc. Roy. Soc. (London), A209 (1951) 542. d) M. Yaqub and J. F. Cochran, Phys. Rev. 137 (1965) A1182; 140 (1965) A2174. For supercooled liquid and single crystals: e) R. W. Powell, Proc. Roy Soc. (London), A209 (1951) 525.

323. D. R. Hamilton and R. G. Seidensticker, J. Appl. Phys., 31 (1960) 1165; 34 (1963) 1450.

324. H. N. Fletcher, J. Cryst. Growth, 35 (1976) 39.

325. J. M. R. Cotterill, J. Cryst. Growth, 40 (1980) 582.

326. K. Kamada, Progr. Cryst. Growth Charact., 3 (1981) 309.

327. J. R. Owen and E. A. D. White, J. Cryst. Growth, 42 (1977) 449.

328. P. Rudolfh, P. Fille, Ch. Genzel, and T. Boeck, Crystal Res. and Technol., 19 (1984) 1073.

329. S. Larsson, L. Broman, C. Raxbergh, and A. Lodding, Z. Naturforsch, 25a (1970) 1472.

330. V. P. Skripov. G. T. Butorin, and V. P. Koverda, Fiz. Met. Metalloved., 31 (1971) 790.

331. Y. Miyazawa and G. M. Pound, J. Cryst. Growth, 23 (1974) 45.

332. a) M. Volmer and O. Z. Schmidt, Z. Phys. Chem. (Leipzig), 85 (1937) 467. b) M. P. Dokhov, S. N. Zadumkin, and A. A. Karashaev, Russ. J. Phys. Chem., 45 (1971) 1061. c) H. Wenzl, A. Fattah, D. Gustin, M. Mihelcic, and W. Uelhoff, J. Cryst. Growth, 43 (1978) 607.

333. a) S. S. Dshandzhgava, E. F. Sidokhin, O. V. Utenkova, and G. V. Shcheberdinskii, Metallofizika, 4 (1982) 118. b) A. C. Carter and C. G. Wilson, Brit. J. Appl. Phys., 1 (1968) 515.

334. M. Elwenspoek and J. P. van der Eerden, J. Phys. A, to be published; see also: V. V. Podolinski, J. Cryst. Growth, 46 (1979) 511.

335. P. Bennema, R. Kern, and B. Simon, Phys. Stat. Sol., 19 (1967) 211.

336. J. S. Langer, R. F. Sekerka, and T. Fujioka, J. Cryst. Growth, 44 (1978) 414.

337. V. T. Borisov, I. N. Golikov, and Y. E. Matveev, Sov. Phys.-Crsty. 13 (1969) 756.

338. a) I. Gutzow, in: 1976 Crystal Growth and Materials, E. Kaldis and H. J. Scheel, eds. (North-Holland, Amsterdam, 1977), p. 379. b) I. Gutzow and E. Pancheva, Kristall. U. Technik, 11 (1976) 793.

339. W. J. Boettinger, F. S. Biancaniello, and S. R. Coriell, Met. Trans., A12 (1981) 321.

340. J. D. Verhoeven, Trans. TMS-AIME, 242 (1968) 1940.

341. W. R. Wilcox, J. Appl. Phys., 35 (1963) 636.

342. P. de la Breteque, Gallium, Bulletin d'Information et de Bibliographie, No. 12 (Alusuisse France, Marseille, 1974), p. 11.

343. R. Kofman, P. Cheyssac, and J. Richard, Phys. Rev., B16 (1977) 5216.

344. H. E. Sostman, Rev. Scient. Instrum., 48 (1977) 127.

345. G. H. Wagner and W. H. Gitzen, J. Chem. Educ., 29 (1952) 162.

346. A. Defrain, Metaux, 417 (1960) 248.

347. G. B. Adams, Jr., H. L. Johnston, and E. C. Kerr, J. Am. Chem. Soc., 74 (1952) 4784.

348. R. W. Powell, M. J. Woodman, and R. P. Tye, Brit. J. Appl. Phys., 14 (1963) 432.

349. Y. Takahashi, H. Kadokura, H. Yokokawa, J. Chem. Therm., 15 (1983) 65.

350. C. J. Smithells, Metals Reference Book, 6th ed., E. A. Brandes, ed. (Butterworths, London, 1983).

351. K. Wade and A. J. Banister, The Chemistry of Al, Ga, In, and Tl (Pergamon Press, New York, 1974).

352. L. Bosio and C. G. Windsor, Phys. Rev. Lett., 35 (1975) 1652.

353. J. H. Perepezko and D. H. Rasmussen, in: Proc. 17th AIAA Ann. Meeting, New Orleans, LA, 1979.

354. O. Hunderi and R. Ryberg, J. Phys., F4 (1974) 2096.

355. F. Greuter and P. Oelhapen, Z. Phyzik, B34 (1979) 123.

356. D. I. Page, D. H. Saunderson, and C. G. Windsor, J. Phys., C6 (1973) 212.

357. M. I. Barker, M. W. Johnson, N. H. March, and D. I. Page, in: Properties of Liquid Metals: Proceedings, S. Takeuchi, ed. (Halsted Press, New York, 1973), p. 99.

358. A. Defrain, J. Chim. Phys., 74 (1977) 851.

359. L. Bosio, R. Cortes, and A. Defrain, J. Chim. Phys., 70 (1973) 357.

360. R. D. Heyding, W. Keeney, and S. L. Segel, J. Phys. Chem. Solids, 34 (1973) 133.

361. A. J. MacKintosh, K. N. Ishihara, and P. H. Shingu, Scripta Met., 17 (1983) 1441.

362. J. D. Stroud and M. J. Stott, J. Phys., F5 (1975) 1667.

363. L. Bosio, A. Defrain, and I. Epelboin, C. R. Acad. Sci., 268 (1969) 1344.

364. A. Jayaraman, W. Klement, R. Newton, and G. J. Kennedy, J. Phys. Chem. Solids, 24 (1963) 7.

365. A. R. Ubbelohde, Melting and Crystal Structure (Clarendon Press, Oxford, 1965).

366. G. Fritsch, R. Lachner, H. Diletti, and E. Lüscher, Phil. Mag., A46 (1982) 829.

367. J. K. Kristensen, R. M. J. Cotterill, Phil. Mag., 36 (1977) 347.

368. G. Fritsch and E. Lüscher, Phil. Mag., A48 (1983) 21.

369. A. R. Ubbelohde, private communication.

370. H. Wenzl ad G. Mair, Z. Physik, B21 (1975) 95.

371. U. König and W. Keck, J. Less-Common Met., 90 (1983) 299.

372. A. R. Miedema and F. J. A. den Broeder, Z. Metallk., 70 (1979) 14.

373. G. J. Abbaschian, J. Less-Common Met., 40 (1975) 329.

374. W. R. Tyson and W. A. Miller, Surf. Sci., 62 (1977) 267.

375. A. A. Karashaev, S. N. Zadumkin, and A. I. Kukhno, Russ. J. Phys. Chem., 3 (1967) 654.

376. E. F. Broome and H. A. Walls, Trans. TMS-AIME, 245 (1969) 739.

377. J. Petit and n. H. Nachtrieb, J. Chem. Phys., 24 (1956) 1027.

378. F. M. Jaeger, P. Terpstra, and H. G. K.. Westenbrink, Z. Krist., 66 (1927) 195.

379. F. Laves, Z. Krist., 84 (1933) 256.

380. A. J. Bradley, Z. Krist., A91 (1935) 302.

381. H. E. Swanson and R. K. Fuyat, Nat. Bur. Stand. Circular, No. 539, 3 (1953) 9.

382. B. D. Sharma and J. Donohue, Z. Krist., 117 (1962) 293.

383. C. S. Barrett and F. J. Spooner, Nature, 207 (1965) 1382.

384. J. Donohue, The Structure of the Elements (J. Wiley, New York, 1972). p. 236.

385. R. W. Powell, Nature, 164 (1949) 153.

386. R. W. Powell, Nature, 166 (1950) 1110.

387. L. Pauling, J. Amer. Chem. Soc., 69 (1947) 542.

388. J. C. Slater, G. F. Koster, and J. H. Wood, Phys. Rev., 126 (1962) 1307.

389. V. Heine, J. Phys., C1 (1968) 222.

390. C. G. Wilson, J. Less-Common Met., 5 (1963) 245.

391. F. J. Spooner and C. G. Wilson, J. Less-Common Met., 10 (1966) 169.

392. N. Durbec, B. Pichaud, and F. Minari, J. Less-Common Met., 82 (1981) 373.

393. N. Burble-Durbec, B. Pichaud, and F. Minari, J. Less-Common Met., 98 (1984) 79.

394. C. G. Wilson, Trans. AIME, 224 (1962) 1293.

395. P. Ascarelli, Phys. Rev., 143 (1966) 36.

396. R. Brözel, D. Handtmann, and H. Richter, Z. Physik, 169 (1978) 374.

397. S. F. French, D. J. Sanders, and G. W. Ingle, J. Phys. Chem., 42 (1938) 265.

398. W. J. Svirbely and S. M. Selis, J. Phys. Chem., 58 (1954) 33.

399. R. M. Evans and R. I. Jaffee, Trans. AIME, 194 (1952) 153.

400. J. P. Denny, J. H. Hamilton, and J. R. Lewis, Trans. AIME, 194 (1952) 39.

401. M. Hansen, Constitution of Binary Alloys, 2nd ed. (McGraw-Hill, New York, 1958), p. 745.

402. A. Gokhale, private communication.

403. P. E. Eriksson, S. J. Larsson, and A. Lodding, Z. Naturforsch, 29a (1974) 893.

404. K. Suzuki and O. Vemura, J. Phys. Chem. Sol., 32 (1971) 1801.

405. B. Predel and A. Eman, J. of the Less-Common Metals, 19 (1969) 385.

406. O. J. Kleppa, J. Chem. Phys., 18 (1950) 1331.

407. H. S. Carslaw and J. C. Jaeger, Conduction of Heat in Solids, 2nd ed. (Oxford Univ. Press, London, 1959).

408. F. C. Frank, Disc. Faraday Soc., 5 (1949) 189.

409. T. W. Clyne, Mat. Sci. Eng., 65 (1984) 111.

410. R. J. Schaeffer and M. E. Glicksman, J. Cryst. Growth, 5 (1969) 44.

411. N. Shamsundar and E. M. Sparrow, J. Heat Transfer, 97 (1975) 333.

412. C. G. Levi Rodriguez, Ph.D. Thesis, Univ. of Illinois, at Urbana-Champaign (1981).

413. E. R. G. Eckert and R. M. Drake, Jr., Heat and Mass Transfer, 2nd Ed. (McGraw-Hill, New York, 1959), p. 239.

414. T. C. Wang, unpublished work, Univ. of Florida (1985).

415. L. J. Briggs, J. Chem. Phys., 26 (1957) 784.

416. C. Y. Ho, R. W. Powell, and P. E. Liley, J. of Phys. and Chem. Ref. Data, 1 (1972) 279.

417. CRC Handbook of Chemistry and Physics, 65th ed., R. C. Weast, ed. (CRC Press, Boca Raton, FL).

418. J. P. Candito, private communication.

419. J. C. Brice, J. Cryst. Growth, 1 (1967) 218.

BIOGRAPHICAL SKETCH

The author was born on March 22, 1957 in Lamia, Greece. He received his diploma in metallurgical and mining engineering from the National Technical University, Athens, Greece, in 1980. Afterwards, he attended the George Washington University in Washington, D.C. and received a Master of Science degree in materials engineering and solid mechanics in 1982. He entered the University of Florida in August, 1982 and has been a candidate for the Doctor of Philosophy degree in materials science and engineering since October, 1983. He is a member of Tau Beta Pi, Alpha Sigma Mu, American Association of Crystal Growth, Materials Research Society, American Institute of Mining, Metallurgical and Petroleum Engineers, American Society of Metals, and the Technical Chamber of Greece.
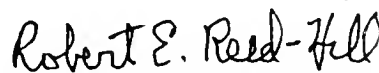
I certify that I have read this study and that in my opinion it conforms to acceptable standards of scholarly presentation and is fully adequate, in scope and quality, as a dissertation for the degree of Doctor of Philosophy.

Gholamreza J. Abbaschian,
Chairman
Professor of Materials Science
and Engineering

I certify that I have read this study and that in my opinion it conforms to acceptable standards of scholarly presentation and is fully adequate, in scope and quality, as a dissertation for the degree of Doctor of Philosophy.

Robert T. DeHoff, Co-Chairman
Professor of Materials Science
and Engineering

I certify that I have read this study and that in my opinion it conforms to acceptable standards of scholarly presentation and is fully adequate, in scope and quality, as a dissertation for the degree of Doctor of Philosophy.

Robert E. Reed-Hill
Professor Emeritus of
Materials Science and
Engineering

I certify that I have read this study and that in my opinion it conforms to acceptable standards of scholarly presentation and is fully adequate, in scope and quality, as a dissertation for the degree of Doctor of Philosophy.
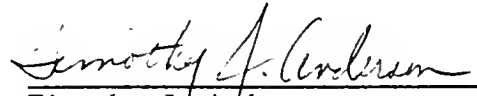
Ranganathan Narayanan
Associate Professor of
Chemical Engineering

I certify that I have read this study and that in my opinion it conforms to acceptable standards of scholarly presentation and is fully adequate, in scope and quality, as a dissertation for the degree of Doctor of Philosophy.
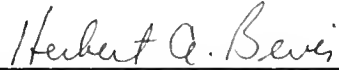
Timothy J. Anderson
Associate Professor of
Chemical Engineering

This dissertation was submitted to the Graduate Faculty of the College of Engineering and to the Graduate School and was accepted as partial fulfillment of the requirements for the degree of Doctor of Philosophy.

December 1986

Dean, College of Engineering

Dean, Graduate School